SYNTHESIS, CHARACTERISATION AND REACTIVITY OF PHOSPHIDE AND METHYLIDENE COMPLEXES OF IRIDIUM

By

KIRAN JOSHI

B.Sc. (Hons.), University of British Columbia, 1985

M.Sc., University of British Columbia, 1987

A THESIS SUBMITTED IN PARTIAL FULFILMENT OF

THE REQUIREMENTS FOR THE DEGREE OF

DOCTOR OF PHILOSOPHY

in

THE FACULTY OF GRADUATE STUDIES

DEPARTMENT OF CHEMISTRY

We accept this thesis as conforming

to the required standard

THE UNIVERSITY OF BRITISH COLUMBIA

August 1990

In presenting this thesis in partial fulfilment of the requirements for an advanced degree at the University of British Columbia, I agree that the Library shall make it freely available for reference and study. I further agree that permission for extensive copying of this thesis for scholarly purposes may be granted by the head of my department or by his or her representatives. It is understood that copying or publication of this thesis for financial gain shall not be allowed without my written permission.

Department of Chemistry

The University of British Columbia
Vancouver, Canada

Date Oct. 3/1990

ABSTRACT

The iridium(III) methyl diarylphosphide complexes, $Ir(CH_3)PR_2[N(SiMe_2CH_2PPh_2)_2]$ (**2a**: R = phenyl, **2b**: R = *meta*-tolyl) had been prepared previous to this work. The iridium(III) dimethylphosphide complex, $Ir(CH_3)PMe_2[N(SiMe_2CH_2PPh_2)_2]$, **2c**, is readily prepared *in situ* by transmetallation of the $Ir(CH_3)I[N(SiMe_2CH_2PPh_2)_2]$ with $KPMe_2$ at -30°C. The synthesis of the phenylphosphide complex $Ir(CH_3)PHPh[N(SiMe_2CH_2PPh_2)_2]$, **2d**, involves deprotonation of the six-coordinate iridium(III) phenylphosphine complex, $Ir(CH_3)I(PH_2Ph)[N(SiMe_2CH_2PPh_2)_2]$, with KO^tBu.

Thermolysis of **2a** and **2b** yields the six-coordinate iridium(III) cyclometallated hydride complexes *fac*-$Ir(\eta^2\text{-}CH_2PR_2)H[N(SiMe_2CH_2PPh_2)_2]$, **3a** and **3b**. The dimethylphosphide complex **2c** undergoes the same rearrangement to afford **3c** but more rapidly. Thermolysis of **3a-3c** yields the square planar iridium(I) phosphine complexes of the formula, $Ir(PCH_3R_2)[N(SiMe_2CH_2PPh_2)_2]$, **4a-4c**. Some of the intermediates proposed in the thermolysis of **2a** are synthesised independently by the reaction of iridium methylidene complex, $Ir{=}CH_2[N(SiMe_2CH_2PPh_2)_2]$, **10**, with $PHPh_2$. The complex *fac*-$Ir(\eta^2\text{-}CHPhPMe_2)H[N(SiMe_2CH_2PPh_2)_2]$ is generated from the reaction of $Ir(CH_2Ph)Br[N(SiMe_2CH_2PPh_2)_2]$ with $KPMe_2$ without intermediacy of the corresponding phosphide complex.

The photolysis of **2a-2c** also yields species **4a-4c**; however, no intermediacy of the cyclometallated hydride complexes **3a-3c** is observed during this transformation.

Upon thermolysis of the phenylphosphide complex **2d**, only the corresponding iridium(I) phosphine complex, $Ir(PHCH_3Ph)[N(SiMe_2CH_2PPh_2)_2]$, **4d**, is obtained, which is also the photolysis product of **2d**.

$Ir(CH_3)PPh_2[N(SiMe_2CH_2PPh_2)_2]$, **2a**, reacts at -78°C with dimethylacetylenedicarboxylate to yield an octahedral iridium(III) complex in which the alkyne has bridged between the phosphide ligand and the phosphine group of the chelating ligand. In addition, one of the phenyl groups from the chelating phosphine has migrated to the metal. On the other hand, $Ir(CH_3)PMe_2[N(SiMe_2CH_2PPh_2)_2]$, **2c**, reacts with the same alkyne to yield a product in which the alkyne has bridged between the phosphide group and the iridium centre. The reaction of **2a** with diphenylacetylene affords $Ir(PhC{\equiv}CPh)[N(SiMe_2CH_2PPh_2)_2]$ and free methyldiphenylphosphine. Complex **2a** reacts with terminal alkynes ($RC{\equiv}CH$; R = H, Ph, ^{t}Bu) to yield acetylide complexes of formula $Ir(CH_3)PHPh_2(C{\equiv}CR)[N(SiMe_2CH_2PPh_2)_2]$.

The methylidene complex, $Ir{=}CH_2[N(SiMe_2CH_2PPh_2)_2]$, **10**, prepared by the reaction of $Ir(CH_3)I[N(SiMe_2CH_2PPh_2)_2]$ with KO^{t}Bu, reacts with phosphines PHR_2 (R = Ph, ^{t}Bu) to afford the cyclometallated hydride complexes, *fac*-$Ir(\eta^2\text{-}CH_2PR_2)H[N(SiMe_2CH_2PPh_2)_2]$, via a five-coordinate methylidene phosphine intermediate. The reaction of **10** with PH_2Ph yields similar cyclometallated hydride product, but in this case the five-coordinate intermediate is not observed. The methylidene complex **10** reacts with the electrophiles MeI and $AlMe_3$ to yield $Ir(\eta^2\text{-}C_2H_4)H(I)[N(SiMe_2CH_2PPh_2)_2]$ and $Ir(\mu\text{-}AlMe_2)H[N(SiMe_2CH_2PPh_2)_2]$, respectively. Reaction of **10** with $HC{\equiv}CH$ affords an η^3-allyl acetylide complex $Ir(\eta^3\text{-}C_3H_5)(C{\equiv}CH)[N(SiMe_2CH_2PPh_2)_2]$. A trimethylenemethane complex, *fac*-$Ir\{\eta^4\text{-}C(CH_2)_3\}[N(SiMe_2CH_2PPh_2)_2]$, is obtained readily upon exposing **10** to 1,2-propadiene. The reaction of **10** with 1,3-butadiene affords a pentenyl product, $Ir(\sigma\text{-}\eta^3\text{-}C_5H_8)[N(SiMe_2CH_2PPh_2)_2]$.

In previous studies, the iridium(I) η^2-cyclooctene species, $Ir(\eta^2\text{-}C_8H_{14})[N(SiMe_2CH_2PPh_2)_2]$, **25**, has served as a useful starting material in the preparation of a number of iridium(I) and iridium(III) amide complexes. This complex is thermally

stable, but upon photolysis, it yields $Ir(H)_2[N(SiMe_2CH_2PPh_2)_2]$ and a mixture (2:1) of free 1,3-and 1,5-cyclooctadiene. This dehydrogenation process proceeds through an η^3-allyl hydride intermediate, $Ir(\eta^3\text{-}C_8H_{13})H[N(SiMe_2CH_2PPh_2)_2]$. The cyclo-octene ligand in **25** can be replaced by 1,3-butadiene and 1,2-propadiene. The products obtained from these reactions are $Ir(\eta^4\text{-}C_4H_6)[N(SiMe_2CH_2PPh_2)_2]$ and $Ir(\eta^2\text{-}C_3H_4)[N(SiMe_2CH_2PPh_2)_2]$, respectively. The reaction of **25** with $AlMe_3$ affords $Ir(\mu\text{-}AlMe_2)Me[N(SiMe_2CH_2PPh_2)_2]$.

TABLE OF CONTENTS

LIST OF TABLES

LIST OF FIGURES

LIST OF ABBREVIATIONS

The following list of abbreviations, most of which are commonly used in the chemical literature, will be employed in this thesis:

A_t	absorbance at time t (UV-Vis)
Å	angstrom, 10^{-8} centimeter
APT	attached proton test (NMR)
atm	atmosphere; 1 atm = 760 mm Hg
br	broad
Bu	butyl, $CH_2(CH_2)_2CH_3$
^tBu	tertiary butyl, $C(CH_3)_3$
Bz	benzyl, $CH_2C_6H_5$
^{13}C	carbon-13
cm	centimeter
COD	cyclooctadiene
COE	cyclooctene
Cp	cyclopentadienyl, η^5-C_5H_5
Cp*	pentamethylcyclopentadienyl, η^5-C_5Me_5
°C	degree Celsius
d	doublet (NMR)
DBU	1,8-diazabicyclo[5.4.0]undec-7-ene
dd	doublet of doublets (NMR)
DMAD	dimethylacetylenedicarboxylate
dt	doublet of triplets
deg	degree

deg	degree
fac	facial
gem	geminal
^1H	proton-1
Hz	Hertz, cycles per second
HETCOR	heteronuclear correlation (NMR)
IR	infra-red
^iPr	iso-propyl, $(CH_3)_2CH$
J	coupling constant, in Hz
k	rate constant
L	ligand
	litre
l	path length
M	central metal atom in a complex
m	multiplet (NMR)
	moderate intensity (IR)
Me	methyl, CH_3
mer	meridional
meta-tol	*meta*-tolyl, $CH_3(C_6H_4)$
min	minute(s)
mL	millilitre
mmol	millimole(s)
mol	mole(s)
nm	nanometer(s)
NMR	nuclear magnetic resonance
NOEDIFF	nuclear Overhauser effect difference
obs	observed

^{31}P	phosphorus-31
Ph	phenyl, C_6H_5
ppm	parts per million
r.d.s.	rate determining step
RT	room temperature
s	singlet (NMR), strong (IR)
T	temperature
t	triplet
tert	tertiary
UV-Vis	ultraviolet-visible
W	Watt
w	weak intensity (IR)
Δ	heat
ε	extinction coefficient (in mol^{-1} L cm^{-1})
λ	wave length
δ	chemical shift (in ppm downfield from TMS)
ν	frequency (cm^{-1})
η	descriptor for hapticity
μ	descriptor for bridging

ACKNOWLEDGEMENTS

I would like to thank Professor M. D. Fryzuk for his guidance, encouragement, and patience throughout the duration of this work. I am also indebted to members of the Fryzuk group (past and present) for their friendship and support. I wish to express my gratitude to the proof-readers for their excellent criticism.

The assistance of the various departmental services is gratefully acknowledged.

Finally, I would like to thank my family for their encouragement and support over the years.

CHAPTER 1

Introduction

1.1 General Introduction

The last three decades have witnessed a tremendous growth in the field of organometallic chemistry. Organometallic compounds, particularly those of the transition metals, are becoming increasingly important in many stoichiometric and catalytic transformations; for example, the speciality chemicals, L-dopa[1] and naproxen,[2] are synthesised via highly specific and selective transformations. Interest in such processes has also provided the impetus for synthesis and reactivity of new organometallic compounds.

This thesis deals with the transformations of a number of iridium complexes that contain phosphide ($-PR_2$), alkyl ($-CR_3$) or alkylidene ($=CR_2$) ligands. Before this work is presented, some background in hybrid ligand strategy, phosphide and carbene chemistry, and cyclometallation process is appropriate to put the thesis work in perspective.

1.2 Hybrid Ligand Design in Organometallic Chemistry

The chemistry of transition metal complexes is largely governed by the electronic and steric properties of the ligands.[3] Even a subtle variation in ligand design can dramatically influence the reactivity of transition metal complexes. Therefore, a considerable effort has been directed towards the synthesis of new ligands.[4]

Sacconi and co-workers have synthesised multi-dentate, neutral ligands with mixed *hard* (e.g. N) and *soft* donors (e.g. P, As) (Figure 1.1).[5] According to the *hard-soft* acid-base theory, "*hard* acids prefer to bind to *hard* bases and *soft* acids prefer to bind to *soft* bases."[6] Transition metal complexes often follow this rule as evidenced from the fact that *soft* late transition metals form a large number of complexes with the *soft* tertiary phosphines.[7] In contrast, few phosphine derivatives of the *hard* early transition metals have been reported.[8]

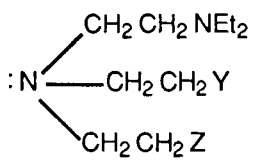

(1) Y = NEt_2; Z = PPh_2
(2) Y = Z = PPh_2
(3) Y = NEt_2; Z = $AsPh_2$
(4) Y = Z = $AsPh_2$

Figure 1.1 Mixed *hard-soft* donor ligands by Sacconi and co-workers[4]

The anionic amido-phosphine tridentate ligand, $^-[N(SiMe_2CH_2PR_2)_2]$ (R = Me, Ph, ^{i}Pr, ^{t}Bu), was first synthesised in our laboratory (Figure 1.2).[9] The impetus for the design of this ligand originated from the aforementioned fact that *soft* tertiary phosphines formed relatively few derivatives of the *hard* early transition metals, while the *hard* amide donors provided only a few stable, late transition metal complexes.[10] Thus, it was thought that incorporation of the amide donor $^-NR_2$ into a chelating array

of phosphines might allow coordination to a wide range of transition metals. This indeed was the case as a variety of amide phosphine complexes of both the early and the late transition metals have been prepared with this tridentate ligand system.[11] Recently, this work has been extended to lanthanides.[12]

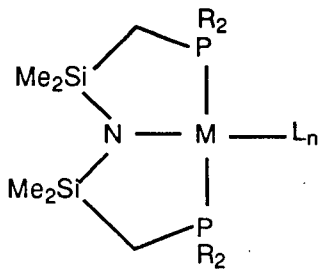

Figure 1.2 Tridentate amido-phosphine ligand bound to a metal centre

In most cases, the tridentate ligand acts as an ancillary (innocent) ligand. Recent studies have shown that it can become involved in certain reactions.[13] Some of these reactions are mentioned in this thesis (Chapters 3-5).

1.3 Transition Metal Phosphide Complexes

Tertiary phosphine complexes of the transition metals (L_nM-PR_3) are numerous due to the fact that they are easily prepared and quite stable. These complexes serve as catalyst precursors for such industrially important processes as hydrogenation, hydroformylation and polymerisation.[14] In addition to the well-known trivalent phosphines, other valencies of phosphorus are known but less studied. These include metallated phosphoranes (-PR_4),[15] terminal phosphides (-PR_2)[16] and phosphinidenes (=PR).[17] Although phosphorane and phosphinidene complexes are rare, the chemistry of the transition metal phosphide complexes has become a rapidly

growing research area. Now terminal phosphide complexes have been synthesised for most of the transition metals.

1.3.1 Synthesis of Transition Metal Phosphide Complexes

There are many ways to synthesise transition metal phosphide complexes. The following examples highlight the primary synthetic methods used to generate this class of compounds.

1.3.1.1 Metathesis with Lithium Phosphides

A variety of phosphide complexes of group 4 transition metals have been prepared via metathesis of the bis(cyclopentadienyl)dihalide complexes of zirconium or hafnium with two equivalents of the lithium phosphide reagents (Equation 1.1).[18] The extensive use of this preparative method is due to the easy accessibility of the required alkali phosphides; in particular, lithium dialkyl and diaryl phosphides are readily prepared from the corresponding secondary phosphines and BuLi (Equation 1.2). Most of the dialkyl and diaryl lithium phosphides can be isolated as solids which are stable at room temperature under an inert atmosphere for extended periods of time.

Equation 1.1

Equation 1.2

A recent publication[19] makes use of a similar metathetical reaction (Equation 1.1) involving the complexes, $Cp^*_2HfCl_2$ and $Cp^*_2ZrCl_2$, but with one equivalent of the secondary lithium phosphide salt, LiPHR (Scheme 1.1). These phosphide complexes were tested as possible precursors of the corresponding phosphinidene complexes via dehydrohalogenation reactions; however, it is believed that a polymeric species containing phosphinidene units was produced.

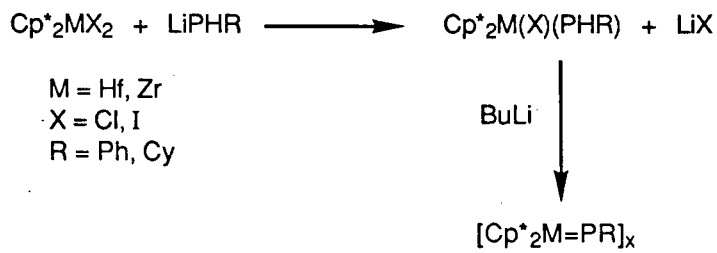

Scheme 1.1

1.3.1.2 Oxidative Addition of Phosphines

The first six-coordinate rhodium(III) and iridium(III) complexes containing PX_2 (X = F, Cl, H) ligands were prepared by the oxidative addition of a PX_2Y species to a low-valent Vaska-type rhodium(I) and iridium(I) complexes (Equation 1.3).[20] The rhodium phosphides reported in the abovementioned study still remain the only phosphide complexes known for this metal.

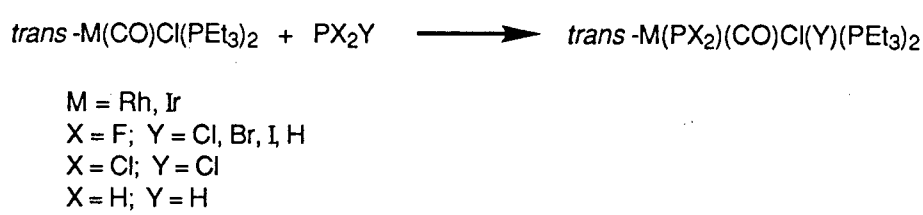

Equation 1.3

1.3.1.3 Deprotonation of Primary and Secondary Phosphines

Primary and secondary phosphine complexes can be deprotonated readily in the presence of strong nucleophilic bases such as 1,8-diazabicyclo[5.4.0]undec-7-ene (DBU), KO^{t}Bu, $NaN(SiMe_3)_2$ or BuLi, to yield terminal phosphide complexes.[21] An example of this preparative method is shown in Equation 1.4.

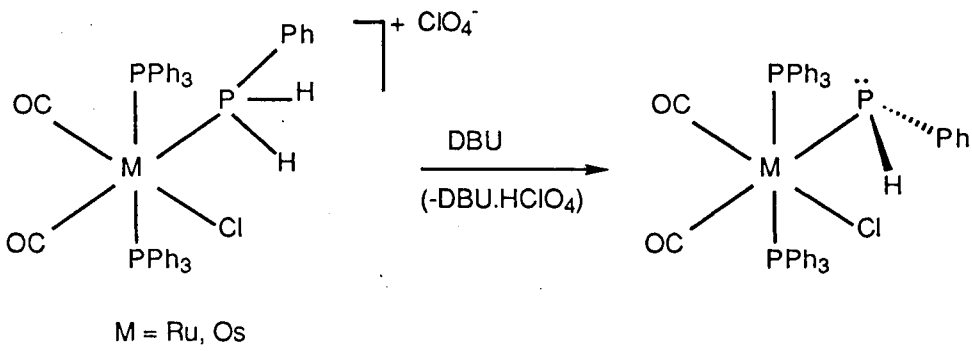

Equation 1.4

1.3.2 Structure and Bonding of the Phosphide Ligand

A terminal phosphide ligand in a mononuclear transition metal complex can either be pyramidal or planar (Figure 1.3).[22] A simple bonding scheme distinguishing these two conformations is shown in **A** and **B**. In the case of pyramidal geometry, the PR_2^- ligand is a two-electron donor and is bound to the metal via a σ-bond; in the planar geometry, the ligand is a four-electron donor and must involve π-bonding with the metal.

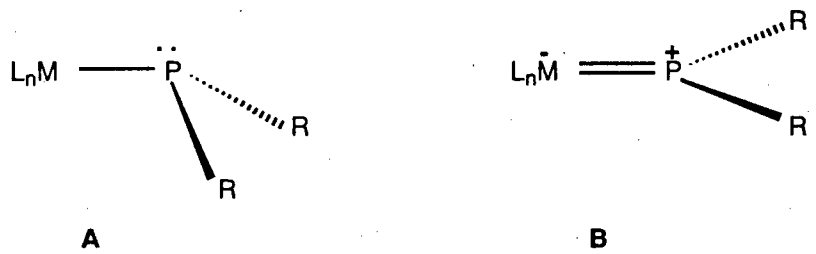

Figure 1.3 A transition metal complex containing (**A**) a pyramidal phosphide ligand (**B**) a planar phosphide ligand

A distinguishable feature of the two configurations is the metal-phosphorus bond length: complexes containing planar phosphide group possess a shorter M-P bond compared to that of complexes containing pyramidal group. In addition, a difference is noted in the metal-phosphorus-substituent bond angles: the ranges are reported to be 127-140° for planar and 106-114° for pyramidal phosphide complexes.[21] These two types of complexes can also be distinguished by ^{31}P NMR spectroscopy. In complexes of type **B**, the ^{31}P NMR resonances are usually shifted to low field as compared to complexes of type **A**. The ^{31}P chemical shifts for pyramidal and planar phosphide complexes reported in the literature range from -270 to +420 ppm and +200 to +400 ppm, respectively.[16]

The iridium(III) methyl diarylphosphide complexes of formula, $Ir(CH_3)PR_2$-$[N(SiMe_2CH_2PPh_2)_2]$ (R = phenyl, *meta*-tolyl), were synthesised via metathesis of the iridium(III) methyl halide complex, $Ir(CH_3)I[N(SiMe_2CH_2PPh_2)_2]$, with the appropriate lithium phosphide, $LiPR_2$, as a part of my M.Sc. thesis.[16a,65] The synthesis and characterisation of the dimethylphosphide complex, $Ir(CH_3)PMe_2$-$[N(SiMe_2CH_2PPh_2)_2]$, and of the phenylphosphide complex, $Ir(CH_3)PHPh$-$[N(SiMe_2CH_2PPh_2)_2]$, are described in this thesis (Chapter 2).

1.4 Intramolecular Carbon-Hydrogen Bond Activation — Cyclometallation

Alkanes are major constituents of natural gas, petroleum and coal liquefaction processes. Their use as feedstocks for large-scale catalytic synthesis of organic molecules by activation of C–H bonds and subsequent functionalisation is of industrial importance.[23] However, the C–H bonds in alkanes are relatively unreactive. This apparent lack of reactivity is partly a consequence of the high C–H bond energies (~400 KJ mol^{-1}).[24] Some soluble transition metal systems have been found which are capable of activating such C–H bonds.[25]

Carbon–hydrogen bond activation by transition metal complexes can be achieved intermolecularly[26] (Equation 1.5) or intramolecularly[27] (Equation 1.6). Related to the intramolecular C–H activation is the cyclometallation of tertiary phosphines which is described in this thesis work.[28]

Equation 1.5

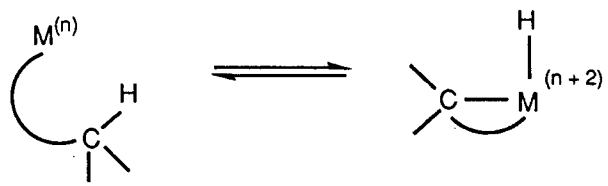

Equation 1.6

One of the earliest structurally well-defined examples of an intramolecular C–H activation involving the formation of ruthenium dimer complexes was reported by Chatt and Davidson in 1965 (Equation 1.7).[29] Later, Tolman and co-workers studied the activation of C–H bonds in CH_3X (X = CN, CO_2Et) by some iron and ruthenium

compounds (Equation 1.8).[30] In these reactions, the reductive elimination of naphthalene to form the corresponding M(0) species was found to be the rate-determining step. In contrast, some alkyl hydride complexes of ruthenium and osmium, *cis*-$(PMe_3)_4Ru(H)Me$[31] and *cis*-$(dmpe)_2OsH(C_{10}H_7)$,[30] are stable toward thermal reductive elimination.

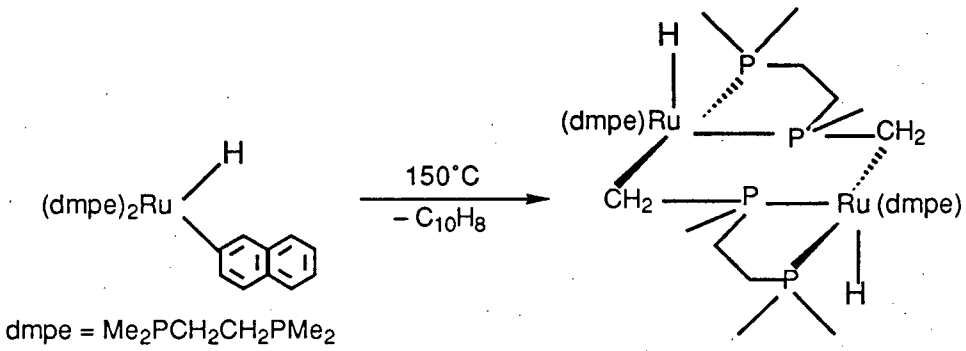

Equation 1.7

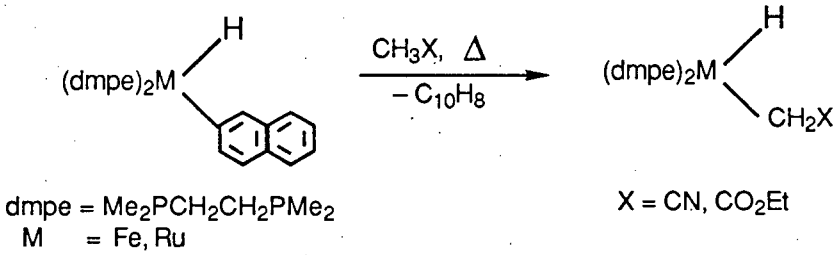

Equation 1.8

However, the complex *cis*-$(PMe_3)_4OsH[CH_2C(CH_3)_3]$ undergoes intramolecular activation of one of the C–H bonds of the bound PMe_3 ligand to form the cyclometallated hydride complex *fac*-$(PMe_3)_3Os(\eta^2\text{-}CH_2PMe_2)H$ at 80°C (Equation 1.9), presumably via the intermediate "$(PMe_3)_4Os$".[32] A similar cyclometallation reaction is observed upon the reduction of ruthenium and osmium complexes with sodium amalgam (Equation 1.10).[33]

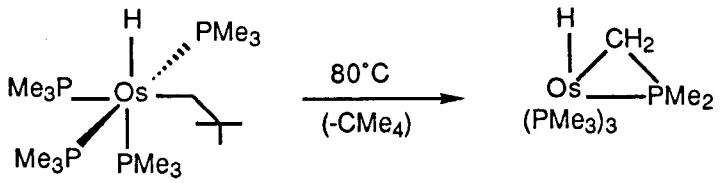

Equation 1.9

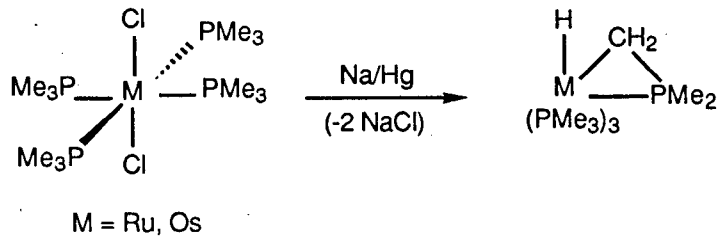

Equation 1.10

Irradiation of rhenium(I) complex, $CpRe(PMe_3)_3$, at 5-10°C in cyclohexane yielded two products originating from intramolecular C–H activation of the PMe_3 ligand (Scheme 1.2). However, when the complex was photolysed in a solvent such as benzene (which is more prone to intermolecular C–H activation compared to cyclohexane), the complex $CpRe(Ph)H(PMe_3)_2$ was produced.[34]

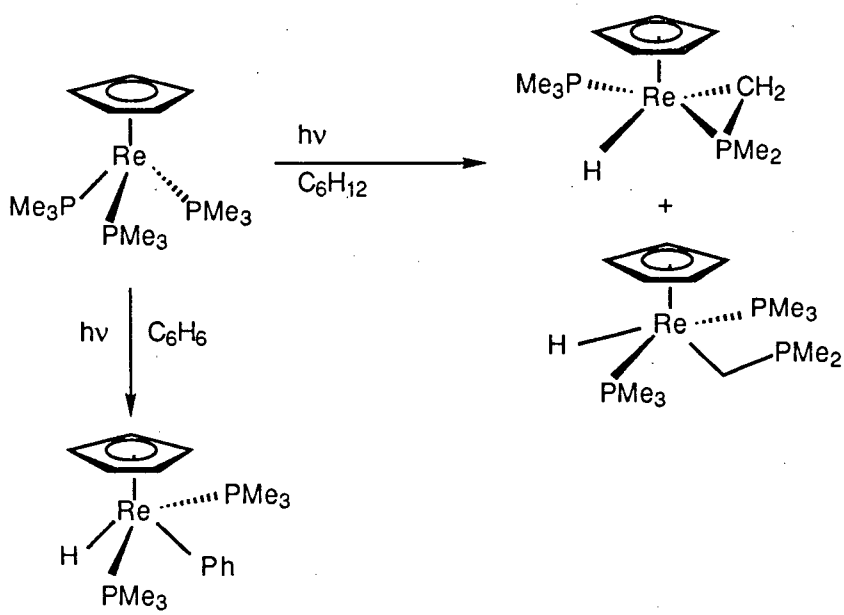

Scheme 1.2

The synthesis of cyclometallated complexes via metathetical reactions has also been reported. The use of a lithiating reagent such as $LiCH_2PR_2$ (R = Me, ^tBu) with $CoCl(PMe_3)_3$ generates $Co(\eta^2\text{-}CH_2PR_2)(PMe_3)_3$ (Equation 1.11).[35] The treatment of $RuCl_2(PMe_3)_4$ with $LiCH_2(=CH_2)PMe_2$ gives a complex containing both three and four-membered rings (Equation 1.12).[36] The reaction of *mer*-$IrCl_3(PMe_2Ph)_3$ with $Li(CH_2)_5Li$ generates the three-membered iridacycle shown in Equation 1.13.[33]

$$CoCl(PMe_3)_3 + LiCH_2PR_2 \xrightarrow[(-LiCl)]{} Co(\eta^2\text{-}CH_2PR_2)(PMe_3)_3$$

R = Me, ^tBu

Equation 1.11

$$RuCl_2(PMe_3)_4 + Me_2P(=CH_2)CH_2Li \xrightarrow[(-LiCl)]{}$$

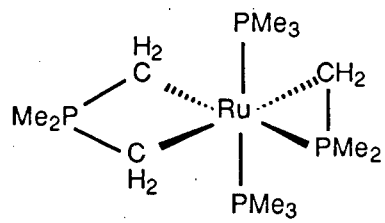

Equation 1.12

$$mer\text{-}IrCl_3(PMe_2Ph)_3 + Li(CH_2)_5Li \xrightarrow[(-LiCl)]{} IrCl_2(\eta^2\text{-}CH_2PMePh)(PMe_2Ph)_2$$

Equation 1.13

Attempts to prepare some ruthenium amide complexes by treating ruthenium halide species with lithium amide salts resulted instead in the metallation of the PMe_3 ligand to give the corresponding three-membered metallacyclic complexes (Equation 1.14).[37] Similar cyclometallation was observed when the iridium system *mer*-$IrCl_3\{P(Me)(CH_2Ph)_2\}_3$ was reacted with $LiN(^iPr)_2$ (Equation 1.15).[36]

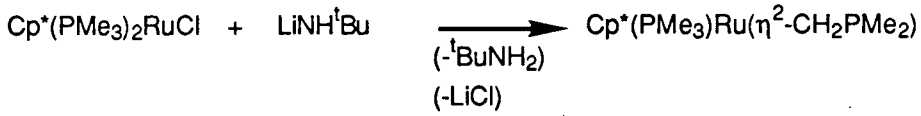

Equation 1.14

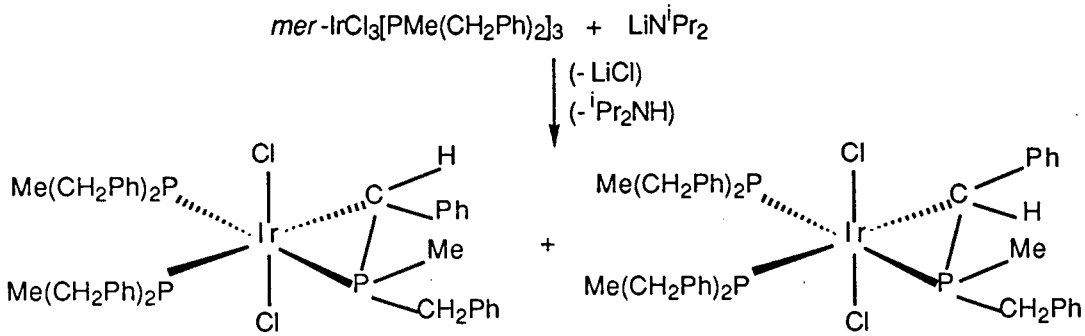

Equation 1.15

In this thesis, cyclometallated hydride complexes of formula $Ir(\eta^2\text{-}CH_2PR_2)H\text{-}[N(SiMe_2CH_2PPh_2)_2]$ are described. These species were synthesised (i) via the thermal rearrangement of the phosphide complexes $Ir(CH_3)PR_2[N(SiMe_2CH_2\text{-}PPh_2)_2]$, (ii) by the reactions of the alkylidene species $Ir{=}CH_2[N(SiMe_2CH_2PPh_2)_2]$ with free phosphines PHR_2 and PH_2R (Chapter 2).

1.5 Transition Metal Carbene Complexes

The ability of transition metal complexes to stabilise very reactive organic fragments, such as carbenes,[38] vinylidenes,[39] benzynes[40] and thiocarbonyls,[41] constitutes a basic facet of organometallic chemistry. Carbenes ($:CR_2$) are short-lived chemical species which can only be isolated by entrapment in low temperature matrices.[42] However, they can also be stabilised by coordination to a metal centre.

Indeed, much has been reported on the formation of transition metal carbene complexes ($M=CR_2$) and the reactivity of the coordinated carbene unit.[38] The importance of metal carbene complexes in a variety of different processes such as olefin metathesis,[43] cyclopropanation,[44] ethylene polymerisation (propagation step in the Ziegler-Natta mechanism)[45] and alkyne co-cyclisation[46] is now well appreciated.[47] Also, surface bound carbenes have been postulated as intermediates in Fischer-Tropsch chemistry.[48]

The first example of a stable transition metal carbene complex was reported by Fischer and Maasbol in 1964.[49] Since then a vast number of carbene complexes have been reported. In these complexes, one or both of the substituents on the carbene carbon are heteroatom (other than C and H) substituents (Figure 1.4 **A**). These complexes are common among the late transition metals, and are generally referred to as "Fischer carbenes".

A series of early transition metal complexes without a heteroatom substituent on the carbene carbon was reported by Schrock (Figure 1.4 **B**).[50] These complexes are often called alkylidenes or "Schrock carbenes".

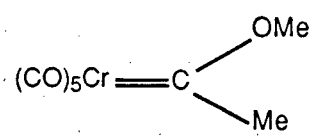

A

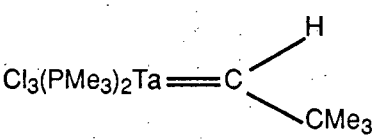

B

Figure 1.4 Example of a Fischer carbene (**A**), and Schrock carbene (**B**)

1.5.1 Synthesis of Transition Metal Carbene Complexes

Since the pioneering work of Fischer's group and Schrock' group, hundreds of transition metal carbene complexes have been prepared by many different synthetic methods. (From this point in the thesis, Fischer and Schrock complexes will be known as transition metal carbene complexes). Examples of some of these routes are mentioned below.

1.5.1.1 Heteroatom Substituted Carbene Complexes

These carbene complexes are still prepared by the method of Fischer and Massbol. This reaction involves the external attack of a carbanionic nucleophile such as R^- in LiR at the carbon atom of a coordinated carbonyl ligand to give an anionic metal acyl complex (Scheme 1.3); subsequent attack of an electrophilic reagent at the acyl oxygen atom converts it into the corresponding carbene complex.[51]

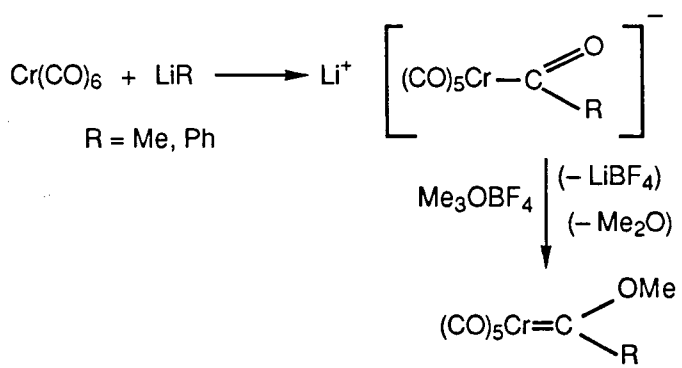

Scheme 1.3

An α-hydroxyalkyne reacts with an iridium(III) complex and affords an iridium(III) bis(oxacyclopentylidene) complex (Equation 1.16).[52] A variety of ruthenium carbene complexes have also been generated in a similar manner.[53]

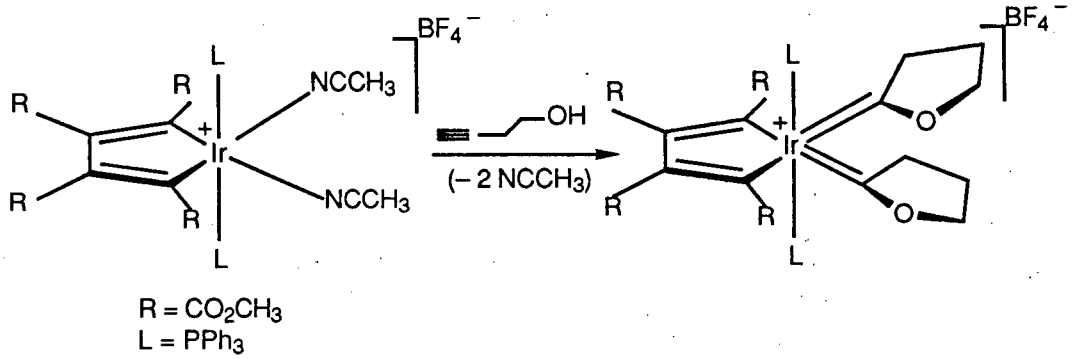

Equation 1.16

Electron-rich olefins such as **A** in Equation 1.17 have been used in the synthesis of a large number of mono-, bis-, tris- and tetracarbene complexes of ruthenium, osmium, rhodium and iridium.[54]

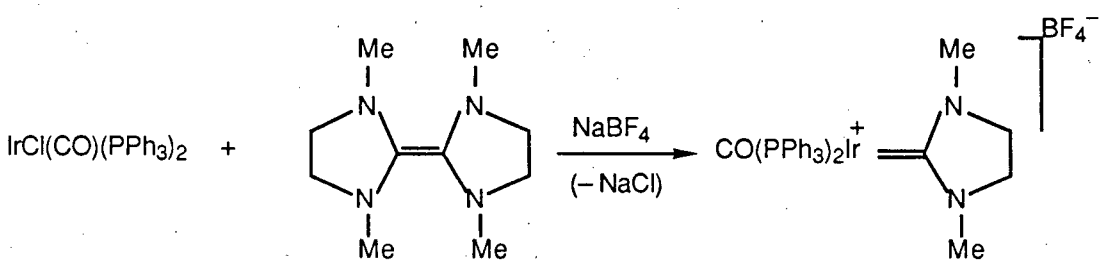

A

Equation 1.17

A variety of late transition metal dihalocarbene complexes have also been reported in recent years. These complexes were prepared by halide abstraction from a trihaloalkyl ligand with Lewis acids such as BF_3 (Equation 1.18).[55]

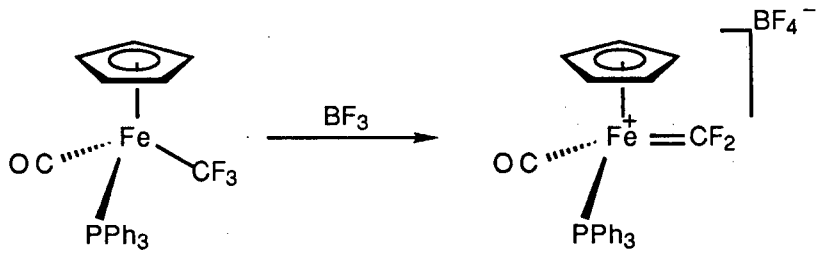

Equation 1.18

1.5.1.2 Alkylidene Complexes

Alkylidene complexes are generally prepared by the removal of an α-hydrogen from an alkyl ligand. In many cases, steric crowding induces the alkane loss, and affords alkylidene formation from group 5 and 6 transition metal dialkyl complexes (Equation 1.19).[56]

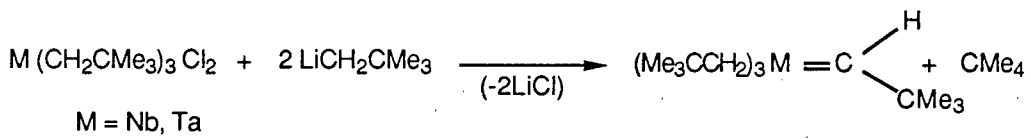

Equation 1.19

The reactions of low-valent Ru, Os and Ir complexes with diazoalkanes provide the most general route to d^8 alkylidene species.[55] The osmium complex, $Os(Cl)NO(PPh_3)_3$, for example, reacted with diazomethane or diazoethane at room temperature to form the stable methylidene or ethylidene complex (Equation 1.20). Diazomethane addition to $Ir(CO)I(PPh_3)_2$ at -50°C yielded $Ir{=}CH_2(I)CO(PPh_3)_2$.[55] This methylidene complex rearranged to the orthometallated ylide complex (Scheme 1.4) when its solution was warmed to room temperature.

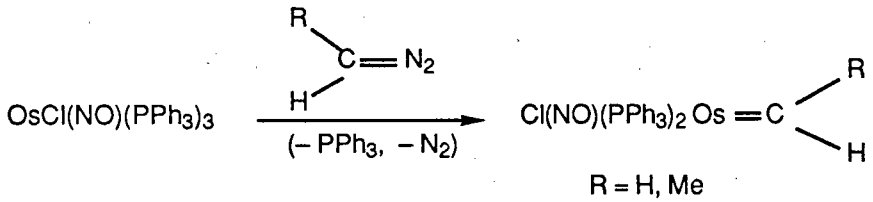

Equation 1.20

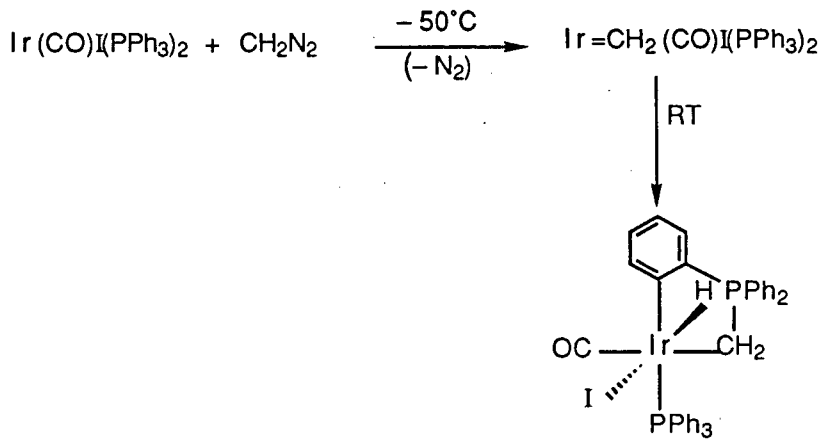

Scheme 1.4

The synthesis of stable cationic rhenium methylidene complexes has been reported by Gladysz and co-workers.[57] The complex, $[Cp^*Re{=}CH_2(NO)(PPh_3)_3]^+$, was prepared by treating the rhenium alkyl complex, $Cp^*Re(CH_3)NO(PPh_3)_3$, with trityl hexafluorophosphate (Equation 1.21).

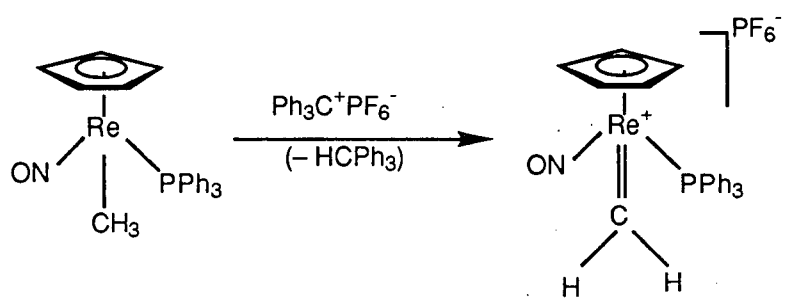

Equation 1.21

The synthesis of an iridium(I) alkylidene species using IrHCl-[^{t}Bu$_2$P(CH$_2$)$_2$CH(CH$_2$)$_2$P^{t}Bu$_2$] as precursor has been described by Shaw's group. Elimination of H_2 from the precursor complex by thermolysis afforded the desired Ir(I) alkylidene complex (Equation 1.22).[58] Although this is considered to be a text book example,[59] poor yields and the irreproducibility of the reaction have prevented any detailed study of this compound.

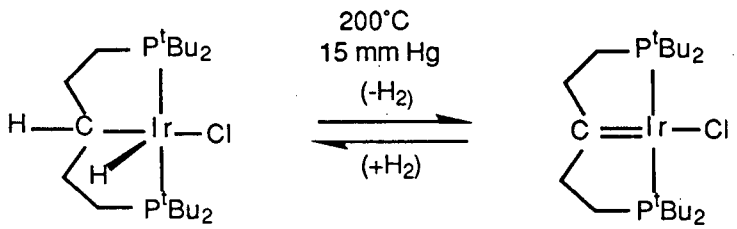

Equation 1.22

A recent example of a cyclopentadienyl iridium alkylidene species is shown in Equation 1.23.[60] The complex Cp*Ir=CH$_2$(PMe$_3$) was prepared by the photoextrusion of acetone from a 2-oxametallacyclic complex at -60°C. At temperatures higher than -40°C, the methylidene complex decomposed.

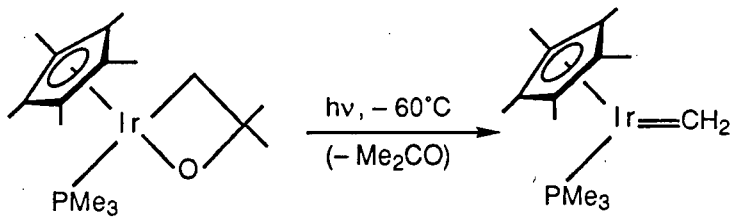

Equation 1.23

In 1985, the preparation of an iridium(I) methylidene complex, Ir=CH$_2$-[N(SiMe$_2$CH$_2$PPh$_2$)$_2$], via photochemical α-hydrogen abstraction (or elimination) from the iridium(III) dialkyl complex, Ir(CH$_3$)(CH$_2$CMe$_3$)[N(SiMe$_2$CH$_2$PPh$_2$)$_2$] (Scheme 1.5) was reported by Fryzuk and co-workers.[61] This complex was the first example of a stable sixteen-electron square-planar late metal-alkylidene species.

The complex $Ir{=}CH_2[N(SiMe_2CH_2PPh_2)_2]$ was isolated in low yields (15-20%), and was characterised by X-ray crystallography (Figure 1.5). The stability of this complex compared to the above mentioned iridium alkylidene complexes is attributed to the tridentate ligand on the metal centre. The phenyl substituents on the phosphine centres of the tridentate ligand seem to provide a "pocket" which protects the methylene unit.

The major product of the reaction was the iridium(III) dihydride species, $Ir(H)_2[N(SiMe_2CH_2PPh_2)_2]$, (Scheme 1.5). An in-depth study of the reactivity of the iridium-alkylidene complex was prevented by the difficulty in obtaining it in good yield.[62]

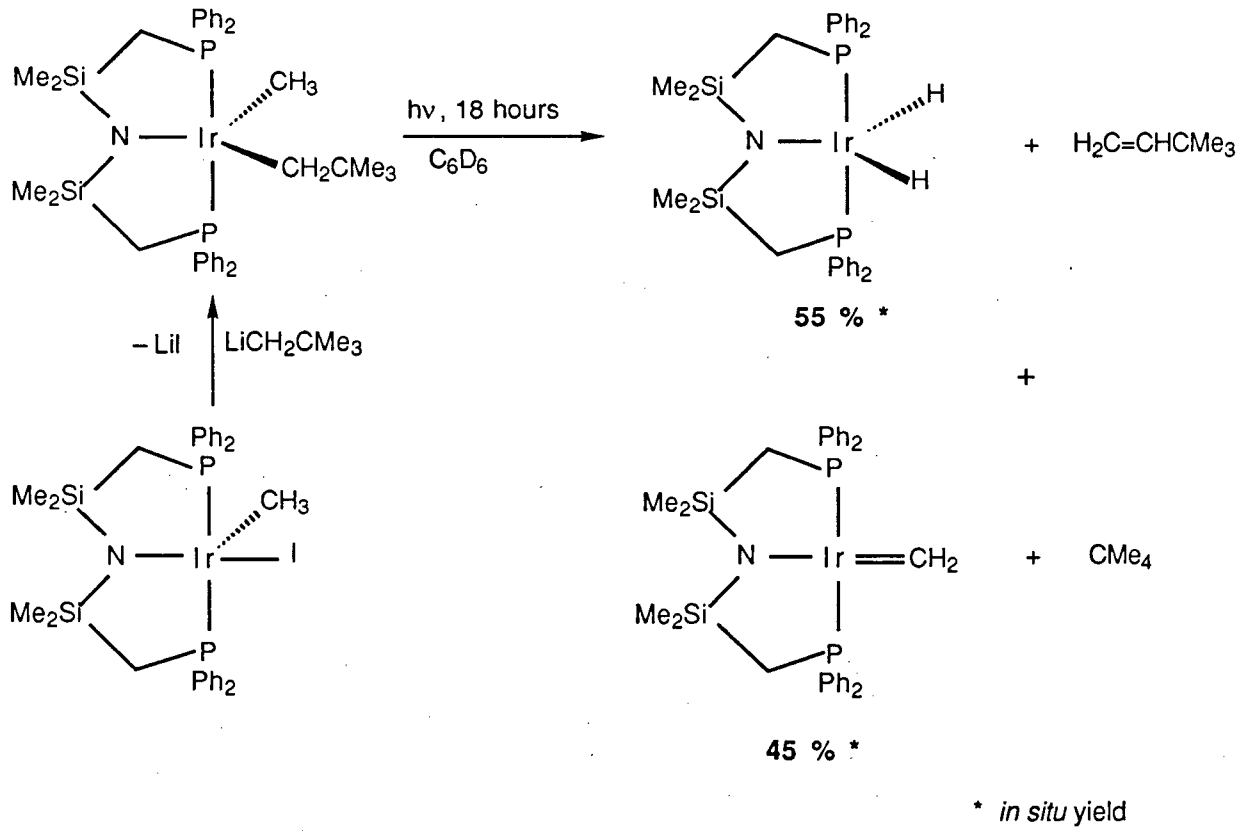

Scheme 1.5

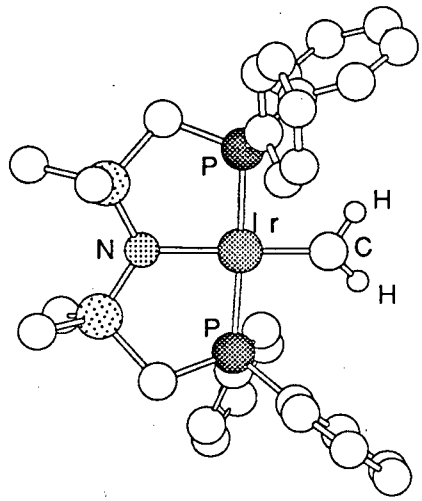

Figure 1.5 Chem-3D^{TM} view of $Ir{=}CH_2[N(SiMe_2CH_2PPh_2)_2]$

1.5.2 Reactivity of Transition Metal Carbene Complexes

A traditional view regarding the reactivity of transition metal carbene complexes suggests that Fischer carbene complexes display electrophilic reactivity at the carbene carbon. In these complexes, replacement of a methoxy group by an amide group, for example, is initiated by the attack of the nucleophile at the carbene carbon (Equation 1.24).[63] In contrast, the alkylidene carbon of Schrock carbenes generally displays nucleophilic behaviour. The nucleophilicity of the methylene ligand in $Cp_2(CH_3)Ta{=}CH_2$ was illustrated by complexation with the electrophile $AlMe_3$ (Equation 1.25).[56a]

$$(CO)_5Cr = C(OMe)Ph \xrightarrow[(-\ MeOH)]{RNH_2} (CO)_5Cr = C(NHR)Ph$$

Equation 1.24

$$Cp_2Ta(CH_3)(CH_2) \xrightarrow{AlMe_3} Cp_2Ta^{+}(CH_3)(CH_2{-}\bar{A}lMe_3)$$

Equation 1.25

However, such a sharp distinction between the electrophilic versus the nucleophilic nature of the metal–carbon double bond does not always hold.[55] For example, an alkylidene ligand can easily become electrophilic when it is part of a cationic species (Equation 1.26).[55]

$$[Cp(NO)(PPh_3)Re = CH_2]^+ \xrightarrow{MeLi} Cp(NO)(PPh_3)Re - CH_2CH_3$$

Equation 1.26

In addition, there are complexes reported in the literature in which the carbene carbon shows amphiphilic (both nucleo- and electrophilic) behaviour.[64] The rhenium alkylidene complex, $Cp(CO)_2Re{=}C[(D)(CH_2CH_2CMe_3)]$, undergoes protonation at the alkylidene carbon upon reaction with HCl at -80°C and affords the corresponding alkyl rhenium species (Scheme 1.6).[64a] It also reacts with the nucleophile PMe_3 to produce the zwitterionic complex (**A**, Scheme 1.6).

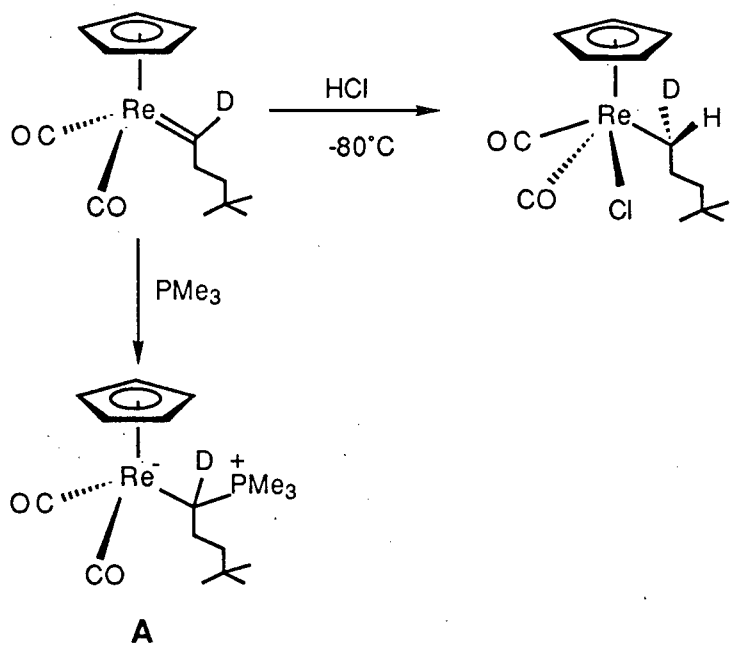

Scheme 1.6

A new and improved synthesis of the methylidene complex, $Ir{=}CH_2$-$[N(SiMe_2CH_2PPh_2)_2]$, is reported in this thesis (Chapter 4). Reactions of this complex with some electrophiles and with some unsaturated hydrocarbons are described.

1.6 Scope of the Thesis

The iridium(III) methyl diarylphosphide complexes, $Ir(CH_3)PR_2$-$[N(SiMe_2CH_2PPh_2)_2]$, (**2a**: R = phenyl, **2b**: R = *meta*-tolyl) were prepared. The photolysis and the reactivity of complex **2a** with small molecules such as H_2, CO and MeI were studied as part of my M.Sc. thesis.[65] These complexes were proposed to be square pyramidal, with the methyl ligand in the apical position (from NOE-DIFF experiments). Furthermore, although inconclusive, the geometry at the phosphide phosphorus nucleus was assigned as pyramidal (from ^{31}P NMR spectral data).[65]

Chapter 2 describes the results of a crystallographic study on complex **2a**. In addition, the syntheses of the dimethylphosphide complex, $Ir(CH_3)PMe_2$-$[N(SiMe_2CH_2PPh_2)_2]$, **2c**, and the phenylphosphide complex, $Ir(CH_3)PHPh$-$[N(SiMe_2CH_2PPh_2)_2]$, **2d**, are discussed. Complexes **2a-2c** undergo thermal rearrangement to yield cyclometallated hydride species of formula $Ir(\eta^2$-$CH_2PR_2)H[N(SiMe_2CH_2PPh_2)_2]$. The results of this process along with the kinetic and mechanistic details constitute the major part of this chapter. Some of the intermediates proposed in the mechanism of the thermolysis reaction of **2a** were prepared via a different synthetic route involving the reaction of the iridium methylidene complex, $Ir{=}CH_2[N(SiMe_2CH_2PPh_2)_2]$, and $PHPh_2$. The characterisation of other cyclometallated hydride complexes prepared by the reaction of $Ir{=}CH_2[N(SiMe_2CH_2PPh_2)_2]$ with PH^tBu_2 and PH_2Ph is also described. Complex

2d shows thermal reactivity different than that of **2a-2c**. The kinetic and mechanistic details of this reaction are presented. Photolytic behaviour of **2a-2d** is also described in this chapter.

Chapter 3 consists of the reactivity of complex **2a** with various alkynes such as diphenylacetylene, phenylacetylene, *tert*-butylacetylene, acetylene, and dimethyl-acetylenedicarboxylate (DMAD). The reaction of complex **2c** with DMAD is also discussed.

An improved synthesis of the iridium methylidene complex, $Ir{=}CH_2$-$[N(SiMe_2CH_2PPh_2)_2]$, is reported in chapter 4. The reactivity of this alkylidene complex with electrophiles such as trimethylaluminum and methyl iodide is described. Furthermore, some interesting reactions were observed on reacting the methylidene complex with 1,3-butadiene, 1,2-propadiene (allene) and acetylene. They are also discussed in chapter 4.

The iridium(I) cyclooctene complex, $Ir(\eta^2\text{-}C_8H_{14})[N(SiMe_2CH_2PPh_2)_2]$, serves as a usefull starting material in a variety of reactions leading to iridium(I) and iridium(III) amide complexes. Chapter 5 consists of a study of the photochemical versus thermal reactivity of this complex, along with its reactions with dienes such as 1,3-butadiene and 1,2-propadiene (allene). The reaction with trimethylaluminum is also mentioned.

Chapter 6 outlines some general conclusions and recommendations for future work.

The experimental procedures used in this thesis work are described in chapter 7.

1.7 References

1 Knowles, W. S. *Accs. Chem. Res.* **1983**, *16*, 206.

2 Haggin, J. *Chem. Eng. News* May 7, **1990**, 58.

3 McAuliffe, C. A. *Compr. Coord. Chem.* **1987**, *2*, 989.

4 Collman, J. P.; Hegedus, L. S.; Norton, J. R.; Finke, R. G. *Principles and Applications of Organotransition Metal Chemistry*; University Science Books: Mill Valley, CA, **1987**, Chapter 3.

5 (a) Bertini, I.; Dapporta, P.; Fallani, G.; Sacconi, L. *Inorg. Chem.* **1971**, *10*, 1703.
(b) Sacconi, L.; Morassi, R. *J. Chem. Soc. (A)* **1969**, 2904.

6 Pearson, R. G. *J. Chem. Ed.* **1968**, *45*, 581 and 643.

7 (a) Levason, W.; MacAuliffe, C. A. *Phosphine, Arsine, and Stibine Complexes of Transition Elements*; Elsevier: Amsterdam, **1979**.
(b) Tolman, C. A. *Chem. Rev.* **1977**, *77*, 313.

8 (a) Fryzuk, M. D.; Haddad, T. S.; Berg, D. J. *Coord. Chem. Rev.* **1990**, *99*, 137.
(b) Datta, S.; Fisher, M. B.; Wreford, S. S. *J. Organomet. Chem.* **1980**, *188*, 353.
(c) Parshall, G .W.; Schrock, R. R. *Chem. Rev.* **1976**, *76*, 243.

9 Fryzuk, M. D.; MacNeil, P. A. *J. Am. Chem. Soc.* **1981**, *103*, 3592.

10 (a) Fryzuk, M. D.; Montgomery, C. D. *Coord. Chem. Rev.* **1989**, *95*, 1.
(b) Bryndza, H. E.; Tam, W. *Chem. Rev.* **1988**, *88*, 1163.
(c) Lappert, M. F.; Power, P. P.; Sanger, A. R.; Srivastava, R. C. *Metal and Metalloid Amides*; Horwood-Wiley: Chichester, New York, **1980**.

11 (a) Fryzuk, M. D.; MacNeil, P. A.; Rettig, S. J.; Secco, A. S.; Trotter, J. *Organometallics* **1982**, *1*, 918.
(b) Fryzuk, M. D.; MacNeil, P. A. *Organometallics* **1983**, *2*, 682.

(c) Fryzuk, M. D.; MacNeil, P. A.; Rettig, S. J. *Organometallics* **1986**, *5*, 2469.

(d) Fryzuk, M. D.; Rettig, S. J.; Westerhaus, A.; Williams, H. D. *Inorg. Chem.* **1985**, *24*, 4316.

(e) Fryzuk, M. D.; Williams, H. D. *Organometallics* **1983**, *2*, 162.

(f) Fryzuk, M. D.; Haddad, T. S.; Rettig, S. J. *Organometallics* **1988**, *7*, 1224.

(g) Fryzuk, M. D.; Haddad, T. S. *J. Am. Chem. Soc.* **1988**, *110*, 8263.

12 Fryzuk, M. D.; Berg, D. J.; Haddad, T. S. unpublished results, **1989**.

13 Fryzuk, M. D.; MacNeil, P. A. *Organometallics* **1982**, *1*, 1540.

14 Alyea, E. C.; Meek, D. W. *Catalytic Aspects of Metal Phosphine Complexes; Advances in Chemistry, 196*; American Chemical Society, Washington, D.C., **1982**.

15 Ebsworth, E. A. V.; Holloway, J. H.; Pilkington, N. J.; Rankin, D. W. H. *Angew. Chem., Int. Ed. Engl.* **1984**, *8*, 630.

16 (a) Fryzuk, M. D.; Joshi, K. *Organometallics* **1989**, *8*, 722.

(b) Crisp, G. T.; Salem, G.; Wild, S. B. *Organometallics* **1989**, *8*, 2360.

(c) Montllo, D.; Svades, J.; Torres, M. R.; Perales, A.; Mathieu, R. *J. Chem. Soc., Chem. Commun.* **1989**, 97.

(d) Hey, E.; Lappert, M. F.; Atwood, J. L.; Bott, S. G. *Polyhedron* **1988**, *7*, 2083.

(e) Fryzuk, M. D.; Bhangu, K. *J. Am. Chem. Soc.* **1988**, *103*, 961.

(f) Buhro, W. E.; Zwick, B. D.; Georgiou, S.; Hutchinson, J. P.; Gladysz, J. A. *J. Am. Chem. Soc.* **1988**, *110*, 2427.

(g) Buhro, W. E.; Chisholm, M. H.; Folting, K.; Huffmann, J. C. *J. Am. Chem. Soc.* **1987**, *109*, 905.

(h) Jorg, K.; Malisch, W.; Reich, W.; Meyer, A.; Schubert, U. *Angew. Chem., Int. Ed. Engl.* **1986**, *25*, 92.

(i) Bohle, D. S.; Jones, T. C.; Rickard, C. E. F.; Roper, W. R. *Organometallics* **1986**, *5*, 1612.

(j) Baker, R. T.; Whitney, J. F.; Wreford, S. S. *Organometallics* **1983**, *2*, 1049.

(j) Baker, R. T.; Whitney, J. F.; Wreford, S. S. *Organometallics* **1983**, *2*, 1049.

(k) Day, V. W.; Tavanaiepour, I.; Abdel-Meguid, S. S.; Kirner, J. F.; Goh, L. Y.; Mutterties, E. L. *Inorg. Chem.* **1982**, *21*, 657.

(l) Rocklage, S. M.; Schrock, R. R.; Churchill, M. R.; Wasserman, H. J. *Organometallics* **1982**, *1*, 1332.

(m) Domaille, P. J.; Foxman, B. M.; McNeese, T. J.; Wreford, S. S. *J. Am. Chem. Soc.* **1980**, *102*, 4114.

(n) Malisch, W.; Alsmann, R. *Angew. Chem., Int. Ed. Engl.* **1976**, *15*, 769.

(o) Buhro, W. E.; Georgiou, S.; Hutchinson, J. P.; Gladysz, J. A. *J. Am. Chem. Soc.* **1985**, *107*, 3346.

(p) Dobbie, R. C.; Hopkinson, M. J.; Whittaker, D. *J. Chem. Soc., Dalton Trans.* **1972**, 1030.

17 (a) Cowley, A. H.; Barron, A. R. *Accs. Chem. Res.* **1988**, *21*, 81.

(b) Arif, A. M.; Cowley, A. H.; Norman, N. C.; Orpen, A. G.; Paulski, M. *Organometallics* **1988**, *7*, 309.

(c) Charrier, C.; Maigrot, N.; Mathey, F. *Organometallics* **1987**, *6*, 586.

(d) Hitchcock, P. B.; Lappert, M. F.; Leung, W. P. *J. Chem. Soc., Chem. Commun.* **1987**, 1282.

(e) Flynn, K. M.; Bartlett, R. A.; Olmstead, M. M.; Power, P. P. *Organometallics* **1986**, *5*, 813.

(f) Marinetti, A.; Mathey, F. *J. Am. Chem. Soc.* **1982**, *104*, 4484.

18 Baker, R. T.; Krusic, P. J.; Tulip, T. H.; Calabrese, J. C.; Wreford, S. S. *J. Am. Chem. Soc.* **1983**, *105*, 6763.

19 Vaughan, G. A.; Hillhouse, G. L.; Rheingold, A. L. *Organometallics* **1989**, 8, 1760.

20 (a) Ebsworth, E. A. V.; Holloway, J. H.; Pilkington, N. J.; Rankin, D. W. H. *Angew. Chem., Int. Ed. Engl.* **1984**, *8*, 630.

(b) Ebsworth, E. A. V.; Mayo, R. *Angew. Chem., Int. Ed. Engl.* **1985**, *24*, 68.

21 Bohle, D. S.; Roper, W. R. *Organometallics* **1986**, *5*, 1607.

22 Reference 18 describes a hafnium phosphide complex containing both a pyramidal and a planar phosphide ligand. The structural parameters (M–P bond length and angle) along with the ^{31}P NMR data typical for a pyramidal versus planar phosphide geometry are discussed.

23 Crabtree, R. H. *Chem. Rev.* **1985**, *85*, 245, and references therein.

24 Benson, S. W. *Thermochemical Kinetics*; Wiley, New York, **1976**, p. 309.

25 Bergman, R. G. *Science* **1984**, *223*, 902 and references 26-32.

26 (a) Shilov, A. E.; Shteinman, A. A. *Coord. Chem. Rev.* **1977**, *24*, 97.
(b) Shilov, A. E. *Activation of Saturated Hydrocarbons by Transition Metal Complexes*; D. Reidel: Hingham, MA, **1984**.
(c) Halpern, J. *Inorg. Chim. Acta* **1985**, *100*, 41.
(d) Deem, M. L. *Coord. Chem. Rev.* **1986**, *10*, 9.

27 (a) Ryabov, A. D. *Chem. Rev.* **1990**, *90*, 403, and references therein.
(b) Evans, D. W.; Baker, G. R.; Newkome, G. R. *Coord. Chem. Rev.* **1989**, *93*, 155.
(c) Omae, I. *Organometallic Intramolecular-coordination Compounds*; Elsevier Scince Publishers: Amsterdam, New York, **1986**.
(d) Rothwell, I. P. *Acc. Chem. Res.* **1988**, *21*, 153.
(e) Parshall, G. W. *Acc. Chem. Res.* **1970**, *3*, 139.

28 In addition to cyclometallation, intramolecular C–H activation is known as orthometallation when an ortho aromatic C–H bond is activated. Examples of orthometallation process can be located in: Collman, J. P.; Hegedus, L. S.; Norton, J. R.; Finke, R. G. *Principles and Applications of Organotransition Metal Chemistry*; University Science Books: Mill Valley, CA, **1987**, p. 298.

29 Chatt, J.; Davidson, J. M. *J. Chem. Soc.* **1965**, 843. The correct structure of the dimer was assigned by: Cotton, F. A.; Hunter, D. L.; Frenz, B. A. *Inorg. Chim. Acta* **1975**, *15*, 155.

30 Tolman, C. A.; Ittel, S. D.; English, A. D.; Jesson, J. P. *J. Am. Chem. Soc.* **1978**, *100*, 4080.

31 Statler, J. A.; Wilkinson, G.; Thornton-Pett, M.; Hursthouse, M. B. *J. Chem. Soc., Dalton Trans.* **1984**, 1731.

32 (a) Shinomoto, R. S.; Desrosiers, P. J.; Harper, T. G. P.; Flood, T. C. *J. Am. Chem. Soc.* **1990**, *112*, 704.
(b) Desrosiers, P. J.; Shinomoto, R. S.; Flood, T. C. *J. Am. Chem. Soc.* **1986**, *108*, 7964.

33 (a) Werner, H.; Werner, R. *J. Organomet. Chem.* **1981**, *209*, C60.
(b) Werner, H.; Gotzig, J. *Organometallics* **1983**, *2*, 547.

34 Wenzel, T. T.; Bergman, R. G. *J. Am. Chem. Soc.* **1986**, *108*, 4856.

35 (a) Karsch, H. H.; Schmidbaur, H. *Z. Naturforsch.* **1977**, *B(32)*, 762.
(b) Karsch, H. H.; Klein, H. F.; Schmidbaur, H. *Angew. Chem., Int. Ed. Engl.* **1975**, 637.

36 Schmidbaur, H.; Blaschke, G. *Z. Naturforsch.* **1980**, *B(75)*, 584.

37 (a) Bryndza, H. E.; Fong, L. K.; Paciello, R. A.; Tam, W.; Bercaw, J. E. *J. Am. Chem. Soc.* **1987**, *109*, 1444.
(b) Mainz, V. V.; Andersen, R. A. *Organometallics* **1984**, *3*, 675.

38 (a) Erker, G. *Angew. Chem., Int. Ed. Engl.* **1989**, *28*, 397.
(b) Dotz, K. H.; Fischer, H.; Hoffmann, P.; Kreissel, F. R.; Schubert, U.; Weiss, K. *Transition Metal Carbene Complexes*; Verlag Chemie, Weinheim **1983**.

39 (a) Fryzuk, M. D.; McManus, N. T.; Rettig, S. J.; White, G. S. *Angew. Chem., Int. Ed. Engl.* **1990**, *29*, 73.
(b) Duran, R. P.; Amorebieta, V. T.; Colussi, A. J. *J. Am. Chem. Soc.* **1987**, *109*, 3154.

40 (a) Buchwald, S. L.; Neilsen, R. B. *Chem. Rev.* **1988**, *88*, 1047.
(b) Bennett, M. A.; Schwemlein, H. *Angew. Chem., Int. Ed. Engl.* **1989**, *10*, 1349.

(c) Hartwig, J. F.; Andersen, R. A.; Bergman, R. G. *J. Am. Chem. Soc.* **1989**, *111*, 2717.

41 (a) Butler, I. M. *Acc. Chem. Res.* **1977**, *10*, 359.
(b) Yaneff, P. V. *Coord. Chem. Rev.* **1977**, *23*, 183.

42 (a) Nefedov, O. M.; Maltsev, A. K.; Mikaelyan, R. G. *Tet. Lett.* **1971**, *44*, 4125.
(b) Trozzolo, A. M.; Gibbons, W. A. *J. Am. Chem. Soc.* **1967**, *89*, 239.

43 (a) Schrock, R. R.; Murdzek, J. S.; Bazan, G. C.; Robbins, J.; DiMare, M.; O'Regan, M. *J. Am. Chem. Soc.* **1990**, *112*, 3875.
(b) Feldman, J.; Murdzek, J. S.; Davis, W. M.; Schrock, R. R. *Organometallics* **1989**, *8*, 2260.
(c) Schrock, R. R.; De Pue, R.; Feldman, J.; Schaverien, C. J.; Dewan, J. C.; Liu, A. H. *J. Am. Chem. Soc.* **1988**, *110*, 1423.
(d) Horton, A. D.; Schrock, R. R. *Polyhedron* **1988**, *7*, 1841.
(e) Grubbs, R. H. *In Comprehensive Organometallic Chemistry*; Wilkinson, G.; Stone, F. G. A.; Abel, E. W.; Eds., Pergamon: New York, **1982**; Vol. 8.

44 (a) Wulff, W. D.; Dragisich, V.; Huffman, J. C.; Kaesler, R. W.; Yang, D. C. *Organometallics* **1989**, *8*, 2196.
(b) Wulff, W. D.; Yang, D. C.; Murray, C. K. *Pure Appl. Chem.* **1988**, *60*, 137.
(c) Fischer, E. O.; Dotz, K. H. *Chem. Ber.* **1972**, *105*, 3966.

45 Soto, J.; Steigerwald, M. L.; Grubbs, R. H. *J. Am. Chem. Soc.* **1982**, *104*, 4479.

46 (a) McKinney, R. J.; Tulip, T. H.; Thorn, D. L.; Coolbaugh, T. S.; Tebbe, F. N. *J. Am. Chem. Soc.* **1981**, *103*, 5584.
(b) Meinhart, J. D.; Anslyn, E. V.; Grubbs, R. H. *Organometallics* **1989**, *8*, 583.
(c) Straus, D. A.; Grubbs, R. H. *J. Mol. Catal.* **1985**, *28*, 9.
(d) Straus, D. A.; Grubbs, R. H. *J. Am. Chem. Soc.* **1981**, *103*, 7358.

47 Also see: Collman, J. P.; Hegedus, L. S.; Norton, J. R.; Finke, R. G. *Principles and Applications of Organotransition Metal Chemistry*; University Science Books: Mill Valley, CA, **1987**, Chapter 16.

48 (a) Brady, R. C.; Pettit, R. *J. Am. Chem. Soc.* **1981**, *103*, 1287.
(b) Brady, R. C.; Pettit, R. *J. Am. Chem. Soc.* **1980**, *102*, 6181.
(c) Herrmann, W. A. *Angew. Chem., Int. Ed. Engl.* **1982**, *21*, 117.
(d) Steinmetz, G. R.; Morrison, E. D.; Geoffroy, G. L. *J. Am. Chem. Soc.* **1984**, *106*, 2559.

49 Fischer, E. O.; Maasbol, A. *Angew. Chem., Int. Ed. Engl.* **1964**, *3*, 580.

50 Schrock, R. R. *J. Am. Chem. Soc.* **1974**, *96*, 6796.

51 Fischer, E. O. *Adv. Organomet. Chem.* **1976**, *14*, 1.

52 O'Connor, J. M.; Pu, L.; Rheingold, A. L. *J. Am. Chem. Soc.* **1989**, *111*, 4129.

53 (a) Chisholm, M. H.; Clark, H. C. *Acc. Chem. Res.* **1973**, *6*, 202.
(b) Bruce, M. I.; Swincer, A. G.; Thomson, B. J.; Wallis, R. C. *Aust. J. Chem.* **1980**, *33*, 2605.

54 Hermann, W. A.; Hubbard, J. L.; Bernal, I.; Korp, J. D.; Haymore, B. L.; Hillhouse, G. L. *Inorg. Chem.* **1984**, *23*, 2978.

55 Gallop, M. A.; Roper, W. R. *Adv. Organomet. Chem.* **1986**, *25*, 121.

56 (a) Schrock, R. R. *Acc. Chem. Res.* **1979**, *12*, 98.
(b) Brow, F. J. *Prog. Inorg. Chem.* **1980**, *27*, 1.

57 (a) Wong, W. K.; Tam, W.; Gladysz, J. A. *J. Am. Chem. Soc.* **1979**, *101*, 5440.
(b) Kiel, W. A.; Lin, G. Y.; Constable, A. G.; McCormick, F. B.; Strouse, C. E.; Eisenstein, O.; Gladysz, J. A. *J. Am. Chem. Soc.* **1982**, *104*, 4865.

58 Crocker, C.; Empsall, H. D.; Errington, R. J.; Hyde, E. M.; McDonald, W. S.; Markham, R.; Norton, M. C.; Shaw, B. L.; Weeks, B. *J. Chem. Soc., Dalton Trans.* **1982**, 1217.

59 Collman, J. P.; Hegedus, L. S.; Norton, J. R.; Finke, R. G. *Principles and Applications of Organotransition Metal Chemistry*; University Science Books: Mill Valley, CA, **1987**, p. 382.

60 Klein, D. P.; Bergman, R. G. *J. Am. Chem. Soc.* **1989**, *111*, 3079.

61 Fryzuk, M. D.; MacNeil, P. A.; Rettig, S. J. *J. Am. Chem. Soc.* **1985**, *107*, 6709.

62 Preliminary reactivity of the methylidene complex were attempted by a previous graduate student in our laboratory. The results of this work are described in chapter 4. Massey, R. L. *M. Sc. Thesis*, University of British Columbia, Vancouver, Cananda, **1989**.

63 Dotz, K. H. *Angew. Chem., Int. Ed. Engl.* **1984**, *23*, 58.

64 (a) Casey, C. P.; Vosejpka, P. C.; Askham, F. R. *J. Am. Chem. Soc.* **1990**, *112*, 3713.
(b) Brothers, P. J.; Roper, W. R. *Chem. Rev.* **1988**, *88*, 1293.
(c) Clark, G. R.; Hoskins, S. V.; Jones, T. C.; Roper, W. R. *J. Chem. Soc., Chem. Commun.* **1983**, 719.

65 Bhangu, K. *M. Sc. Thesis*, University of British Columbia, Vancouver, Canada, **1987**.

CHAPTER 2

Synthesis and Characterisation of the Iridium(III) Phosphide Complexes and Their Thermolytic and Photolytic behaviour

2.1 Introduction

As noted in chapter 1, the preparation and spectral characterisation of the iridium(III) diarylphosphide complexes, $Ir(CH_3)PR_2[N(SiMe_2CH_2PPh_2)_2]$, (R = phenyl, *meta*-tolyl, **2a-2b**), have been reported previously.[1] The geometry at the phosphide phosphorus atom was suggested to be pyramidal from the $^{31}P\{^1H\}$ NMR data. On the basis of NOE-DIFF experiments, the structure of these complexes in solution was proposed to be intermediate between trigonal bipyramidal and square pyramidal with the methyl ligand in the apical position. However, results of an X-ray crystal study show that the structure in the solid-state is different from the previously reported solution structure. The results of this study are discussed in this chapter. The synthesis and characterisation of $Ir(CH_3)PMe_2[N(SiMe_2CH_2PPh_2)_2]$, **2c**, and of $Ir(CH_3)PHPh[N(SiMe_2CH_2PPh_2)_2]$, **2d**, are described here. Under thermal and photolytic conditions, complexes **2a-2c** rearrange to give new products arising from C–H bond cleavage and P–C bond formation.[2] However, for the complex **2d**, only P–C bond formation is observed both upon thermolysis and photolysis. This intriguing

difference is explored in more detail in this chapter. The kinetic and mechanistic results of some of the thermal processes are also discussed.

2.2 Solid-State Structure of $Ir(CH_3)PPh_2[N(SiMe_2CH_2PPh_2)_2]$, 2a

Diffraction quality crystals of the methyl-diphenylphosphide complex, $Ir(CH_3)$-$PPh_2[N(SiMe_2CH_2PPh_2)_2]$, **2a**, were finally obtained after many earlier attempts. Some pertinent bond lengths and bond angles are listed in Tables 2.1 and 2.2, respectively. Figure 2.1 shows that the overall geometry at the iridium centre is best described as a distorted square pyramid. The tridentate hybrid ligand is arranged in a quasi-meridional fashion (P(1)–Ir–P(2) = 166.68°). The angle between the methyl carbon (C(43)) and the phosphide phosphorus atom (P(3) = 87.4°) is close to the expected 90° angle for a square pyramidal geometry. However, the angle between the phosphide group and the amide ligand (N–Ir–P(3) = 113.2°) is greater by ~23° from the expected 90° for an apical phosphide. Interestingly, the methyl ligand is out of the square pyramid base plane by 21° (C(43)–Ir–N = 159.0°) which is very close to the 23° distortion observed for the phosphide ligand. This apparent rotation of the phosphide–iridium–methyl unit around the phosphine–iridium–phosphine bonds of the tridentate ligand may be ascribed to the steric bulk of the diphenylphosphide moiety and/or repulsion between the amide and phosphide lone pairs of electrons. Crystal packing effects might also be contributing to the distortion. The magnitude of Ir–P(3)–C(31) (108.4°) and Ir–P(3)–C(37) (117.7°) seems to indicate that the geometry at the phosphorus in the PPh_2 ligand is pyramidal.

The solution data have been reinterpreted in terms of the solid-state structure. An NOE–DIFF experiment conducted on a benzene solution of **2a** showed a small enhancement of the methyl (Ir–CH_3) resonance upon irradiation of one of the two sets of methylene proton (PCH_2Si) resonances. No enhancement of the methyl proton

resonance was observed upon irradiation of the other set of the methylene signals. This result suggests that the methyl ligand is not in the apical position, but a distortion from the square pyramid base plane may still account for the observed enhancement.

Although the solid-state geometry for **2a** is a distorted square pyramid, in this thesis this molecule will be drawn as a square pyramid with the methyl ligand *trans* to the amide centre and the phosphide ligand in the apical position.

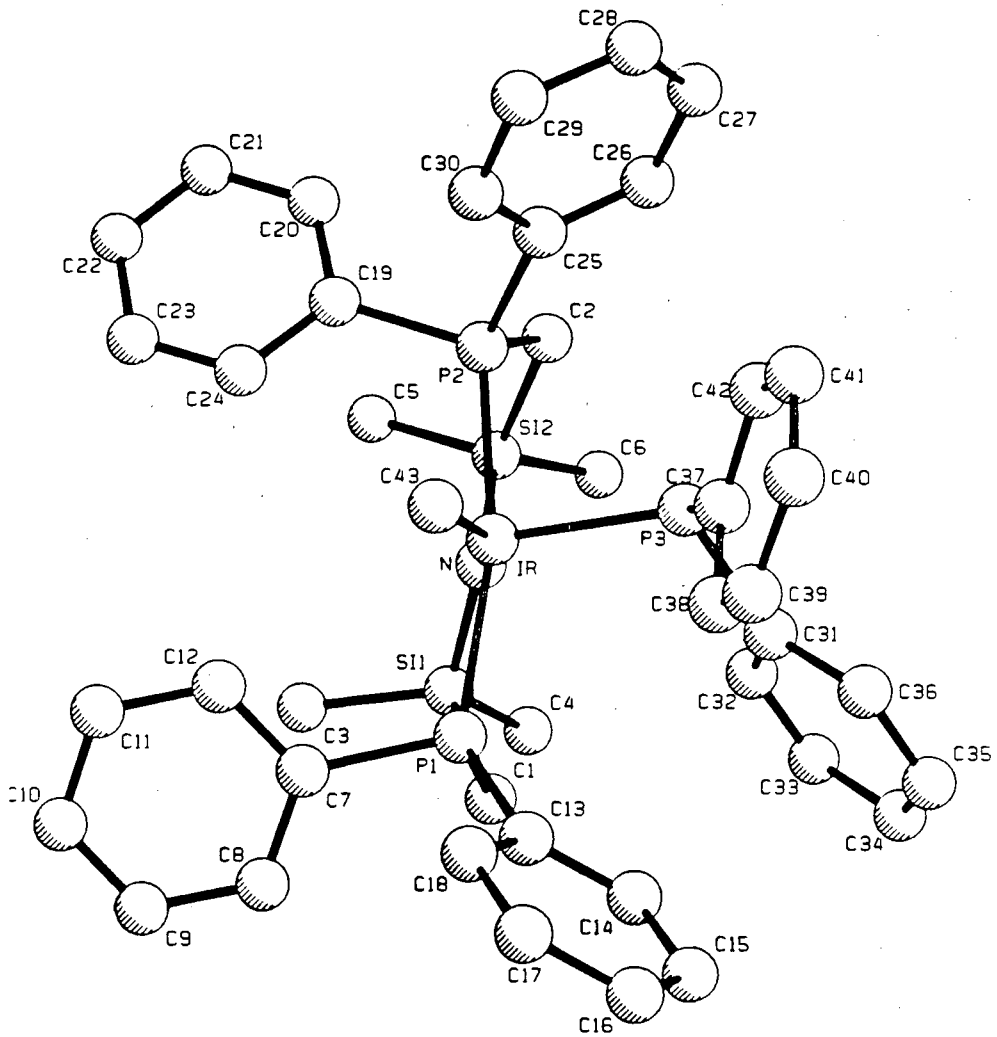

Figure 2.1 X-ray crystal structure of $Ir(CH_3)PPh_2[N(SiMe_2CH_2PPh_2)_2]$, **2a**

Table 2.1 Selected Bond Lengths (Å) for $Ir(CH_3)PPh_2[N(SiMe_2CH_2PPh_2)_2]$, **2a**[a]

Ir—P(1)	2.309(2)
Ir—P(2)	2.312(2)
Ir—P(3)	2.297(2)
Ir—C(43)	2.126(9)
Ir—N	2.126(6)

Table 2.2 Selected Bond Angles (deg) for $Ir(CH_3)PPh_2[N(SiMe_2CH_2PPh_2)_2]$, **2a**[a]

C(43)—Ir—N	159.0(3)
C(43)—Ir—P(1)	91.2(2)
C(43)—Ir—P(2)	90.3(2)
C(43)—Ir—P(3)	87.4(2)
N—Ir—P(1)	87.4(2)
N—Ir—P(2)	86.5(2)
N—Ir—P(3)	113.2(2)
P(1)—Ir—P(2)	166.68(2)
P(3)—Ir—P(1)	105.35(9)
P(3)—Ir—P(2)	87.95(8)
Ir—P(3)—C(31)	108.4(3)
Ir—P(3)—C(37)	117.7(3)

a. A complete list of the bond distances and the bond angles is compiled in Appendix A1.

2.3 Synthesis and Characterisation of the Iridium Dimethylphosphide Complex, $Ir(CH_3)PMe_2[N(SiMe_2CH_2PPh_2)_2]$, 2c

The iridium(III) methyl dimethylphosphide complex, $Ir(CH_3)PMe_2$-$[N(SiMe_2CH_2PPh_2)_2]$, **2c**, was synthesised by a transmetallation reaction of the square pyramidal iridium(III) methyl-iodide complex, $Ir(CH_3)I[N(SiMe_2CH_2PPh_2)_2]$, **1**, with stoichiometric amounts of potassium dimethylphosphide (Equation 2.1). The reaction proceeded over an hour at -30°C with the deep green colour of the methyl iodide derivative changing slowly to the characteristic[1] dark purple of the phosphide complex. The phosphide complex, **2c**, is thermally unstable (*vide infra*) at temperatures higher than -30°C, and, therefore, has been prepared only *in situ*.

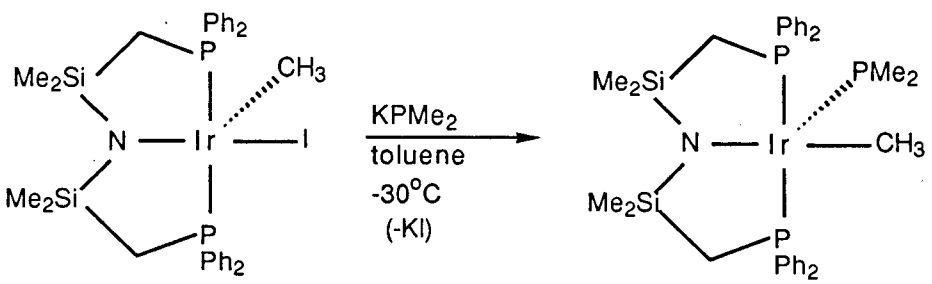

1 **2c**

Equation 2.1

Spectral characterisation of **2c** was carried out at -30°C and the proposed structure was found to be very similar to that of the diarylphosphide complexes **2a-2b**. Its ^1H NMR spectrum is shown in Figure 2.2. The $Si(CH_3)_2$ resonances consist of two sharp singlets of equal intensity at -0.03 and 0.26 ppm indicating inequivalent environments above and below the metal tridentate plane, in keeping with the earlier work on five coordinate complexes stabilised by this tridentate ligand.[3] An AB quartet of virtual triplets at 1.99 and 2.12 ppm (J_{gem} = 12.0, J_{app} = 4.9 Hz) for the CH_2P protons is indicative of a *trans* orientation of the chelating phosphines.

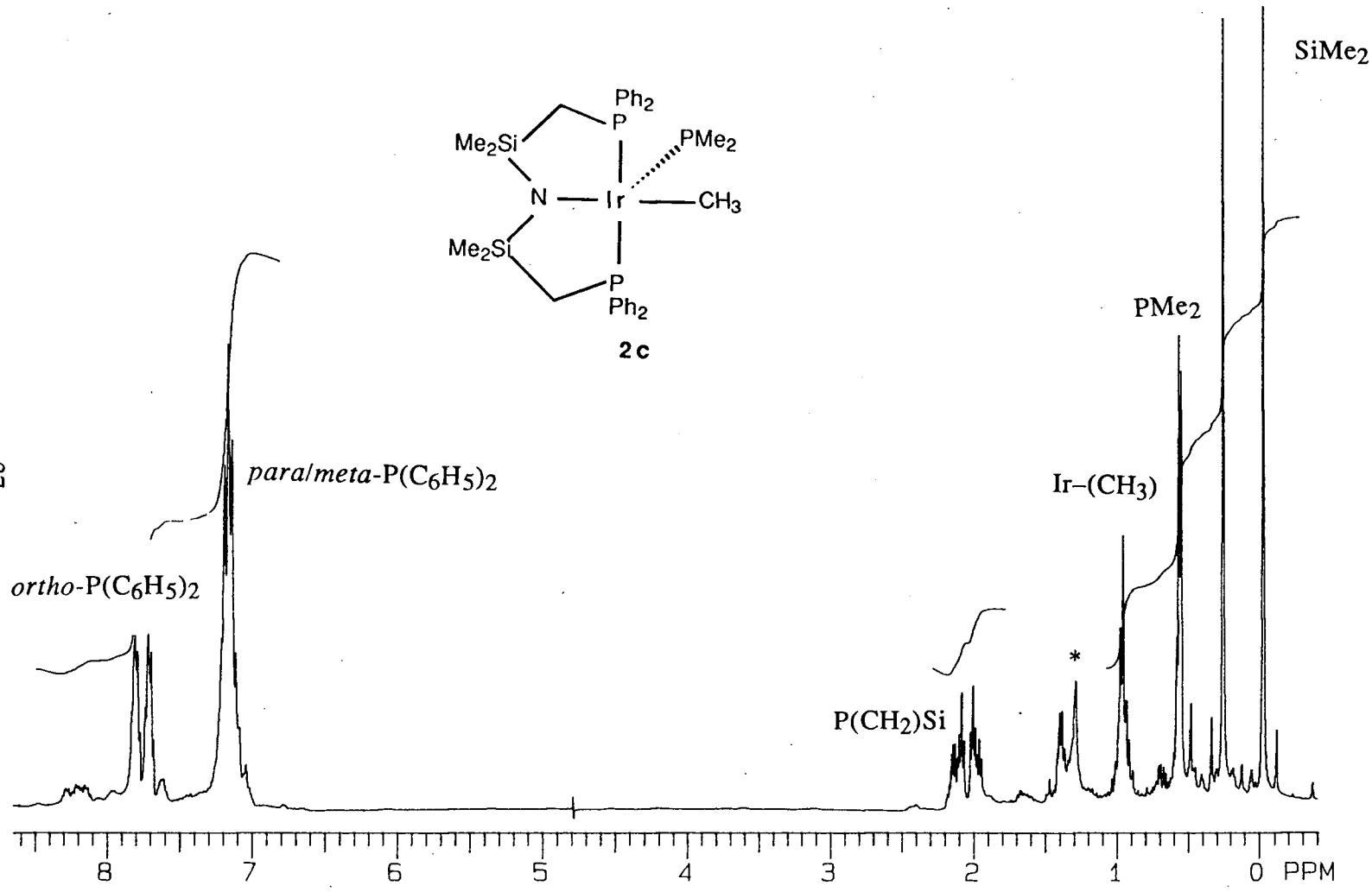

Figure 2.2 ^{1}H NMR spectrum (300 MHz, C_7D_8, -30°C) of $Ir(CH_3)PMe_2[N(SiMe_2CH_2PPh_2)_2]$, **2c**
(* indicates solvent hexanes protons)

Brookes and Shaw have demonstrated that virtual coupling arises in such AA'BB'XX' spin systems when $J_{XX'}$ is very large.[4] In the complex **2c**, because the phosphines are strongly coupled, this spin system simplifies to an $(AB)_2X_2$ pattern for the CH_2P protons. The resonances for the *para* and *meta* phenyl protons are observed as a multiplet and are separated from the *ortho* protons' resonances by 0.67 ppm. A chemical shift difference of 0.6 and 1.0 ppm between the *ortho* and *para/meta* protons of the phosphine phenyl groups (in deuterated aromatic solvents) is also indicative of the *trans* orientation of the chelating phosphines.[5]

As pointed out earlier (Chapter 1, Section 1.2), the phosphide ligand can possess either a pyramidal geometry or a planar geometry. The $^{31}P\{^1H\}$ chemical shifts are usually reliable, although not conclusive, in distinguishing the geometry at the phosphide phosphorus. The respective phosphorus chemical shifts for pyramidal and planar phosphide complexes reported in the literature range form -270 to +420 ppm and +200 to +400 ppm.[6] The $^{31}P\{^1H\}$ shift of 94.30 ppm (t, $^2J_{P,P}$ = 25.1 Hz) for the dimethylphosphide ligand points to the presence of a pyramidal phosphide donor in this complex.

Because the spectral data for the dimethylphosphide complex **2c** are similar to those of the crystallographically characterised diphenylphosphide analogue **2a**, complex **2c** has been assigned as having square-pyramidal geometry with the methyl ligand *trans* to the amide centre and the dimethylphosphide moiety at the apical site of the pyramid.

2.4 Synthesis and Characterisation of the Iridium Phenylphosphide Complex, $Ir(CH_3)PHPh[N(SiMe_2CH_2PPh_2)_2]$, 2d

The synthesis of the phenylphosphide derivative $Ir(CH_3)PHPh-[N(SiMe_2CH_2PPh_2)_2]$, **2d**, was achieved by the deprotonation of an octahedral

iridium(III) phenylphosphine complex, $Ir(CH_3)PH_2Ph(I)[N(SiMe_2CH_2PPh_2)_2]$, **9** with potassium *tert*-butoxide, KO^tBu, (Scheme 2.1). The reaction proceeded within minutes at room temperature as the yellow colour of the octahedral phosphine complex changed to a brick red colour. The phenylphosphide complex **2d** was isolated as brick red crystals from hexanes at -30°C in good yield (80%). The synthesis of complex **2d** was also attempted by the abstraction of HI from **9** using the base, 1,8-diazabicyclo[5.4.0]undec-7-ene (DBU), but no reaction was observed.

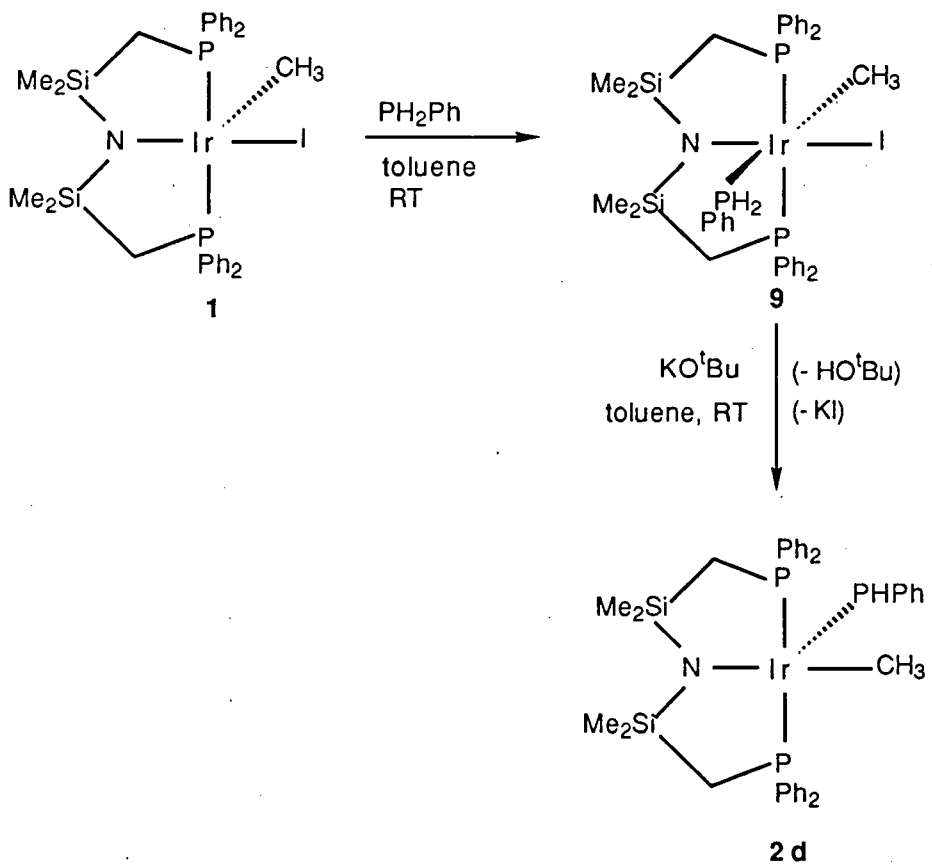

Scheme 2.1

Alternatively, the complex **2d** could be prepared by reacting freshly prepared *in situ* LiPHPh or $Mg(PHPh)_2$.TMEDA with the iridium(III) methyl iodide complex, $Ir(CH_3)I[N(SiMe_2CH_2PPh_2)_2]$, **1**, but there were problems associated with these metathetical reactions. Along with the formation of the desired iridium(III)

phenylphosphide complex, **2d**, there was a competitive reaction of the free phenylphosphine with **1** regenerating **9**. The free PH_2Ph may arise from the slow hydrolysis of the lithium and magnesium phenylphosphide reagents.

The complex $Ir(CH_3)PHPh[N(SiMe_2CH_2PPh_2)_2]$, **2d**, exhibits simple ^1H and $^{31}P\{^1H\}$ NMR spectra. The ^1H NMR spectrum (Figure 2.3) consists of a sharp singlet at 0.37 ppm and a broad peak at -0.10 ppm for the silyl methyl protons at room temperature. As the temperature of the solution is lowered, the peak at -0.10 ppm broadens and then splits into two singlets which are observed at -0.05 and 0.14 ppm (T_c = 280 K, $\Delta G^{\ddagger}$ = 58 ± 4 KJ mol^{-1}). In addition, the broad methylene resonance (2.00 ppm) and the phenyl resonance (7.80 ppm) split into multiplets. The different orientations of the substituents on the chiral phosphide ligand with respect to the tridentate ligand protons on the same side of the phosphide may result in different environments for those particular ligand protons (for example, the silyl methyls marked a and b in Scheme 2.2 and Figure 2.3). The silyl methyl protons on the side opposite to the phosphide ligand (labelled c and d in Scheme 2.2 and Figure 2.3) remain relatively unaffected by the different orientations of the phosphide ligand, and therefore, only single coincidental resonance is observed. The spectral data can be explained by invoking inversion at the chiral phosphide phosphorus in the pyramidal phenylphosphide ligand (Scheme 2.2). In complexes $CpRe(PHPh)NO(PPh_3)$[7] and $CpFe(PHPh)\{1,2\text{-}C_6H_4(PMePh)_2\}$,[8] the inversion barriers reported for the pyramidal phenylphosphide ligand are 48 and 60 KJ mol^{-1}, respectively. Thus, the activation barrier of 58 KJ mol^{-1} for the phosphide inversion mecahnism in **2d** seems reasonable.

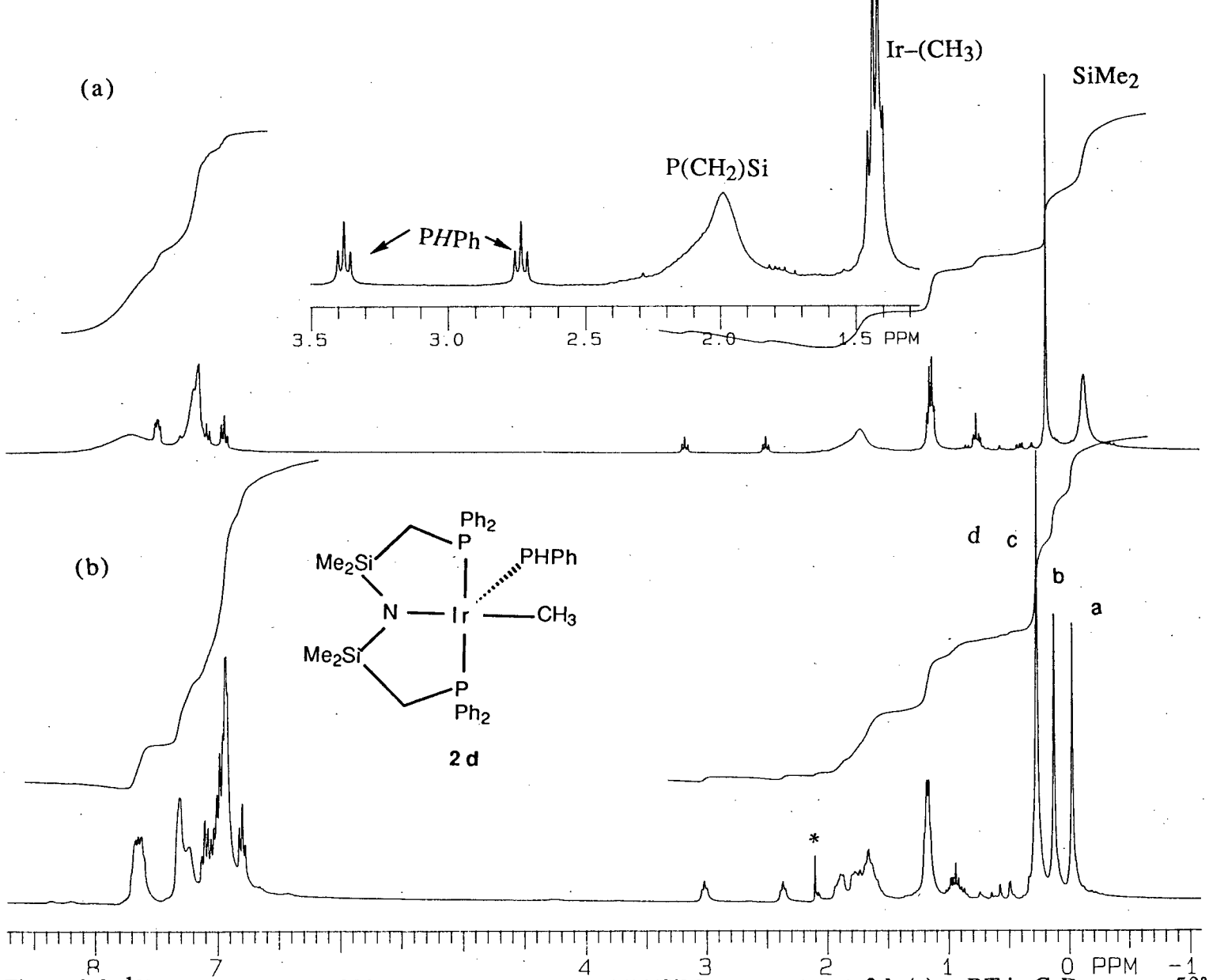

Figure 2.3 ^{1}H NMR spectrum (300 MHz) of $Ir(CH_3)PHPh[N(SiMe_2CH_2PPh_2)_2]$, **2d**, (a) at RT in C_6D_6, (b) at -50°C in C_7D_8 (* indicates toluene peak)

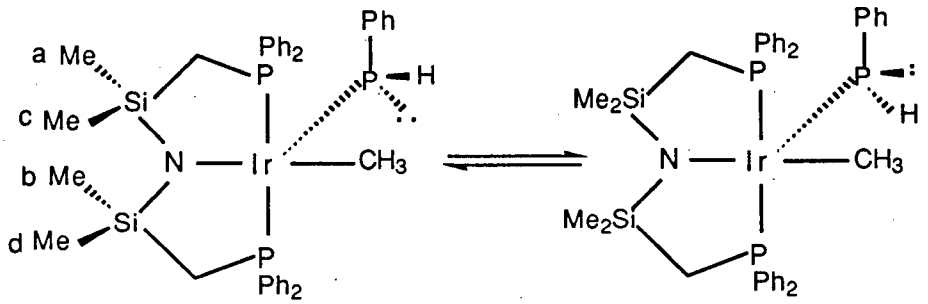

Scheme 2.2

In solution, the phenylphosphide complex **2d** is less stable thermally than its diphenylphosphide analogue **2a** but more stable compared to the dimethylphosphide complex **2c**. Details of this difference are described in the following sections (Section 2.5 for the complexes **2a-2c**, Section 2.8 for **2d**).

2.5 Thermolysis of the Phosphide Complexes 2a-2c

The diphenyl and di-*meta*-tolyl phosphide complexes, $Ir(CH_3)PR_2$-$[N(SiMe_2CH_2PPh_2)_2]$, **2a-b**, are quite stable thermally in the solid form and can be stored at room temperature for months under an inert atmosphere without any noticeable decomposition. However, when thermolysed in hydrocarbon solvents, typically benzene, toluene or hexanes (50°C in the dark for about five hours), complexes **2a** and **2b** were converted cleanly and quantitatively to the cyclometallated hydride species *fac*-$Ir(\eta^2\text{-}CH_2PR_2)H[N(SiMe_2CH_2PPh_2)_2]$, **3a-b** (Equation 2.2).

The dimethylphosphide complex $Ir(CH_3)PMe_2[N(SiMe_2CH_2PPh_2)_2]$, **2c**, is less stable than **2a** and **2b**, and, as mentioned before, has been prepared only *in situ* at -30°C. When the sample was warmed from -30°C to room temperature, it cleanly converted to the cyclometallated hydride derivative *fac*-$Ir(\eta^2\text{-}CH_2PMe_2)H$-$[N(SiMe_2CH_2PPh_2)_2]$, **3c**. The complexes **3a-3c** were isolated in > 80% yield as

pale yellow crystalline solids which were stable under inert atmosphere for months at room temperature. These complexes have been characterised by various NMR spectral techniques and X-ray diffraction (for the η^2-CH_2PPh_2 complex).

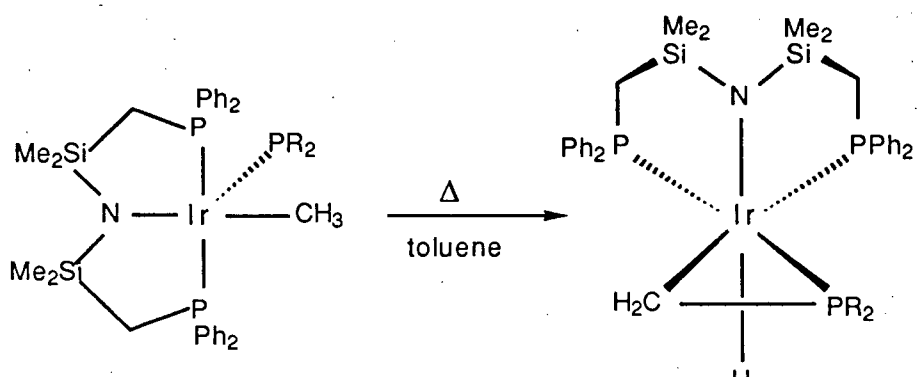

2a R = phenyl
2b R = *meta*-tolyl
2c R = methyl

3a-3c

Equation 2.2

The ^1H and $^{31}P\{^1H\}$ NMR spectra of the complex **3a** will serve to illustrate the typical spectral behaviour of these complexes. In the ^1H NMR spectrum (Figure 2.4), four singlet resonances at -0.22, 0.65, 0.68 and 0.81 ppm are observed for the silyl methyl groups in the tridentate ligand backbone. Both pairs of the methylene protons of the hybrid ligand backbone display four sets of resonances at 1.40 ppm (t, J_{app} = 13.7 Hz), 1.75 ppm (t, J_{app} = 13.7 Hz), 2.10 (m) and 2.49 (m). The CH_2 protons of the η^2-CH_2PPh_2 moiety are observed as two diastereotopic multiplets at 1.32 ppm (br) and 2.00 ppm (br, t). The hydride ligand *trans* to the amide resonates at -19.90 ppm (td, $^2J_{P,H}$ = 16.7 Hz, $^2J_{P,H}$ = 9.9 Hz). Hydride chemical shift values are related to the *trans* influence order (CO > P > N) of the ligand positioned *trans* to the hydride.[9] In octahedral complexes containing the hybrid tridentate ligand,[10] a hydride *trans* to the amide centre typically resonates at -19 to -25 ppm; however, when it is *trans* to a

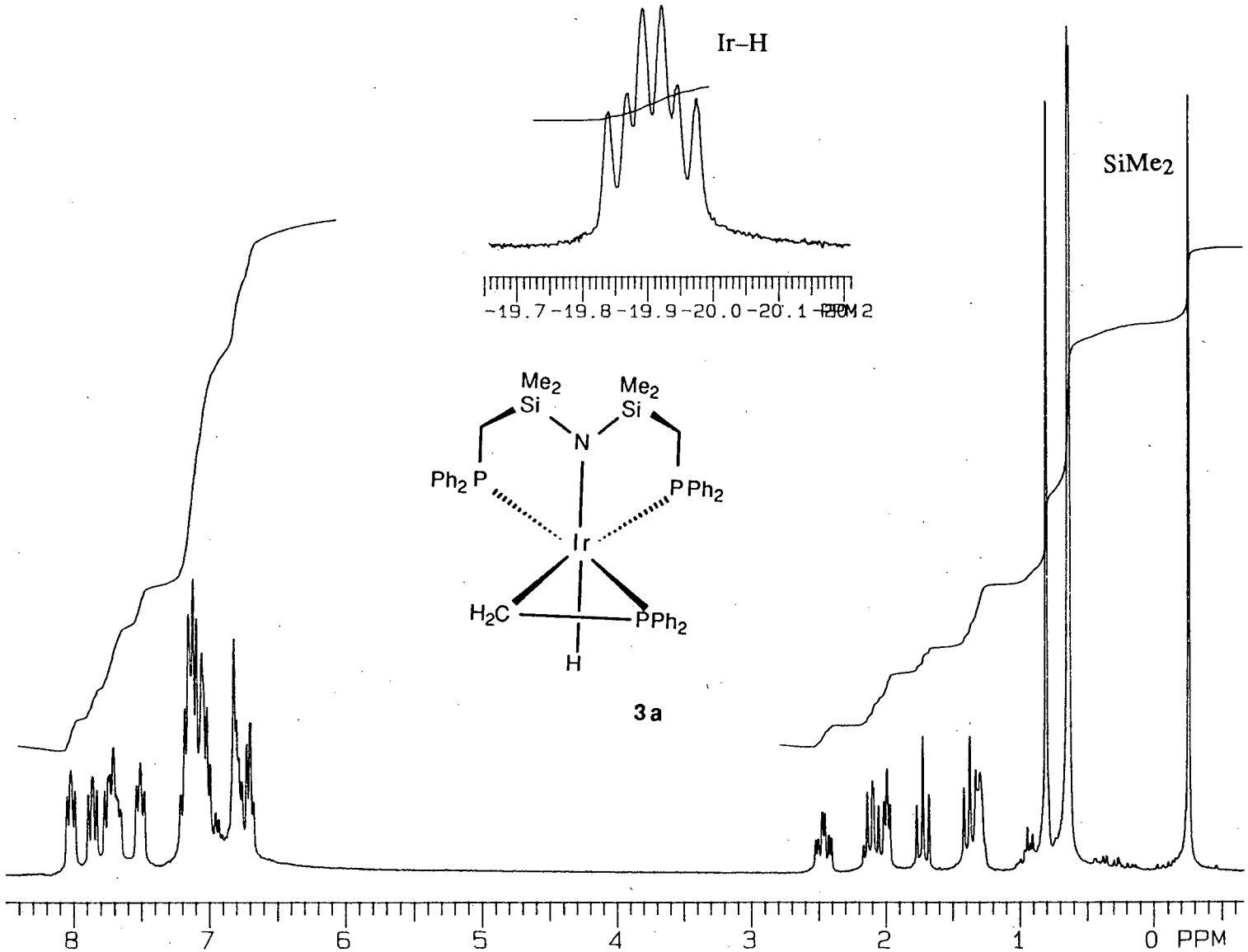

Figure 2.4 ^{1}H NMR spectrum (300 MHz, C_6D_6) of *fac*-Ir(η^2-CH_2PPh_2)H[$N(SiMe_2CH_2PPh_2)_2$], **3a**

phosphine, the chemical shift range is -9 to -12 ppm. The hydride *trans* to a carbonyl moiety is normally observed between -6 to -7 ppm.

The $^{31}P\{^{1}H\}$ NMR spectrum of **3a** shows an AMX pattern for this molecule indicating that all three phosphorus centres are non-equivalent. Two of the phosphorus nuclei are strongly coupled to each other, but weakly coupled to the third. The chemical shifts of the phosphorus nuclei belonging to the tridentate ligand [12.39 ppm (dd, $^{2}J_{PA,\,PX}$ = 32.0 Hz, $^{2}J_{PM,\,PX}$ = 5.5 Hz) and 15.60 ppm (dd, $^{2}J_{PA,\,PM}$ = 298.2 Hz, $^{2}J_{PM,\,PX}$ = 6.4 Hz)] are well within the expected range; however, the resonance of the phosphorus nucleus in the η^2-CH_2PPh_2 moiety is shifted upfield (-46.80 ppm, dd, $^{2}J_{PA,\,PM}$ = 297.9 Hz, $^{2}J_{PA,\,PX}$ = 30.4 Hz), a phenomenon which has been observed before in other metallacyclic structures.[11]

The X-ray crystal structure of **3a** is shown in Figure 2.5. Selected bond lengths and bond angles are listed in Tables 2.3 and 2.4 respectively. The structure reveals that the ancillary tridentate ligand has isomerised to the facial coordination mode (P(2)-Ir-P(3) = 104.5°) with the hydride ligand *trans* to the amide donor; the η^2-CH_2PPh_2 moiety occupies the remaining *cis* sites of the distorted octahedron. The distortions from true octahedral geometry in the molecule are not unexpected given the steric demands of the tridentate ligand and the η^2-CH_2PPh_2 metallacyclic ring. The crystallographically determined iridium-hydride bond length of 1.51 Å is consistent with other reported Ir-H distances.[12] The Ir-P(1) bond length in the three-membered ring is 0.03 Å and 0.05 Å shorter than the other two Ir-P bond lengths of the hybrid tridentate ligand. The shortening of Ir-P(1) bond may be the result of the bridging methylene unit. In the related complex $IrCl_2(\eta^2\text{-}CH_2PMePh)(PMe_2Ph)_2$ the parameters reported for the metallacycle are analogous.[12]

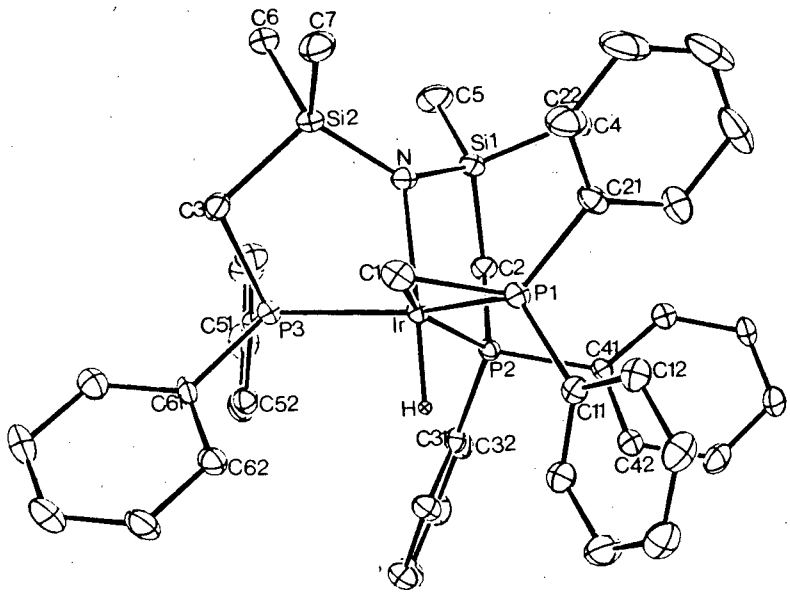

Figure 2.5 X-ray crystal structure of *fac*-Ir(η^2-CH_2PPh_2)H[$N(SiMe_2CH_2PPh_2)_2$], **3a**

Table 2.3 Selected Bond Lengths (Å) for *fac*-Ir(η^2-CH_2PPh_2)H[$N(SiMe_2CH_2PPh_2)_2$], **3a**[a]

Ir—P(1)	2.241(2)
Ir—P(2)	2.272(2)
Ir—P(3)	2.291(2)
Ir—C(1)	2.203(7)
Ir—N	2.277(6)
Ir—H	1.51(6)
P(1)—C(1)	1.760(8)

Table 2.4 Selected Bond Angles (deg) for *fac*-Ir(η^2-CH_2PPh_2)H[$N(SiMe_2CH_2PPh_2)_2$], **3a**[a]

C(1)—Ir—N	97.6(3)	P(1)—Ir—H	70(3)
C(1)—Ir—H	87(3)	P(2)—Ir—H	157.5(2)
C(1)—Ir—P(1)	46.7(2)	P(3)—Ir—H	112(3)
C(1)—Ir—P(2)	157.5(2)	N—Ir—H	167(3)
C(1)—Ir—P(3)	97.9(2)		
N—Ir—P(1)	103.8(2)		
N—Ir—P(2)	88.4(2)		
N—Ir—P(3)	79.7(1)		
P(1)—Ir—P(2)	110.9(1)		
P(1)—Ir—P(3)	144.5(1)		
P(2)—Ir—P(3)	104.5(1)		

a. A complete list of the bond distances and the bond angles is compiled in Appendix A1

Complexes **3a-3c** are stable in the solid-state at room temperature under an inert atmosphere; however, heating benzene or toluene solutions of **3a-3c** for 24 hours at 100°C results in the formation of the iridium(I) phosphine complexes, $Ir(PR_2CH_3)[N(SiMe_2CH_2PPh_2)_2]$, **4a-4c** (Equation 2.3).

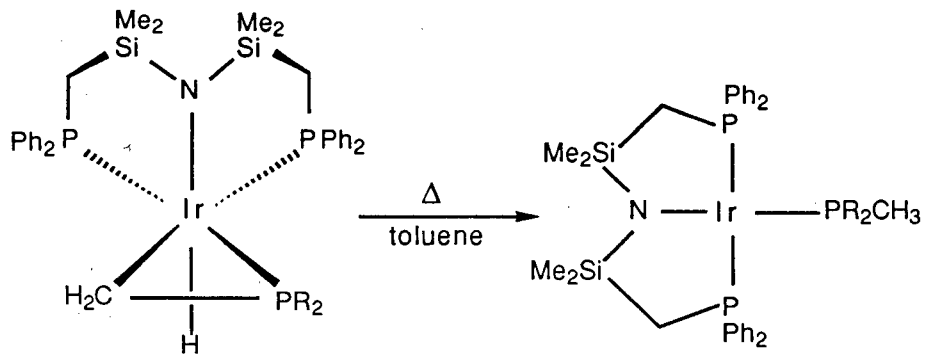

3a-3c **4a-4c**

Equation 2.3

These complexes were characterised by ^1H and $^{31}P\{^1H\}$ NMR spectra. The ^1H NMR spectrum of **4a** (Figure 2.6) consists of a sharp singlet at 0.20 ppm for the silyl methyl protons indicating an equivalent environment above and below the metal tridentate plane. The ligand backbone methylene proton resonances are observed as a triplet (1.91 ppm, J_{app} = 5.2 Hz) and thus are indicative of the meridional arrangement of the hybrid ligand. The methyl protons of the PPh_2Me ligand are observed as a doublet at 1.38 ppm ($^3J_{P,H}$ = 7.5 Hz). The phenyl protons are observed at 6.90 -7.10 ppm (m, *para/meta*) and 7.53, 7.75 ppm (m, *ortho*).

In summary, the rearrangement of a methyl-phosphide complex $L_nM(CH_3)PR_2$ to $L_nM(\eta^2\text{-}CH_2PR_2)H$ is unprecedented. However, as mentioned in chapter 1 (Section 1.4), the cyclometallation of coordinated phosphines does lead to complexes with the $\eta^2\text{-}CH_2PR_2$ unit, although, as discussed above, this certainly is not occurring in this system.

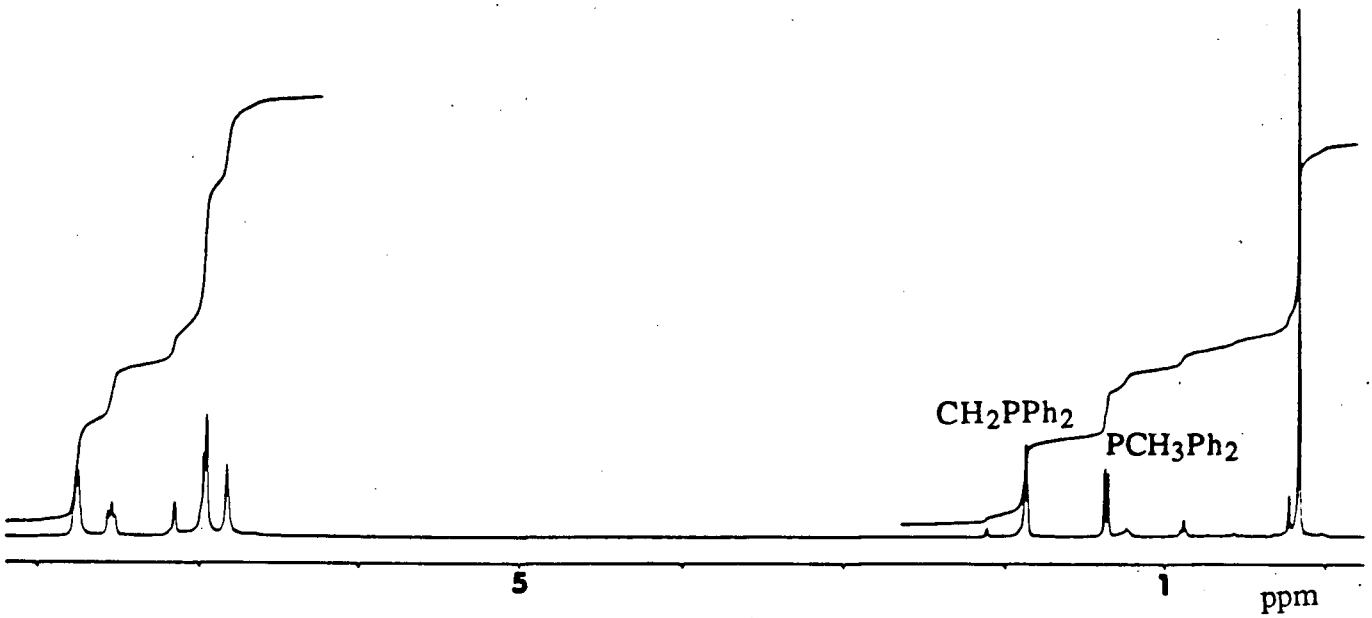

Figure 2.6 ^{1}H NMR spectrum (C_6D_6, 400 MHz) of $Ir(PCH_3Ph_2)[N(SiMe_2CH_2PPh_2)_2]$, **4a**

2.6 Kinetic and Mechanistic Studies of the Thermolysis of $Ir(CH_3)PPh_2[N(SiMe_2CH_2PPh_2)_2]$, 2a, and *fac*-$Ir(\eta^2\text{-}CH_2PPh_2)H[N(SiMe_2CH_2PPh_2)_2]$, 3a

2.6.1 Kinetic Data

A kinetic study was undertaken of the thermolytic conversion of $Ir(CH_3)PPh_2[N(SiMe_2CH_2PPh_2)_2]$, **2a**, to *fac*-$Ir(\eta^2\text{-}CH_2PPh_2)H[N(SiMe_2CH_2PPh_2)_2]$, **3a**, and of **3a** to $Ir(PMePh_2)[N(SiMe_2CH_2PPh_2)_2]$, **4a**, in order to elucidate some mechanistic details for these transformations. Because the phosphide complex **2a** is coloured (λ_{max} = 538 nm, ε = 2850 mol^{-1} L cm^{-1}), presumably due to d-d transitions, its rearrangement to **3a** in toluene was conveniently studied by following the decrease in the intensity of the band at 538 nm with time using UV-Vis spectroscopy (Figure 2.7, Table 2.5). Analysis of the spectral changes showed that the thermolysis rates were first order in the concentration of **2a** (data taken for at least three half-lives or more),

as demonstrated by the linear plot of $\ln(A_t - A_\infty)$ versus time (Figure 2.7). Measurements of the reaction rates were carried out at four different temperatures between 73 and 108°C (Table 2.6). The plot of $\ln(k_{obs}/T)$ versus $1/T$ yielded a straight line, from which the following activation parameters were calculated: $\Delta H^{\ddagger} = 52 \pm 15$ KJ mol^{-1} , $\Delta S^{\ddagger} = -163 \pm 40$ J K^{-1} mol^{-1} (Figure 2.8). The $\Delta S^{\ddagger}$ value was found to be a rather large negative number in toluene, suggesting an ordered transition state. A reaction pathway involving solvation of the phenyl rings of "PPh_2" by the solvent toluene is an attractive possibility. To test this, the thermolysis was performed in hexanes. It was found that the activation parameters were remarkably different in hexanes [$\Delta H^{\ddagger} = 103 \pm 20$ KJ mol^{-1} , $\Delta S^{\ddagger} = -16 \pm 3$ J K^{-1} mol^{-1} (Figure 2.8, Table 2.6)]. The activation enthalpy was almost doubled but this was now offset by a less negative activation entropy value, thus suggesting that the solvation effects were contributing to the overall activation parameters when the solvent was toluene. The kinetic isotope effect (k_H/k_D) for this process was also determined. Thermolysis of **2a**-CD_3 in hexanes at 67°C was followed by UV-Vis spectroscopy, and the k_H/k_D was found to be 1.6 ± 0.1, which indicated that C–H bond breaking was involved in the transition state.

The cyclometallated hydride complex, *fac*-$Ir(\eta^2\text{-}CH_2PPh_2)H[N(SiMe_2CH_2\text{-}PPh_2)_2]$, **3a**, shows an absorption band at 360 nm ($\varepsilon = 5425$ mol^{-1} L cm^{-1}) in the UV-Vis spectrum. The freshly prepared samples of **3a** were thermolysed in toluene, and decrease in the absorption band at 360 nm was followed as **3a** converted to the corresponding phosphine complex, $Ir(PCH_3Ph_2)[N(SiMe_2CH_2PPh_2)_2]$, **4a** (Figure 2.9, Table 2.7). Again, the reaction was first order in the concentration of **2a** with $k_{obs} = 6.59 \times 10^{-5}$ s^{-1} at 112°C. The transformation rates, determined at four temperatures 91-112°C, yielded the following activation parameters: $\Delta H^{\ddagger} = 107 \pm 2$ KJ mol^{-1} and $\Delta S^{\ddagger} = -49 \pm 6$ J K^{-1} mol^{-1} (Figure 2.10, Table 2.8). The kinetic isotope effect was

Table 2.5 First-Order Analysis of the Absorption Spectral Changes for the Conversion of $Ir(CH_3)PPh_2[N(SiMe_2CH_2PPh_2)_2]$, **2a**, to *fac*-$Ir(\eta^2\text{-}CH_2PPh_2[N(SiMe_2CH_2PPh_2)_2]$, **3a** at 83°C[a] in toluene

$[\mathbf{2a}] = 3.26 \times 10^{-4}$ mol L^{-1}

Time (s)	A_t (538 nm)	$\ln(A_t - A_\infty)$
0	0.881	-0.196
200	0.824	-0.268
400	0.765	-0.348
700	0.658	-0.512
1000	0.573	-0.665
1300	0.509	-0.798
1800	0.388	-1.110
2300	0.298	-1.430
4000	0.127	-2.290
A_∞	0.059	—

$k_{obs} = 0.84 \times 10^{-3}$ s^{-1}

a. Temperature deviation ± 1°C

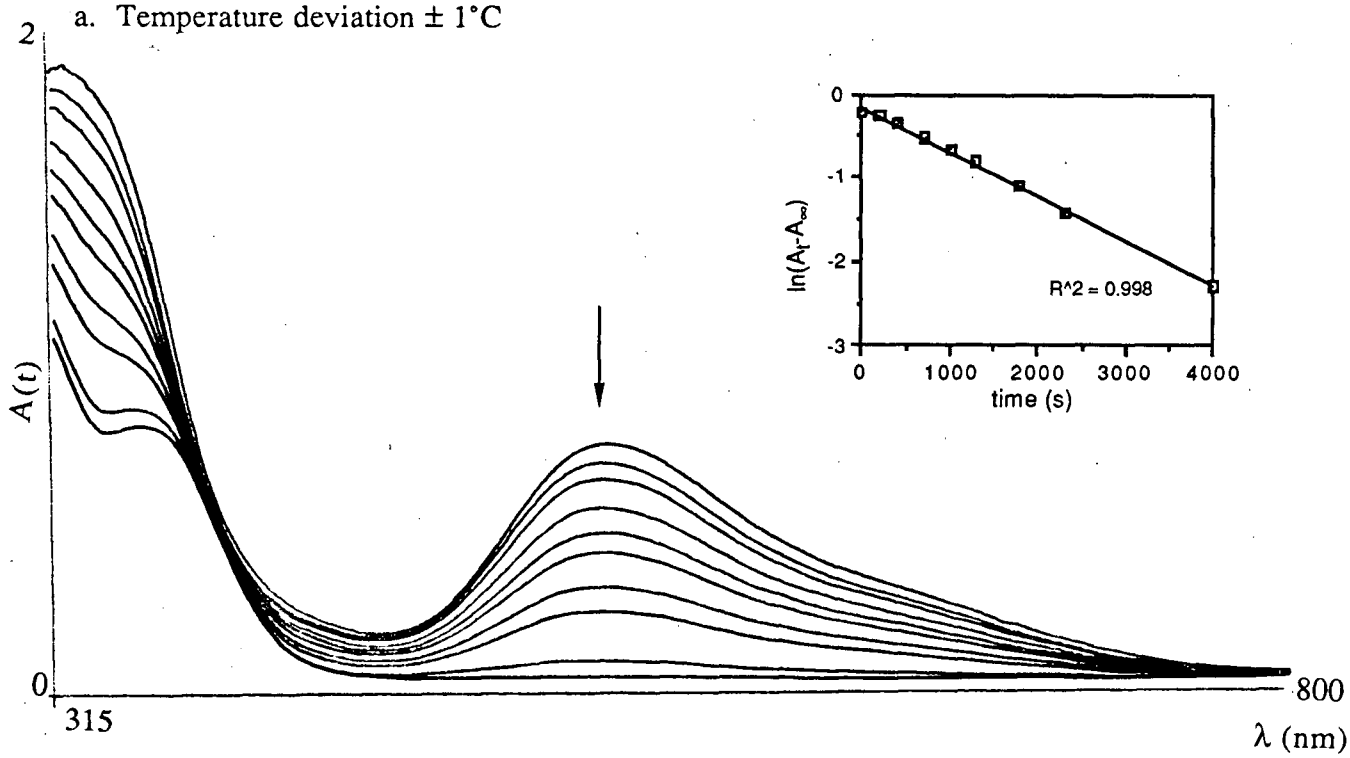

Figure 2.7 Absorption spectral changes upon thermolysis of **2a** at 83°C in toluene

determined by heating **3a**-CD_2 deuteride complex at 112°C in toluene. Comparison of the observed rate constants yields k_H/k_D to be 1.6 ± 0.1 which coincidently is the same as the k_H/k_D value observed for the thermolysis of **2a** to **3a** at 67°C in hexanes.

Table 2.6 Observed Rate Constants and Activation Parameters for the Conversion of $Ir(CH_3)PPh_2[N(SiMe_2CH_2PPh_2)_2]$, **2a**, to *fac*-$Ir(\eta^2\text{-}CH_2PPh_2)H[N(SiMe_2CH_2PPh_2)_2]$, **3a**

in Toluene		in Hexanes	
Temp (°C)	$k_{obs} \times 10^3$, s^{-1}	Temp (°C)	$k_{obs} \times 10^3$, s^{-1}
73	0.54	60	0.06
83	0.84	67	0.14
97[b]	1.04	78	0.42
108	1.90	87	1.10
$\Delta H^{\ddagger}$ = 52 ±15 KJ mol^{-1}		$\Delta H^{\ddagger}$ = 103 ± 20 KJ mol^{-1}	
$\Delta S^{\ddagger}$ = -163 ± 40 J K^{-1} mol^{-1}		$\Delta S^{\ddagger}$ = -16 ± 3 J K^{-1} mol^{-1}	

a. The data for each run are given in Appendix A2. b. The run at 97°C was repeated, k_{obs} = 1.07 x 10^{-3} s^{-1}. Thus the uncertainty of 0.03 x 10^{-3} in the k_{obs} values was used to determine the error in the $\Delta H^{\ddagger}$ and $\Delta S^{\ddagger}$ values.

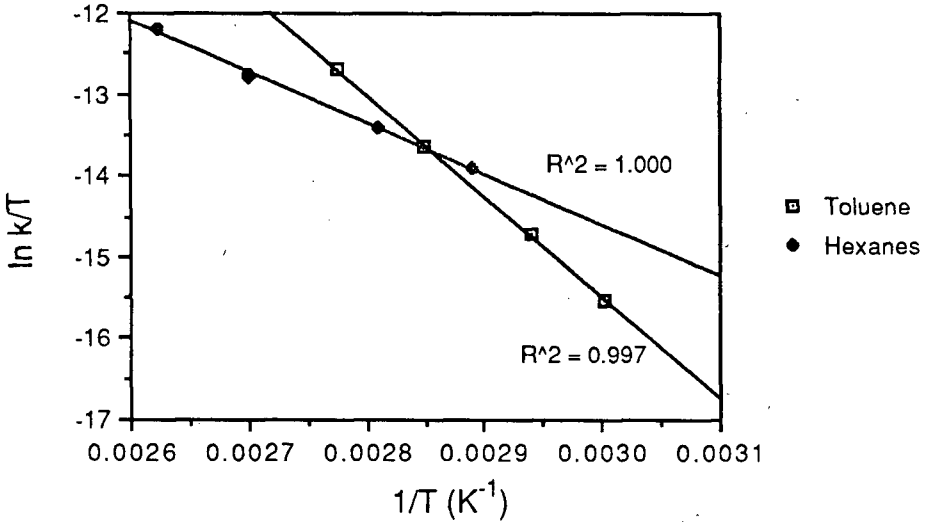

Figure 2.8 Eyring plot for the conversion of **2a** to **3a** in toluene and hexanes

Table 2.7 First-Order Analysis of the Absorption Spectral Changes for the Conversion of *fac*-Ir(η^2-CH_2PPh_2)H[$N(SiMe_2CH_2PPh_2)_2$], **3a**, to Ir(PCH_3Ph_2)[$N(SiMe_2CH_2PPh_2)_2$], **4a** at 112°C[a] in Toluene

[**3a**] = 2.04 x 10^{-4} mol L^{-1}

Time (s)	A_t (360 nm)	$\ln(A_t-A_\infty)$
0	1.066	-0.406
4000	0.928	-0.639
8000	0.810	-0.892
12550	0.697	-1.214
16550	0.621	-1.509
20550	0.584	-1.693
38270	0.454	-2.919
A_∞	0.400	—

k_{obs} = 6.59 x 10^{-5} s^{-1}

a. Temperature deviation ± 1°C

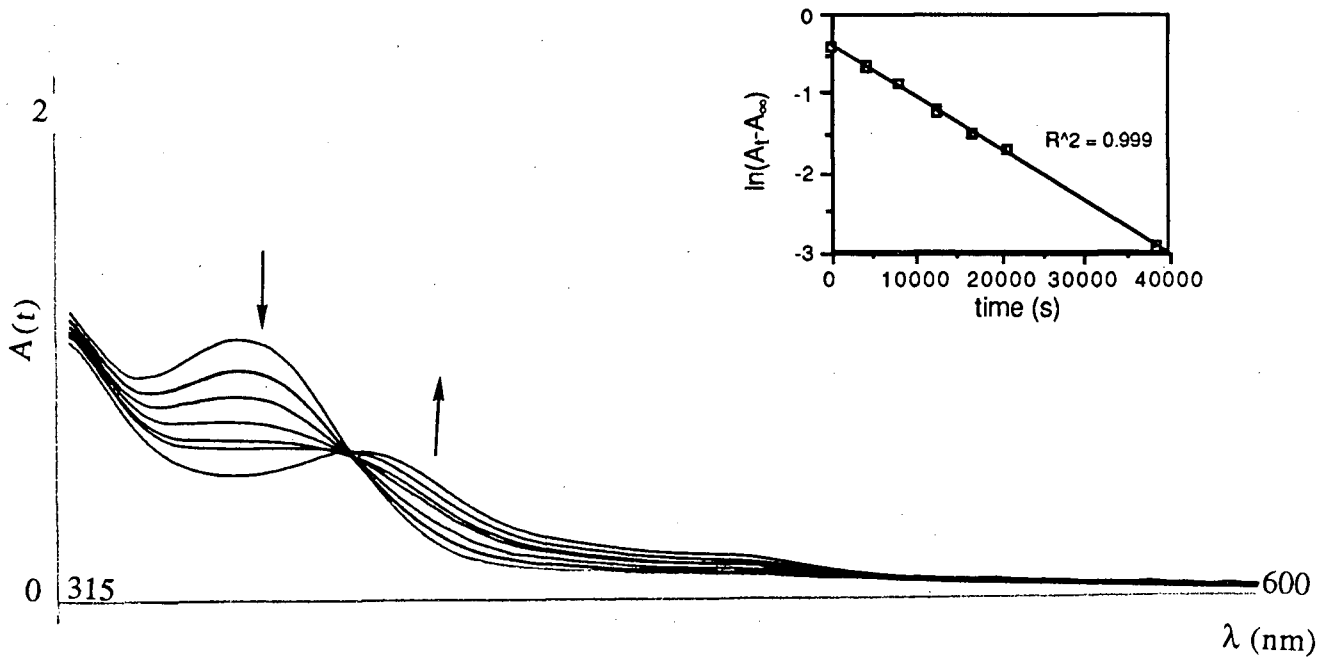

Figure 2.9 Absorption spectral changes upon thermolysis of **3a** at 112°C in toluene

Table 2.8 Observed Rate Constants and Activation Parameters for the Thermolytic Conversion of *fac*-Ir(η^2-CH_2PPh_2)H[$N(SiMe_2CH_2PPh_2)_2$], **3a**, to Ir(PCH_3Ph)[$N(SiMe_2CH_2PPh_2)_2$], **4a** in Toluene[a]

Temp (°C)	k_{obs} x 10^5, s^{-1}
91[b]	0.87
94	1.03
102	2.31
112	6.59

$\Delta H^{\ddagger} = 107 \pm 2$ KJ mol^{-1}

$\Delta S^{\ddagger} = -49 \pm 6$ J K^{-1} mol^{-1}

a. The data for each run are given in Appendix A2. b. The run at 91°C was repeated and $k_{obs} = 0.94 \times 10^{-5}$ s^{-1}. An error of 0.07×10^{-5} was used in all the k_{obs} values in calculating the errors in the activation parameters.

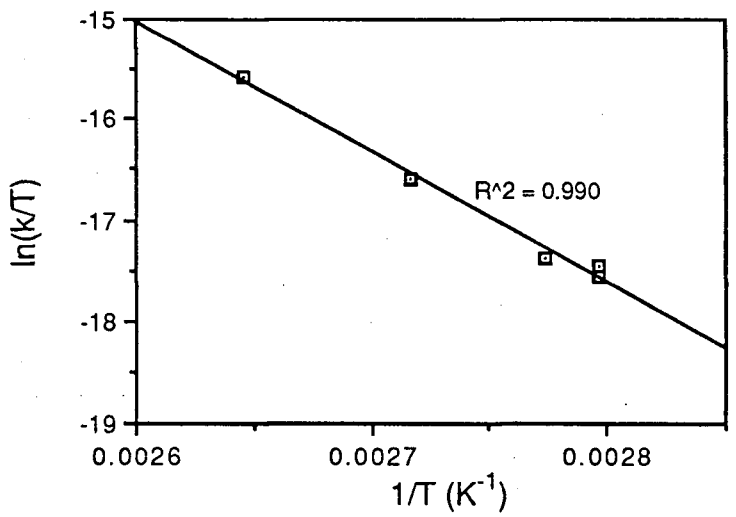

Figure 2.10 Eyring plot for the conversion of **3a** to **4a** in toluene

2.6.2 Mechanistic Considerations

A possible mechanism put forth for the aforementioned thermolysis transformations is shown in Scheme 2.3. The first step involves α-hydride

abstraction[13] by the phosphide group from the coordinated methyl ligand yielding $Ir{=}CH_2(PHR_2)[N(SiMe_2CH_2PPh_2)_2]$, **5**. The six-coordinate hydride-phosphide intermediate **A** then forms via oxidative addition of the phosphine P–H bond at the metal centre. This is followed by the migratory insertion of the methylene ligand into the iridium-phosphide bond thus yielding the intermediate **B**. The lone pair on the uncoordinated phosphine of **B** can then bind to the coordinatively unsaturated iridium(III) centre to generate the species **3** or **6**. As proposed in Scheme 2.3, the conversion of **3** to **4** proceeds via an intermediate involving C–H bond formation.

During the thermolytic transformation of **2a** to **3a** and **3a** to **4a**, none of the proposed intermediates in Scheme 2.3 were observed by the ^1H and $^{31}P\{^1H\}$ NMR spectroscopy; however, the mechanism was supported via some independent experiments. The addition of one equivalent of diphenylphosphine to a toluene solution of $Ir{=}CH_2$-$[N(SiMe_2CH_2PPh_2)_2]$, **10**,[14] at -78°C caused the purple colour of **10** to change to wine red (Scheme 2.4). This colour persisted up to -30°C, above which it started to fade away to light yellow. The reaction was monitored by $^{31}P\{^1H\}$ and ^1H NMR spectroscopy. The complex formed at -78°C was characterised as the diphenyl-phosphine adduct of the methylidene complex, $Ir{=}CH_2(PHPh_2)[N(SiMe_2CH_2\text{-}PPh_2)_2]$, **5a**. The methylidene protons in this complex are observed as a four line pattern at +12.08 ppm ($^3J_{P,H}$ = 15.0 Hz) in the ^1H NMR spectrum (Figure 2.11 a), because of similar coupling to three phosphorus nuclei, whereas in the starting complex, a triplet at +16.44 ppm ($^3J_{P,H}$ = 14.4 Hz) is observed.[14] The silyl-methyl protons are observed as two singlets, indicating inequivalent environments above and below the Ir-P-N-P plane. The P*H*Ph_2 proton would be expected to resonate as a doublet of triplets. One part of this resonance was observed at 5.90 ppm but the other half was presumably obscured by the PPh_2 resonances.

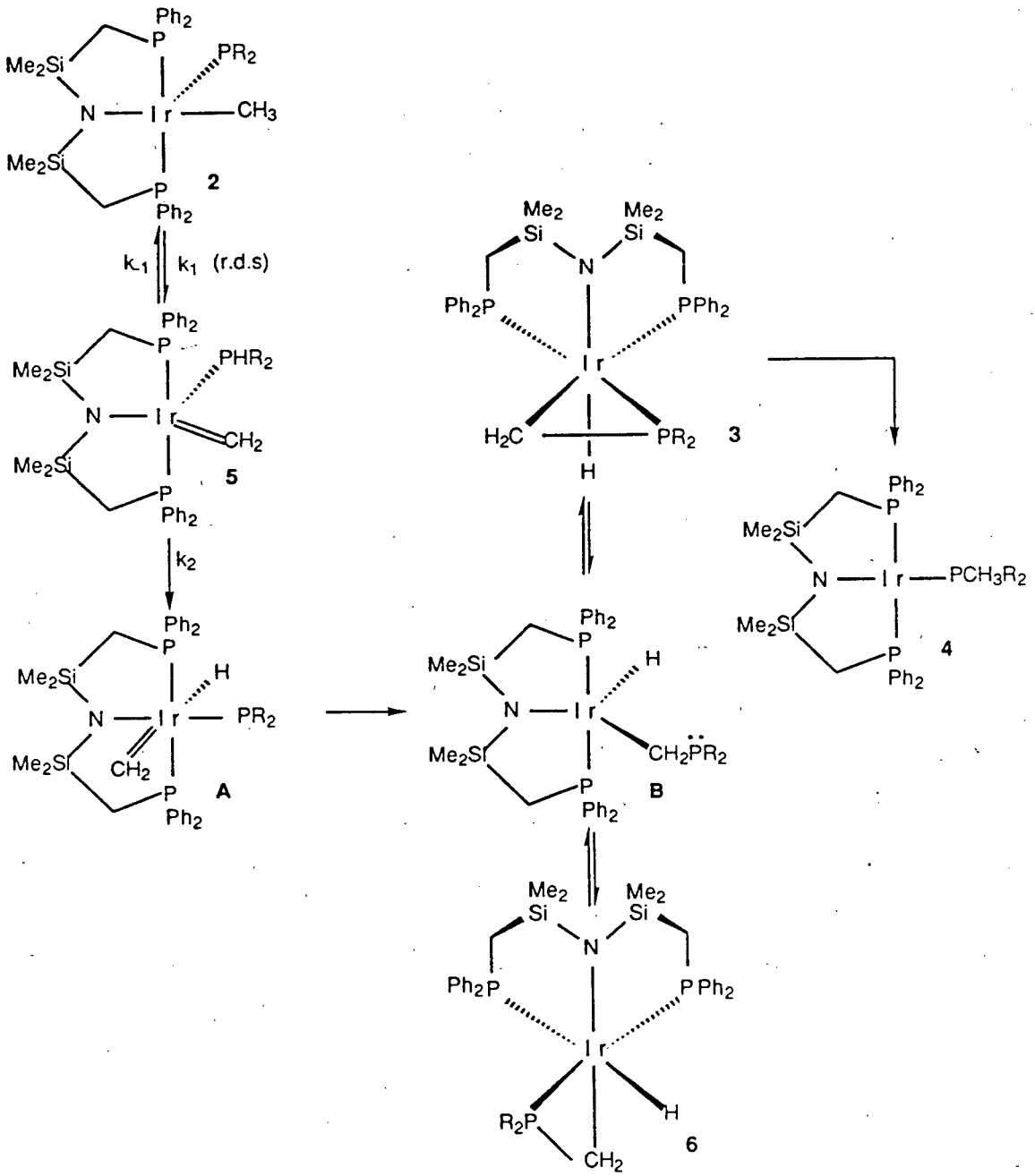

Scheme 2.3

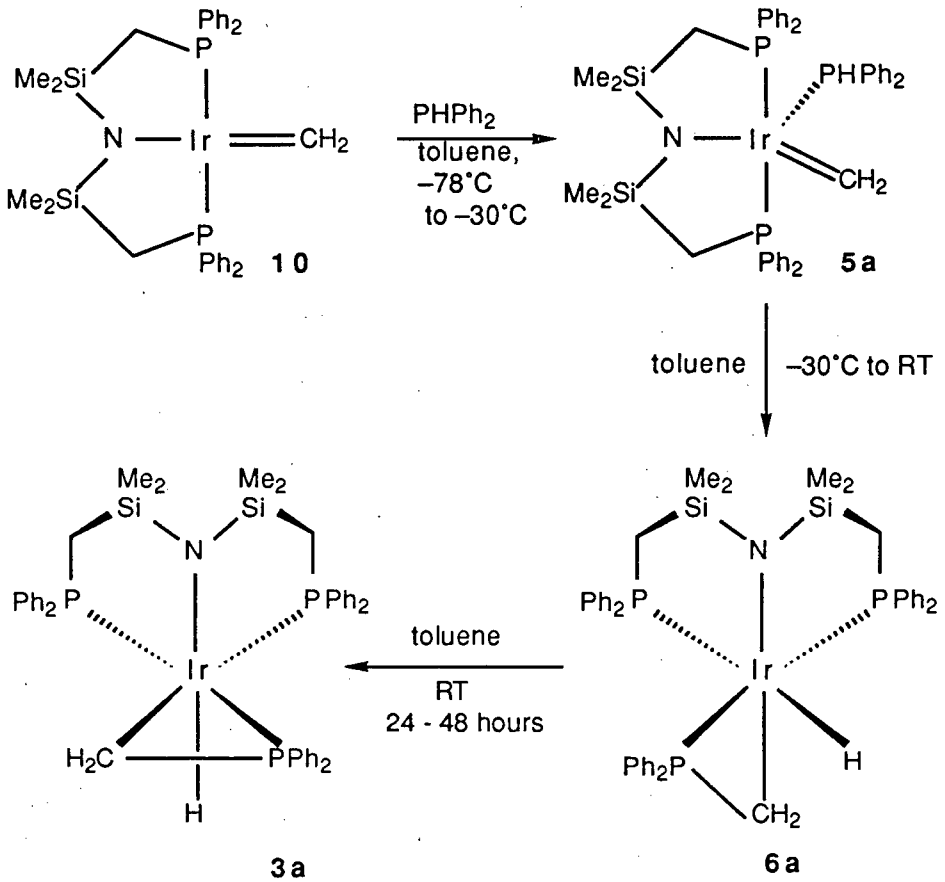

Scheme 2.4

The $^{31}P\{^{1}H\}$ NMR spectrum (Figure 2.12 a) shows two singlets at 13.45 ppm (for the phosphorus nuclei belonging to the tridentate ligand) and 3.90 ppm (for the $PHPh_2$ ligand) in the integral ratio of 2:1. No coupling is observed between the coordinated diphenylphosphine and the tridentate ligand phosphine donors. There are only two other examples of iridium methylidene phosphine complexes reported in the literature.[15] As mentioned in chapter 1 (Section 1.5), the complexes $Cp^*Ir{=}CH_2(PMe_3)$ and $Ir{=}CH_2(I)CO(PPh_3)_2$ have been prepared *in situ* at low temperatures only. The former complex decomposed above -40°C, whereas the latter species yielded the corresponding ylide complex at temperatures higher than -50°C via intramolecular cyclometallation. With the hybrid tridentate ligand system, the

trimethylphosphine adduct of the methylidene complex, $Ir{=}CH_2(PMe_3)$-$[N(SiMe_2CH_2PPh_2)_2]$, was found to be stable only below 0°C.[16] This species converted to $Ir(PMe_3)[N(SiMe_2CH_2PPh_2)_2]$ above 0°C losing ethylene.

The solution of $Ir{=}CH_2(PHPh_2)[N(SiMe_2CH_2PPh_2)_2]$, **5a**, when warmed above -30°C, slowly rearranged to *fac*-$Ir(\eta^2\text{-}CH_2PPh_2)H[N(SiMe_2CH_2PPh_2)_2]$, **6a**, in which the hydride ligand was *trans* to one of the phosphorus nuclei. The transformation was clean and no other species were detected during this process. The $^{31}P\{^1H\}$ NMR spectrum consists of an AMX pattern indicating all three phosphorus nuclei are nonequivalent (Figure 2.12 b). In the ^1H NMR spectrum (Figure 2.11 b) four singlets for the silyl-methyl protons, four multiplets for the ligand backbone methylene protons are observed. One of the most informative features is the hydride resonance which is observed as a doublet of doublet of doublets at -11.88 ppm (*trans* to a phosphorus nucleus) that shows a large *trans* coupling ($^2J_{P,H\ (trans)}$ = 133.3 Hz) to one of the phosphorus nuclei and *cis* couplings to the other two phosphorus centres ($^2J_{P,H\ (cis)}$ = 19.8 Hz, $^2J_{P,H\ (cis)}$ = 11.8 Hz). The complex **6a** was stable in solution only for a few hours at room temperature but it could be isolated as pale yellow crystals which were stored under an inert atmosphere at room temperature for long periods of time. Within 48 hours in solution, however, it completely isomerised to the complex **3a**, in which the hydride ligand was *trans* to the amide donor (observed by ^1H and $^{31}P\{^1H\}$ NMR spectroscopy).

For the conversion of **6a** to **3a**, standard first-order kinetics was observed (Figure 2.13). The appearance of complex **3a** was followed by UV-Vis spectroscopy at 360 nm (Figure 2.13, Table 2.9). The observed rate constants at various temperatures (36-59°C) are listed in Table 2.10. An Eyring plot of the data, ln(k/T) versus 1/T (Figure 2.14), yielded the activation enthalpy and entropy, $\Delta H^{\ddagger} = 95 \pm 10$ KJ mol^{-1} , $\Delta S^{\ddagger} = -3 \pm 2$ J K^{-1} mol^{-1}, respectively.

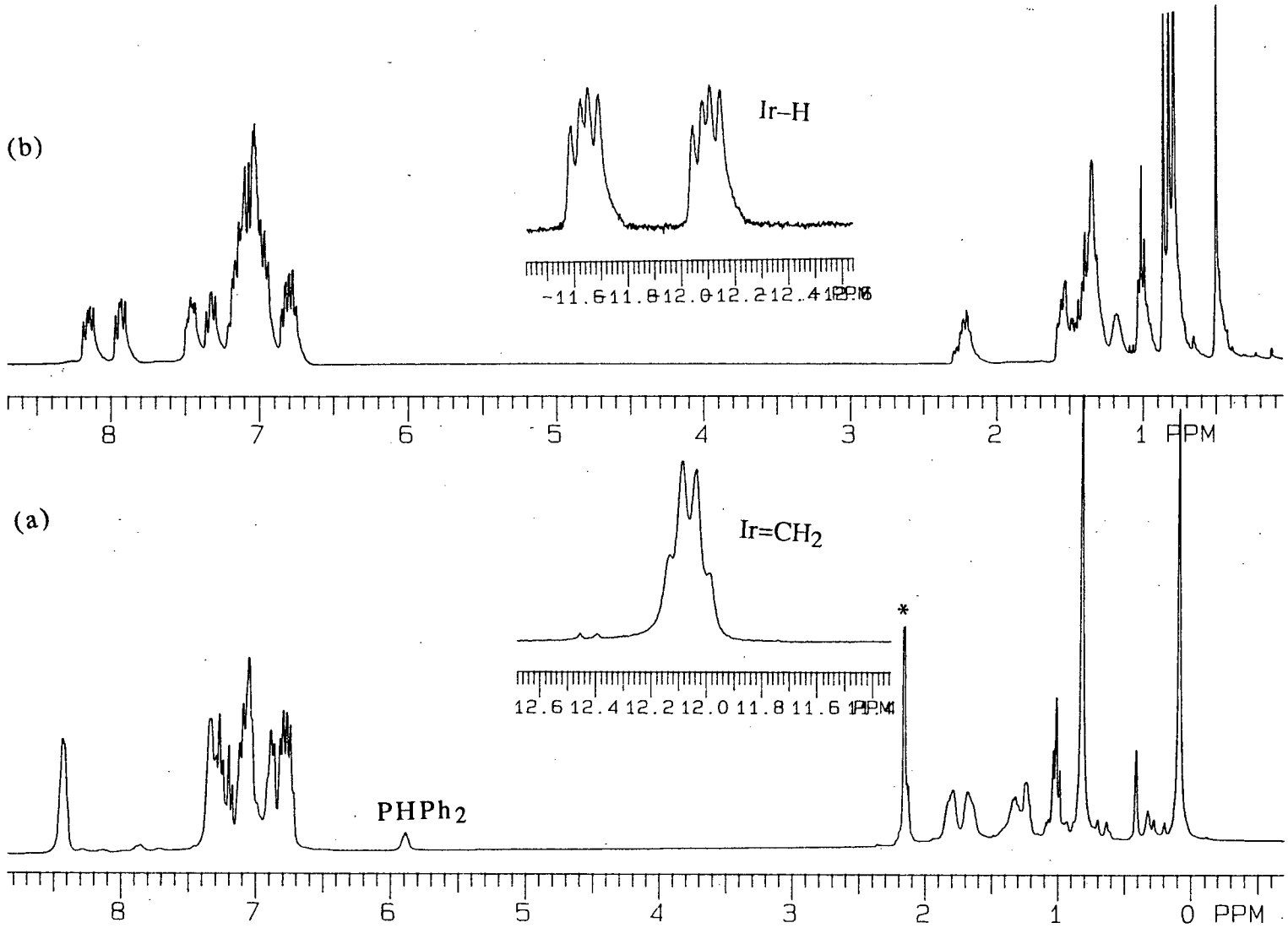

Figure 2.11 ^1H NMR spectrum (300 MHz) of $Ir{=}CH_2[N(SiMe_2CH_2PPh_2)_2]$ + $PHPh_2$ (a) at -78°C in C_7D_8, (b) at RT in C_6D_6 (* indicates toluene protons)

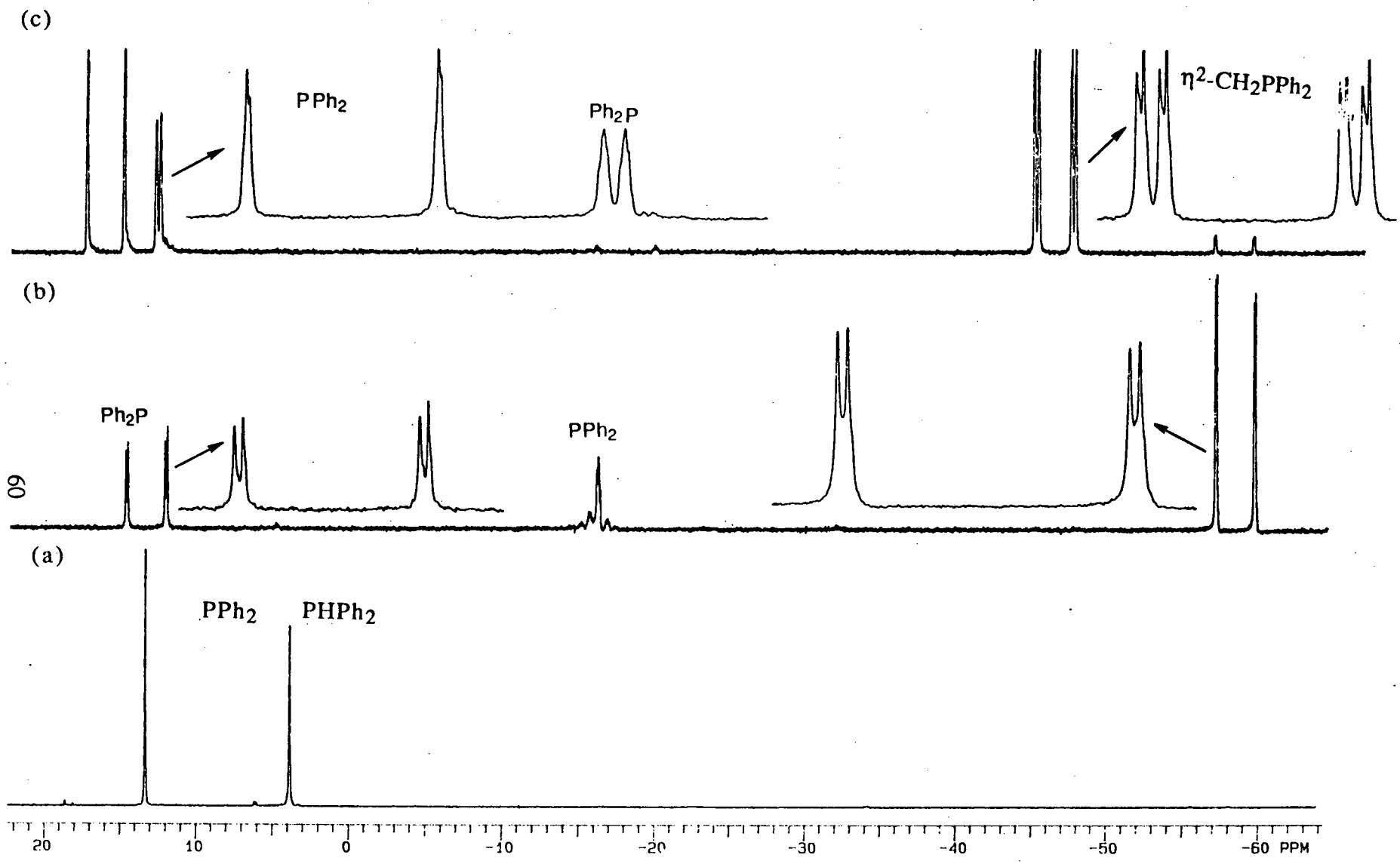

Figure 2.12 $^{31}P\{^{1}H\}$ NMR spectrum (121.4 MHz, C_7D_8) of $Ir{=}CH_2[N(SiMe_2CH_2PPh_2)_2]$ + $PHPh_2$ (a) at -78°C, (b) at -20°C, (c) at RT after 48 hours

Table 2.9 First-Order Analysis of the Absorption spectral changes for the isomerisation of **6a** to **3a** at 46°C in toluene

$[\mathbf{6a}] = 2.08 \times 10^{-4}$ mol L^{-1}

Time (s)	A_t (360 nm)	$\ln(A_t - A_\infty)$
0	0.458	-0.443
600	0.528	-0.559
1200	0.581	-0.656
1800	0.633	-0.761
2400	0.678	-0.863
3200	0.732	-1.000
4200	0.792	-1.178
5200	0.840	-1.347
6200	0.883	-1.528
8200	0.963	-1.988
9700	0.992	-2.226
A_∞	1.100	—

$k_{obs} = 1.84 \times 10^{-4}$ s^{-1}

a. Temperature deviation ± 1°C

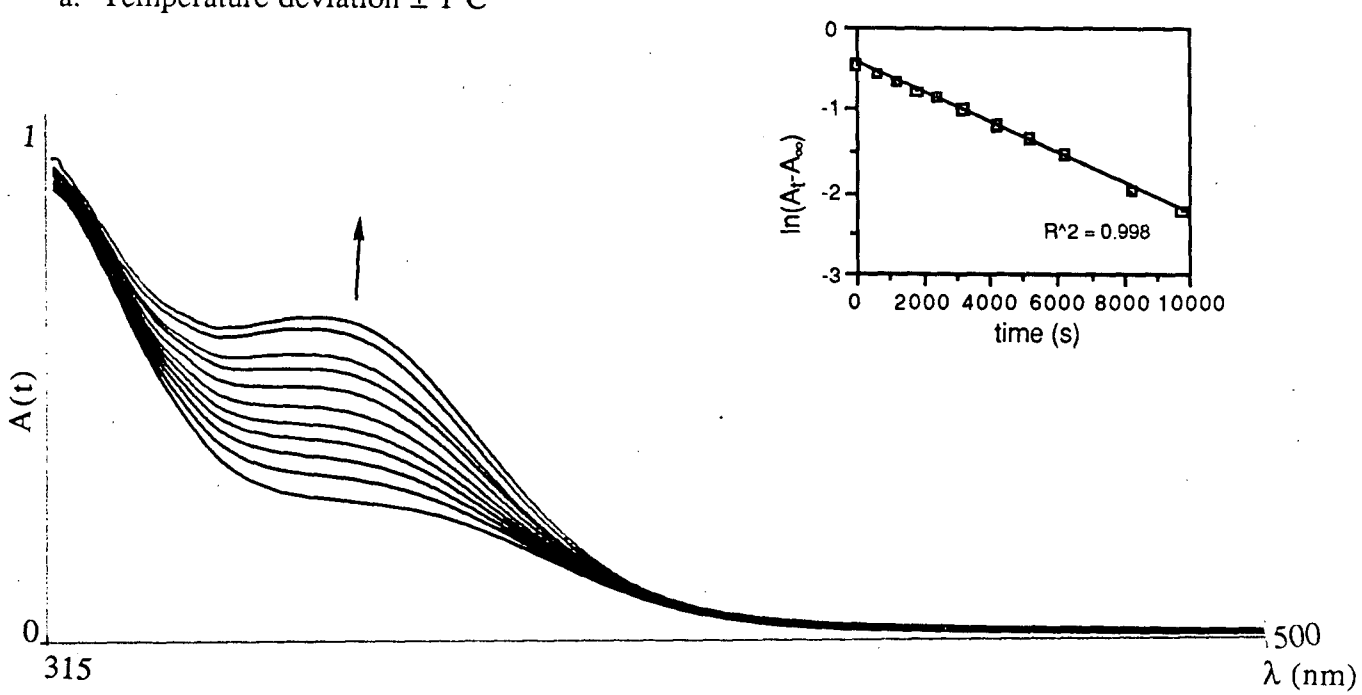

Figure 2.13 Absorption spectral changes for the thermolysis of **6a** at 46°C in toluene

Table 2.10 Observed Rate Constants and Activation Parameters for the Isomerisation of **6a** to **3a** in Toluene[a]

Temp (°C)	k_{obs} x 10^4, s^{-1}
36	0.50
46	1.84
56	4.87
59	7.15

$\Delta H^{\ddagger} = 95 \pm 10$ KJ mol^{-1}

$\Delta S^{\ddagger} = -3 \pm 2$ J K^{-1} mol^{-1}

a. The data for each run are given in Appendix A2.

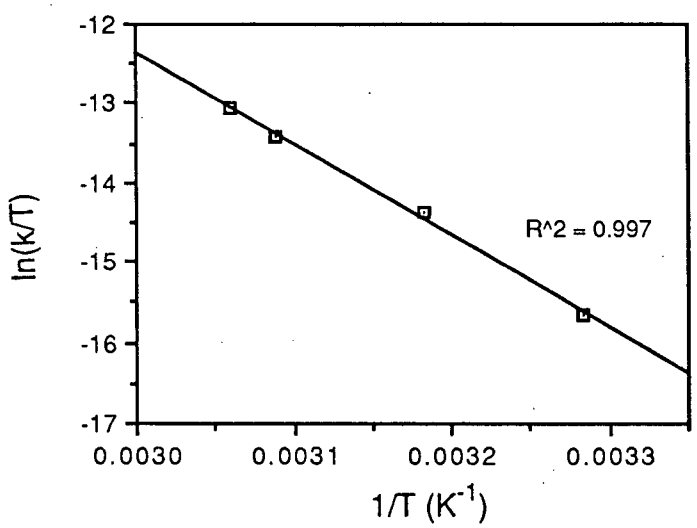

Figure 2.14 Eyring plot for the thermolytic conversion of **6a** to **3a** in toluene

A five-coordinate iridium(III) hydride complex **B** is proposed as an intermediate in the isomerisation of **6a** to **3a**. There exists indirect evidence for the involvement of **B** via a trapping experiment. Exposing the benzene solution of **6a** or **3a** to one atmosphere of CO gas at room temperature for 48 hours afforded a six

coordinate iridium(III) hydrido carbonyl species **7a** containing the η^1-CH_2PPh_2 ligand (Scheme 2.5). This complex was isolated as pale yellow crystals. The reaction of **6a** with CO gas was followed by UV-Vis spectroscopy at 46°C and the k_{obs} (1.82×10^{-4} s^{-1}) was found to be essentially identical with the k_{obs} value for the isomerisation of **6a** to **3a** at this temperature (Table 2.10).

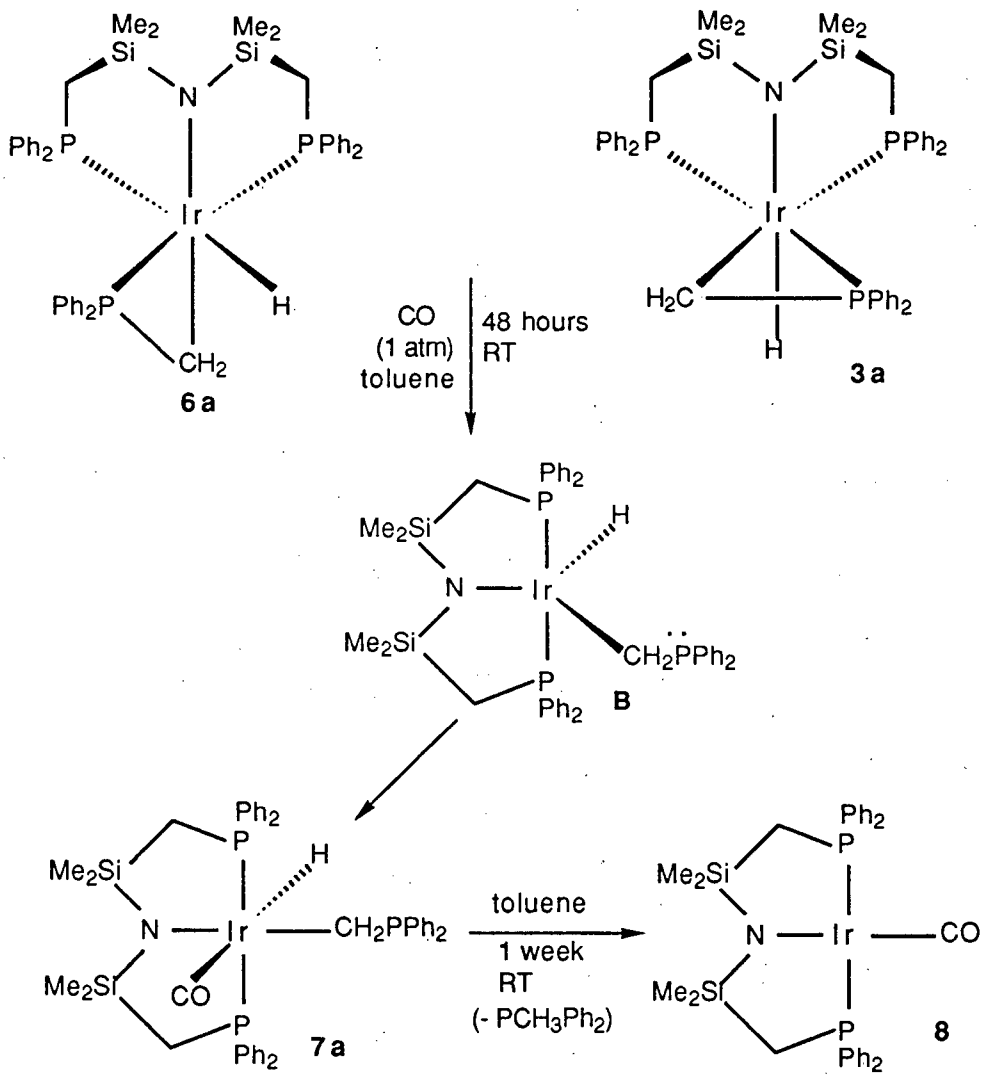

Scheme 2.5

The ^1H NMR spectrum of **7a** (Figure 2.15) consists of two sharp singlets for the silyl methyl protons, two sets of doublets of virtual triplets for the $SiCH_2P$ protons

of the ligand backbone thus indicating *trans* disposition of the chelating phosphines. Most informative is the hydride region which is comprised of a triplet of doublets at -6.50 ppm ($^2J_{P,H}$ = 18.0 Hz, $^3J_{P,H}$ = 9.0 Hz). The $^2J_{H,C}$ coupling (54.0 Hz) observed in the ^1H NMR spectrum of ^{13}CO enriched complex helped to determine the *trans* disposition of the hydride and carbonyl ligands. The iridium-carbonyl stretching frequency is at 1965 cm^{-1} in its infrared spectrum in toluene solution, and the ν_{Ir-H} band is at 1925 cm^{-1}. In the $^{13}C\{^1H\}$ NMR spectrum, the ^{13}CO ligand is observed as a doublet of triplets at 179.88 ppm ($^2J_{P,C}$ = 11.0 Hz, $^3J_{P,C}$ = 5.9 Hz). This chemical shift and the above mentioned IR data are quite typical for a late transition metal carbonyl functionality.[17]

Examples of transition metal complexes containing η^1-CH_2PR_2 ligand are rare.[18] The complex $CpRe(\eta^1\text{-}CH_2PMe_2)H(PMe_3)_2$ could be prepared only *in situ* at temperatures below 10°C.[18b] At room temperature in benzene solution, it converted to $CpRe(Ph)H(PMe_3)_2$ and generated one equivalent of free trimethylphosphine. Similarly, the hydrido carbonyl species, $Ir(\eta^1\text{-}CH_2PPh_2)H(CO)[N(SiMe_2CH_2\text{-}PPh_2)_2]$, **7a**, reductively eliminated methyldiphenylphosphine in solution (benzene) over a period of a week at room temperature and converted to a previously reported iridium(I) carbonyl complex, $Ir(CO)[N(SiMe_2CH_2PPh_2)_2]$, **8**.[3a]

Another piece of evidence for the involvement of the intermediates similar to **B** in the formation of the metallacyclic species such as **3** involves the reaction of $LiCH_2PPh_2$•TMEDA with $Ir(CH_3)I[N(SiMe_2CH_2PPh_2)_2]$, **1**. The species $Ir(CH_3)\text{-}(\eta^2\text{-}CH_2PPh_2)[N(SiMe_2CH_2PPh_2)_2]$ was produced, in which the tridentate ligand had facial geometry (as indicated by the ^1H and $^{31}P\{^1H\}$ NMR spectroscopy). The reaction presumably proceeds via a five coordinate complex containing the

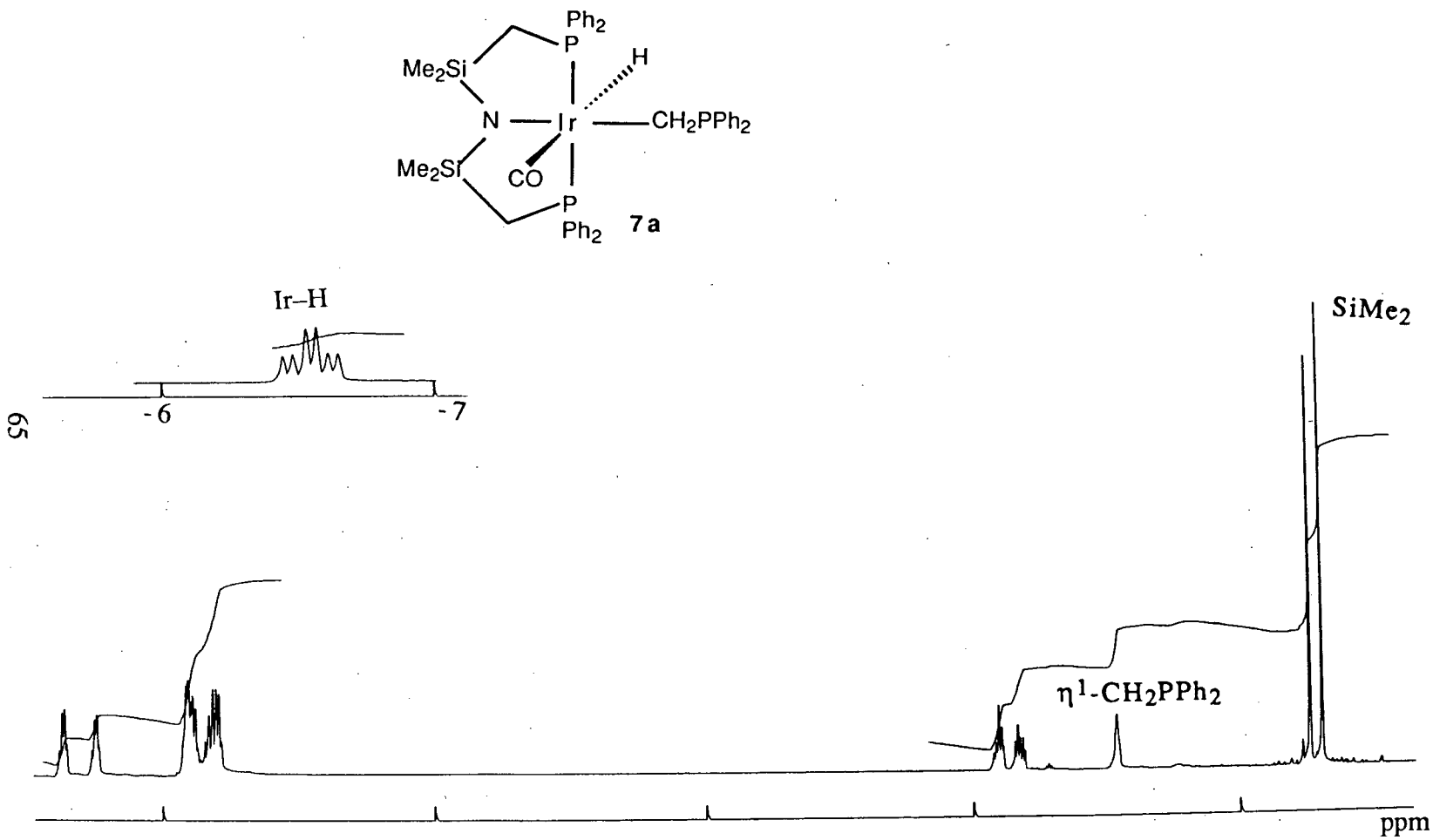

Figure 2.15 ^{1}H NMR spectrum (400 MHz, C_6D_6) of Ir(η^1-CH_2PPh_2)H(CO)[N($SiMe_2CH_2PPh_2$)$_2$], **7a**

η^1-CH_2PPh_2 ligand which undergoes ring closure to form the six coordinate η^2-CH_2PPh_2 complex. The species $Ir(CH_3)(\eta^2\text{-}CH_2PPh_2)[N(SiMe_2CH_2PPh_2)_2]$ was found to be unstable in solution as it decomposed within a day.

2.6.3 Discussion of the Kinetic and Mechanistic Experiments

The aforementioned kinetic experiments revealed that thermolysis of the methyl diphenylphosphide complex, **2a**, in toluene produced the cyclometallated hydride species, **3a**, cleanly and quantitatively and that the conversion is first order in **2a**. The activation parameters for this process are $\Delta H^{\ddagger} = 52 \pm 15$ KJ mol^{-1} and $\Delta S^{\ddagger} = -163 \pm 40$ J K^{-1} mol^{-1}. In hexanes, the cyclometallation occurs with very different parameters: $\Delta H^{\ddagger} = 103 \pm 20$ KJ mol^{-1} and $\Delta S^{\ddagger} = -16 \pm 3$ J K^{-1} mol^{-1}. The activation enthalpy is almost doubled but this is now offset by less negative activation entropy value. While negative entropy of activation may be explained by invoking an ordered transition state, the difference in the $\Delta S^{\ddagger}$ values in toluene and hexanes strongly suggests that solvation in the transition state is important, and the solvation effects are likely to be contributing to the overall activation enthalpy value.

The formation of complex **3a** via thermolysis of the phosphide complex **2a** is slower than its production from the reaction of the methylidene complex **10** with diphenylphosphine; therefore, the rate determining step in the thermolysis reaction must be before the formation of the methylidene phosphine adduct **5a**. Thus, the above mentioned $\Delta H^{\ddagger}$ and $\Delta S^{\ddagger}$ values for the thermolysis reaction refer to the k_1 step (Scheme 2.3). The activated complex is suggested to be **C** (Scheme 2.6) and resembles closely to the starting material; in other words, the transition state is reactant like. A small primary kinetic isotope effect (1.6 ± 0.1) also supports the transition state **C** in which only a slight breaking of the C–H bond in the methyl ligand has taken place.

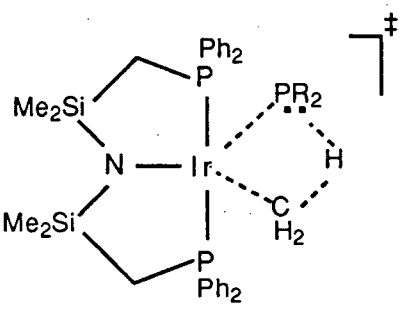

C

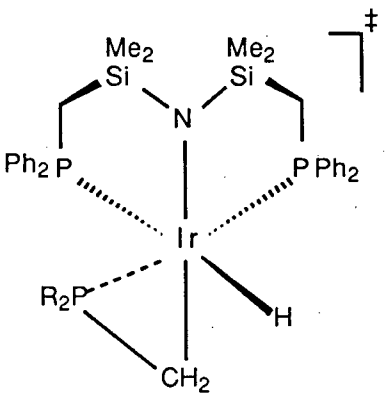

D

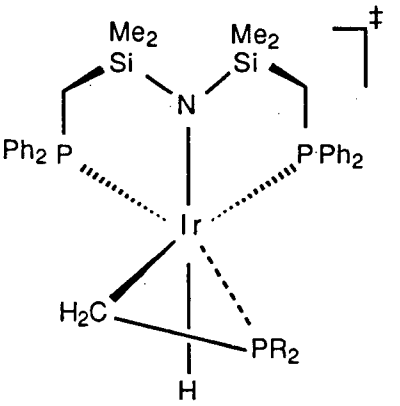

E

Scheme 2.6

No methylidene phosphine complex **5a** can be observed during thermolysis of **2a**, which suggests that it gets consumed as quickly as it forms therefore implying that k_2 must be much larger than k_1 (see Scheme 2.3). Furthermore, the complex **5a**, prepared by the alternative route, does not convert to the phosphide complex **2a** indicating that the k_2 value should also be much larger than the k_{-1} value. Because k_1 is the rate-determining step, the activation parameters listed above should have no contribution from the rest of the steps in the mechanism.

It is interesting to compare the kinetic parameters obtained from the cyclometallation of the phosphide system **2a** with that of the alkoxide complex $Zr(OAr')_2(CH_2Ph)_2$ where OAr' = 2,6-di-*tert*-butylphenoxide. This species

undergoes intramolecular activation of one of the C–H bonds of the *tert*-butyl groups when thermolysed in toluene, and affords the corresponding cyclometallated complex, $Zr(OC_6H_3{}^tBuCMe_2CH_2)(OAr')(CH_2Ph)$ and one equivalent of toluene.[19] Kinetic measurements of the cyclometallation step showed the reaction to be unimolecular with the following activation parameters: $\Delta H^{\ddagger}$ = 90 KJ mol^{-1}, $\Delta S^{\ddagger}$ = -80 J K^{-1} mol^{-1}. On the basis of the moderately large and negative activation entropy, a 4-centre transition state is proposed for the activation step analogous to that for the cyclometallation of **2a**.

The next isolable species in the mechanism is **6a** which upon thermolysis isomerises to its more stable form **3a**. The isomerisation occurs with a barrier of 95 ± 10 KJ mol^{-1} and is proposed to proceed via the dissociation of the phosphine end of the metallacyclic ring. Thus the 95 KJ mol^{-1} value represents enthalpy of activation for phosphine dissociation from **6a** in toluene solvent. Because the activated complex (**D**, Scheme 2.6) resembles closely to the five-coordinate intermediate (**B**, Scheme 2.3), the 95 KJ mol^{-1} can be approximated to the bond dissociation energy of Ir–P bond, assuming that the solvation effects are negligible.

The rearrangement of **3a** to **4a** takes place by a clean first order process in which $\Delta H^{\ddagger}$ = 107 ± 2 KJ mol^{-1} and $\Delta S^{\ddagger}$ = -49 ± 6 J mol^{-1} K^{-1}. For this conversion, a small primary kinetic isotope effect of 1.6 ± 0.1 was found. The intermediate suggested for this transformation is the five coordinate species, **B** (Scheme 2.3). An early transition state is proposed (**E**) (Scheme 2.6). The measured $\Delta H^{\ddagger}$ value of 107 KJ mol^{-1} represents the enthalpy of activation for Ir-P bond dissociation from **3a** in toluene.

There are limited data available on transition metal–phosphorus bond dissociation energies. During the isomerisation of *trans*-$RuCl_2(CO)(PPh_3)_3$ to its *cis*

form, dissociation of a phosphine ligand is proposed to be the key step.[20] The measured activation parameters for this step in chlorobenzene are: $\Delta H^{\ddagger} = 129 \pm 2$ KJ mol^{-1} and $\Delta S^{\ddagger} = 33 \pm 8$ J K^{-1} mol^{-1}. A $\Delta H^{\ddagger}$ value of 128 ± 13 KJ mol^{-1} is reported for the Ru–P bond dissociation in the hydrogenolysis of the ruthenium acyl complex, $RuCl(COC_7H_9)(CO)_2(PPh_3)_2$, in toluene.[21] Since M–L bond strengths generally increase down a column in the periodic table,[22] higher $\Delta H^{\ddagger}$ values will be expected for the Ir–P bond compared to that of the Ru–P bond. The measured activation enthalpy values of Ir–P bond (107 ± 10 and 95 ± 10 KJ mol^{-1}) in complexes **6a** and **3a** are lower perhaps because of the strain in the three-membered metallacyclic rings.

2.7 Photolysis of $Ir(CH_3)PR_2[N(SiMe_2CH_2PPh_2)_2]$, 2a-2c

The complexes $Ir(PCH_3R_2)[N(SiMe_2CH_2PPh_2)_2]$, **4a-4c**, were produced upon photolysis of the corresponding iridium(III) phosphide complexes, $Ir(CH_3)PR_2$-$[N(SiMe_2CH_2PPh_2)_2]$, **2a-2c**. The diarylphosphide complexes **2a** and **2b** were photolysed in a benzene solution at room temperature for 24 hours, using a 140 W Hg lamp as the light source. However, due to the thermal instability of the dimethylphosphide complex **2c**, its photolysis was carried out at -30°C in toluene using a N_2 laser. The completion of this photolytic transformation took approximately three hours. Even though the intermediate η^2-cyclometallated hydride, **3a-3c**, was not observed during the photolysis process, the transformation could proceed via the same mechanism as proposed for the thermolysis of **2a-2c**. Migration of the phosphide ligand into the iridium-methyl bond is another possibility.

2.8 Thermolysis of $Ir(CH_3)PHPh[N(SiMe_2CH_2PPh_2)_2]$, 2d

The complex $Ir(CH_3)PHPh[N(SiMe_2CH_2PPh_2)_2]$, **2d**, is thermally sensitive. Heating a benzene solution of **2d** at 60°C for one hour resulted in its transformation to the corresponding iridium(I) phosphine complex, $Ir(PHPhCH_3)[N(SiMe_2CH_2$-

$PPh_2)_2]$, **4d** (Equation 2.4). No intermediacy of the cyclometallated hydride complex was observed in the ^1H and $^{31}P\{^1H\}$ NMR spectra during this process in contrast to the thermal transformations of the diaryl and dialkylphosphide complexes **2a-2c**.

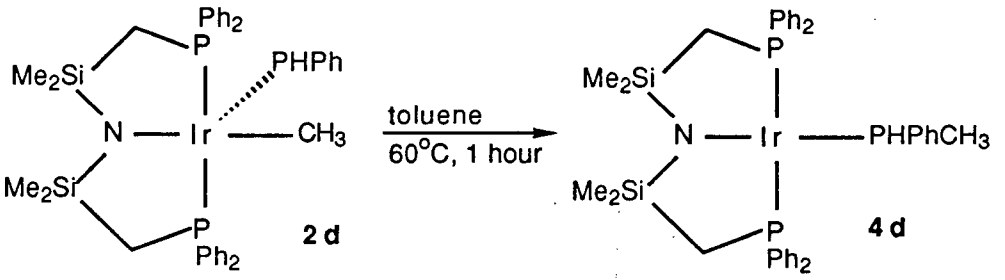

Equation 2.4

2.9 Kinetic and Mechanistic Experiments on the Thermolysis of 2d

2.9.1 Kinetic Experiments

Because the phenylphosphide complex, **2d**, is coloured (λ_{max} = 462 nm, ε = 1820 mol^{-1} L cm^{-1}), its thermal conversion to the phosphine complex, **4d**, is easily followed by UV-Vis spectrophotometry. The decrease in the band intensity at 462 nm was followed with time. First order kinetics were observed for this conversion. Rates were determined at four temperatures in toluene in the range of 69-93°C (Table 2.12). A typical $\ln(A_t - A_\infty)$ versus time plot is shown in Figure 2.16. The activation parameters $\Delta H^‡$ and $\Delta S^‡$ are 82 ± 10 KJ mol^{-1} and -71 ± 7 J K^{-1} mol^{-1}, respectively (Figure 2.17, Table 2.12). Thermolysis of the phenylphosphide complex was also followed in hexanes (λ = 515 nm, ε = 1951 mol^{-1} L cm^{-1}), and the activation parameters ($\Delta H^‡$ = 77 ± 8 KJ mol^{-1} , $\Delta S^‡$ = -83 ± 8 J K^{-1} mol^{-1}) obtained were similar to the activation data in toluene (Tables 2.11 and 2.12, Figure 2.16); therefore, any involvement of the solvent in the transition state, which might be reflected in the negative $\Delta S^‡$ value, was precluded. No primary kinetic isotope effect was observed

Table 2.11 First-Order Analysis of the Absorption Spectral Changes for the Thermolysis of the $Ir(CD_3)PHPh[N(SiMe_2CH_2PPh_2)_2]$, **2d-$CD_3$**, at 74°C[a] in Hexanes

$[\mathbf{2d\text{-}CD_3}] = 1.12 \times 10^{-3}$ mol L^{-1}

Time (s)	A_t (515 nm)	$\ln(A_t - A_\infty)$
0	1.611	0.334
150	1.225	0.011
400	1.185	-0.029
600	1.020	-0.216
800	0.879	-0.408
1000	0.771	-0.585
1200	0.678	-0.768
1400	0.604	-0.942
1700	0.485	-1.306
2000	0.397	-1.698
2500	0.283	-2.674
A_∞	0.214	—

$k_{obs} = 9.937 \times 10^{-4}$ s^{-1}

a. Temperature deviation ± 1°C

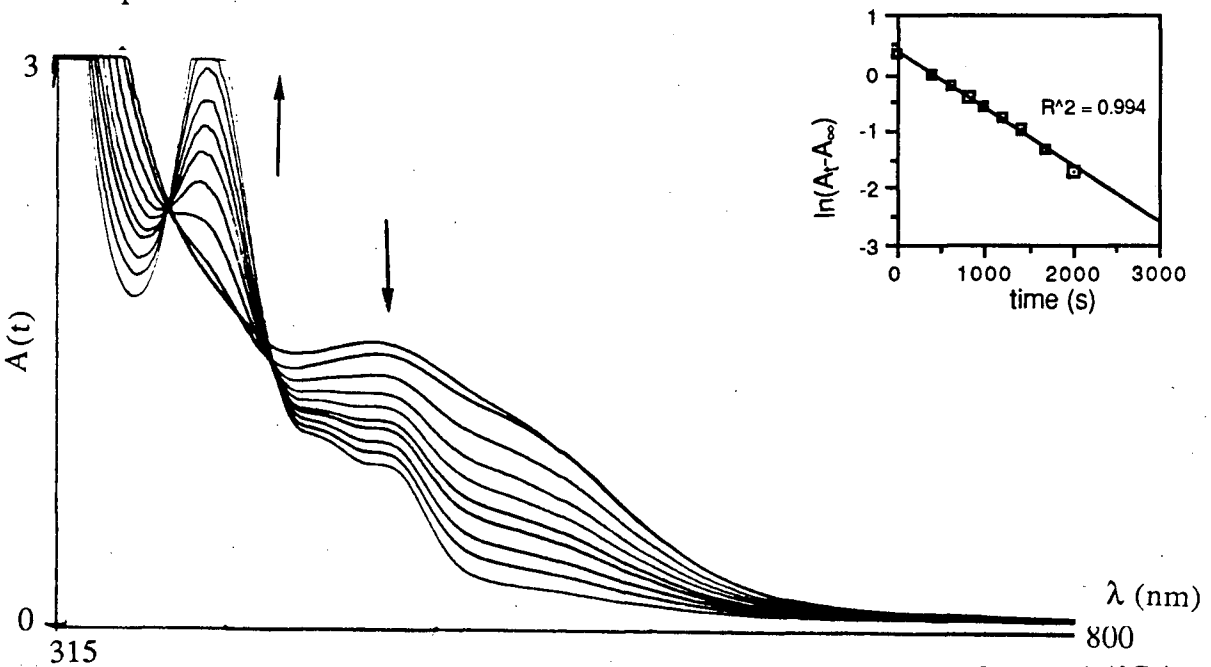

Figure 2.16 Absorption spectral changes upon thermolysis of **2d**-CD_3 at 74°C in hexanes

for this transformation (k_H/k_D = 1.0 ± 0.1 at 74°C in hexanes) indicating no carbon-hydrogen bond breaking is involved in the transition state.

Table 2.12 Observed Rate Constants and Activation Parameters for the Thermolytic Conversion of $Ir(CH_3)PHPh[N(SiMe_2CH_2PPh_2)_2]$, **2d**, to $Ir(PHCH_3Ph)[N(SiMe_2CH_2PPh_2)_2]$, **4d**

in Toluene		in Hexanes	
Temp (°C)	k_{obs} x 10^3, s^{-1}	Temp (°C)	k_{obs} x 10^3, s^{-1}
69	0.430	54[b]	0.176
82	1.600	65	0.476
86	2.102	74	1.008
93	2.800	79	1.327
$\Delta H^{\ddagger}$ = 82 ± 10 KJ mol^{-1}		$\Delta H^{\ddagger}$ = 77 ± 8 KJ mol^{-1}	
$\Delta S^{\ddagger}$ = - 71 ± 20 J K^{-1} mol^{-1}		$\Delta S^{\ddagger}$ = - 83 ± 8 J K^{-1} mol^{-1}	

a. The data for each run are given in Appendix A2. b. The run at 54°C was repeated and k_{obs} = 0.178 x 10^{-3} s^{-1}. Therefore, an error of 0.002 x 10^{-3} in the k_{obs} values was used to calculate the uncertainity in the activation parameters.

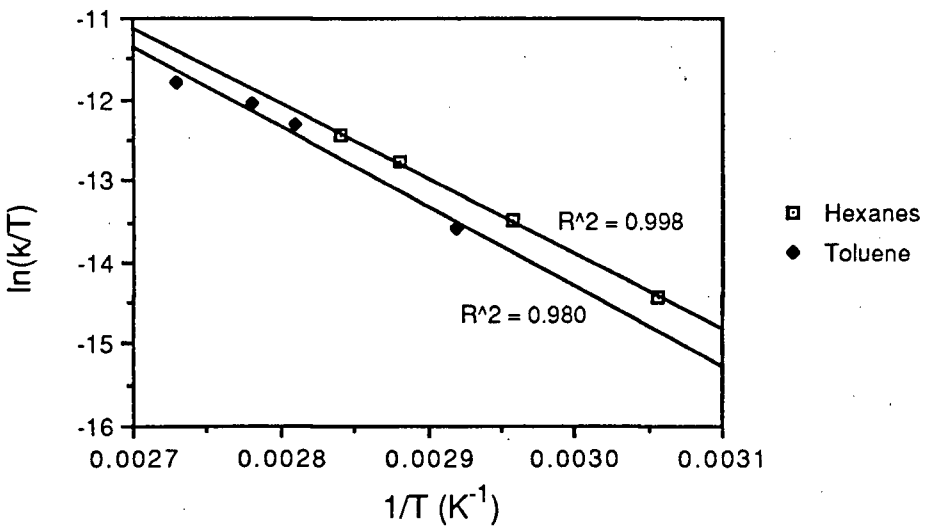

Figure 2.17 Eyring plot for the thermolysis of **2d** to **4d** in toluene and hexanes

2.9.2 Mechanistic Considerations

It is possible that the thermolysis of the phenylphosphide complex, **2d**, also proceeds through the same mechanism as the one established above for the diphenyl, di-*meta*-tolyl and dimethylphosphide complexes, **2a-2c**. However, the experimental evidence does not favour it, but points more towards migration of the phosphide ligand into the iridium-methyl bond. The lack of primary kinetic isotope effect is readily explained by this migration process. Furthermore, the fact that an intermediate cyclometallated hydride species is not seen can be either because it never becomes concentrated enough to be observed by NMR spectroscopy, or it does not form at all during the thermolysis process. A separate experiment involving the reaction of free phenylphosphine with the methylidene complex, $Ir{=}CH_2[N(SiMe_2CH_2PPh_2)_2]$, **10**, was conducted in order to access the cyclometallated hydride species (Equation 2.5).

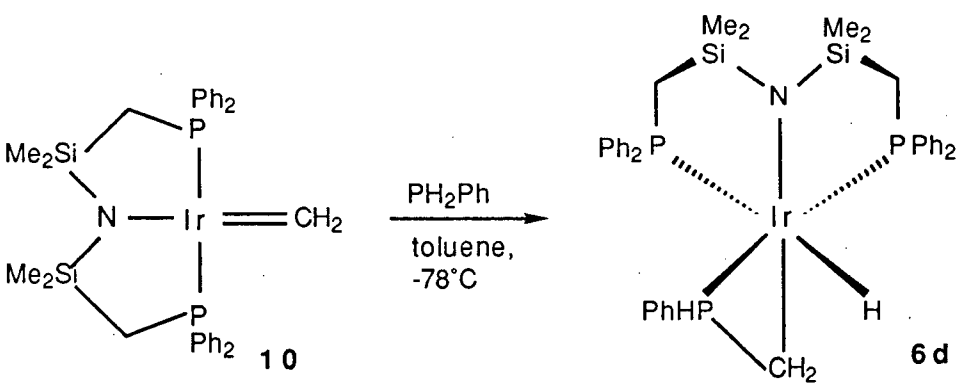

Equation 2.5

The reaction proceeded instantaneously at -78°C and the purple colour of the methylidene solution changed to light yellow. The light yellow complex was characterised as *fac*-$Ir(\eta^2\text{-}CH_2PHPh)H[N(SiMe_2CH_2PPh_2)_2]$, **6d**, by ^1H and $^{31}P\{^1H\}$ NMR spectroscopy (Figure 2.18). In this complex, the hydride ligand is

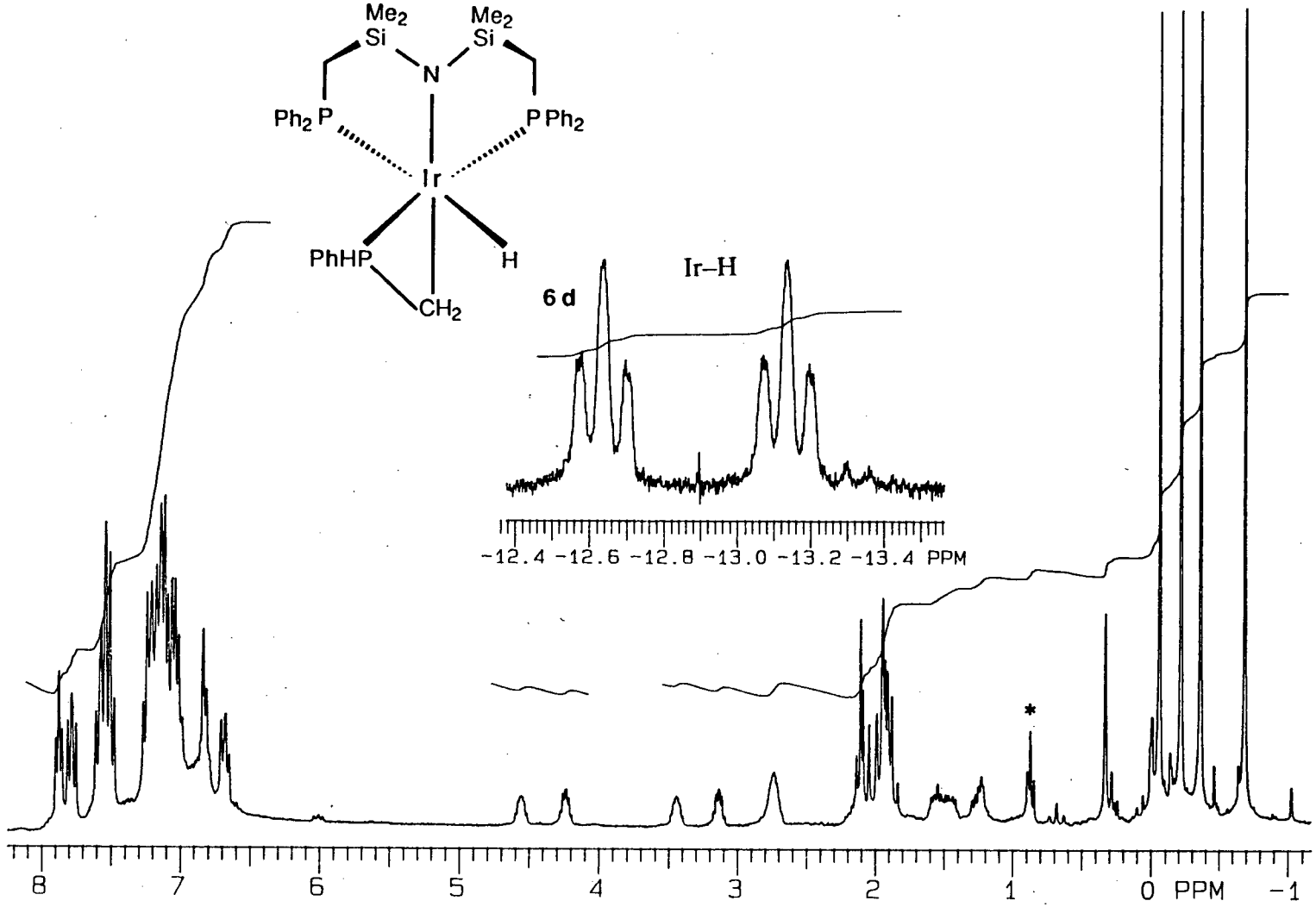

Figure 2.18 ^{1}H NMR spectrum (300 MHz, C_6D_6) of *fac*-Ir(η^2-CH_2PHPh)H[$N(SiMe_2CH_2PPh_2)_2$], **6d** (* indicates hexanes protons)

trans to a phosphine centre of the tridentate ligand (-12.87 ppm, dt, $^2J_{P,H\ (trans)}$ = 149.3 Hz, $^2J_{P,H\ (cis)}$ = 19.1 Hz). However, the geometry at the chiral phosphorus in η^2-CH_2PHPh ligand could not be ascertained from the NMR data. This complex in solution does not isomerise to the other expected cyclometallated complex in which the hydride ligand is *trans* to the amide moiety, and neither does it convert to the square planar phosphine complex, $Ir(PHCH_3Ph)[N(SiMe_2CH_2PPh_2)_2]$, **4d**. Heating the toluene solution of this complex at 80°C for 30 minutes resulted in decomposition. These observations do suggest that the cyclometallated hydride route is not likely to be involved in the thermolysis of **2d**.

2.9.3 Discussion on the Kinetics and the Mechanism

The formation of the phosphine complex, **4d**, from thermolysis of the phosphide complex, **2d**, proceeds smoothly with activation parameters $\Delta H^{\ddagger}$ = 82 ± 10 KJ mol^{-1} and $\Delta S^{\ddagger}$ = -71 ± 7 J mol^{-1} K^{-1} in toluene. The activation data obtained in hexanes ($\Delta H^{\ddagger}$ = 77.0 ± 7 KJ mol^{-1}, $\Delta S^{\ddagger}$ = -83 ± 8 J mol^{-1} K^{-1}) are similar to the parameters reported above in toluene; therefore, any involvement of the solvent in the transition state which might be contributing to the activation parameters is precluded. No primary isotope effect was observed in this transformation (k_H/k_D = 1.0 ± 0.1); therefore, no C-H bond breaking is suggested in the transition state. The transition state is likely to be ordered as indicated by the large negative $\Delta S^{\ddagger}$ value and a possibility is shown below (**F**). The activation enthalpy value $\Delta H^{\ddagger}$ then is a combination of Ir-C bond breaking and P-C bond forming energies.

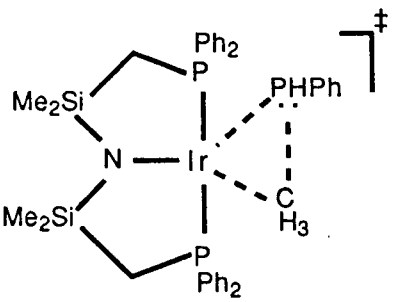

F

Why does there exist such a drastic change in the kinetic data (k_H/k_D), and therefore in mechanism, upon going from diphenylphosphide complex **2a** to the phenylphosphide complex **2d**? The difference is likely not due to the higher basicity of the phenylphosphide ligand as compared to the diphenylphosphide, because even the very basic dimethylphosphide ligand follows the same thermal conversion as the diphenyl and di-*meta*-tolylphosphide ligands in the corresponding complexes.[23] However, the different reactivities can be rationalised in terms of the transition states. A 4-centre transition state (labelled **C** in Scheme 2.6) might be necessary in the diphenylphosphide complex because of steric strain which only allows access to the C–H bond of the methyl ligand. For the less sterically encumbered phenylphosphide complex, a 3-centre transition state is proposed (labelled **F** above), where direct C–P bond formation occurs instead.

2.10 Photolysis of $Ir(CH_3)PHPh[N(SiMe_2CH_2PPh_2)_2]$, 2d

The photolysis of the iridium(III) phenylphosphide complex, $Ir(CH_3)PHPh[N(SiMe_2CH_2PPh_2)_2]$, **2d**, (140 W Hg lamp, 18 hours, C_6D_6) proceeded cleanly to yield the same product, $Ir(PHCH_3Ph)[N(SiMe_2CH_2PPh_2)_2]$, **4d**, as obtained form the thermolysis of **2d**. Again, no intermediates were observed during the photolysis process.

2.11 Synthesis of Other Cyclometallated hydride complexes

2.11.1 Reaction of $Ir{=}CH_2[N(SiMe_2CH_2PPh_2)_2]$, 10, with HP^tBu_2

The reactivity of $Ir{=}CH_2[N(SiMe_2CH_2PPh_2)_2]$ with diphenylphosphine to generate the cyclometallated species **3a** and **6a** turned out to be a useful synthetic route to access other cyclometallated hydride species which could not be obtained via the phosphide route. The complex $Ir(CH_3)I[N(SiMe_2CH_2PPh_2)_2]$, **1**, did not react with KP^tBu_2 even at elevated temperatures (80°C, 5 hours). However, the reaction of $Ir{=}CH_2[N(SiMe_2CH_2PPh_2)_2]$ with HP^tBu_2 at -78°C afforded the phosphine adduct $Ir{=}CH_2(PH^tBu_2)[N(SiMe_2CH_2PPh_2)_2]$, **5e**, (Scheme 2.7). Above -30°C, this complex rearranged to the cyclometallated hydride complex, *fac*-$Ir(\eta^2\text{-}CH_2P^tBu_2)H$-$[N(SiMe_2CH_2PPh_2)_2]$, **6e**, with the hydride ligand disposed *trans* to one of the phosphorus nuclei. Within 24-48 hours, **6e** rearranged to its more stable form, **3e**, in which the hydride ligand was *trans* to the amide moiety. The $^{31}P\{^1H\}$ NMR spectral changes for this reaction sequence are shown in Figure 2.19.

2.11.2 Limitations of the Reactions of $Ir(R)X[N(SiMe_2CH_2PPh_2)_2]$ with MPR'_2

There likely exists some steric hindrance between the alkyl ligand on the iridium centre and the substituents on the phosphide precursor. The reaction also seems to be dependent upon the counterion M in the phosphide salt. These observations were made from the following experiments. When the methyl ligand on the iridium centre was replaced by a phenyl group, the starting material, $Ir(Ph)I[N(SiMe_2CH_2PPh_2)_2]$, failed to react with $LiPPh_2$, but the reaction with $LiPMe_2$ produced $Ir(PMe_2Ph)[N(SiMe_2CH_2PPh_2)_2]$ without any apparent intermediacy of the desired phosphide complex (by ^1H and $^{31}P\{^1H\}$ NMR spectroscopy). A variety of different combinations of the iridium halide complexes and

the lithium phosphide salts were tried, but in the cases shown below no reaction was observed (Equation 2.6).

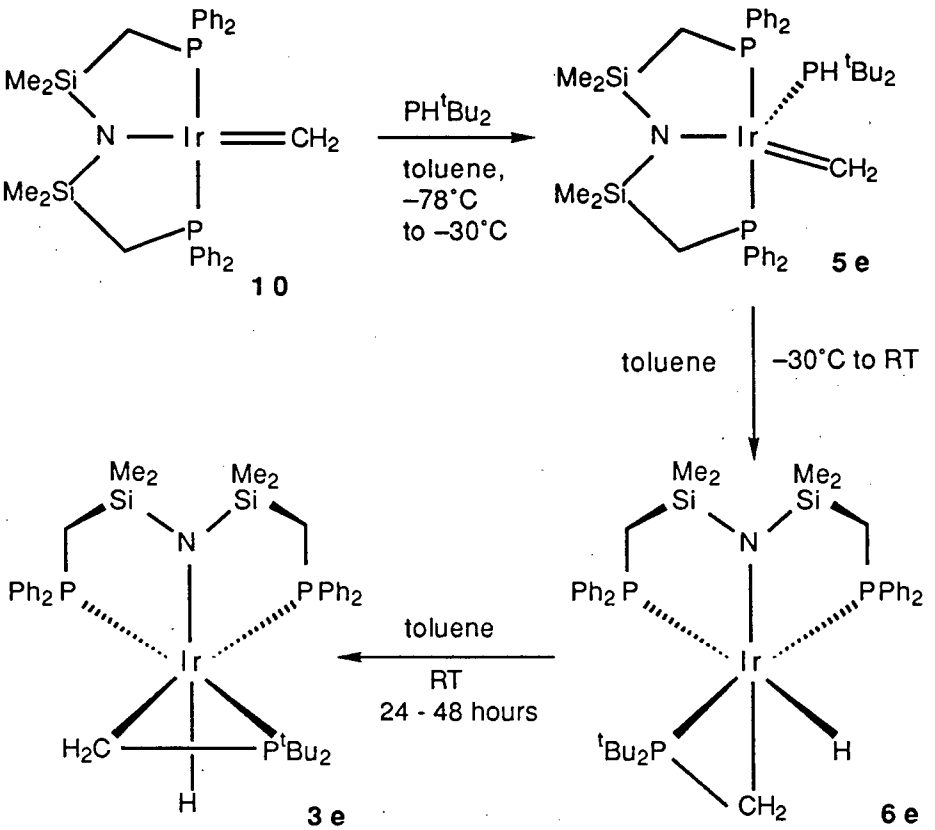

Scheme 2.7

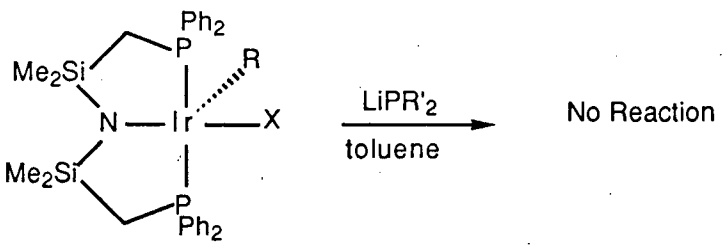

R	R'	X
CH_3	*ortho*-tol	I
CH_3	^{i}Pr	I
Ph	Ph	I
CH_2Ph	Ph	Br

Equation 2.6

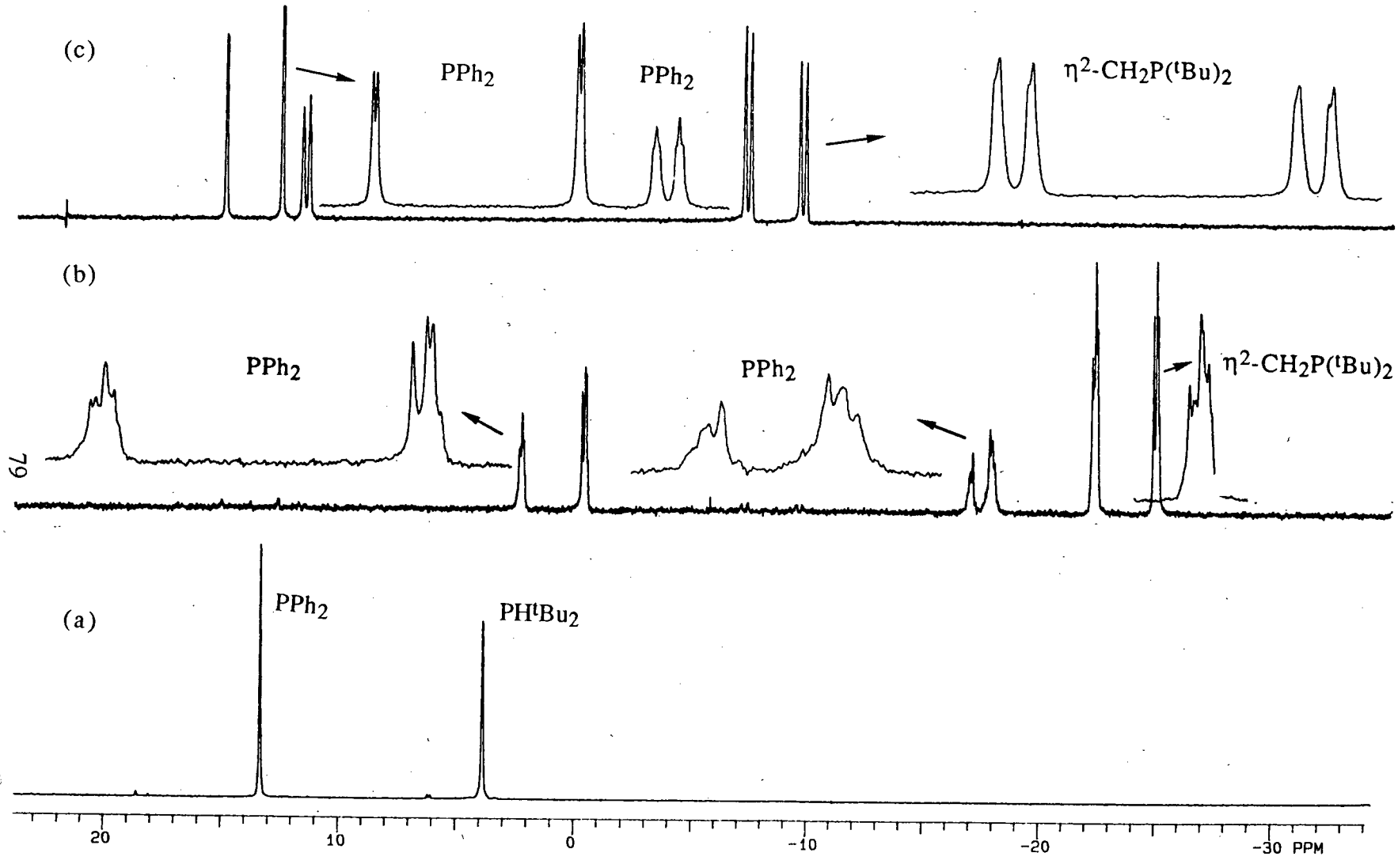

Figure 2.19 $^{31}P\{^{1}H\}$ NMR spectrum (121.4 MHz, C_7D_8) of $Ir{=}CH_2[N(SiMe_2CH_2PPh_2)_2]$ + PH^tBu_2 (a) at -78°C, (b) at -10°C, (c) at RT after 48 hours

Furthermore, the iridium(III) benzyl bromide complex, $Ir(CH_2Ph)Br$-$[N(SiMe_2CH_2PPh_2)_2]$, showed no reactivity toward $LiPMe_2$ at room temperature over a week; however, its reaction with $KPMe_2$ proceeded smoothly at ambient temperature with a noticeable colour change over a period of half an hour (Scheme 2.8). The green colour of the benzyl bromide complex changed to light yellow of *fac*-$Ir(\eta^2$-$CHPhPMe_2)H[N(SiMe_2CH_2PPh_2)_2]$, **6f**, (Scheme 2.8). The product was isolated as pale yellow crystals in good yield (~80%).

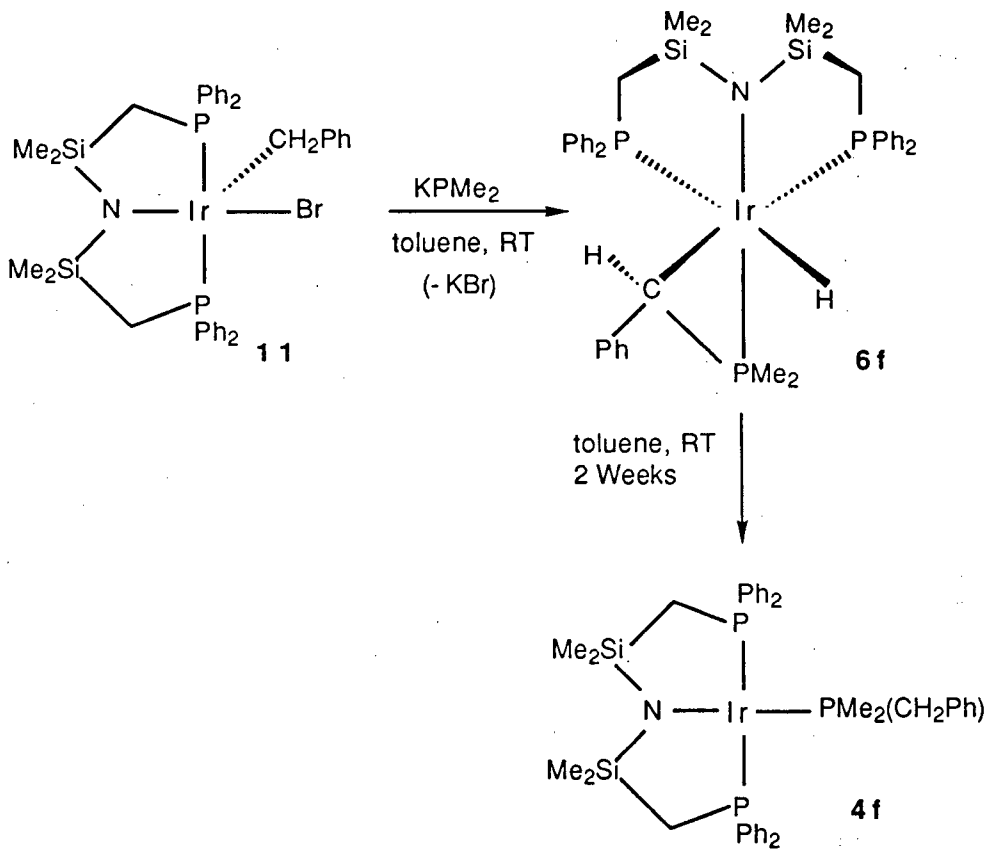

Scheme 2.8

The $^{31}P\{^1H\}$and ^1H NMR spectra provide excellent handles for deducing the stereochemistry at the iridium centre and also the arrangement of the hybrid tridentate ligand. But, the geometry at the chiral carbon of the metallacycle is not apparent from the NMR data. Based on steric considerations, it is assumed that the phenyl ring on

the carbon centre is pointing away from the phenyl moieties on the tridentate ligand. The $^{31}P\{^{1}H\}$ NMR spectrum of this complex exhibits three resonances which are weakly coupled in the integral ratio of 1:1:1. Of these, a simple triplet for the PMe_2 ligand (-11.19 ppm, $^{2}J_{P,P}$ = 9.0 Hz) appears to arise from coupling to the two *cis* phosphorus atoms of the hybrid tridentate ligand. The phosphorus nuclei of the hybrid ligand are coupled (*cis*) to one another and also to the PMe_2 ligand and thus are observed as two sets of four lines (-7.39 ppm, 2.62 ppm, $^{2}J_{P,P}$ = 9.5 Hz, $^{2}J_{P,P}$ = 9.3 Hz). Complex **6f** exhibits a most informative feature in the high field region in the ^{1}H NMR spectrum (Figure 2.20). The hydride resonance is a doublet of doublet of doublets at -10.82 ppm and shows a large *trans* coupling ($^{2}J_{P,H}$ = 153.0 Hz) to one of the phosphorus centres and *cis* couplings ($^{2}J_{P,H}$ = 20.0 Hz, $^{2}J_{P,H}$ = 9.0 Hz) to the other two phosphorus nuclei. The C*H*Ph proton resonance at 2.11 ppm (m) was identified by comparing the ^{1}H NMR spectrum of the protiated compound with that of the deuterated sample *fac*-Ir(η^2-$CDC_6D_5PMe_2$)D[$N(SiMe_2CH_2PPh_2)_2$].

The formation of complex **6f** proceeds with remarkable stereoselectivity, since only one isomer is observed in the crude reaction mixture (by ^{1}H and $^{31}P\{^{1}H\}$ NMR spectroscopy). A reported reaction between *mer*-$IrCl_3\{P(Me)(CH_2Ph)_2\}_3$ and $LiN^{i}Pr_2$ afforded a pair of geometrical isomers of the formula Ir{η^2-CHPh-($PMeCH_2Ph$)}$Cl_2\{P(Me)(CH_2Ph)_2\}_2$ (see Chapter 1, Section 1.4).[11b]

This iridium(III) hydride complex, *fac*-Ir(η^2-$CHPhPMe_2$)H[$N(SiMe_2CH_2$-$PPh_2)_2$], **6f**, rearranged to the iridium(I) phosphine complex, Ir(PMe_2CH_2Ph)-[$N(SiMe_2CH_2PPh_2)_2$], **4f**, in solution at room temperature over a period of two weeks (Scheme 2.6). During this process, no other hydride intermediate was observed in contrast to some of the transformations mentioned above.

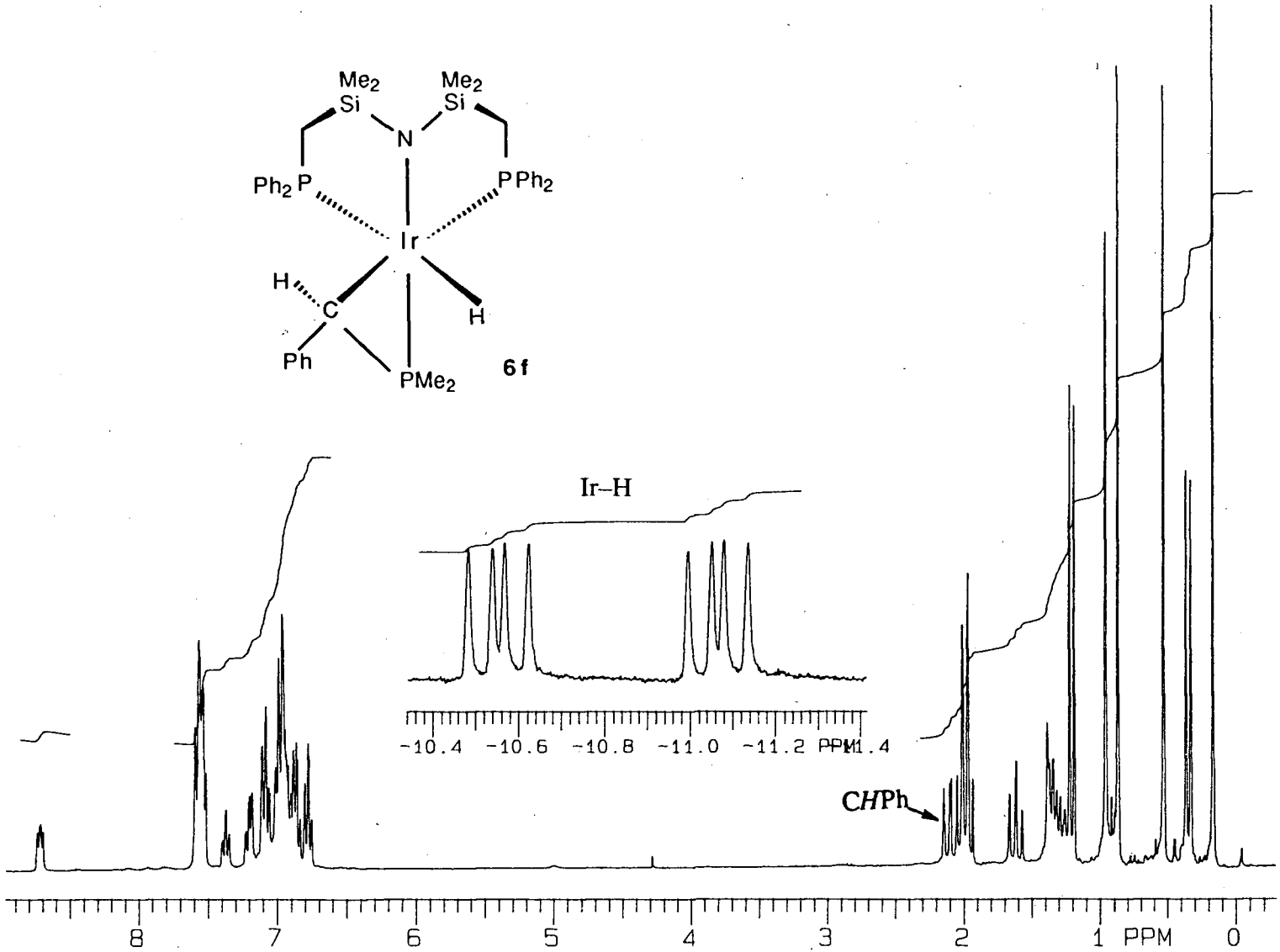

Figure 2.20 ^{1}H NMR spectrum (300 MHz, C_6D_6) of *fac*-Ir(η^2-CHPhPMe$_2$)H[N(SiMe$_2$CH$_2$PPh$_2$)$_2$], **6f**

2.12 References

1 (a) Fryzuk, M. D.; Joshi, K. *Organometallics* **1989**, *8*, 722.
(b) Fryzuk, M. D.; Bhangu, K. *J. Am. Chem. Soc.* **1988**, *110*, 961.

2 Fryzuk, M. D.; Joshi, K. *J. Am. Chem. Soc.* **1989**, *111*, 4498.

3 (a) Fryzuk, M. D.; MacNeil, P. A.; Rettig, S. J. *Organometallics* **1986**, *5*, 2469.
(b) Fryzuk, M. D.; MacNeil, P. A.; Massey, R. L.; Ball, R. G. *J. Organomet Chem.* **1989**, *368*, 213.

4 Brookes, P. R.; Shaw, B. L. *J. Chem. Soc. A.* **1967**, 1079.

5 Moore, D. S.; Robinson, S. D. *Inorg. Chim. Acta.* **1981**, *53*, L171.

6 (a) Montllo, D.; Svades, J.; Torres, M. R.; Perales, A.; Mathieu, R. *J. Chem. Soc., Chem. Commun.* **1989**, 97.
(b) Hey, E.; Lappert, M. F.; Atwood, J. L.; Bott, S. G. *Polyhedron* **1988**, *7*, 2083.
(c) Buhro, W. E.; Zwick, B. D.; Georgiou, S.; Hutchinson, J. P.; Gladysz, J. A. *J. Am. Chem. Soc.* **1988**, *110*, 2427.
(d) Buhro, W. E.; Chisholm, M. H.; Folting, K.; Huffmann, J. C. *J. Am. Chem. Soc.* **1987**, *109*, 905.
(e) Jorg, K.; Malisch, W.; Reich, W.; Meyer, A.; Schubert, U. *Angew. Chem., Int. Ed. Engl.* **1986**, *25*, 92.
(f) Bohle, D. S.; Jones, T. C.; Rickard, C. E. F.; Roper, W. R. *Organometallics* **1986**, *5*, 1612.
(g) Baker, R. T.; Whitney, J. F.; Wreford, S. S. *Organometallics* **1983**, *2*, 1049.
(h) Day, V. W.; Tavanaiepour, I.; Abdel-Meguid, S. S.; Kirner, J. F.; Goh, L. Y.; Mutterties, E. L. *Inorg. Chem.* **1982**, *21*, 657.
(i) Rocklage, S. M.; Schrock, R. R.; Churchill, M. R.; Wasserman, H. J. *Organometallics* **1982**, *1*, 1332.
(j) Domaille, P. J.; Foxman, B. M.; McNeese, T. J.; Wreford, S. S. *J. Am. Chem. Soc.* **1980**, *102*, 4114.

(k) Malisch, W.; Alsmann, R. *Angew. Chem., Int. Ed. Engl.* **1976**, *15*, 769.
(l) Buhro, W. E.; Georgiou, S.; Hutchimson, J. P.; Gladysz, J. A. *J. Am. Chem. Soc.* **1985**, *107*, 3346.
(m) Dobbie, R. C.; Hopkinson, M. J.; Whittaker, D. *J. Chem. Soc., Dalton Trans.* **1972**, 1030.
(n) Roddick, D. M.; Santarsiero, B. D.; Bercaw, J. E. *J. Am. Chem. Soc.* **1985**, *107*, 4670.

7 Buhro, W. E.; Gladysz, J. A. *Inorg. Chem.* **1985**, *24*, 3505.

8 Crisp, G. T.; Salem, G.; Wild, S. B. *Organometallics* **1989**, *8*, 2360.

9 Appleton, T. G.; Clark, H. C.; Mazner, L. E. *Coord. Chem. Rev.* **1973**, *10*, 335.

10 Fryzuk, M. D.; MacNeil, P. A.; Rettig, S. J. *J. Am. Chem. Soc.* **1987**, *109*, 2803.

11 (a) Mainz, V. V.; Andersen, R. A. *Organometallics* **1984**, *3*, 675.
(b) Schimdbaur, H; Blaschke, G. *Z. Naturforsch. B.* **1980**, *35*, 584.
(c) Werner, H.; Werner, R. J. *J. Organomet. Chem.* **1981**, *C60*, 209.

12 Al-Jibori, S.; Crocker, C.; McDonald, W. S.; Shaw, B. L. *J. Chem. Soc., Dalton Trans.* **1981**, 1572.

13 (a) Crocker, C.; Empsall, H. D.; Ernington, R. J.; Hyde, E. M.; McDonald, W.S.; Markam, R.; Norton, M. C.; Shaw, B. L. *J. Chem. Soc., Dalton Trans.* **1982**, 1217.
(b) Ling, S. S.; Puddephatt, R. J. *J. Chem. Soc., Chem. Commun.* **1982**, 412.

14 Fryzuk, M. D.; MacNeil, P. A.; Rettig, S. J. *J. Am. Chem. Soc.* **1985**, *107*, 6708.

15 (a) Klein, D. P.; Bergman, R. G. *J. Am. Chem. Soc.* **1989**, *111*, 3079.
(b) Clark, G. R.; Roper, W. R.; Wright, A. H. *J. Organomet. Chem.* **1984**, *C17*, 273.

16 Massey, R. L. *M. Sc. Thesis*, University of British Cloumbia, Vancouver, Cananda, **1989**.

17 (a) Deutsch, P. P.; Eisenberg, R. *Organometallics* **1990**, *9*, 709.
(b) Mann, B. E.; Taylor, B. F. *^{13}C NMR Data for Organometallic Compounds*; Academic: New York, **1981**.

18 (a) Blandy, C.; Locke, S. A.; Young, S. J.; Schore, N. E. *J. Am. Chem. Soc.* **1988**, *110*, 7540.
(b) Wenzel, T. T.; Bergman, R. G. *J. Am. Chem. Soc.* **1986**, *108*, 4856.
(c) Karsch, H. H.; Appelt, A. *Phosphorus Sulfur* **1983**, *18*, 287.
(d) Engelhard, L. M.; Jacobsen, G. E.; Raston, C. L.; White, A. H. *J. Chem. Soc., Chem. Commun.* **1984**, 220.
(e) Chiu, K. W.; Wong, W. K.; Wilkinson, G.; Galas, A. M. R.; Hursthouse, M. B. *Polyhedron* **1982**, *1*, 37.

19 Latesky, S. L.; McMullen, A. K.; Rothwell, I. P.; Huffmann, J. C. *J. Am. Chem. Soc.* **1985**, *107*, 5981.

20 Krassowki, D. W.; Nelson, J. H.; Brower, K. R.; Hauenstein, D.; Jacobson, R. A. *Inorg. Chem.* **1988**, *27*, 4294.

21 Joshi, A. M.; James, B. R. *Organometallics* **1990**, *9*, 199.

22 Collman, J. P.; Hegedus, L. S.; Norton, J. R.; Finke, R. G. *Principles and Applications of Organotransition Metal Chemistry*; University Science Books: Mill Valley, CA, **1987**, Chapter 4, p 239.

23 Kosolapoff, G. M. *Organophosphorus Compounds;* John Wiley: New York, **1950**, Chapter 1, p. 24.

CHAPTER 3

Reactivity of the Iridium(III) Phosphide Complexes with Alkynes

3.1 Introduction

In the last ten years, several reports on the reactivity of terminal phosphide complexes have been published.[1] Due to the presence of a lone pair of electrons on the pyramidal phosphide (See Chapter 1, Section 1.3.2), nucleophilic properties are normally associated with this type of phosphorus centre.[2] For example, the complex *trans*-[$Cp(CO)_2(PMe_3)Mo(PPh_2)$] reacts with the electrophilic reagents MeI or HCl to yield products in which the phosphide ligand has been methylated or protonated, respectively (Scheme 3.1).[3] On the other hand, the formal charges present in planar phosphide derivatives (Chapter 1, Section 1.3.2) suggest that this phosphorus centre should display electrophilic character. Since complexes containing planar phosphide ligands are rare, little is known about their reactivity patterns.[4] However, the following example will serve to illustrate the electrophilic nature of this type of phosphorus centre. The complex $Cp(CO)_2W[P(CMe_3)_2]$ undergoes spontaneous reaction with ROH (R = H, Me, Et) to form the derivative in which the alcohol group has added across the metal–phosphorus double bond with the nucleophilic RO^- group adding to the phosphorus (Equation 3.1).[5]

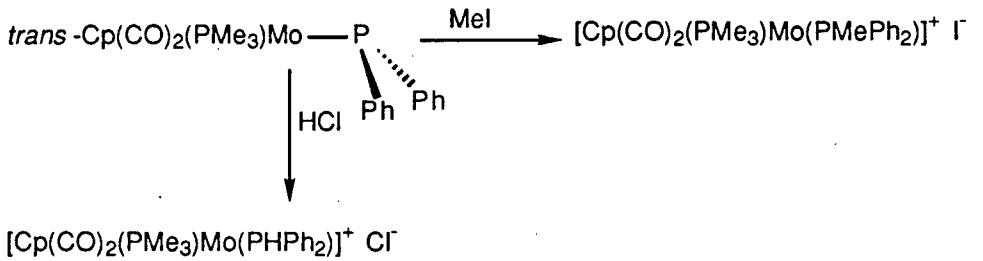

Scheme 3.1

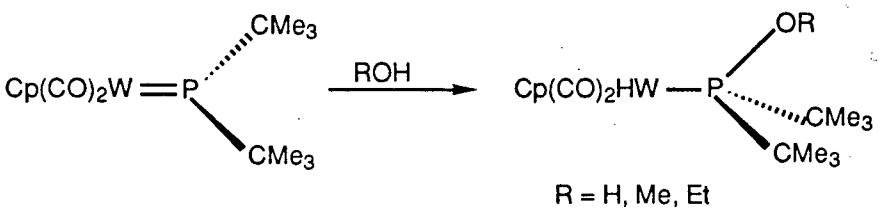

Equation 3.1

To our knowledge, there is no report in the literature describing the reactivity of mononuclear phosphide complexes with alkynes, but some reactions of binuclear complexes containing bridging phosphide ligands with alkynes have been published.[6] Relevant to the thesis work is the following example: the complex $[Fe(CO)_3]_2$-$(\mu$-$PHPh)_2$, when exposed to one equivalent of dimethylacetylenedicarboxylate (DMAD) in the presence of the base piperidine, undergoes a Michael-type addition reaction[7] with the alkyne to yield two products (Equation 3.2).[8] In the product **A**, the alkyne binds to one of the phosphide ligands; whereas, in the product **B**, both the carbons of the alkyne are bridged between the two phosphide ligands.

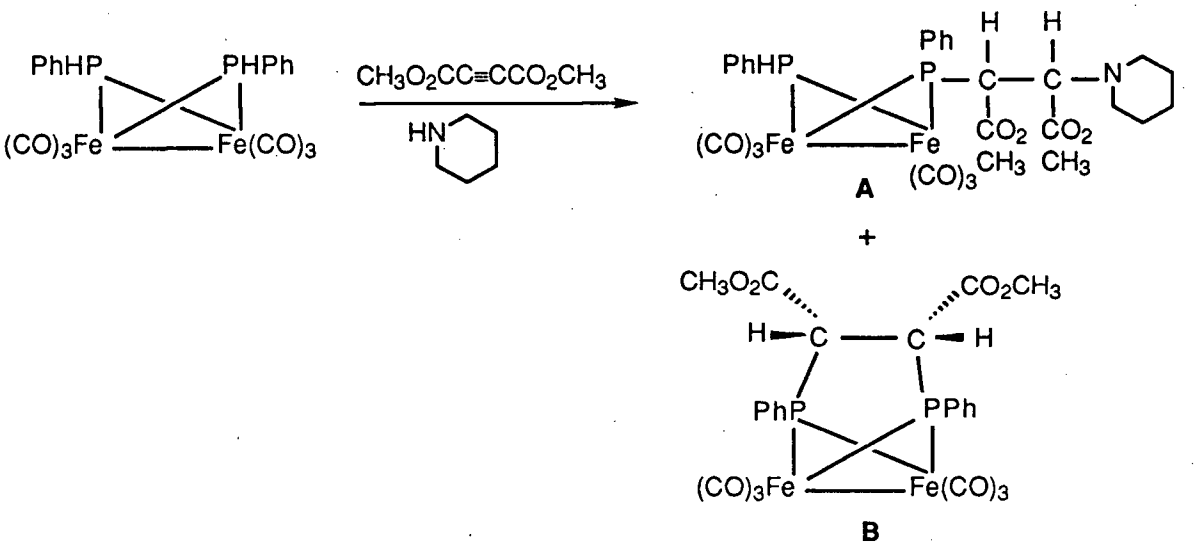

Equation 3.2

As a part of an ongoing study on the reactivity of iridium(III) phosphide complexes,[9] the reactions of $Ir(CH_3)PR_2[N(SiMe_2CH_2PPh_2)_2]$ (**2a**: R = Ph, **2c**: R = Me) with various alkynes were investigated in an attempt to generate complexes in which the alkyne has bridged between the nucleophilic phosphide phosphorus and the unsaturated metal centre (in other words to generate metallacyclophosphinobutene-type complexes, shown below as **C**). This chapter describes the reactivity of **2a** and **2c** with DMAD, and the reactions of **2a** with the following alkynes: PhC≡CPh, RC≡CH (R = H, Ph, ^{t}Bu).

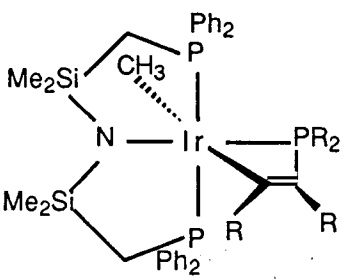

C

3.2 Reaction of $Ir(CH_3)PPh_2[N(SiMe_2CH_2PPh_2)_2]$, 2a, with DMAD

Addition of one equivalent of DMAD to the toluene solution of the iridium(III) diphenylphosphide, $Ir(CH_3)PPh_2[N(SiMe_2CH_2PPh_2)_2]$, **2a**, at -78°C resulted in the immediate colour change from purple to burgundy (Equation 3.3); recrystallisation from toluene/hexanes at -30°C afforded the new complex, **12**, in good yields (~ 82%).

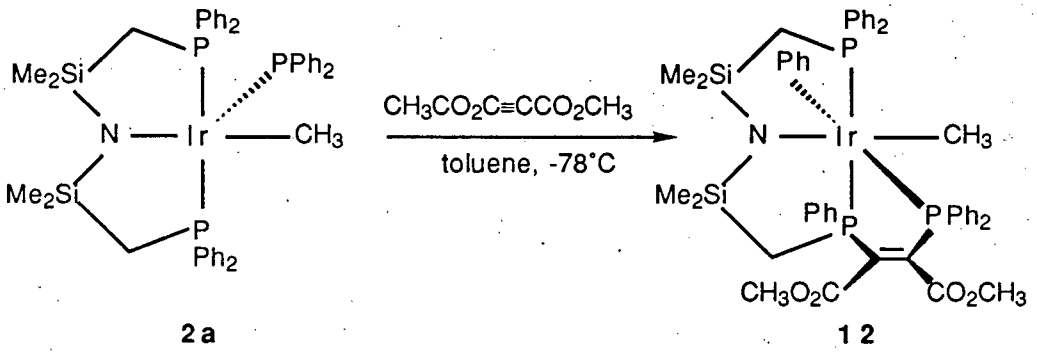

2a **12**

Equation 3.3

The geometry of the product **12** was not obvious from the available NMR spectral information; however, the X-ray crystal structure (Figure 3.1) revealed that one of the phosphorus phenyl substituents had migrated to the iridium centre. The phosphide group is now part of a tetradentate ligand joined by the DMAD unit, and the newly formed tetradentate ligand is in the *cis*-β configuration [P(1)–Ir–P(3) = 96.16°]. The methyl ligand is oriented *trans* to the amide [C(49)–Ir–N = 173.6°]. The C=C bond length of 1.34 Å is the same as reported for several alkenyl complexes.[10] Some selected bond lengths and bond angles are listed in Tables 3.1 and 3.2.

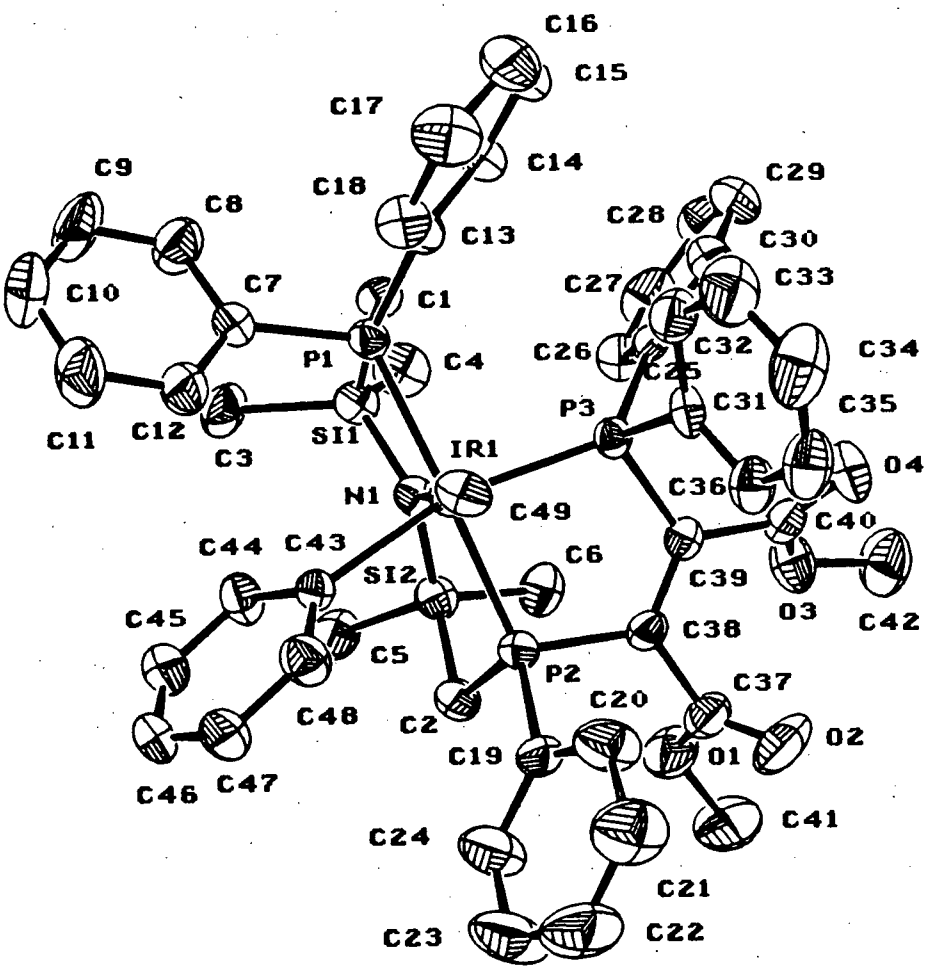

Figure 3.1 X-ray crystal structure of $Ir(CH_3)PPh_2\{C_2(CO_2Me)_2\}$-$[N(SiMe_2CH_2PPh_2)_2]$,**12**

Table 3.1 Selected Bond Lengths (Å) for $Ir(CH_3)PPh_2\{C_2(CO_2Me)_2\}[N(SiMe_2CH_2PPh_2)_2]$, **12**[a]

Ir—P(1)	2.352(2)
Ir—P(2)	2.288(2)
Ir—P(3)	2.335(2)
Ir—C(43)	2.145(7)
Ir—C(49)	2.119(7)
Ir—N	2.281(5)
C(38)—C(39)	1.34(1)

Table 3.2 Selected Bond Angles (deg) for $Ir(CH_3)PPh_2\{C_2(CO_2Me)_2\}[N(SiMe_2CH_2PPh_2)_2]$, **12**[a]

C(43)—Ir—N	89.2(2)	C(49)—Ir—N	173.6(2)
C(43)—Ir—P(1)	98.8(2)	C(49)—Ir—P(1)	90.9(2)
C(43)—Ir—P(2)	81.1(2)	C(49)—Ir—P(2)	99.1(2)
C(43)—Ir—P(3)	164.5(2)	C(49)—Ir—P(3)	89.2(2)
N—Ir—P(1)	84.9(1)	C(43)—Ir—C(49)	86.7(3)
N—Ir—P(2)	85.1(1)		
N—Ir—P(3)	96.1(1)		
P(1)—Ir—P(2)	169.98(6)		
P(1)—Ir—P(3)	96.16(7)		
P(2)—Ir—P(3)	84.88(7)		

a. A complete list of the bond distances and the bond angles is compiled in Appendix A1.

The information provided by various NMR spectra on this complex is consistent with the solid-state data. In the ^{1}H NMR spectrum of **12** (Figure 3.2), silyl-methyl groups and the methylene protons of the ligand backbone resonate as four singlets and four sets of multiplets, respectively. Two sharp singlets at 2.92 and 3.05 ppm are observed for the OCH_3 protons. In addition, the IR data (KBr disc) are also consistent with the formulation owing to the $\nu_{(C=O)}$ absorptions at 1711.7 and 1746.9 cm^{-1} and $\nu_{(C=C)}$ absorption at 1620 cm^{-1}.[8] The three phosphorus nuclei show an AMX pattern in the $^{31}P\{^{1}H\}$ NMR spectrum; the chemical shifts of the PPh_2 phosphorus nuclei are at 41.25 ppm ($^{2}J_{PA,\ PM}$ = 398.3 Hz, $^{2}J_{PA,\ PX}$ = 6.1 Hz) and -17.65 ppm ($^{2}J_{PA,\ PM}$ = 389.8 Hz, $^{2}J_{PM,\ PX}$ = 14.6 Hz). The PPh resonance is observed at 26.85 ppm ($^{2}J_{PA,\ PX}$ = 4.8 Hz, $^{2}J_{PM,\ PX}$ = 7.3 Hz).

One possible mechanism (Scheme 3.2) for the formation of **12** involves prior coordination of the alkyne to the metal centre to generate an octahedral intermediate **A**, which then undergoes nucleophilic attack by the phosphide ligand to form the metallacyclobutene complex (**B**). The alkenyl-phosphine ring in **B** can be considered as a resonance form of the carbene-ylide form (**B'**). Such a representation allows for the migratory insertion of the carbene unit[11] into one of the tridentate phosphine arms of the ancillary ligand yielding **C**, which is followed by the phenyl group migration to the metal.

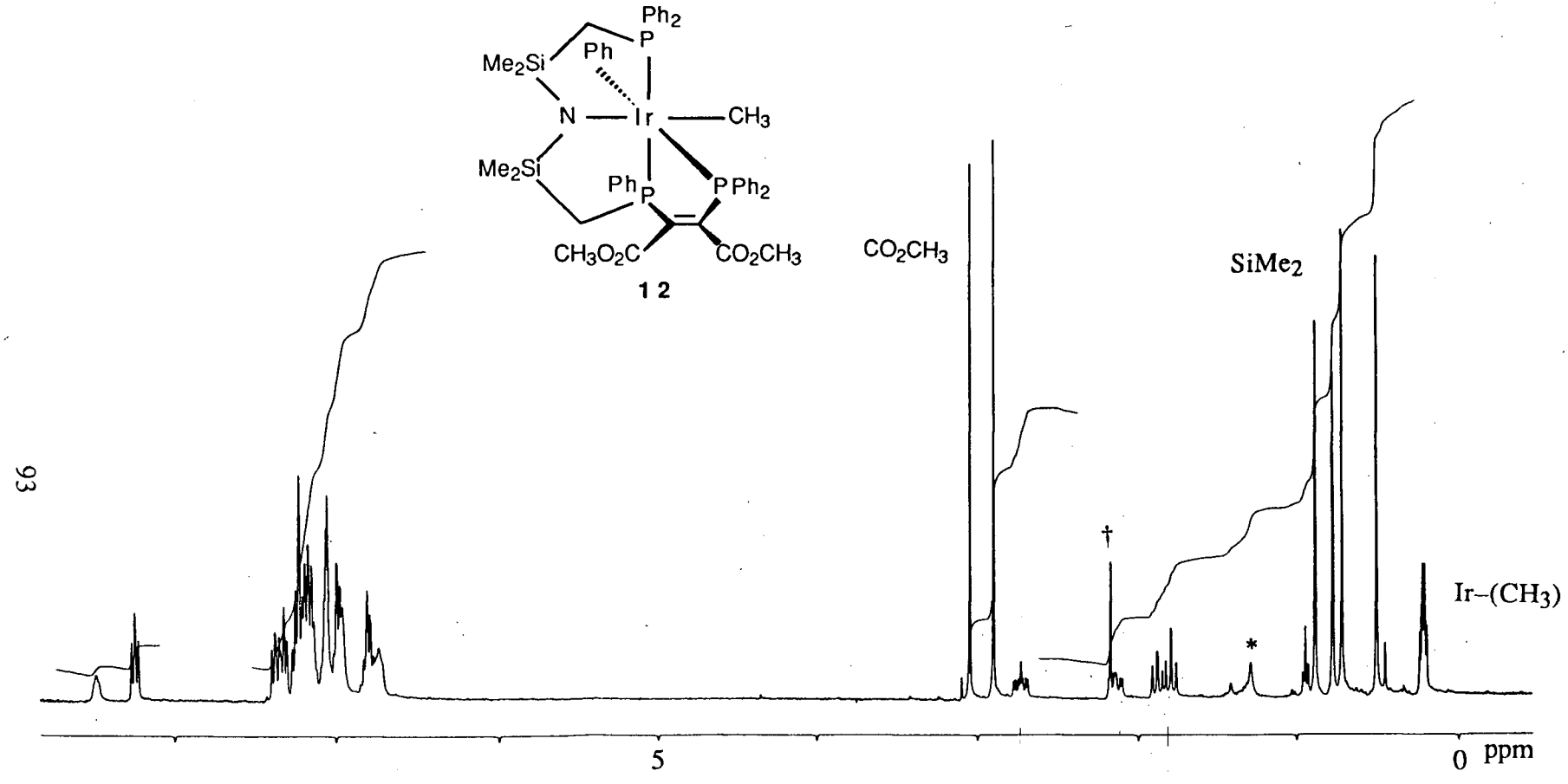

Figure 3.2 ^{1}H NMR spectrum (400 MHz, C_6D_6) of $Ir(CH_3)PPh_2\{C_2(CO_2Me)_2\}[N(SiMe_2CH_2PPh_2)_2]$, **12**, (* indicates hexanes protons, † indicates toluene protons)

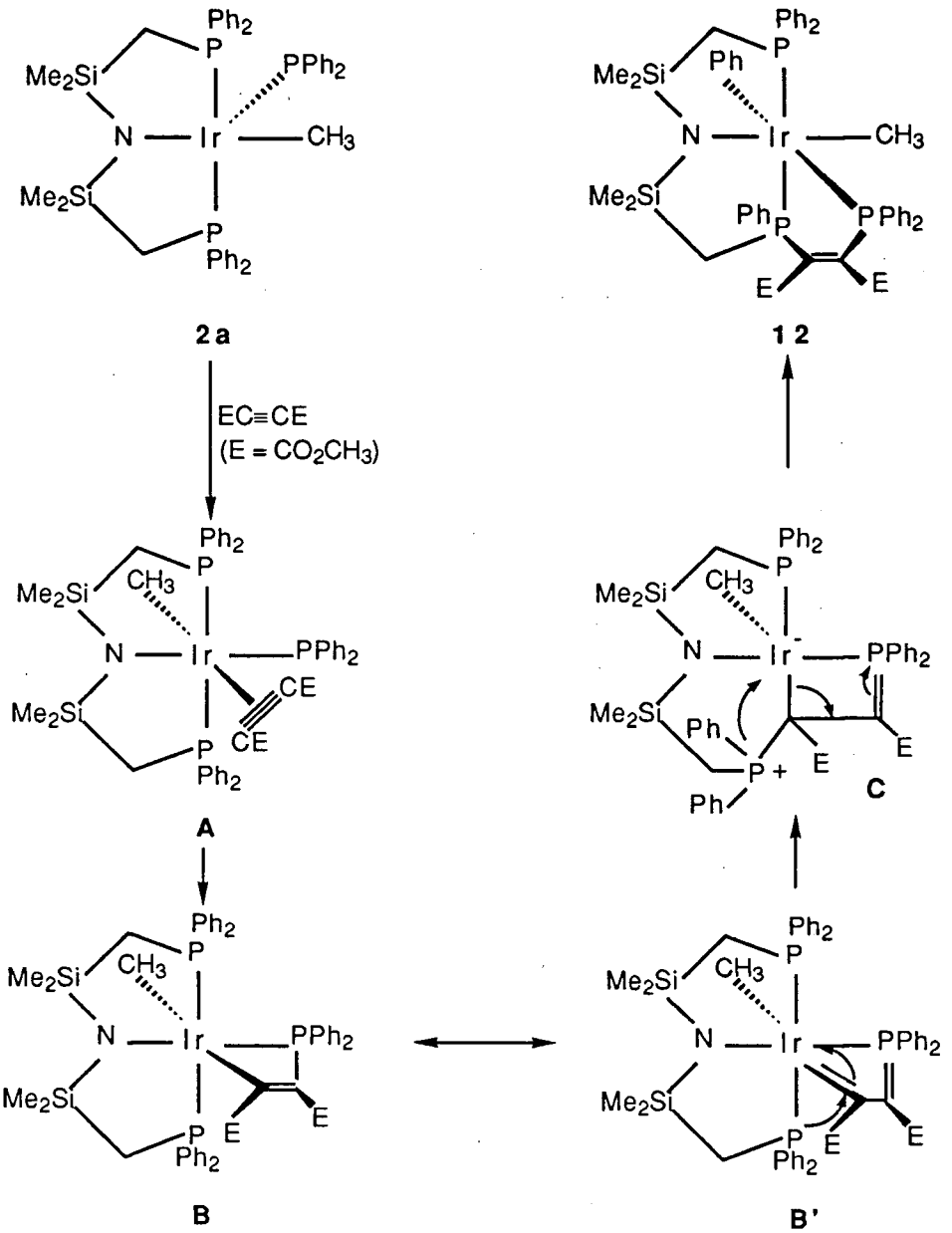

Scheme 3.2

Examples of binuclear systems involving phenyl migration from a coordinated phosphine ligand have been reported in the literature.[12] However, these transformations usually occur at high temperatures. The reaction of $[Fe_2(CO)_7(\mu\text{-dppm})]$ with acetylene produces $\{Fe_2(CO)_5(\mu\text{-CH=CHCO})\text{-}[\mu\text{-}PPh_2CH_2PPh_2]\}$ (shown as **A** in Scheme 3.3) under photolytic conditions.[13] The

complex **A** exists in equilibrium with **A'** via rapid breaking and reforming of the carbon–carbon bond linking the "alkyne" and CO, thus exchanging the ketonic and the terminal CO between the two ends of the alkyne. At ~90°C, complex **A** converts to **B**, which in turn slowly isomerises to **C** in which the phenyl group from one of the phosphine ligands has migrated to one of the methylene ligands. Complexes **A**-**C** were characterised by X-ray crystallography, but the authors did not comment on how these species were formed.

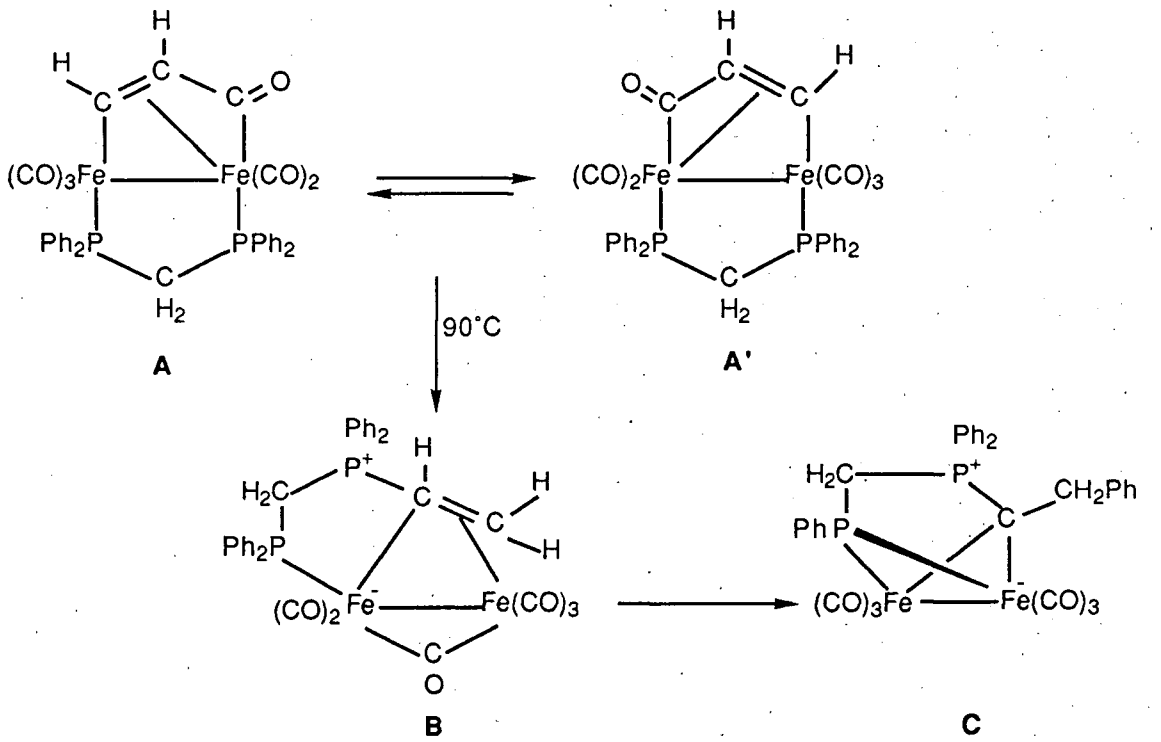

Scheme 3.3

As mentioned before (Chapter 1, Section 1.2), the amido-diphosphine ligand generally acts as an ancillary ligand. There are few other reports where this rather innocent ligand participated in the reaction.[14] One of the examples involved the migratory insertion of CO into nickel(II) carbon bond of Ni(R)[N(SiMe$_2$CH$_2$PPh$_2$)$_2$] (R = CH$_3$, CH=CH$_2$, C$_6$H$_5$) and promoted a rearrangement of the tridentate ligand to generate a nickel(0) dicarbonyl derivative of formula Ni(CO)$_2$[RCON-

$(SiMe_2CH_2PPh_2)_2]$ (Equation 3.4). The next section describes another example where the tridentate ligand has become involved in the reaction.

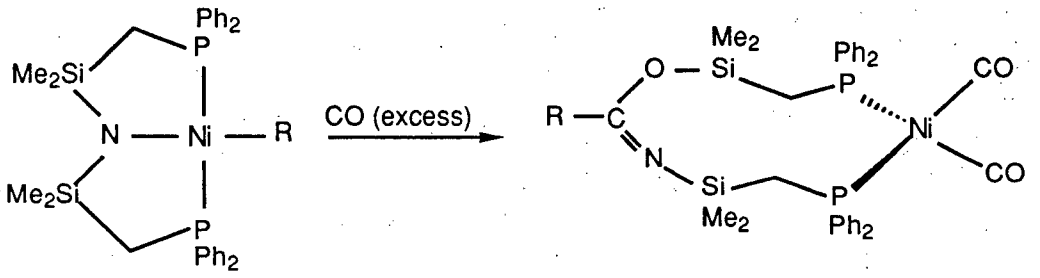

R = CH_3, $CH{=}CH_2$, C_6H_5

Equation 3.4

3.3 Reaction of $Ir(CH_3)PMe_2[N(SiMe_2CH_2PPh_2)_2]$, 2c, with DMAD

Treatment of the purple-coloured toluene solution of $Ir(CH_3)PMe_2$-$[N(SiMe_2CH_2PPh_2)_2]$, **2c**, with one equivalent of DMAD at -30°C yielded a burgundy-coloured solution within minutes; recrystallisation from hexanes/toluene afforded burgundy crystals of **13** (Equation 3.5).

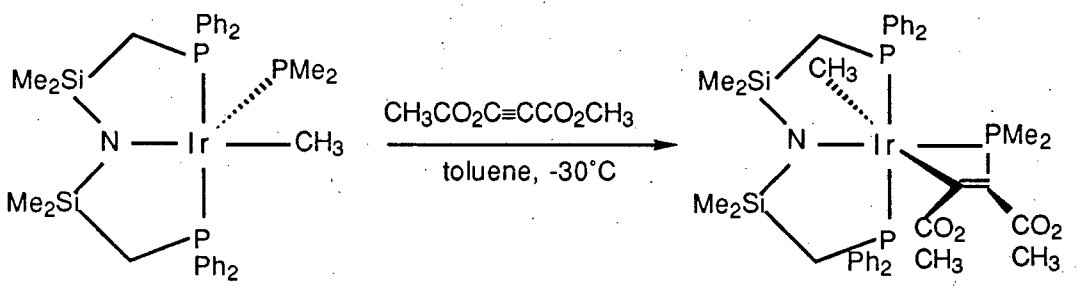

2c **13**

Equation 3.5

The ^1H and $^{31}P\{^1H\}$ NMR spectra of **13** are simpler compared to the spectral features observed for the complex **12**. In the ^1H NMR spectrum (Figure 3.3), two

silyl-methyl singlets and the AB quartet of virtual triplets for the CH_2P protons indicate the two faces of the iridium complex are inequivalent. In addition, the OCH_3 protons are two sharp singlets at 3.27 and 3.88 ppm. Further evidence for this structure is the AX_2 pattern in the $^{31}P\{^1H\}$ NMR spectrum: a doublet at 2.99 ppm ($^2J_{P,P}$ = 23.8 Hz) for the phosphorus nuclei of the ligand backbone, and a triplet at -106.70 ppm.($^2J_{P,P}$ = 23.5 Hz) for the PMe_2 phosphorus centre are observed. Such a high shielding of the phosphorus nucleus of the PMe_2 group is consistent with metallacyclic structures.[15]

From the crude reaction mixture (Equation 3.5), a small amount of burgundy crystals was isolated, which was initially thought to be of the product **13**, and therefore analysed by X-ray crystallography. But, the crystals, characterised as $Ir(CH_3)I\{C_2(CO_2Me)_2\}[N(SiMe_2CH_2PPh_2)_2]$, **14**, originated from the reaction of DMAD with some left-over starting material $Ir(CH_3)I[N(SiMe_2CH_2PPh_2)_2]$, **1**, used in preparing the *in situ* dimethylphosphide complex **2c** (see Chapter 2, Section 2.2). In order to analyse the product **14** fully, it was synthesised in larger quantities by reacting pure **1** with DMAD (Equation 3.6). The reaction proceeded rapidly at room temperature as the green colour of **1** turned burgundy due to the formation of **14**.

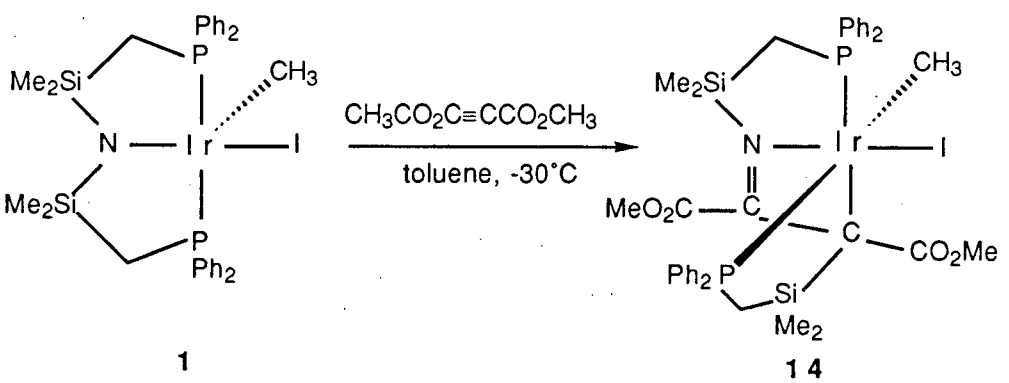

1 **14**

Equation 3.6

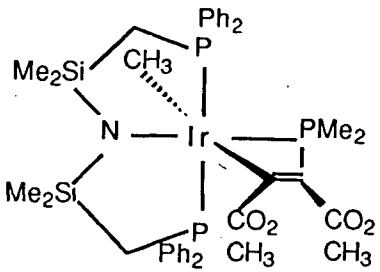

1 3

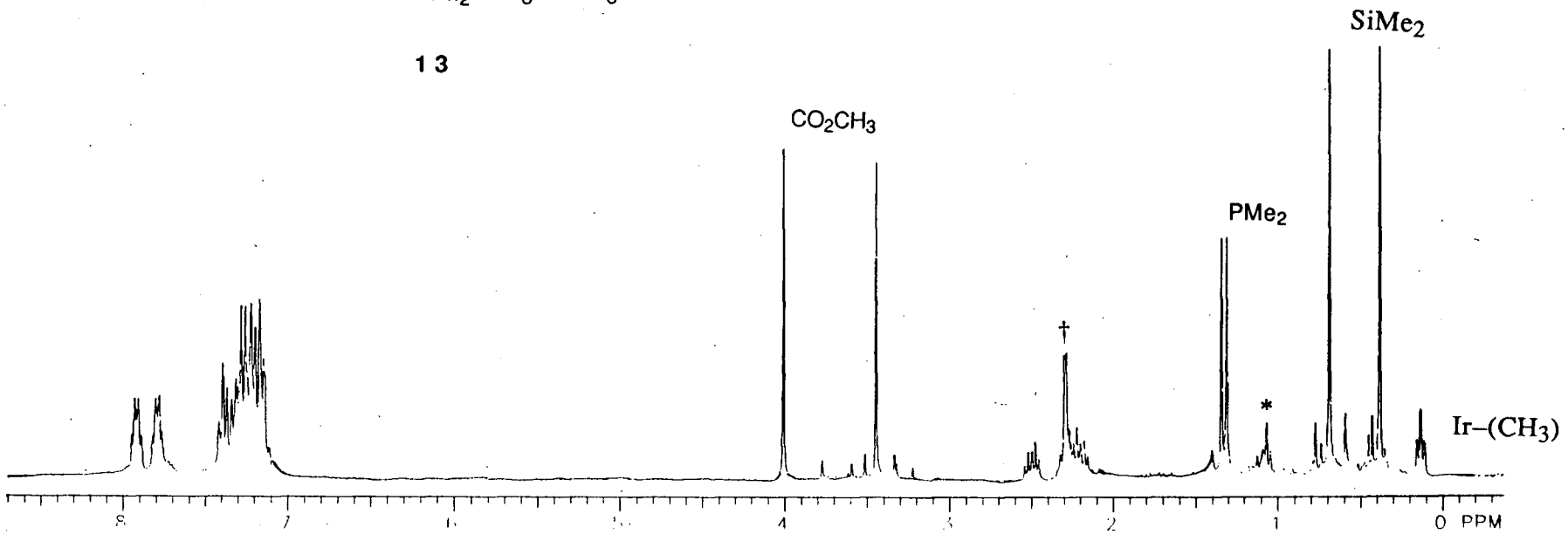

Figure 3.3 ^{1}H NMR spectrum (300 MHz, C_6D_6) of $Ir(CH_3)PMe_2\{C_2(CO_2Me)_2\}[N(SiMe_2CH_2PPh_2)_2]$, **13**,
(* indicates hexanes protons, † indicates toluene protons)

The solid-state structure of **14** (Figure 3.4) reveals that the DMAD unit has been incorporated into the backbone of the ligand between the amide and the silicon atoms. The insertion results in the formation of a carbon–nitrogen double bond, based on the N–C(2) distance of 1.28 Å (Tables 3.3, 3.4), and a new iridium–carbon bond. The N-C(2) bond length coincides well with other known N=C distances (1.28 Å).[17] Similar to complex **12**, the newly formed tridentate ligand is arranged in cis-β configuration [P(1)–Ir–P(2) = 96.37°].

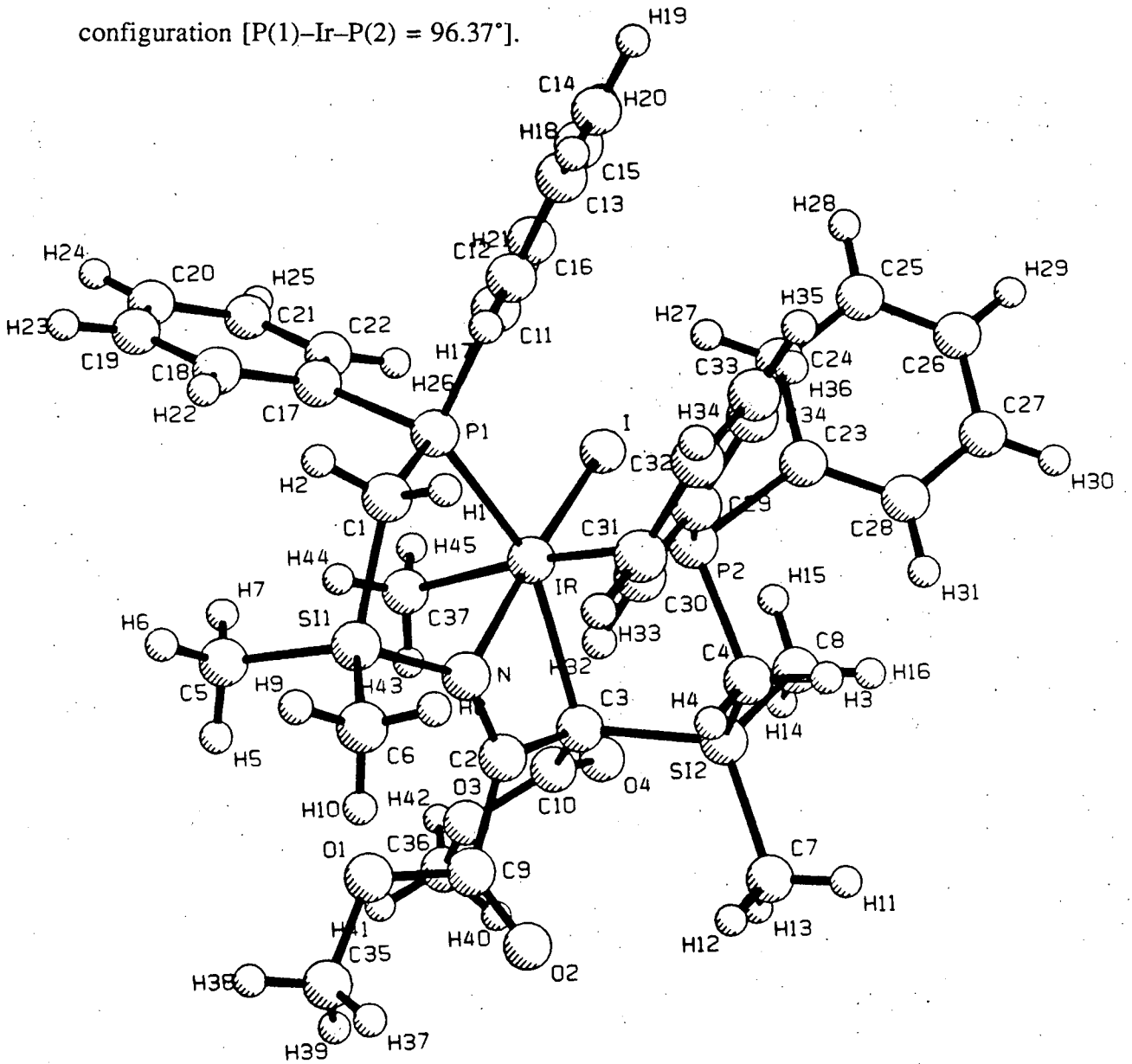

Figure 3.4 X-ray structure of $Ir(CH_3)I\{C_2(CO_2Me)_2\}[N(SiMe_2CH_2PPh_2)_2]$, **14**

Table 3.3 Selected Bond Lengths (Å) for $Ir(CH_3)I\{C_2(CO_2Me)_2\}[N(SiMe_2CH_2PPh_2)_2]$, **14**[a]

Ir—P(1)	2.278(3)
Ir—P(2)	2.433(2)
Ir—C(37)	2.146(9)
Ir—I	2.6929(9)
Ir—N	2.044(9)
Ir—C(3)	2.32(1)
C(2)—C(3)	1.51(1)
N—C(2)	1.28(1)

Table 3.4 Selected Bond Angles (deg) for $Ir(CH_3)I\{C_2(CO_2Me)_2\}[N(SiMe_2CH_2PPh_2)_2]$, **14**[a]

C(37)—Ir—N	85.1(4)	C(3)—Ir—N	64.3(3)
C(37)—Ir—P(1)	91.5(3)	C(3)—Ir—P(1)	155.2(3)
C(37)—Ir—P(2)	172.1(3)	C(3)—Ir—P(2)	88.8(2)
C(37)—Ir—I	84.7(3)	C(3)—Ir—I	104.5(2)
N—Ir—P(1)	91.1(2)		
N—Ir—P(2)	93.7(2)		
N—Ir—I	165.6(2)		
P(1)—Ir—P(2)	96.37(9)		
P(1)—Ir—I	99.24(7)		
P(2)—Ir—I	95.13(7)		

a. A complete list of the bond distances and the bond angles is compiled in Appendix A1.

The spectral information obtained on this complex is consistent with the solid-state structure. The ^1H NMR spectrum of **14** (Figure 3.5) consists of four singlet resonances for the silyl-methyl groups, a set of multiplets for the methylene protons of the ligand backbone, and two singlets for the OCH_3 protons. In the $^{31}P\{^1H\}$ NMR spectrum, the two phosphines being inequivalent show resonances at -20.56 ppm (d, $^2J_{P,P}$ = 7.4 Hz) and +42.34 ppm (d, $^2J_{P,P}$ = 11.0 Hz). The IR spectrum (KBr disc) has two moderate intensity bands at 1676.8 and 1732.8 cm^{-1} ascribed to the $\nu_{(C=O)}$ of the acyl ligands.

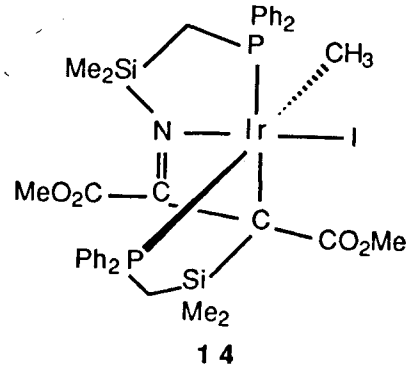

1 4

Figure 3.5 ^{1}H NMR spectrum (400 MHz, C_6D_6) of $Ir(CH_3)I\{C_2(CO_2Me)_2\}[N(SiMe_2CH_2PPh_2)_2]$, **14**,
(* indicates hexanes protons, † indicates toluene protons)

Analogous to the mechanism invoked for the formation of the complex **12**, the synthesis of **14** is thought to involve prior coordination of the alkyne at the iridium centre to afford **A** (Scheme 3.4). Previous work done on the reactivity of **1** with ligands L = CO or PMe_3 has shown that L coordinates *trans* to the methyl ligand and generates octahedral complexes of formula $Ir(CH_3)I(L)[N(SiMe_2CH_2PPh_2)_2]$.[17] The nucleophilic attack by the amide nitrogen at the bound alkyne carbon in a pseudo-Michael-type reaction followed by insertion into N–Si bond leads to the product .

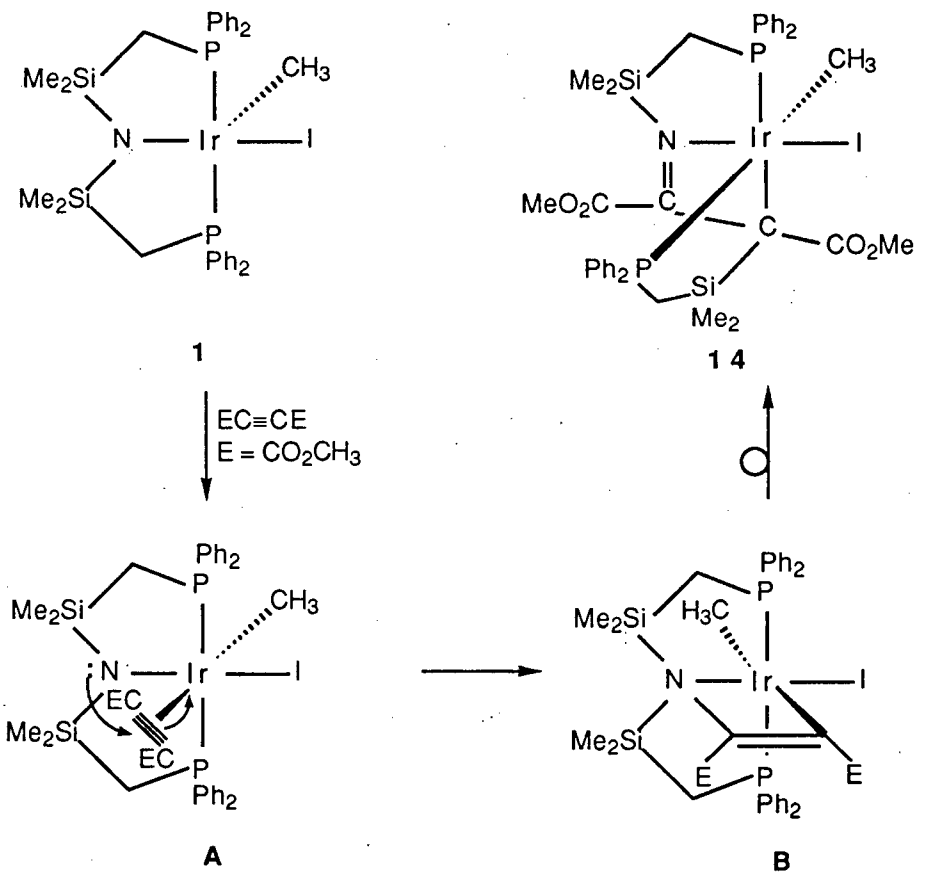

Scheme 3.4

3.4 Reaction of 2a with PhC≡CPh

The complex $Ir(CH_3)PPh_2[N(SiMe_2CH_2PPh_2)_2]$, **2a**, reacted with PhC≡CPh at room temperature within ten minutes with the purple colour of **2a** changing to orange (Equation 3.7). By ^1H and $^{31}P\{^1H\}$ NMR spectroscopy, the product was readily identified as $Ir(PhC{\equiv}CPh)[N(SiMe_2CH_2PPh_2)_2]$, **15**, because it had been prepared previously by the reaction of the iridium(III) dihydride complex $Ir(H)_2[N(SiMe_2CH_2PPh_2)_2]$ with PhC≡CPh.[18]

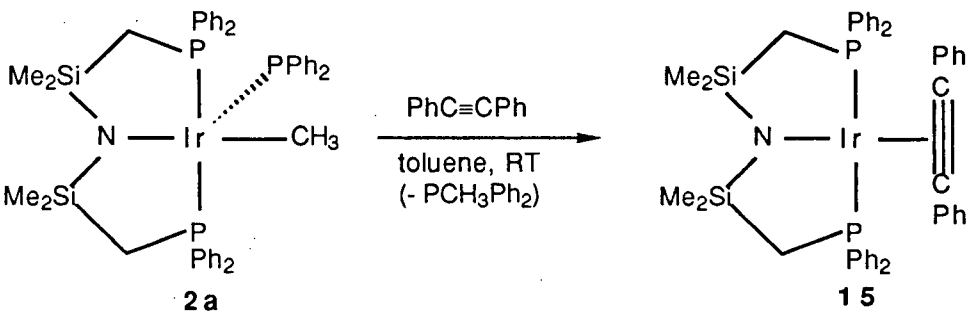

Equation 3.7

The reaction presumably proceeds via the prior coordination of PhC≡CPh at the metal centre. Reductive coupling and elimination of PCH_3Ph_2 (observed by ^1H and $^{31}P\{^1H\}$ NMR spectroscopy) from the metal coordination sphere affords the complex **15**. The work done on the reactivity of the diphenylphosphide complex $Ir(CH_3)PPh_2[N(SiMe_2CH_2PPh_2)_2]$, **2a**, with CO has shown similar results.[19] The reaction of **2a** with excess CO afforded two isomers of formula $Ir(CH_3)PPh_2(CO)$-$[N(SiMe_2CH_2PPh_2)_2]$ (Scheme 3.5). Within 24 hours in solution, these complexes were converted to the iridium(I) carbonyl species $Ir(CO)[N(SiMe_2CH_2PPh_2)_2]$ yielding free methyldiphenylphosphine.

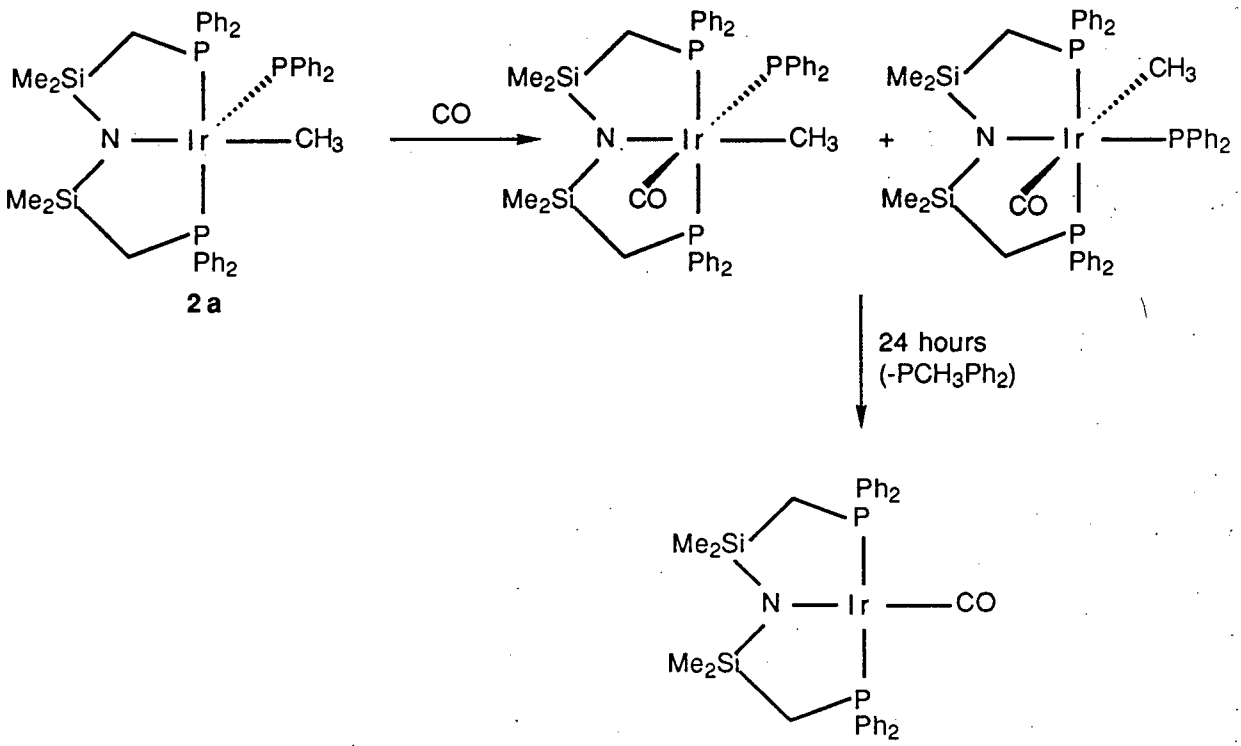

Scheme 3.5

3.5 Reaction of 2a with RC≡CH (R = H, Ph, ^{t}Bu)

The iridium(III) diphenylphosphide complex $Ir(CH_3)PPh_2[N(SiMe_2CH_2PPh_2)_2]$, **2a**, reacted with the terminal alkynes RC≡CH (R = H, Ph, ^{t}Bu) over the period of an hour as the purple solution of **2a** slowly changed to light yellow (Equation 3.8). By ^1H and $^{31}P\{^1H\}$ NMR spectroscopy, the products are formulated as $Ir(CH_3)PHPh_2(C{\equiv}CR)[N(SiMe_2CH_2PPh_2)_2]$, **16-18**. However, none of these species could be isolated because decomposition resulted when solutions of the complexes were left for crystallisation under an inert atmosphere.

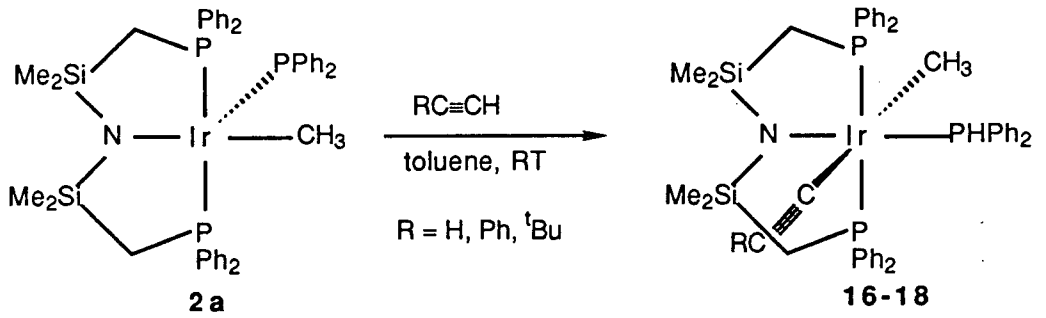

2a **16-18**

Equation 3.8

The ^1H NMR spectra of the products are straightforward. The NMR spectral data of **18** will serve to illustrate this point. Once again, the methylene resonances, observed as an AB quartet of virtual triplets, are indicative of the meridional arrangement of the tridentate ligand. The P*H*Ph$_2$ proton is observed as a doublet of triplets centred at 5.30 ppm ($^1J_{P,H}$ = 360.0 Hz, $^3J_{P,H}$ = 7.2 Hz). This large value of $^1J_{P,H}$ has been observed before in complexes such as Ir(H)$_2$PHPh$_2$-[N(SiMe$_2$CH$_2$PPh$_2$)$_2$] ($^1J_{P,H}$ = 334.7 Hz, $^3J_{P,H}$ = 9.7 Hz).[20] The ^{t}Bu protons resonate as a singlet at 1.72 ppm.

There are three possible stereoisomers for the structures of the complexes **16-18** (Scheme 3.6). The isomer O3 was readily ruled out from the ^1H NMR data for which the methyl protons of the Ir–CH$_3$ ligand would be expected to resonate as a doublet of triplets because of its larger *trans* coupling with the phosphorus of the PHPh$_2$ ligand than its *cis* couplings with the chelating phosphine donors; rather it is observed as a four line pattern (-0.95 ppm, $^3J_{P,H}$ = 5.3 Hz). In the complex Ir(CH$_3$)I-(PCH$_3$Ph$_2$)[N(SiMe$_2$CH$_2$PPh$_2$)$_2$],[19] where the methyl and the methyldiphenyl-phosphine ligands are *trans* oriented, the Ir–CH$_3$ resonance is a doublet of triplets ($^3J_{P,H\ (trans)}$ = 20.0 Hz, $^3J_{P,H\ (cis)}$ = 6.0 Hz).

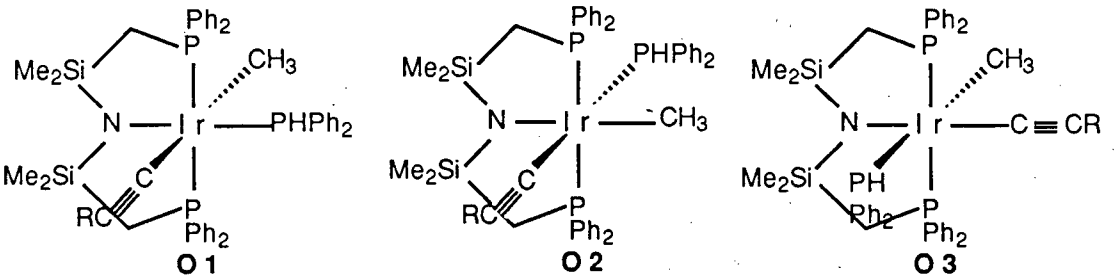

Scheme 3.6

The isomer O2, in which the acetylide and the phosphine ligands are *trans*, is unlikely to form from a mechanistic point of view; that is with the assumption that the product forms via an intramolecular proton abstraction by the phosphide ligand from the alkyne, both the ligands would expected to be *cis*-oriented.

3.6 Summary

The reactivity of **1** and **2a** with DMAD is unusual. Some examples of modification of ancillary phosphine ligands are reported in the literature.[12,13] The results described in this study are the first examples involving the hybrid tridentate ligand where P–C bond formation/cleavage has taken place.

Because of the electron-withdrawing substituents on the DMAD, the alkyne reacts with the electron-rich sites (phosphide and amide) in the complexes **1**, **2a** and **2c**. In the species **2a** and **2c**, which contain two electron-rich centres, namely phosphide and amide, the alkyne preferentially binds to the phosphide site which suggests that the phosphide is likely more basic than the amide centre.

The alkyne PhC≡CPh promotes the elimination of the methyldiphenylphosphine from **2a** which is pehaps because of the steric bulk of the phenyl substituents. In the case of a terminal alkyne (RC≡CH), where an acidic proton is present, after being

coordinated to the metal centre, the alkyne undergoes a proton abstraction by the phosphide ligand to afford an acetylide phosphine complex.

3.7 References

1 Collman, J. P.; Hegedus, L. S.; Norton, J. R.; Finke, R. G. *Principles and Applications of Organotransition Metal Chemistry*; University Science Books: Mill Valley, CA, **1987**, Chapter 3, p.77.

2 Bohle, D. S.; Jones, T. C.; Rickard, C. E. F.; Roper, W. R. *Organometallics* **1986**, *5*, 1612, and references therein.

3 Malish, W.; Maisch, R.; Colquhoun, I. J.; MacFarlane, W. *J. Organomet. Chem.* **1981**, 220, C1.

4 Roddick, D. M.; Santarsiero, B. D.; Bercaw, J. E. *J. Am. Chem. Soc.* **1985**, *107*, 4670, and references therein.

5 Jorg, K.; Malish, W.; Reich, W.; Meyer, A.; Schubert, U. *Angew. Chem., Int. Ed. Engl.* **1986**, *25*, 92.

6 (a) Nucciarone, D.; Taylor, N. J.; Carty, A. J. *Organometallics*, **1988**, *7*, 127.
(b) Iggo, J. A.; Mays, M. J.; Raithby, P. R. *J. Chem. Soc., Dalton Trans.* **1983**, 205.

7 For example, see: March, J. *Advanced Organic Chemistry*; Wiley Interscience: New York, **1985**, Chapter 15, p. 665.

8 Seyferth, D.; Wood, T. G. *Organometallics* **1988**, *7*, 714.

9 (a) Fryzuk, M. D.; Joshi, K. *Organometallics*, **1989**, *8*, 1722.
(b) Fryzuk, M. D.; Bhangu, K. *J. Am. Chem. Soc.* **1988**, *110*, 961.

10 Balegroune, F.; Braunstein, P.; Carneiro, T. M.; Grandjean, D.; Matt, D. *J. Chem. Soc., Chem. Commun.* **1989**, 582.

11 Some examples of carbene insertion into iridium-phosphorus bond have been discussed in chapters 1 and 2. Also see Clark, G. R.; Roper, W. R.; Wright, A. H. *J. Organomet Chem.* **1984**, *C17*, 273.

12 (a) Powell, J.; Sawer, J. F.; Shiralian, M. *Organometallics*, **1989**, *8*, 577.
(b) Chakravarty, A. R.; Cotton, F. A.; Tocher, D. A. *J. Am. Chem. Soc.* **1984**, *106*, 6409.

(c) Farrugia, L. J.; Miles, A. D.; Stone, F. G. A. *J. Chem. Soc., Dalton Trans.* **1984**, 2415.

13 Hogarth, G.; Knox, S. A. R.; Lloyd, B. R.; Macpherson, K. A.; Morton, D. A. V.; Orpen, A. G. *J. Chem. Soc., Chem. Commun.* **1988**, 360.

14 (a) Fryzuk, M. D.; MacNeil, P. A. *Organometallics* **1982**, *1*, 1540.
(b) Fryzuk, M.D.; McManus, N. T.; Rettig, S. J.; White, G. S. *Angew. Chem., Int. Ed. Engl.* **1990**, *29*, 73; also see chapters 4 and 5.

15 (a) Mainz, V. V.; Andersen, R. A. *Organometallics* **1984**, *3*,675.
(b) Werner, H.; Werner, R. J. *J. Organomet. Chem.* **1981**, *C60*, 209.

16 Bohme, H.; Viehe, H. G., Eds. *Iminium Salts in Organic Chemistry, Part I.* Wiley: New York, **1976**, 89.

17 Fryzuk, M. D.; MacNeil, P. A., Rettig, S. J. *Organometallics* **1986**, *5*, 2469.

18 Block, G. *B. Sc. Thesis*, University of British Columbia, Vancouver, Canada, **1986**.

19 Bhangu, K. *M. Sc. Thesis*, University of British Columbia, Vancouver, Canada, **1987**.

20 Some examples of proton abstraction by the phosphide ligand from a coordinated ligand have been discussed in chapter 2 of this thesis; also see reference 9b.

CHAPTER 4

Synthesis and Reactivity of an Iridium Methylidene Complex

4.1 Introduction

The synthesis and characterisation of the iridium methylidene complex, $Ir{=}CH_2[N(SiMe_2CH_2PPh_2)_2]$, **10**, have been reported previously.[1] However, the usual photochemical preparative route (Chapter 1, Scheme 1.5) gives low isolated yield of the methylidene complex with $Ir(H)_2[N(SiMe_2CH_2PPh_2)_2]$ formed as the major product. It was found that the reaction of $Ir(CH_3)I[N(SiMe_2CH_2PPh_2)_2]$, **1**, with KO^tBu gave $Ir{=}CH_2[N(SiMe_2CH_2PPh_2)_2]$, **10**, in higher yield. This chapter describes the synthesis of $Ir{=}CH_2[N(SiMe_2CH_2PPh_2)_2]$, **10**, its reactivity with the electrophiles, MeI and Me_3Al, and with the unsaturated hydrocarbons, 1,2-propadiene (allene), 1,3-butadiene and acetylene. Its reactivity with the nucleophiles, $PHPh_2$, PH^tBu_2 and PH_2Ph, has been discussed in chapter 2.

4.2 Improved Synthesis of $Ir{=}CH_2[N(SiMe_2CH_2PPh_2)_2]$, 10

The iridium methylidene complex, $Ir{=}CH_2[N(SiMe_2CH_2PPh_2)_2]$, **10**, was prepared by the reaction of the iridium(III) methyl-iodide derivative, $Ir(CH_3)I$-

$[N(SiMe_2CH_2PPh_2)_2]$, **1**, with excess (~5 equivalents) potassium *tert*-butoxide in toluene (Equation 4.1). The reaction proceeded over two hours with a noticeable colour change from initial deep green to purple colour due to the formation of the iridium methylidene species. The isolated yield of the product is ~60%. The methylidene complex **10** is stable toward the by-product *tert*-butanol for about 24 hours, beyond which it decomposes as the *tert*-butanol presumably reacts with the ligand backbone. The ^1H NMR spectrum of **10** shows the resonance for the methylidene protons at +16.44 ppm (t, $^3J_{P,H}$ = 14.4 Hz).

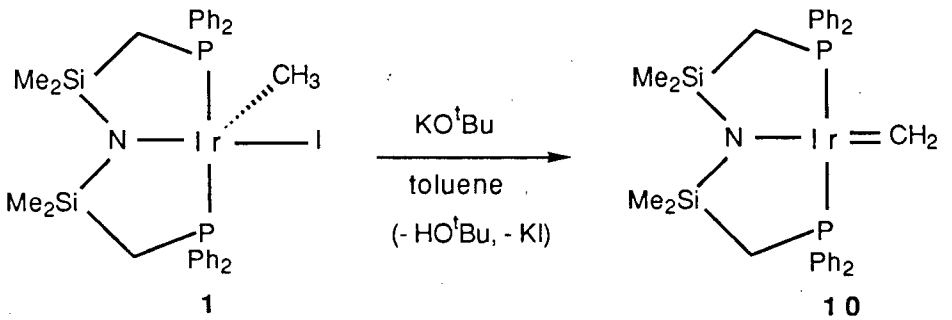

1 **10**

Equation 4.1

In agreement with the iridium(III) methyl-phosphide[2] and the dialkyl chemistry,[3] it is proposed that the synthesis of **10** might proceed through the formation of the iridium(III) methyl *tert*-butoxide intermediate **A** (Scheme 4.1a). The next step involves an intramolecular α-hydride abstraction from the methyl ligand by the butoxide group to generate the methylidene butanol intermediate **B**. The *tert*-butanol ligand dissociates yielding the product **10**. The formation of **10** was followed by ^1H and $^{31}P\{^1H\}$ NMR spectroscopy but no intermediates were observed. An alternative mechanism is shown in Scheme 4.1b which involves intermolecular deprotonation of the α-proton from the methyl ligand by the butoxide base.

The synthesis of the methylidene complex **10** was also attempted by the reaction of the methyl-iodide derivative **1** with $LiN(SiMe_3)_2$, BuLi and $LiNH^tBu$.

While no reaction was observed with $LiN(SiMe_3)_2$, the reaction with BuLi resulted in decomposition. However, the reaction with $LiNH^tBu$ yielded $Ir(H)_2[N(SiMe_2CH_2PPh_2)_2]$ quantitatively, presumably by the loss of $H_2C{=}N^tBu$ (Equation 4.2).

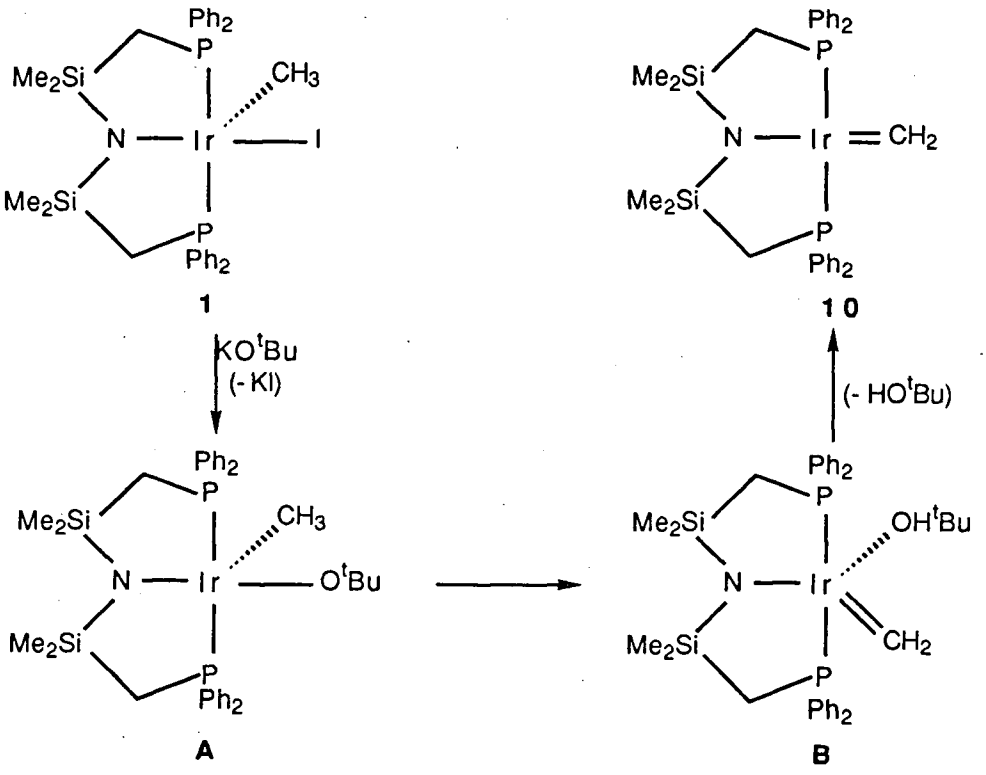

Scheme 4.1a

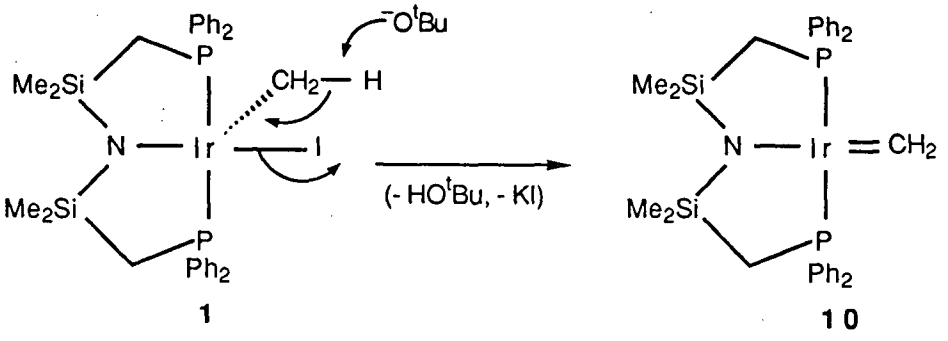

Scheme 4.1b

It was speculated that the dihydride complex might be forming via the iridium(III) methyl *tert*-butylamide, $Ir(CH_3)NH^tBu[N(SiMe_2CH_2PPh_2)_2]$ (**A**), and the methylidene amine, $Ir{=}CH_2(NH_2{}^tBu)[N(SiMe_2CH_2PPh_2)_2]$ (**B**), intermediates (Scheme 4.2). To test this hypothesis, one equivalent of $^tBuNH_2$ was added to the toluene solution of the methylidene complex $Ir{=}CH_2[N(SiMe_2CH_2PPh_2)_2]$, **10** (Equation 4.3). The reaction proceeded over two hours to yield *fac*-$Ir(\eta^2\text{-}CH_2NH^tBu)H[N(SiMe_2CH_2PPh_2)_2]$, **19**. No methylidene amine intermediate **B** was detected by ^1H and $^{31}P\{^1H\}$ NMR spectroscopy. Complex **19** was isolated as pale yellow crystals in good yields (~75%). The ^1H NMR spectrocopic features of this complex are similar to its phosphine analogues, *fac*-$Ir(\eta^2\text{-}CH_2PR_2)H[N(SiMe_2CH_2\text{-}PPh_2)_2]$, described in chapter 2. The hydride ligand, being *trans* to the amide centre of the tridentate ligand, is observed as a doublet of doublets at -20.85 ppm ($^2J_{P,H\ (cis)}$ = 19.5 Hz, $^2J_{P,H\ (cis)}$ = 9.6 Hz). The complex **19** is stable in solution for extended periods of time and does not convert to $Ir(H)_2[N(SiMe_2CH_2PPh_2)_2]$, thus indicating that the formation of the dihydride complex is not proceeding through the intermediates proposed in Scheme 4.2.

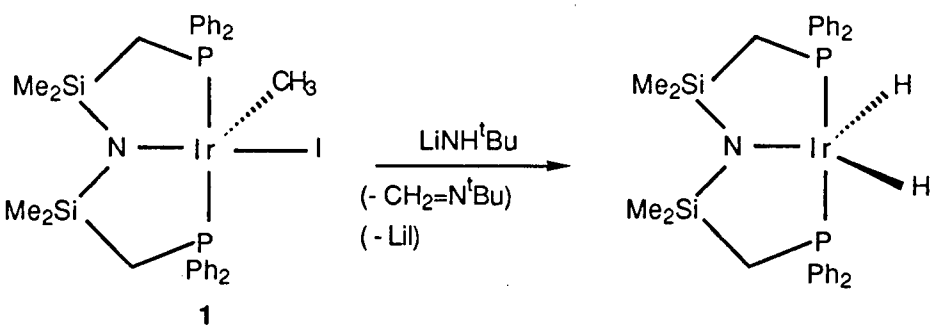

1

Equation 4.2

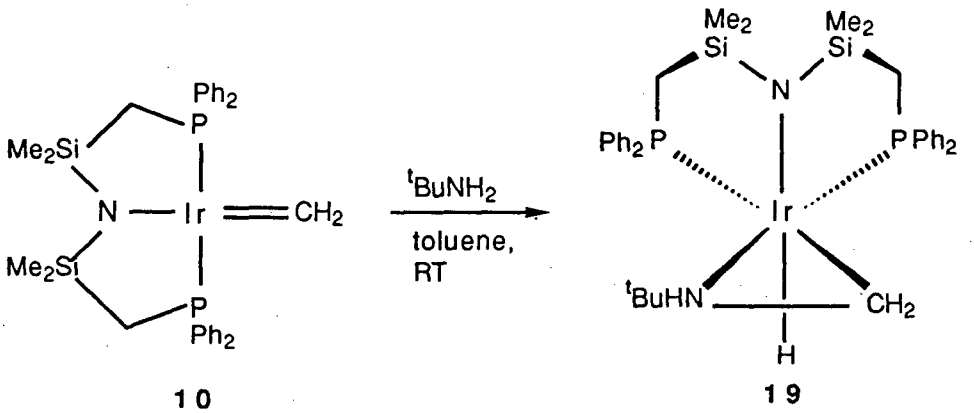

10 19

Equation 4.3

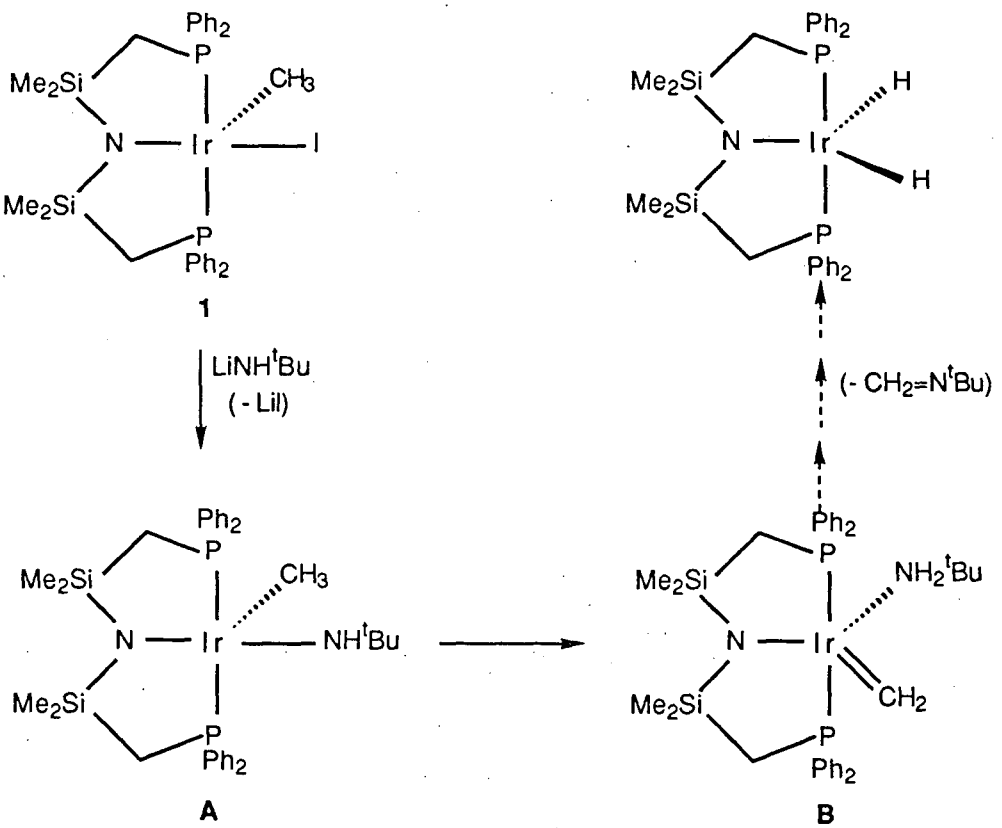

Scheme 4.2

The aforementioned procedure (Equation 4.1) to synthesise **10** could not be extended to generate other alkylidene species. For example, the reaction of the rhodium methyl-iodide complex, $Rh(CH_3)I[N(SiMe_2CH_2PPh_2)_2]$, with KO^tBu

resulted only in decomposition. Furthermore, the reactions of Ir(Ph)I-[$N(SiMe_2CH_2PPh_2)_2$], Ir(CH_2Ph)Br[$N(SiMe_2CH_2PPh_2)_2$], or Ir(CH_2CO_2Me)Br-[$N(SiMe_2CH_2PPh_2)_2$] with KO^{t}Bu to produce the corresponding benzyne, benzylidene or the carbene complex, respectively, were also unsuccessful as decomposition was observed.

4.3 Reactivity of Ir=CH_2[$N(SiMe_2CH_2PPh_2)_2$], 10

Preliminary reactivity patterns of the methylidene complex **10** were investigated by a previous graduate student in our laboratory as a part of her M.Sc. thesis.[4] The reactions of **10** with CO and PMe_3 yielded the iridium(I) complexes of formula Ir(L)[$N(SiMe_2CH_2PPh_2)_2$] (L = CO, PMe_3) and free ethylene (Scheme 4.3). In the case of L = PMe_3, the intermediate Ir=CH_2(PMe_3)[$N(SiMe_2CH_2PPh_2)_2$] was detected below 0°C. The reaction of **10** with ethylene afforded two products: the iridium(I) π-bound ethylene species, Ir(η^2-C_2H_4)[$N(SiMe_2CH_2PPh_2)_2$], and the iridium(III) allyl hydride complex, Ir(η^3-C_3H_5)H[$N(SiMe_2CH_2PPh_2)_2$] in the ratio of 1:2 (Scheme 4.3). Some NMR scale reactions of **10** with methyl iodide and acetylene were also conducted. However, these two latter reactions are re-investigated and are described below along with the reactivity of **10** with trimethylaluminum, 1,3-butadiene and allene.

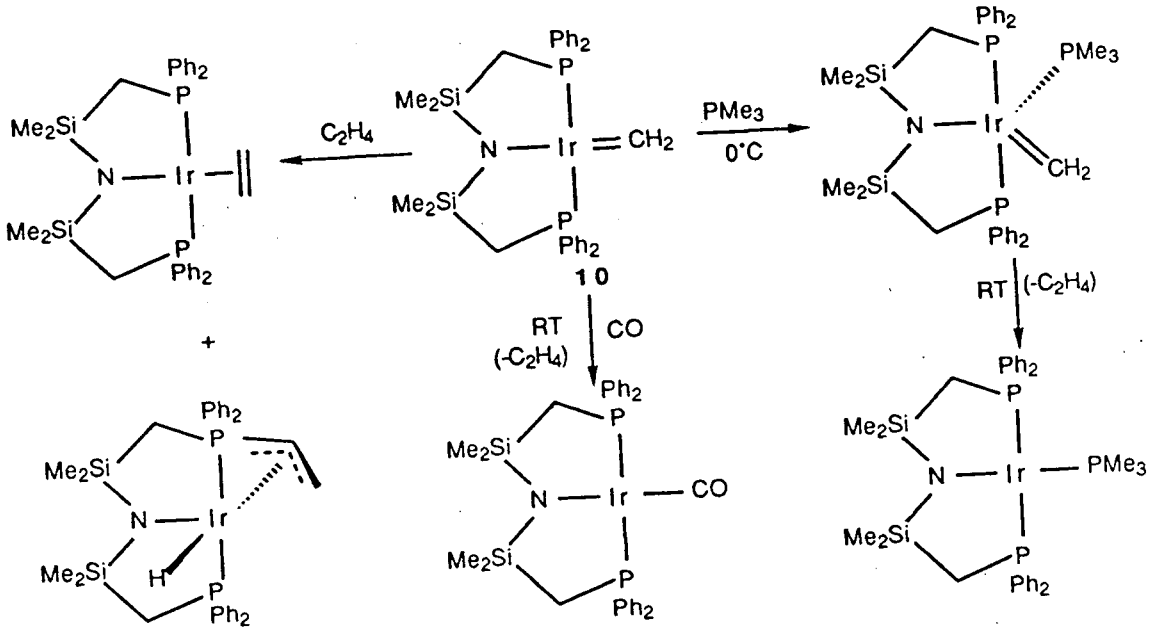

Scheme 4.3

4.3.1 Reactivity with $AlMe_3$ and MeI

As mentioned before (Chapter 1, Section 1.5), Schrock and co-workers examined the reactivity of $Cp_2Ta{=}CH_2(CH_3)$ with the electrophiles $AlMe_3$ and MeI which yielded $Cp_2Ta(CH_2AlMe_2)CH_3$ and $Cp_2Ta(\eta^2\text{-}C_2H_4)I$, respectively.[5] That study along with the reactions with several other substrates pointed towards the nucleophilic nature of the carbene carbon.

The following two sections describe the reactions of $Ir{=}CH_2[N(SiMe_2CH_2\text{-}PPh_2)_2]$, **10**, with $AlMe_3$ and MeI. However, before this work is presented, a brief look at the reactivity of the vinylidene complex, $Ir{=}C{=}CH_2[N(SiMe_2CH_2PPh_2)_2]$ with the same reagents is necessary, because both **10** and the vinylidene complex give rise

to analogous products apparently via similar mechanisms in the presence of these reagents.[6]

The complex $Ir{=}C{=}CH_2[N(SiMe_2CH_2PPh_2)_2]$ reacted cleanly with AlR_3 (R = Me, Et) at room temperature to yield a complex (shown in Figure 4.1) in which the iridium–carbon double bond has inserted into the R group of AlR_3 to generate the isopropenyl ligand, and the AlR_2 moiety has bridged between the iridium–nitrogen bond. The initial step in this reaction is proposed to be the oxidative addition of the AlR_3 reagent at the metal centre in a *cis*-manner.

The reaction of $Ir{=}C{=}CH_2[N(SiMe_2CH_2PPh_2)_2]$ with MeI afforded the iridium(III) allyl iodide complex, $Ir(\eta^3\text{-}C_3H_5)I[N(SiMe_2CH_2PPh_2)_2]$, over the period of 48 hours. The intermediates in this transformation, which are shown in Scheme 4.4, were detected by ^1H and $^{31}P\{^1H\}$ NMR spectroscopy.

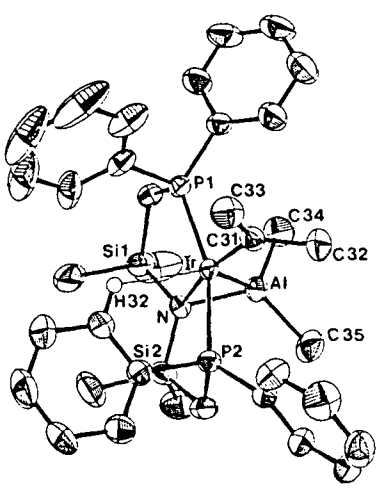

Figure 4.1 X-ray crystal structure of
$Ir(\mu\text{-}AlMe_2)[C(=CH_2)CH_3][N(SiMe_2CH_2PPh_2)_2]$

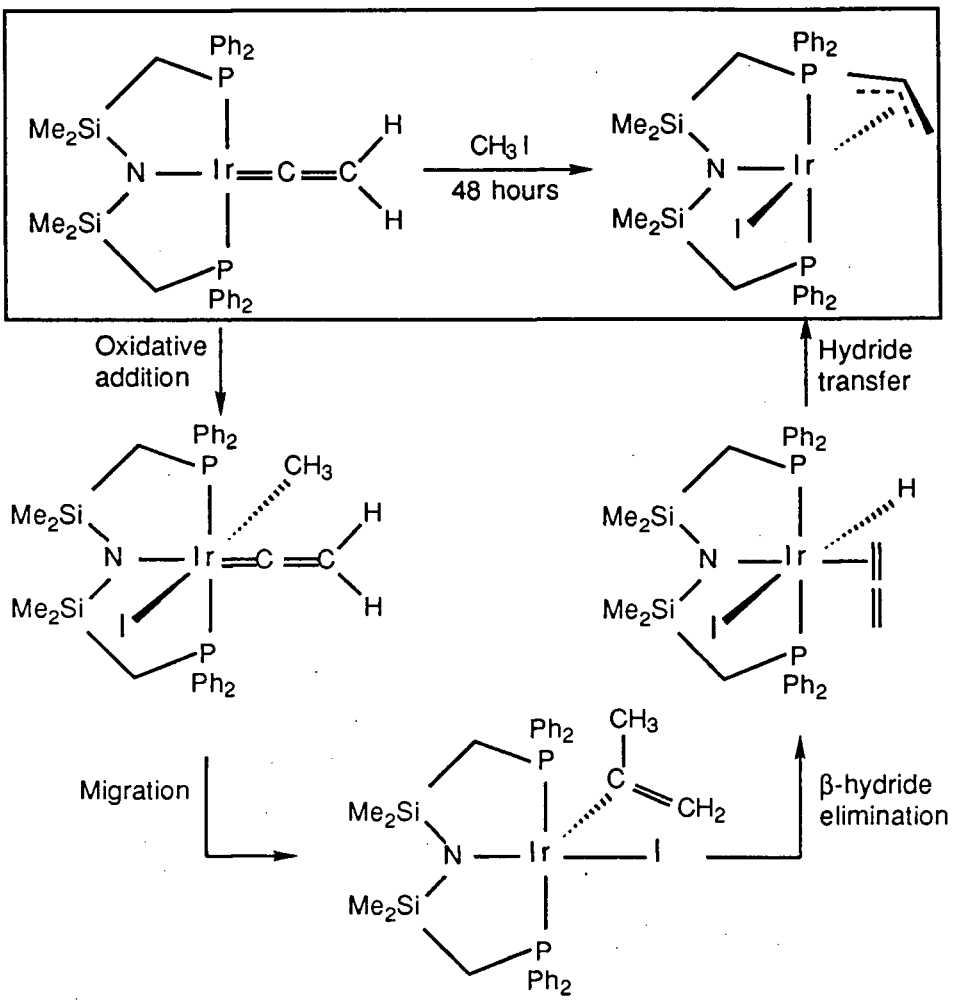

Scheme 4.4

4.3.1.1 Reaction with Trimethylaluminum

Addition of one equivalent of trimethylaluminum to the toluene solution of the iridium methylidene complex, $Ir{=}CH_2[N(SiMe_2CH_2PPh_2)_2]$, **10**, at -78°C resulted in the immediate loss of purple colour and formation of the yellow-orange solution (Equation 4.4); recrystallisation from hexanes at -30°C afforded the new complex **20** in ~70% yield.

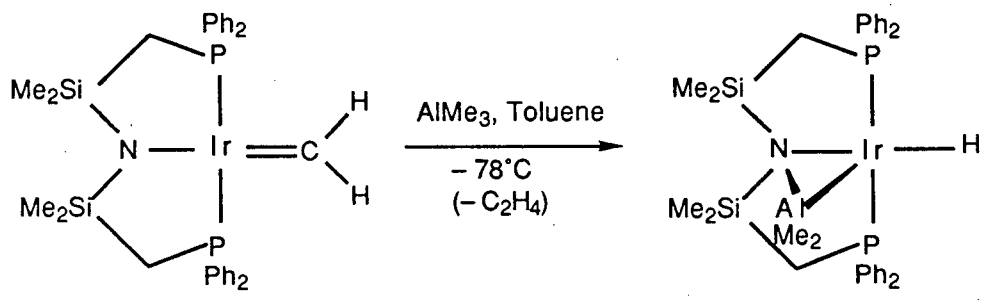

10 **20**

Equation 4.4

In the ^1H NMR spectrum of **20** (Figure 4.2), the silyl methyl protons are observed as two singlets. The methylene protons resonate as two broad multiplets at 2.47 and 2.65 ppm. One set of the *ortho* phenyl protons is also a broad resonance (8.15 ppm). The broadening of the certain peaks might be due to the presence of a quadrupolar nucleus [^{27}Al (I = 5/2)] in the molecule. The methyl protons in the $AlMe_2$ ligand are observed as a singlet at 0.78 ppm. The iridium-hydride ligand resonance is observed as a triplet at -13.47 ppm ($^2J_{P,H}$ = 16.3 Hz). Free ethylene was detected in the ^1H NMR spectrum (5.48 ppm, s, C_6D_6) on conducting the reaction in a sealed NMR tube. The proposal that the $AlMe_2$ ligand is bridged between the Ir–N bond is based upon the above mentioned results obtained from the reactivity of the iridium vinylidene complex, $Ir{=}C{=}CH_2[N(SiMe_2CH_2PPh_2)_2]$, with AlR_3 (R = Me, Et).

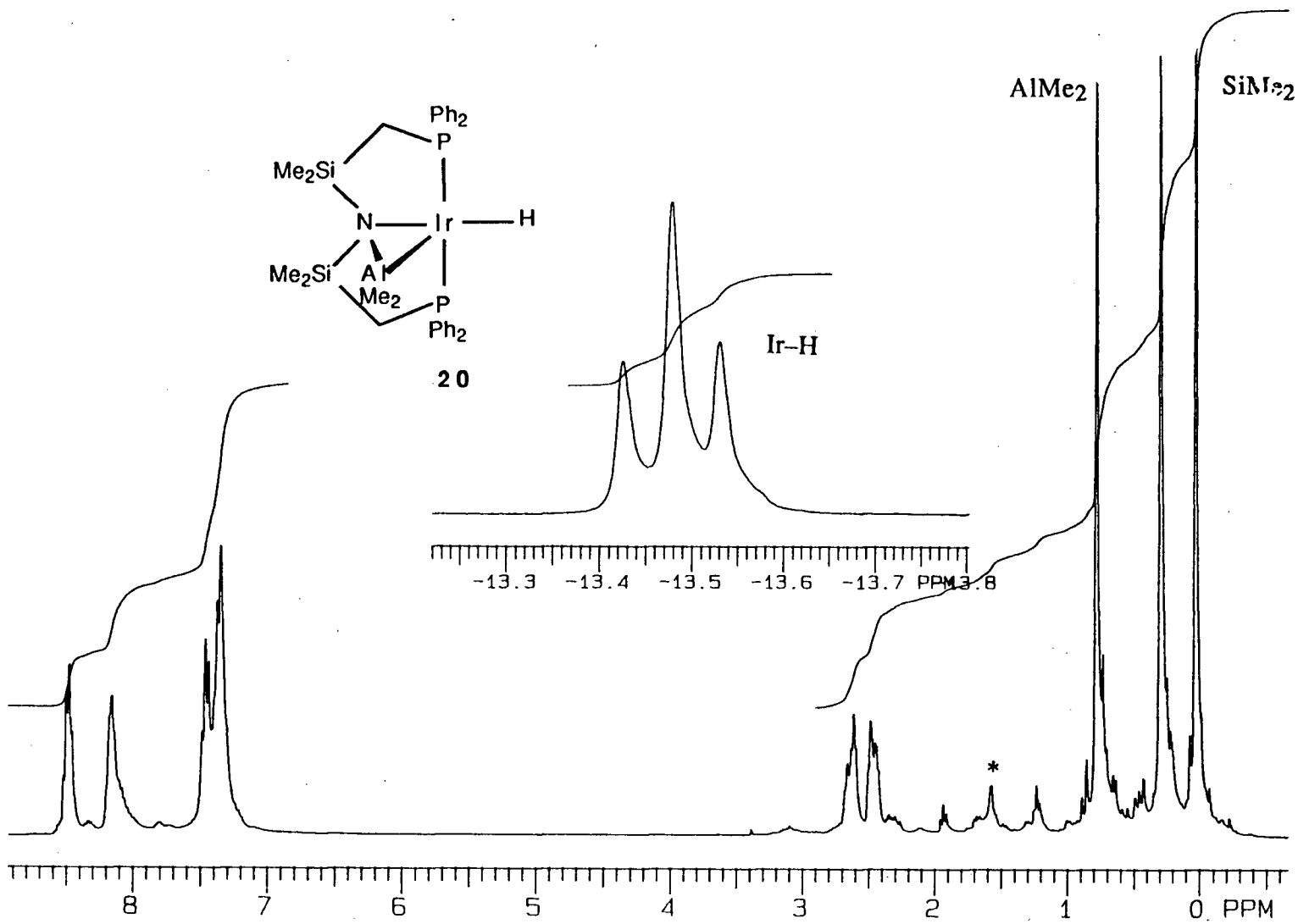

Figure 4.2 ^{1}H NMR spectrum (300 MHz, C_6D_6) of Ir(μ-$AlMe_2$)H[N($SiMe_2CH_2PPh_2$)$_2$], **20**
(* indicates hexanes protons)

A mechanism proposed for the formation of $Ir(\mu\text{-}AlMe_2)H[N(SiMe_2CH_2\text{-}PPh_2)_2]$, **20**, is shown in Scheme 4.5. To keep in line with the vinylidene chemistry, it is proposed that the reaction is likely to involve the oxidative addition of $AlMe_3$ at the metal centre to generate a transient species having an $AlMe_2$ ligand, an alkyl and a methylidene ligand (**A**). Aluminum-alkyl bond cleavage via oxidative addition reaction of trialkylaluminum reagents is rare; however, a recent report by Thorn and Harlow described the oxidative addition of trimethylindium with $IrMe(PMe_3)_4$ to yield *cis*-$Ir(Me)_2InMe_2(PMe_3)_3$.[7] Given that the oxidative addition of $AlMe_3$ reagent at the iridium centre proceeds in a *cis* manner, another possible isomer of **A** can be generated (shown as **A'** in Scheme 4.5). However, the next step which involves the migration of the methyl unit into the iridium methylidene moiety to form the ethyl ligand (**B**) will prefer **A** in which the methylidene unit and the methyl ligand are disposed *cis* to each other, thus excluding the isomer **A'**. Insertion reactions of carbene ligands into alkyl ligands are known,[8] and are considered to be analogous to the migratory insertion reactions of carbonyl complexes.[9] The next step involves the β-hydride elimination from the ethyl ligand in **B** thus yielding the iridium ethylene hydride intermediate (**C**). The elimination of the ethylene moiety from the metal centre followed by the formation of the $AlMe_2$ bridge between the amide N atom and the Al atom yields the final product.

The iridium-aluminum adduct **20** is extremely moisture sensitive in solution. Trace amounts of water from the glassware or the solvents were enough to convert it to $Ir(H)_2[N(SiMe_2CH_2PPh_2)_2]$ (as observed by ^1H NMR spectroscopy) and presumably "$HOAlMe_2$".

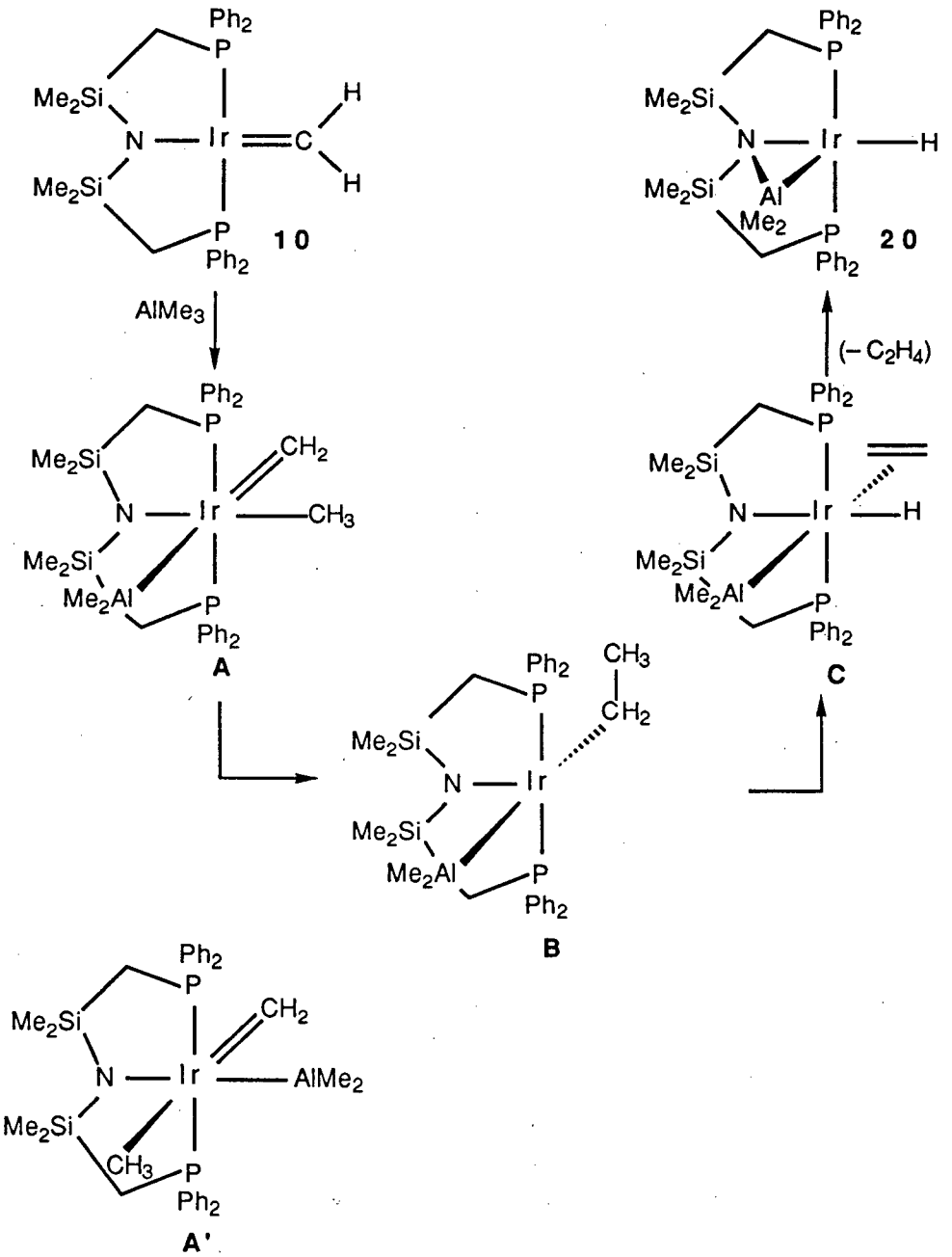
Ph2
P
Me2Si
N
Ir
C
H
Me2Si
P
Ph2
10
AlMe3
CH2
CH3
Me2Al
A
20
(– C2H4)
B
A'
AlMe2

Scheme 4.5

4.3.1.2 Reaction with Methyl Iodide

The methylidene species **10** reacts faster (10 min) with excess MeI than the vinylidene complex (48 hours). The reaction proceeds with a noticeable colour change from initially purple to green and eventually to yellow due to the formation of octahedral iridium(III) ethylene hydrido iodide complex **21** (Equation 4.5).

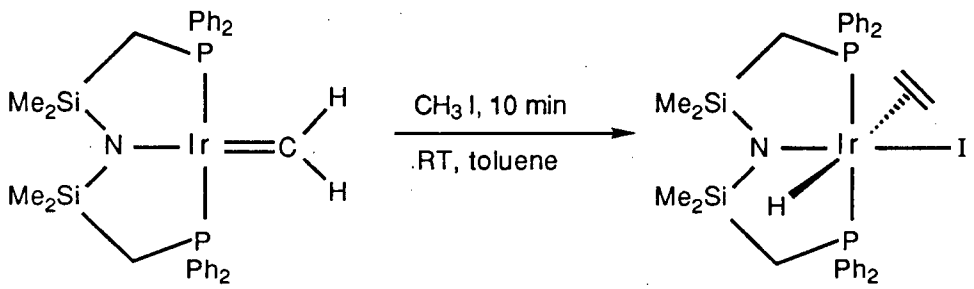

10 **21**

Equation 4.5

The ^1H NMR spectrum (Figure 4.3) provides an excellent handle on the identity and the stereochemistry of this hydride complex. Once again, the resonances of the ligand backbone methylene protons are observed as an AB quartet of virtual triplets and thus are indicative of the meridional arrangement of the tridentate ligand. The resonance for the ethylene protons is a triplet centered at 2.26 ppm ($^3J_{P,H}$ = 3.6 Hz). A triplet at -13.14 ppm ($^2J_{P,H}$ = 8.7 Hz) is due to the Ir–H ligand which can exist *trans* to the amide or the iodide or the ethylene ligand. The former two possibilities are readily ruled out from the ^1H NMR data available on similar complexes. In the complex $Ir(\eta^2\text{-}CH_2PPh_2)H[N(SiMe_2CH_2PPh_2)_2]$, the hydride ligand, which is oriented *trans* to the amide donor, is observed at -19.90 ppm;[10] whereas, when the hydride is oriented *trans* to the iodo ligand in the complex, $Ir(H)_2I[HN(SiMe_2CH_2PPh_2)_2]$, the resonance is observed at -19.39 ppm.[11]

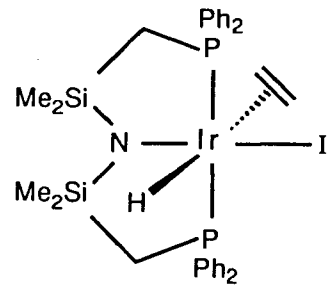

21

Figure 4.3 ^{1}H NMR spectrum (300 MHz, C_6D_6) of $Ir(\eta^2\text{-}C_2H_4)H(I)[N(SiMe_2CH_2PPh_2)_2]$, **21**
{† indicates hexanes protons, * indicates impurities from $Ir(CH_3)I_2[HN(SiMe_2CH_2PPh_2)_2]$}

To account for the formation of **21**, a mechanism is proposed (Scheme 4.6): it involves the oxidative addition of methyl iodide at the metal centre (to form **A**),[12] followed by migratory insertion of the methylene ligand into the iridium-alkyl bond thus yielding the iridium(III) ethyl iodide intermediate (**B**). By analogy with other green-coloured square-pyramidal iridium alkyl halide complexes,[13] the green colour observed in the early stages of the reaction is suggested to originate from the square pyramidal ethyl iodide complex **B**. The β-hydride elimination from the ethyl ligand in **B** would result in the final ethylene hydride complex except that the ethylene and the hydride ligand should be *cis*-oriented to each other. Therefore, hydride abstraction from the ethyl ligand by the amide centre is invoked (which affords **C**), which following inversion at the amine (**D**) and N-H oxidative addition to the metal, gives the desired complex. Complexes which contain both the olefin and the hydride ligands *cis* to each other are rare[14] because the intramolecular migration of a hydride to an olefin to yield an alkyl is quite facile. Some compounds containing both the olefin and the hydride ligands are recognised, and as in complex **21**, these species possess these two ligands in the *trans* orientation.[15]

The presence of excess methyl iodide around **21** causes further reaction to give the methyl bis-iodo-amine complex, $Ir(CH_3)(I)_2[HN(SiMe_2CH_2PPh_2)_2]$ and free ethylene. The same species has also been observed in the reaction of the aforementioned iridium vinylidene complex with excess methyl iodide.

From the above mentioned reactions of **10** with $AlMe_3$ and MeI, it is clear that the methylidene complex $Ir{=}CH_2[N(SiMe_2CH_2PPh_2)_2]$ does not react in the same manner as the Schrock carbene. Instead, the reactions seem to proceed at the metal first due to the unsaturation at the iridium centre, then this is followed by the products resulting from C–C bond formation. Similar results are apparent from the reactions of **10** with various unsaturated hydrocarbons, as described in the following sections.

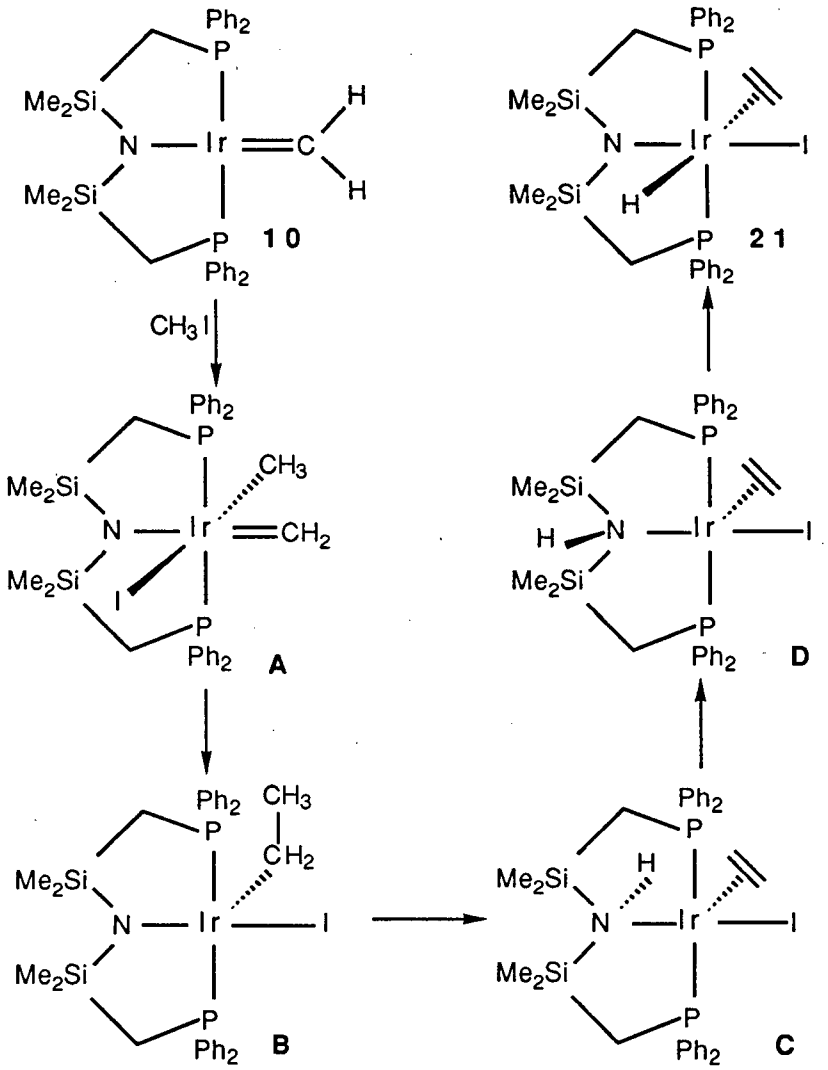

Scheme 4.6

4.3.2 Reactions with Unsaturated Hydrocarbons

4.3.2.1 Reaction with Acetylene

The cycloaddition reaction of a transition metal carbene with an alkyne to give a metallacyclobutene complex is a well-known process.[16] For example, the titanocene methylidene complex, shown in Equation 4.6, reacted cleanly with diphenylacetylene to form the corresponding metallacyclobutene species.[17]

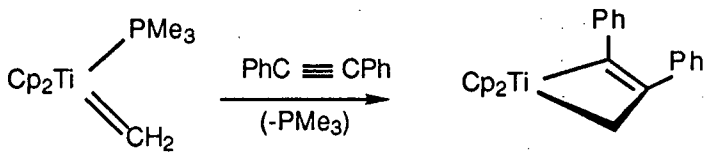

Equation 4.6

The reaction of the iridium methylidene complex **10** with excess acetylene (~5 equivalents) proceeded over two hours in toluene at room temperature (Equation 4.7). The product obtained is the iridium(III) allylic-acetylide species, Ir(η^3-C_3H_5)(C≡CH)[N($SiMe_2CH_2PPh_2$)$_2$], **22**.

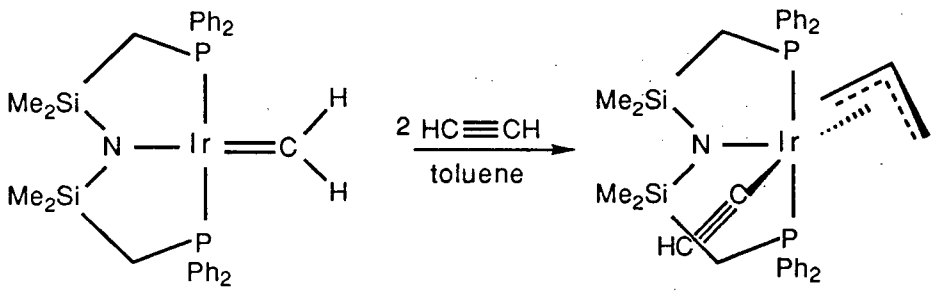

10 **22**

Equation 4.7

The allylic protons in the ^{1}H NMR spectrum (Figure 4.4) of **22** are observed at 3.17 ppm (H_{syn}, dd, $^3J_{P,H}$ = 8.9 Hz, $^2J_{Hsyn,\ Hcentral}$ = 5.2 Hz), 3.95 ppm (H_{anti}, d, $^2J_{Hanti,\ Hcentral}$ = 9.3 Hz) and 4.48 ppm ($H_{central}$, m).[18] The acetylide proton is a singlet at 2.12 ppm. The terminal carbon atoms of the allylic ligand resonate at 53.6 and 54.2 ppm in the $^{13}C\{^1H\}$ NMR spectrum. The central carbon resonance is observed at 110.3 ppm. The α-carbon of the acetylide ligand is found at 90.1 ppm, whereas the β-carbon is observed at 140.0 ppm. The definite assignments of the above mentioned ^{13}C resonances are based on an APT experiment, and are in agreement with the data reported in the literature.[18b,d]

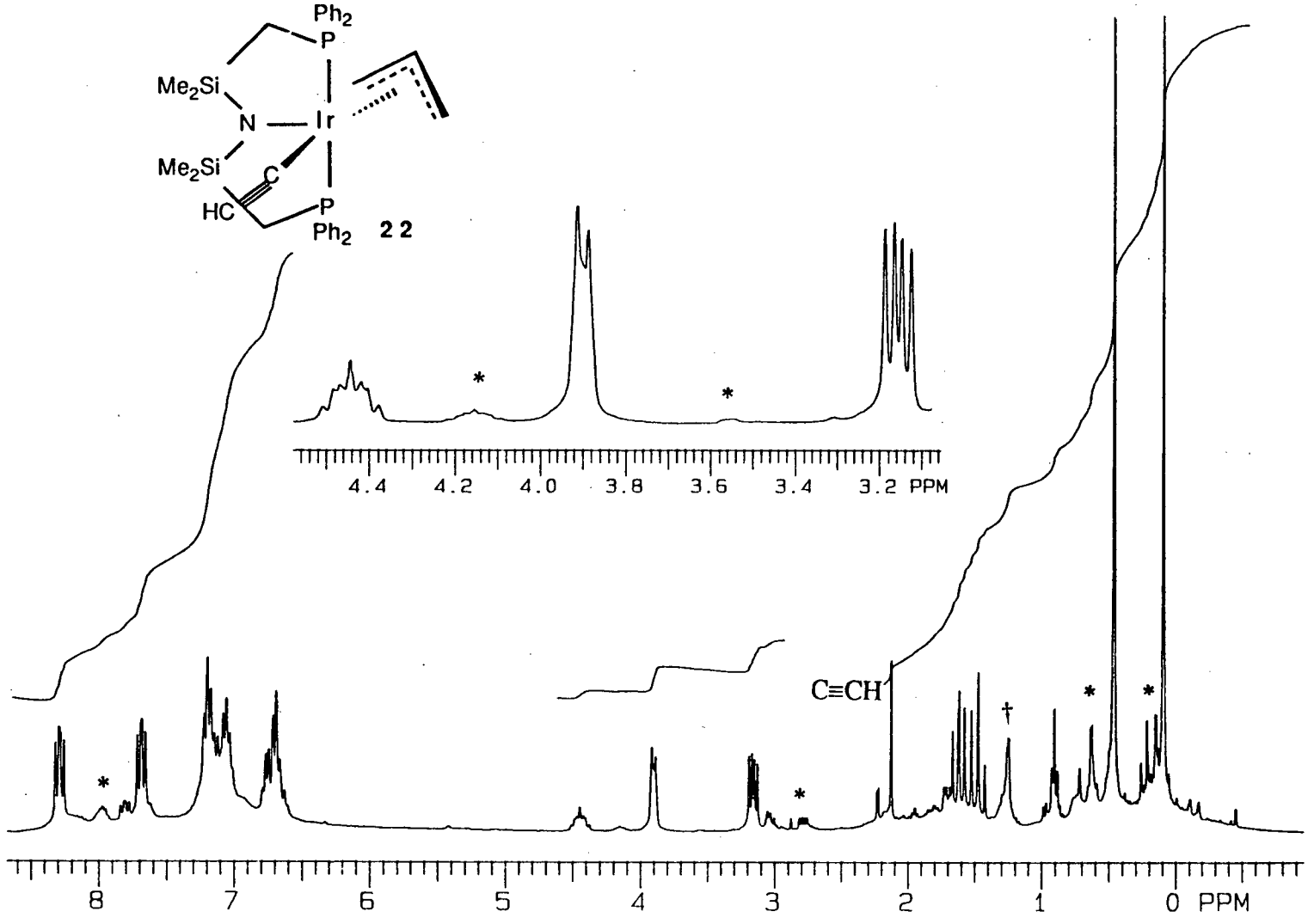

Figure 4.4 ^{1}H NMR spectrum (300 MHz, C_6D_6) of Ir(η^3-C_3H_5)(C≡CH)[N($SiMe_2CH_2PPh_2$)$_2$], **22**
(† indicates hexanes protons, * indicates peaks due to an unknown product)

A proposed mechanism for the formation of **22** is shown in Scheme 4.7. It is likely that the first step involves the coordination of an acetylene ligand at the metal centre (to generate **A**) which is followed by cycloaddition with the methylidene ligand to form the metallacyclobutene intermediate (**B**). Coordination of another acetylene molecule at the empty site on the metal centre (to give **C**) followed by transfer of a proton from the acetylene ligand to the nearest carbon of the metallacycle generates the product.

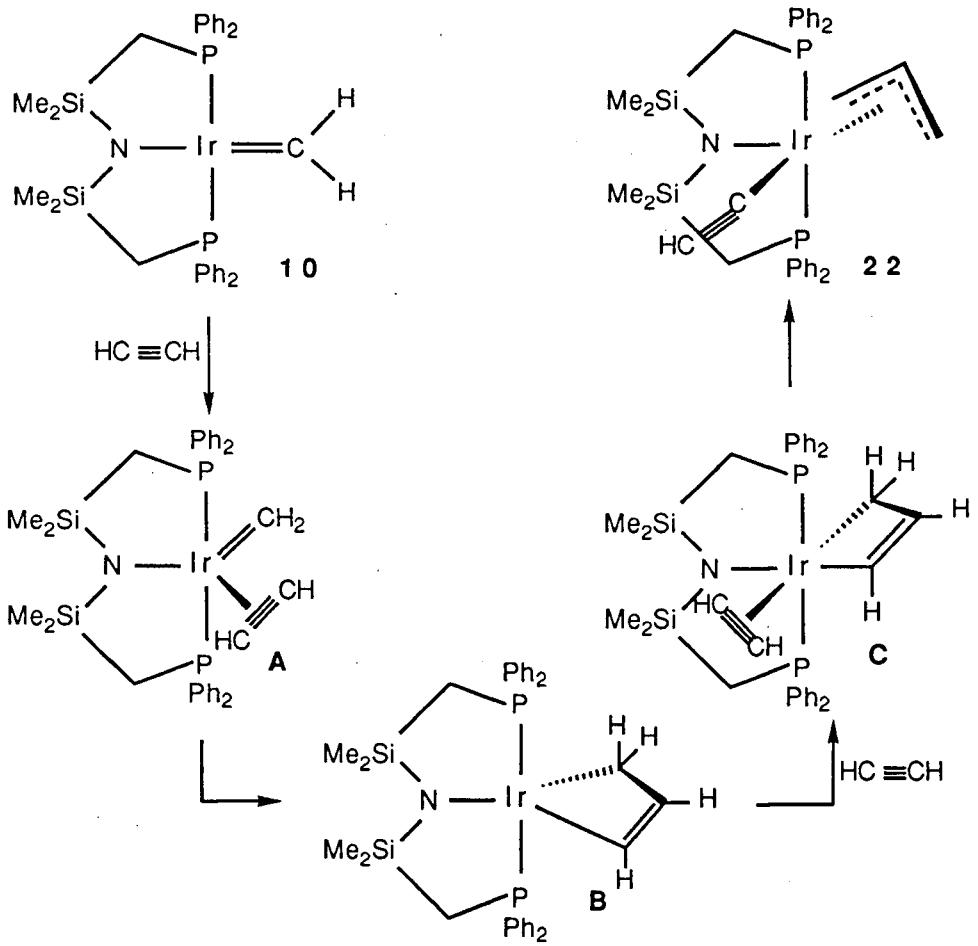

Scheme 4.7

4.3.2.2 Reaction with 1,3-Butadiene

The reaction of the methylidene complex **10** with excess 1,3-butadiene (~5 equivalents) in a toluene solution at room temperature afforded a σ-η^3-pentenyl complex (Equation 4.8). The reaction proceeds over an hour with a colour change from purple to light yellow. The complex $Ir(\sigma\text{-}\eta^3\text{-}C_5H_8)[N(SiMe_2CH_2PPh_2)_2]$ was isolated in >80% yield.

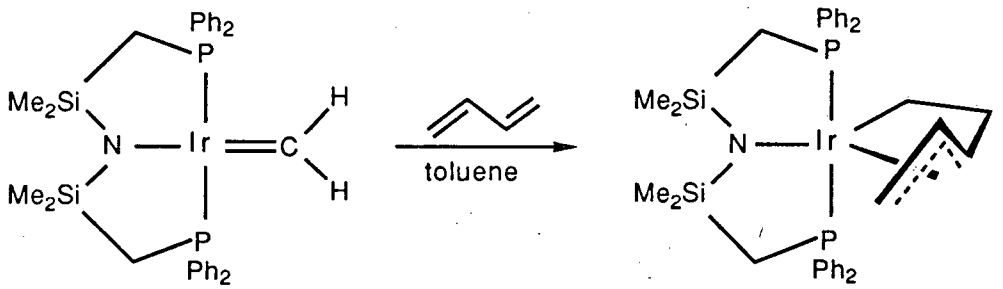

10 **23**

Equation 4.8

The carbon–carbon coupling reaction between the $Ir{=}CH_2$ unit and 1,3-butadiene proceeded with remarkable stereoselectivity. Of two possible diastereomers (characterised by the syn versus anti arrangement of the H(3) and H(4) atoms, Table 4.1), only one product was detected by ^1H and $^{31}P\{^1H\}$ NMR spectroscopy. The vicinal coupling constants displayed are for the anti-protons (11-12 Hz, Table 4.1), and are comparable with the known anti-substituted η^3-allylic ligands in other complexes.[19] The corresponding protons and five ^{13}C resonances for the pentenyl group were identified by the use of ^{13}C-^1H heteronuclear correlation maps (Figure 4.5).

The orientation of the tridentate ligand (meridional versus facial) is not apparent from the NMR data. The phenyl region is quite complicated in the ^1H NMR spectrum, but is similar to that of the phenyl resonances observed for the

crystallographically characterised analogue $Ir(\eta^3\text{-}C_3H_5)I[N(SiMe_2CH_2PPh_2)_2]$ in which the tridentate ligand is arranged meridionally.[6b]

A probable mechanism for the formation of this complex is shown in Scheme 4.8. 1,3-Butadiene first coordinates to the metal centre (**A**). This is followed by the insertion of the methylidene ligand into one of the double bonds of the coordinated butadiene to generate the metallacyclic isomer (**B**) which rearranges to the $\sigma\text{-}\eta^3$-pentenyl product via 1,3-σ,π shift.

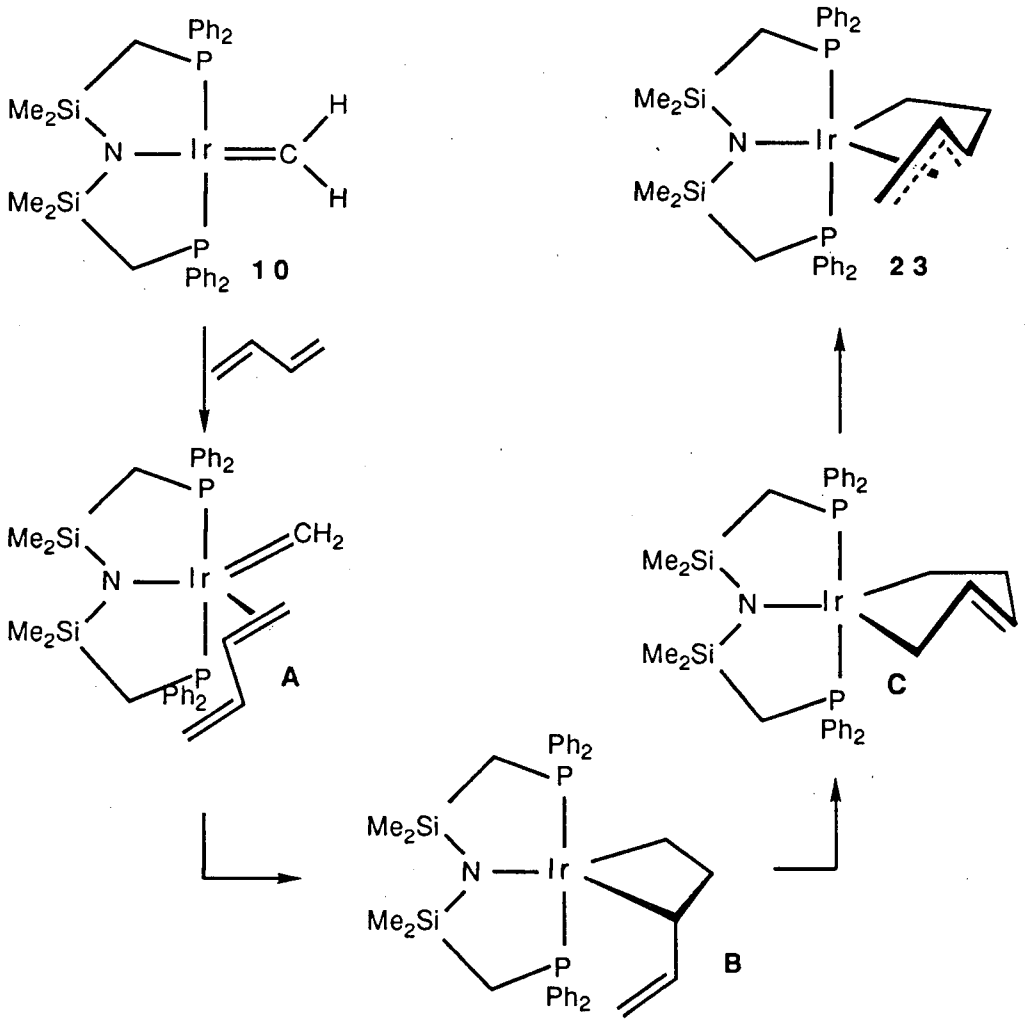

Scheme 4.8

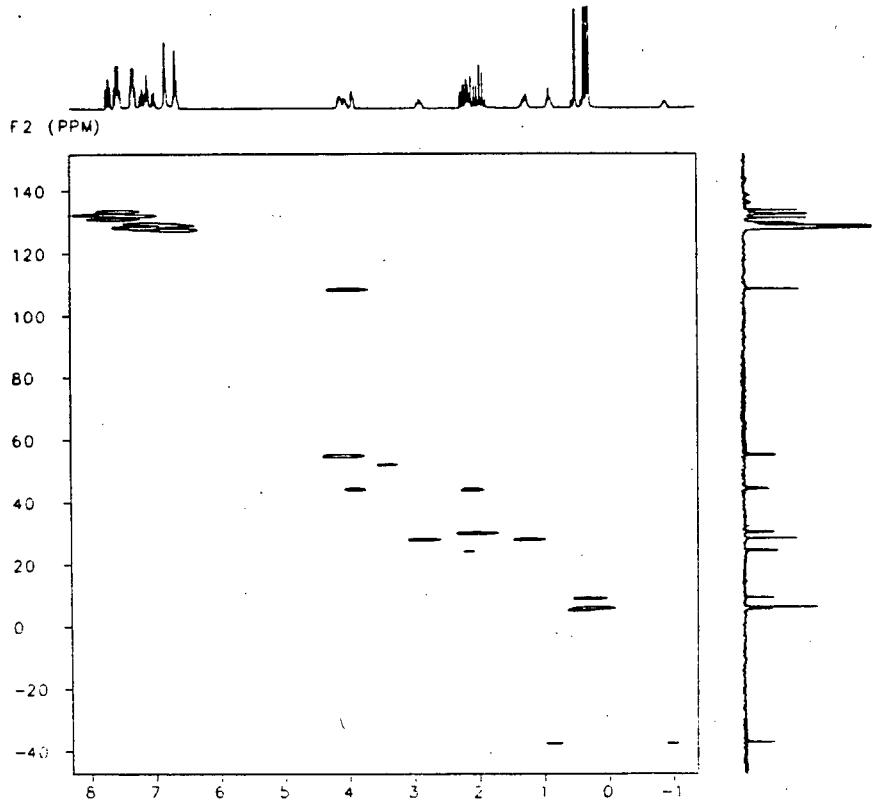

Figure 4.5 ^{13}C-^{1}H HETCOR spectrum (300 MHz, C_6D_6) of Ir(σ-η^3-C_5H_8)-[N($SiMe_2CH_2PPh_2$)$_2$], **23**

A series of complexes containing σ-η^3-allyl ligands has been reported by Erker's and Nakamura's groups.[20] These complexes were synthesised by the coupling reaction between a transition metal–bound diene and an alkene. For example, the complex Cp_2Hf(s-*cis*-diene) reacted with ethylene at -10°C to give the cyclic σ-allyl complex which at 25°C rearranged to the isomeric σ-η^3-allyl complex (Scheme 4.9).[21]

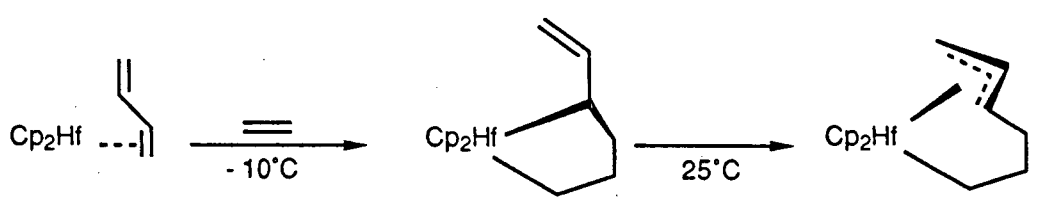

Scheme 4.9

Table 4.1 Chemical Shift and Coupling Constants for the Pentenyl Ligand Protons in $Ir(\sigma\text{-}\eta^3\text{-}C_5H_8)[N(SiMe_2CH_2PPh_2)_2]$, **23**

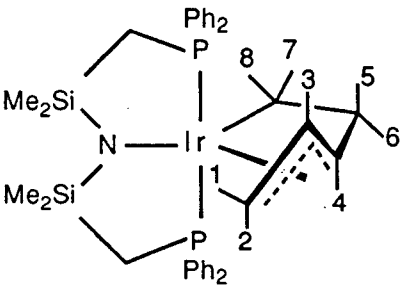

Nucleus	Chemical Shift (ppm)	Coupling Constant (Hz)
H(1)	3.96	^2J (1,2) = 2.1
H(2)	2.25	.....
H(3)	4.15	^3J(1,3) = 7.7
		^3J(2,3) = 11.3,
		^3J(3,4) = 11.6
H(4)	4.08	^3J(4,6) = 11.3
H(5)	2.29	^3J(4,5) = 11.3
		^2J(5,6) = 2.1
H(6)	1.31	^3J(6,8) = 10.3
		^3J(6,7) = 1.9
H(7)	0.92	^2J(7,8) = 5.9
H(8)	-0.85	.....

Table 4.2 $^{13}C\{^1H\}$ NMR Data for the Pentenyl Ligand in $Ir(\sigma\text{-}\eta^3\text{-}C_5H_8)[N(SiMe_2CH_2PPh_2)_2]$, **23**

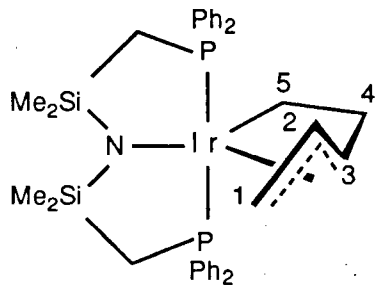

Nucleus	Chemical Shift (ppm)	Coupling Constant (Hz)
C(1)	44.16 (d)	$^2J(C_1,P) = 22.3$
C(2)	108.35 (s)	.....
C(3)	54.90 (d)	$^2J(C_3,P) = 23.5$
C(4)	28.01 (s)	.....
C(5)	-37.26 (s)	.....

4.3.2.3 Reaction with Allene

Transition metal carbenes react with allene to give either methylene-cyclopropane[22] or trimethylenemethane complexes.[23] The reaction of benzylidene-pentacarbonyl tungsten species with 1,1-dimethylallene generated the corresponding methylenecyclopropane complex (Equation 4.9).[22] The reaction proceeded in a stereoselective manner as the carbene ligand was transferred only to the substituted end of the allene. Another report[23] described the synthesis of the trimethylene-methane complexes of chromium and iron by a coupling reaction between allene and the M=C bond of the carbene complexes (Equation 4.10).

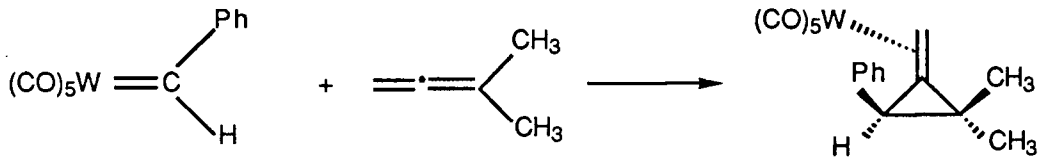

Equation 4.9

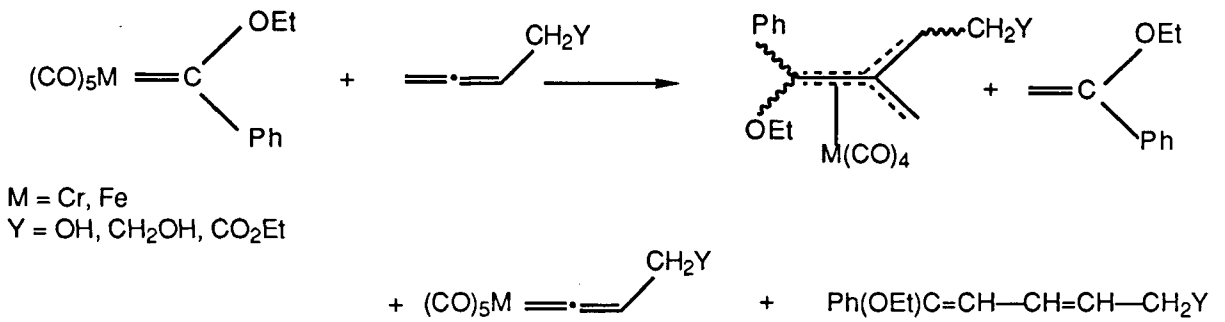

Equation 4.10

The reaction of **10** with allene (~5 equivalents) proceeded at -78°C over a period of an hour. The only product obtained was the trimethylenemethane complex, $Ir\{\eta^4\text{-}C(CH_2)_3\}[N(SiMe_2CH_2PPh_2)_2]$, **24** (Equation 4.11). The product was isolated as colourless crystals in 75% yield. It was apparent from the ^1H NMR spectrum (Figure 4.6) of **24** that the methylidene unit and allene had coupled to generate a trimethylenemethane moiety because three resonances typical for the trimethylene-methane ligand were observed (see Table 4.3).[24]

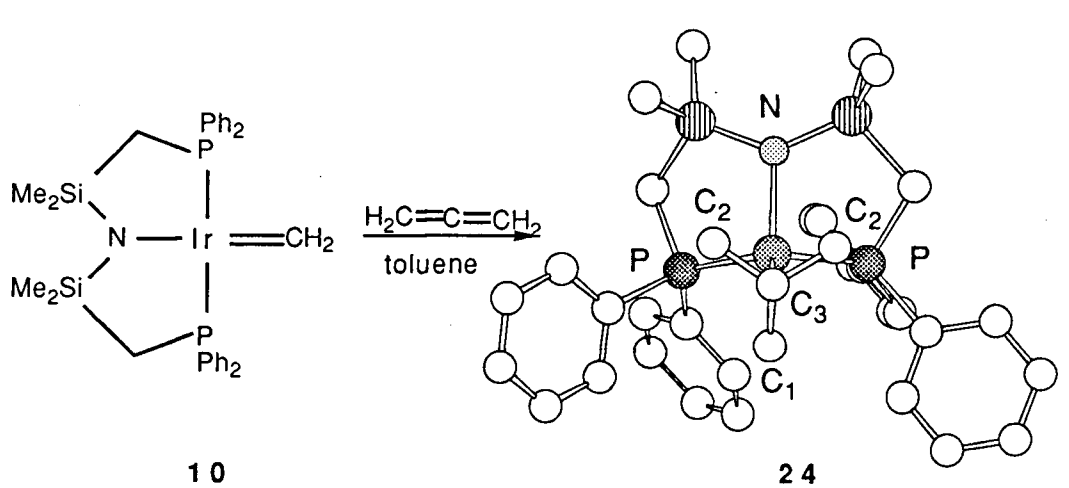

10 **24**

Equation 4.11

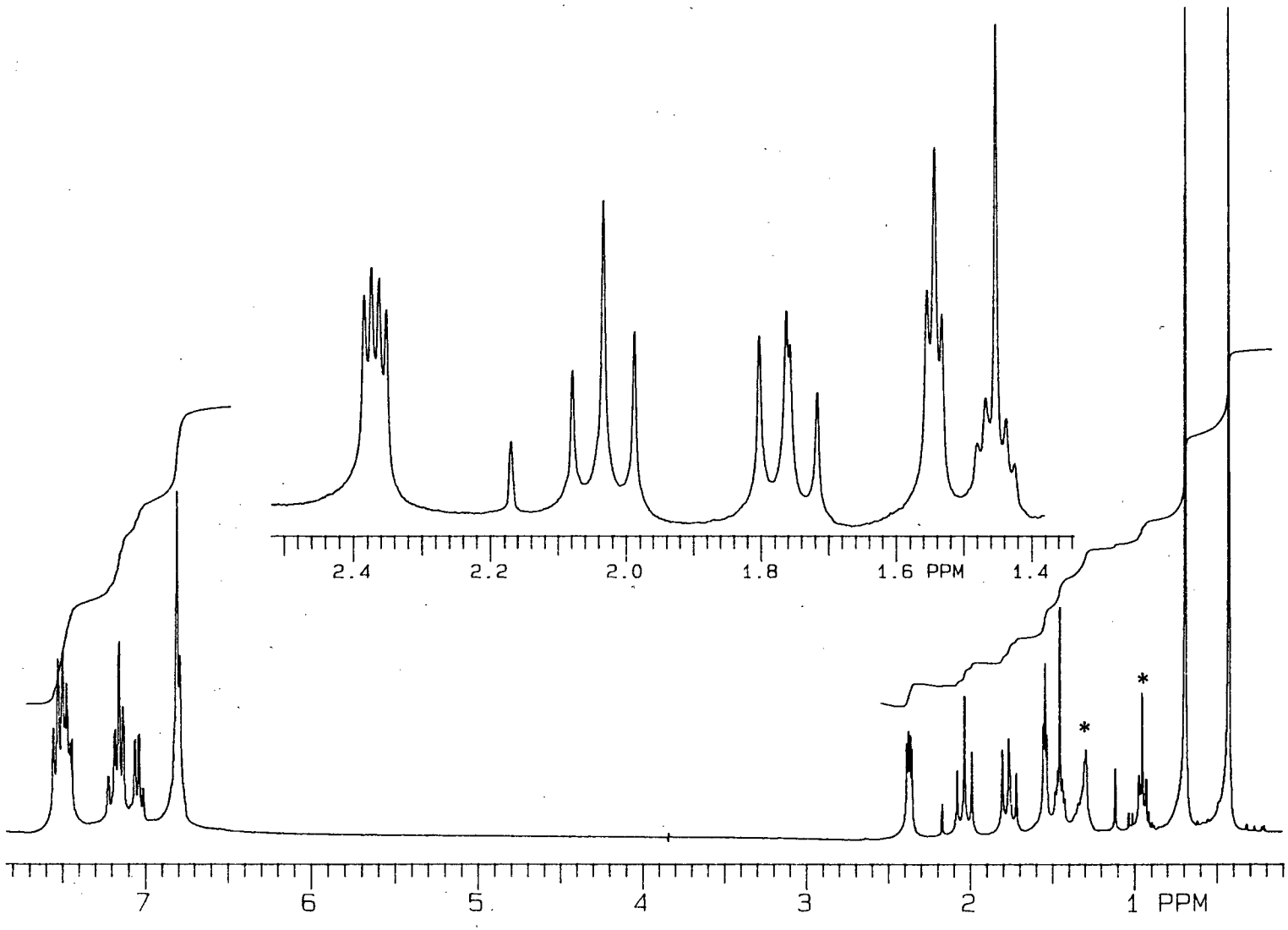

Figure 4.6 ^{1}H NMR spectrum (300 MHz, C_6D_6) of *fac*-Ir{η^4-C$(CH_2)_3$}[N$(SiMe_2CH_2PPh_2)_2$], **24**
(* indicates hexanes protons)

Table 4.3 Chemical Shift and Coupling Constants for the Trimethylenemethane Ligand Protons and Carbons in *fac*-Ir{η^4-C(CH_2)$_3$}[N($SiMe_2CH_2PPh_2$)$_2$], **24**

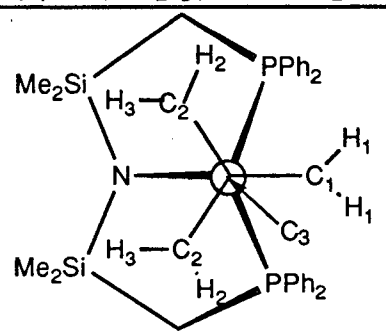

the complex is viewed along the C(3)–Ir axis

Nucleus	Chemical Shift (ppm)	Coupling Constant (Hz)
H(1)	1.54	^4J (H_1,H_3) = 3.0,
		^3J (H_1,P) = 3.0
H(2)	1.45	^2J (H_2,H_3) = 4.6
		^3J (H_2,P) = 9.2
H(3)	2.36	^4J (H_1,H_3) = 3.3
		^3J(H_3,P) = 9.3

Nucleus	Chemical Shift (ppm)	Coupling Constant (Hz)
C(1)	31.89 (d)	^2J(C_1,P) = 4.2
C(2)	47.64 (d)	^2J(C_2,P) = 44.3
C(3)	101.00 (s)	.....

The trimethylenemethane formulation was also confirmed by a single-crystal X-ray determination; the result is shown in Figure 4.7. Some selected bond lengths and bond angles are listed in Tables 4.4 and 4.5 . The meridional arrangement of the ancillary tridentate ligand in **10** changes to facial in the trimethylenemethane complex **24** as indicated by the P(1)–Ir–P(2) bond angle of 106.49 (5)°. The C–C bond lengths of the trimethylenemethane ligand are quite similar (C(31)–C(32), 1.426 (7) Å; C(31)–C(33), 1.437 (7) Å; C(31)–C(34), 1.441 (7) Å). The central carbon, C(31), of the trimethylenemethane ligand is closest to the iridium center (Ir–C(31), 2.055 (5)

Å), and the three terminal methylene carbons are all at similar distances (range from 2.19 to 2.22 Å). This results in the trimethylenemethane unit adopting the characteristic "umbrella" shape. In analogy to the reported iridium trimethylene-methane system, Ir{η^4-C(CH_2)$_3$}Cl(CO)PPh_3,[24] the complex **24** can be considered to possess an octahedral geometry with the η^4-C(CH_2)$_3$ unit and the Ir[N($SiMe_2CH_2PPh_2$)$_2$] moiety in a staggered conformation.

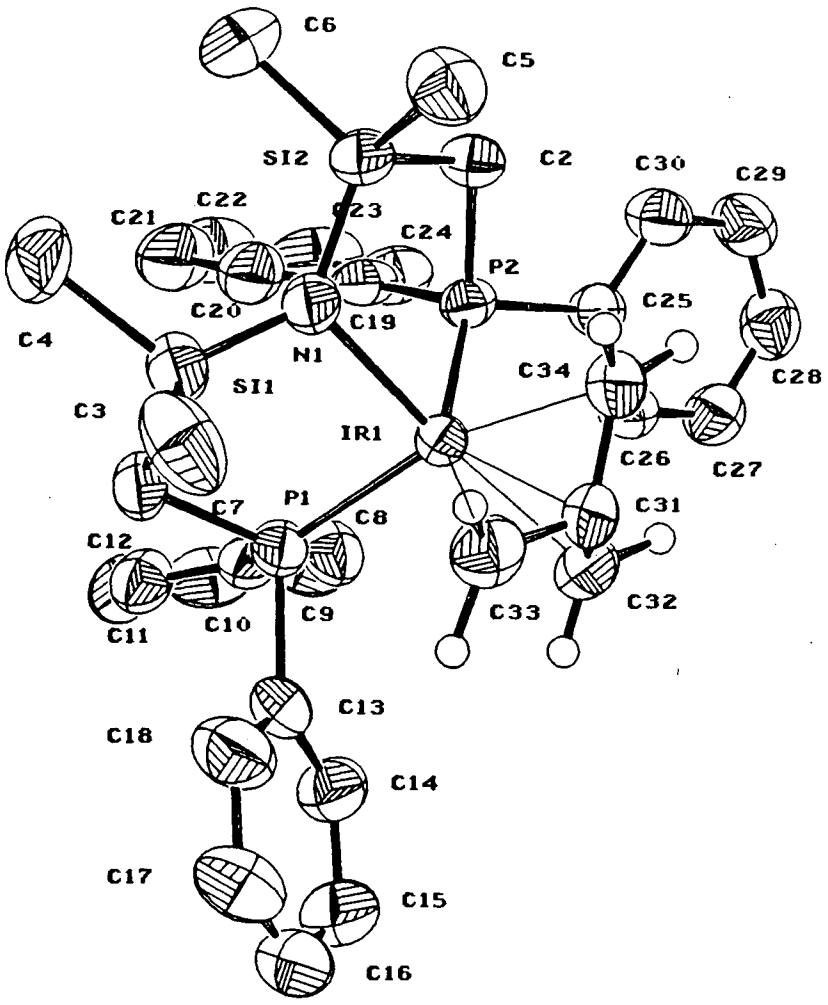

Figure 4.7 X-ray crystal structure of *fac*-Ir{η^4-C(CH_2)$_3$}[N($SiMe_2CH_2PPh_2$)$_2$], **24**

Table 4.4 Selected Bond Lengths (Å) for *fac*-Ir{η^4-C$(CH_2)_3$}[N$(SiMe_2CH_2PPh_2)_2$], **24**[a]

Ir—P(1)	2.296 (1)	Ir—C(33)	2.222 (5)
Ir—P(2)	2.295 (1)	Ir—C(34)	2.202 (5)
Ir—N	2.198 (4)	C(31)—C(32)	1.426 (7)
Ir—C(31)	2.055 (5)	C(31)—C(33)	1.437 (7)
Ir—C(32)	2.189 (5)	C(31)—C(34)	1.441 (7)

Table 4.5 Selected Bond Angles (deg) for *fac*-Ir{η^4-C$(CH_2)_3$}[N$(SiMe_2CH_2PPh_2)_2$], **24**[a]

P(1)—Ir—P(2)	106.49 (5)	P(2)—Ir—C(34)	90.4 (2)
P(1)—Ir—N	87.0 (1)	N—Ir—C(31)	126.2 (2)
P(1)—Ir—C(31)	123.1 (1)	N—Ir—C(32)	165.3 (2)
P(1)—Ir—C(32)	101.9 (2)	N—Ir—C(33)	101.1 (2)
P(1)—Ir—C(33)	97.1 (2)	N—Ir—C(34)	101.6 (2)
P(1)—Ir—C(34)	161.9 (1)	C(31)—Ir—C(32)	39.1 (2)
P(2)—Ir—N	83.0 (1)	C(31)—Ir—C(33)	39.0 (2)
P(2)—Ir—C(31)	120.7 (1)	C(31)—Ir—C(34)	39.4 (2)
P(2)—Ir—C(32)	105.3 (2)	C(32)—Ir—C(33)	66.4 (2)
P(2)—Ir—C(33)	156.3 (2)	C(32)—Ir—C(34)	66.7 (2)
P(2)—Ir—C(34)	90.4 (2)	C(33)—Ir—C(34)	65.8 (2)

a. A complete list of the structural parameters is in Appendix A1.

There are a few examples of structurally characterised monomeric trimethylenemethane complexes in the literature.[25] Parameters obtained for η^4-$C(CH_2)_3$ ligand in complex **24** are slightly different than those reported in the following example. In the phenylmethylenemethane iron complex $Fe\{\eta^4\text{-}C(CH_2)_2\text{-}(CHC_6H_5)\}(CO)_3$,[26] carbon-carbon bond distances within the trimethylenemethane moiety are : C(1)–C(2) = 1.405 (±.013) Å, C(1)–C(3) = 1.406 (±.013) Å, C(1)–C(4) = 1.436 (±.012) Å. In this complex, the central carbon [C(1)] is closest to the iron centre: Fe–C(1) = 1.932 (±.010) Å, Fe–C(2) = 2.098 (±.010) Å, Fe–C(3) = 2.118 (±.010) Å, Fe–C(4) = 2.160 (±.009) Å. This difference in the bond lengths compared to the parameters observed in complex **24** might be a consequence of the phenyl group on the trimethylenemethane ligand in the iron complex.

Similar to other iridium trimethylenemethane complexes, in the complex **24**, the rotation of the trimethylenemethane unit about the Ir–centroid bond (Ir–C(3)) is slow on the NMR time scale because its ^1H NMR spectral parameters remain unchanged between -85°C and +80°C Also, the rotation is slow on the chemical time scale also as observed by the following labelling experiments. The reaction of the ^{13}C-labelled material $Ir=^{13}CH_2[N(SiMe_2CH_2PPh_2)_2]$ with allene generated a material having only the C_1 carbon labelled. Furthermore, the exposure of $Ir=CD_2[N(SiMe_2CH_2PPh_2)_2]$ to allene afforded the product in which only the H_1 protons were labelled with deuterium. These results suggest that the transition state for this carbon-carbon coupling process is product like (shown below as **A**).

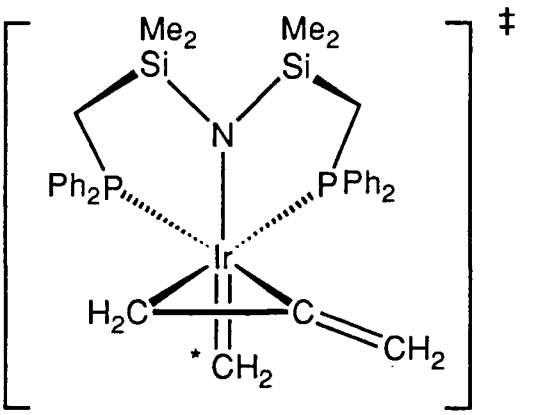

A

Trimethylenemethane, which is a structural isomer of 1,3-butadiene, exists only fleetingly under ambient conditions.[27] However, as evident from the reactions above (Equations 4.9-4.11), this reactive fragment can be stabilised by coordination to a metal centre. Such complexes have been known for many years.[25, 28] The parent trimethylenemethane ligand is synthesised from preformed C-4 fragments via three main routes: (i) the ring opening of alkylidenecyclopropane (Equation 4.12),[29] (ii) the dehalogenation of α-α' dihalogen substituted precursors (Equation 4.13),[30] and (iii) the thermal extrusion of CH_4 (Equation 4.14)[31] or Me_3SiCl from allyl complexes (Scheme 4.10).[32] Thus, the coupling reactions (shown in Equations 4.9-4.11) between M=C bond and allene open up another general route to trimethylenemethane complexes.

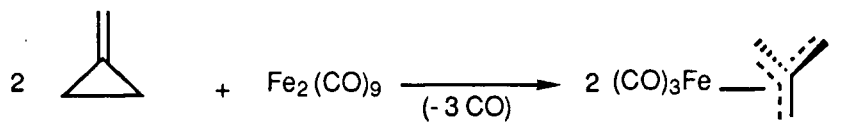

Equation 4.12

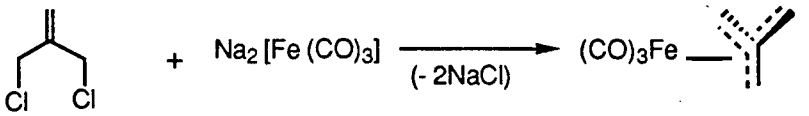

Equation 4.13

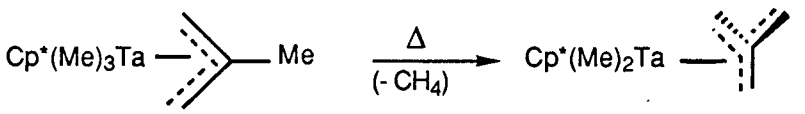

Equation 4.14

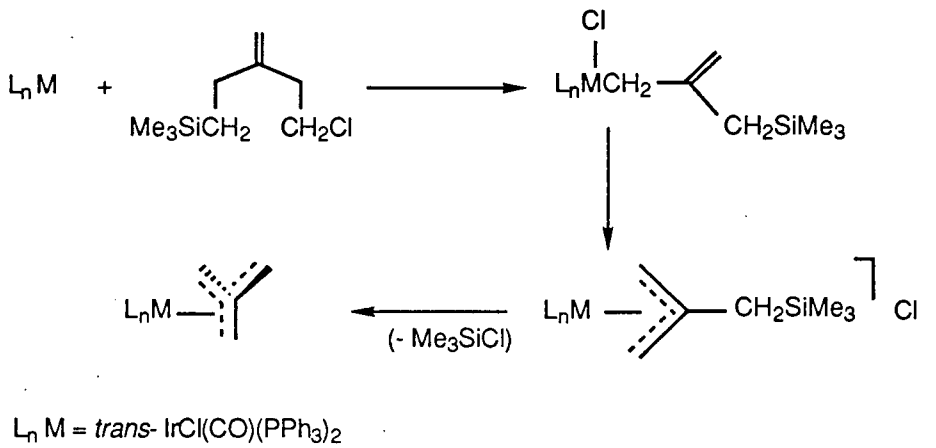

Scheme 4.10

4.4 Summary

A methylidene complex **10** which is easy to prepare in quantity and pure form has been described. The C–C bond formation reactions between the alkylidene group and the reagents MeI, $AlMe_3$, HC≡CH, 1,3-butadiene and allene appear to involve the coordination of the reagents first to iridium, implying that the metal is electron-deficient. The remarkable stereoselectivity observed in the reaction of 1,3-butadiene and allene with **10** may be due to the steric constraints imposed by the tridentate ligand.

4.5 References

1 Fryzuk, M. D.; MacNeil, P. A.; Rettig, S. J. *J. Am. Chem. Soc.* **1985**, *107*, 6709.

2 Fryzuk, M. D.; Joshi, K. *Organometallics* **1989**, *8*, 722.

3 Fryzuk, M. D.; MacNeil, P. A.; Massey, R. L.; Ball, R. G. *J. Organomet Chem.* **1989**, *368*, 213.

4 Massey, R. L. *M. Sc. Thesis*, University of British Columbia, Vancouver, Canada, **1989**.

5 (a) Schrock, R. R.; Sharp, P. R. *J. Am. Chem. Soc.* **1978**, *100*, 2389.
(b) Schrock, R. R. *Acc. Chem. Res.* **1979**, *12*, 98.

6 (a) AlR_3 reactivity: Fryzuk, M. D.; McManus, N. T.; Rettig, S. J; White, G. S. *Angew. Chem., Int. Ed. Engl.* **1990**, *29*, 73.
(b) MeI reactivity: Fryzuk, M. D.; White, G. S.; Paglia, P. L. unpublished results, **1990**.

7 Thorn, D. L.; Harlow, R. L. *J. Am. Chem. Soc.* **1989**, *111*, 2575.

8 (a) Thorn, D. L.; Tulip, T. H. *J. Am. Chem. Soc.* **1981**, *103*, 5984.
(b) Kleitzeir, H.; Werner, H.; Serhadli, P.; Ziegler, M. L. *Angew. Chem., Int. Ed. Engl.* **1983**, *22*, 46.
(c) Jernakoff, P.; Cooper, N. T. *J. Am. Chem. Soc.* **1984**, *106*, 3026.

9 Collman, J. P.; Hegedus, L. S.; Norton, J. R.; Finke, R. G. *Principles and Applications of Organotransition Metal Chemistry*; University Science Books: Mill Valley, CA, **1987**, p. 379-380.

10 Fryzuk, M. D.; Joshi, K. *J. Am. Chem. Soc.* **1989**, *111*, 4498. Also see chapter 2 of this thesis.

11 Fryzuk, M. D.; MacNeil, P. A.; Rettig, S. J. *J. Am. Chem. Soc.* **1987**, *109*, 2803.

12 Oxidative addition reaction of alkyl halides at a metal centre proceeds kinetically to generate the *trans* product: Collman, J. P.; Hegedus, L. S.;

Norton, J. R.; Finke, R. G. *Principles and Applications of Organotransition Metal Chemistry*; University Science Books: Mill Valley, CA, **1987**, p. 280.

13 Fryzuk, M. D.; MacNeil, P. A.; Rettig, S. J. *Organometallics* **1986**, *5*, 2469.

14 (a) Halpern, J.; Okamoto, T. *Inorg. Chim. Acta.* **1984**, *89*, L53.
(b) Roe, D. C. *J. Am. Chem. Soc.* **1983**, *105*, 7771.
(c) Doherty, N. M.; Bercaw, J. E. *J. Am. Chem. Soc.* **1985**, *107*, 2670.

15 (a) Olgemoller, B.; Beck, W. *Angew. Chem. Int., Ed. Engl.* **1980**, *19*, 834.
(b) Deeming, A. J.; Johnson, B. F. G.; Lewis, J. *J. Chem. Soc., Dalton Trans.* **1973**, 1848.

16 (a) Tebbe, F. N.; Parshall, G. W.; Overnall, D. W. *J. Am. Chem. Soc.* **1979**, *101*, 5074.
(b) Tebbe, F. N.; Harlow, R. L. *J. Am. Chem. Soc.* **1980**, *102*, 6149.
(c) McKinney, R. J.; Tulip, T. H.; Thorn, D. L.; Coolbaugh, T. S.; Tebbe, F. N. *J. Am. Chem. Soc.* **1981**, *103*, 5584.
(d) Schlund, R.; Schrock, R. R.; Crowe, W. E. *J. Am. Chem. Soc.* **1989**, *111*, 8004, and references therein.

17 Meinhart, J. D.; Anslyn, E. V.; Grubbs, R. H. *Organometallics* **1989**, *8*, 583.

18 ^{1}H NMR data for an allylic ligand are decribed in these references:
(a) Tulip, T. H.; Ibers, J. A. *J. Am. Chem. Soc.* **1979**, *101*, 4201.
(b) McGhee, W. D.; Bergman, R. G. *J. Am. Chem. Soc.* **1988**, *110*, 4246.
(c) Batchelor, R. J.; Einstein, F. W. B.; Jones, R. H.; Zhuang, J. M.; Sutton, D. *J. Am. Chem. Soc.* **1989**, *111*, 3468.
(d) Collman, J. P.; Hegedus, L. S.; Norton, J. R.; Finke, R. G. *Principles and Applications of Organotransition Metal Chemistry*; University Science Books: Mill Valley, CA, **1987**, p. 177.

19 Brown, P. R.; Green, M. L. H.; Hare, P. M. Bandy, J. A. *Polyhedron* **1988**, *7*, 1819.

20 (a) Erker, G. *Angew. Chem., Int. Ed. Engl.* **1989**, *28*, 397.
(b) Yasuda, H.; Nakamura, A. *Angew. Chem., Int. Ed. Engl.* **1988**, *7*, 1819.

21 Erker, G.; Engel, K.; Dorf, U.; Atwood, J. L.; Hunter, W. E. *Angew. Chem., Int. Ed. Engl.* **1983**, *21*, 914.

22 Fisher, H.; Bidell, W.; Hofmann, J. *J. Chem. Soc., Chem. Commun.* **1990**, *12*, 858.

23 (a) Aumann, R.; Trentmann, B. *Chem. Ber.* **1989**, 1977.
(b) Aumann, R.; Uphoff, J. *Angew. Chem., Int. Ed. Engl.* **1987**, *26*, 357.

24 The ^{1}H and $^{13}C\{^{1}H\}$ NMR assignments for the $\{\eta^4\text{-}C(CH_2)_3\}$ ligand in **24** are based upon the reported NMR analysis of $\{\eta^4\text{-}C(CH_2)_3\}$ in $Ir\{\eta^4\text{-}C(CH_2)_3\}Cl(CO)PPh_3$: Jones, M. D.; Kemmitt, R. D. W.; Platt, A. W. G. *J. Chem. Soc., Dalton Trans.* **1986**, 1411.

25 Marr, G.; Rockett, B. W. in *Chemistry of the Metal–Carbon Bond*; Eds. F. R. Hartley, S. Patai **1982**, *1*, p. 388.

26 Churchill, M. R.; Gold, K. *Inorg. Chem.* **1969**, *8*, 401.

27 Baseman, R. J.; Pratt, D. W.; Chow, M.; Dowd, P. *J. Am. Chem. Soc.* **1976**, *98*, 5726.

28 (a) Emerson, G. F.; Ehrlich, K.; Giering, W. P.; Lauterber, P. C. *J. Am. Chem. Soc.* **1966**, *88*, 3172.
(b) Otsuka, S.; Nakamura, A. *Adv. Organomet. Chem.* **1975**, *14*, 245.
(c) Trost, B. M. *Angew. Chem., Int. Ed. Engl.* **1986**, *25*, 1.

29 Pinhas, A. R.; Samuelson, A. G.; Risenberg, R.; Arnold, E. V.; Clardy, J.; Carpenter, B. K. *J. Am. Chem. Soc.* **1981**, *103*, 1668.

30 (a) Grosselin, J. M.; Le Bozece, H.; Moinet, C.; Toupet, L.; Dixneuf, P. H. *J. Am. Chem. Soc.* **1985**, *107*, 2809.
(b) Ehrlich, K.; Emerson, G. F. *J. Am. Chem. Soc.* **1972**, *94*, 2464.

31 Mayer, J. M.; Curtis, C. J.; Bercaw, J. E. *J. Am. Chem. Soc.* **1983**, 105, 2651.

32 Jones, M. D.; Kemmitt, R. D. W. *J. Chem. Soc., Chem. Commun.* **1985**, 811.

CHAPTER 5

Reactivity of the Iridium(I) η^2-Cyclooctene Complex

5.1 Introduction

Studies on iridium(I) complexes have greatly contributed to the understanding of some of the basic processes in organometallic chemistry. For example, a number of two-electron oxidative addition reactions at the iridium(I) centre in Vaska's complex, *trans*-$IrCl(CO)(PPh_3)_2$, have been examined (Scheme 5.1).[1] While the reagents O_2, H_2 and R_3SiH undergo *cis*-addition at the metal centre, oxidative addition of MeI proceeds kinetically to generate the *trans* adduct.

In our group, the iridium(I) η^2-cyclooctene complex, $Ir(\eta^2\text{-}C_8H_{14})$-$[N(SiMe_2CH_2PPh_2)_2]$, **25**, has been used as a key starting material for the preparation of a wide variety of iridium(I) and iridium(III) amide complexes either via replacement of the cyclooctene moiety by other neutral ligands such as CO, HC≡CH, $H_2C{=}CH_2$ and PR_3 (R = Me, Ph), or by oxidative addition of reagents such as H_2 and RX (R = Me, X = Cl, Br, I; R = CH_2Ph, X = Br; R = CH_2CO_2Me, X = Br) at the metal centre (Scheme 5.2).[2]

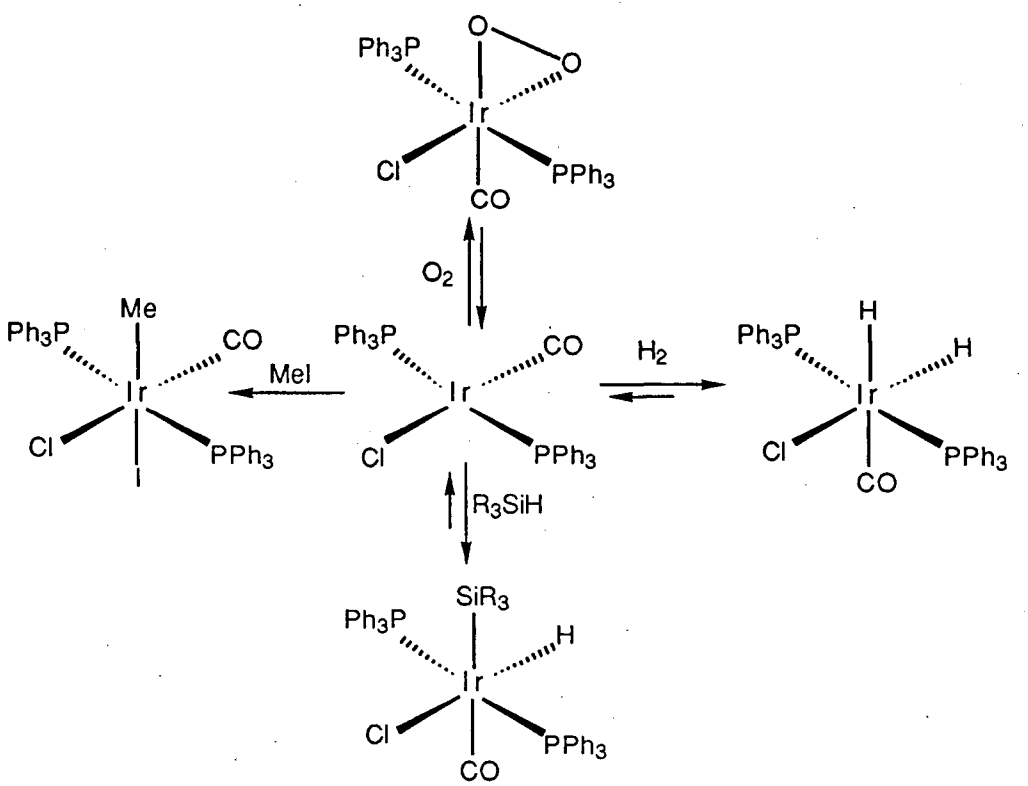

Scheme 5.1

During the course of this thesis work, some interesting chemical properties of $Ir(\eta^2\text{-}C_8H_{14})[N(SiMe_2CH_2PPh_2)_2]$, **25**, were observed and therefore investigated in detail. This chapter describes the photochemical carbon–hydrogen bond activation of the cyclooctene ligand in **25**, and its reactivity with 1,3-butadiene, allene and trimethylaluminum.

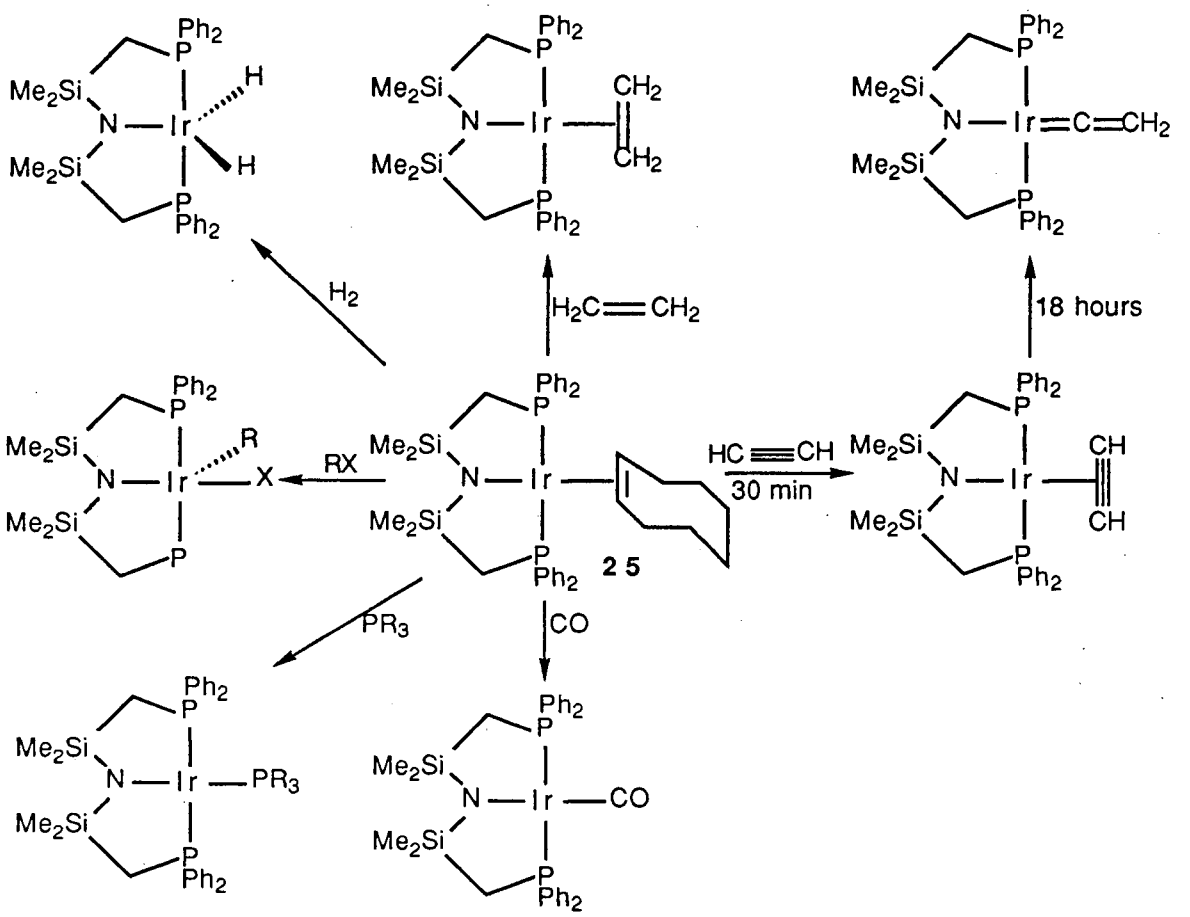

Scheme 5.2

5.2 Photochemical Carbon–Hydrogen Bond Activation of the Coordinated Cyclooctene in $Ir(\eta^2\text{-}C_8H_{14})[N(SiMe_2CH_2PPh_2)_2]$, 25

As discussed in chapter 1, some transition metal complexes have been found which are capable of adding alkane or arene C–H bonds oxidatively.[3] However, in only a few systems has the product of C–H insertion been converted into organic products either stoichiometrically or catalytically.[4]

In 1979, Crabtree and co-workers described the dehydrogenation of a number of alkanes by $[IrH_2(Me_2CO)_2(PPh_3)_2]BF_4$ and *tert*-butylethylene in chlorinated

solvents (Equation 5.1).[5] An η^3-allyl hydride complex was proposed as one of the intermediates in this transformation.

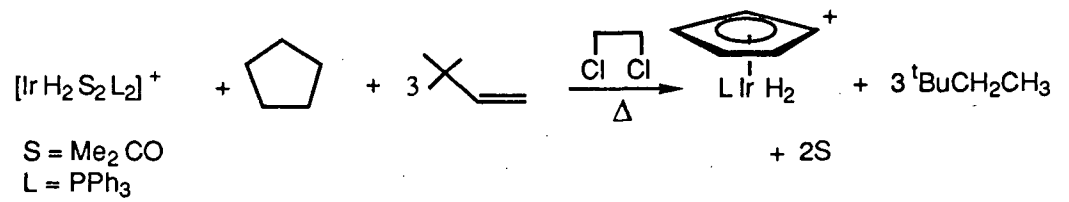

Equation 5.1

This section describes the photochemical dehydrogenation of the cyclooctene ligand in $Ir(\eta^2\text{-}C_8H_{14})[N(SiMe_2CH_2PPh_2)_2]$, **25**, to yield $Ir(H)_2[N(SiMe_2CH_2\text{-}PPh_2)_2]$, **26**, and free cyclooctadienes. The reaction proceeded through an η^3-allyl hydride intermediate $Ir(\eta^3\text{-}C_8H_{13})H[N(SiMe_2CH_2PPh_2)_2]$, **27**, which was isolated and characterised. This photochemical activity of **25** was detected during the attempts to make an iridium imide complex of formula, $Ir{=}(NSiMe_3)[N(SiMe_2CH_2PPh_2)_2]$, by conducting the reaction of **25** with $SiMe_3N_3$ under photolytic conditions.

Although the iridium(I) cyclooctene complex **25** is thermally stable even upon heating to 80°C for 24 hours, when photolysed (140 W, Hg lamp) for 6 hours, it rearranges to the iridium(III) η^3-cyclooctenyl hydride derivative, $Ir(\eta^3\text{-}C_8H_{13})H\text{-}[N(SiMe_2CH_2PPh_2)_2]$, **27** (Scheme 5.3). This transformation proceeded with a noticeable colour change as the orange solution of **25** turned deep red. Complex **27** was isolated as red crystals from hexanes/toluene solution at -30°C. Some of the important features in the ^1H NMR spectrum (Figure 5.1) of **27** include the allyl resonances belonging to the cyclooctenyl ring [4.56 ppm ($H_{central}$, t, $^2J_{H,H}$ = 7.6 Hz) and 4.10 ppm (two H_{syn}, m)] and the hydride resonance [-21.65 ppm (t, $^2J_{P,H}$ = 16.7 Hz)].

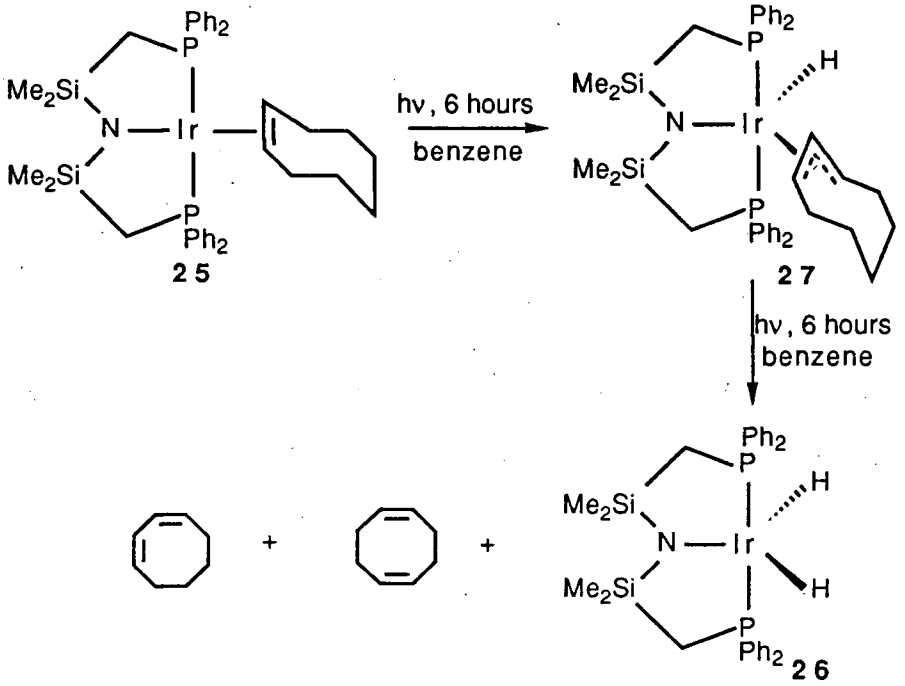

Scheme 5.3

It was noticed that upon continuing the photolysis of **27** for six more hours, the red colour of the solution slowly changed to yellow because of the formation of the iridium(III) dihydride complex, $Ir(H)_2[N(SiMe_2CH_2PPh_2)_2]$, **26** (as observed by ^1H NMR spectroscopy).[2b] A mixture of free 1,3- and 1,5-cyclooctadiene (COD) in the ratio of 2:1 was also detected in the ^1H NMR spectrum. The iridium(III) dihydride complex **26** and the cyclooctenyl hydride species **27** were found to be in equilibrium in the ratio of 90:10, long after the photolysis process had been stopped. However, addition of five equivalents of 1,5-cyclooctadiene to the benzene solution of this mixture under non-photolytic conditions shifted the equilibrium towards the cyclooctenyl hydride complex **27**.

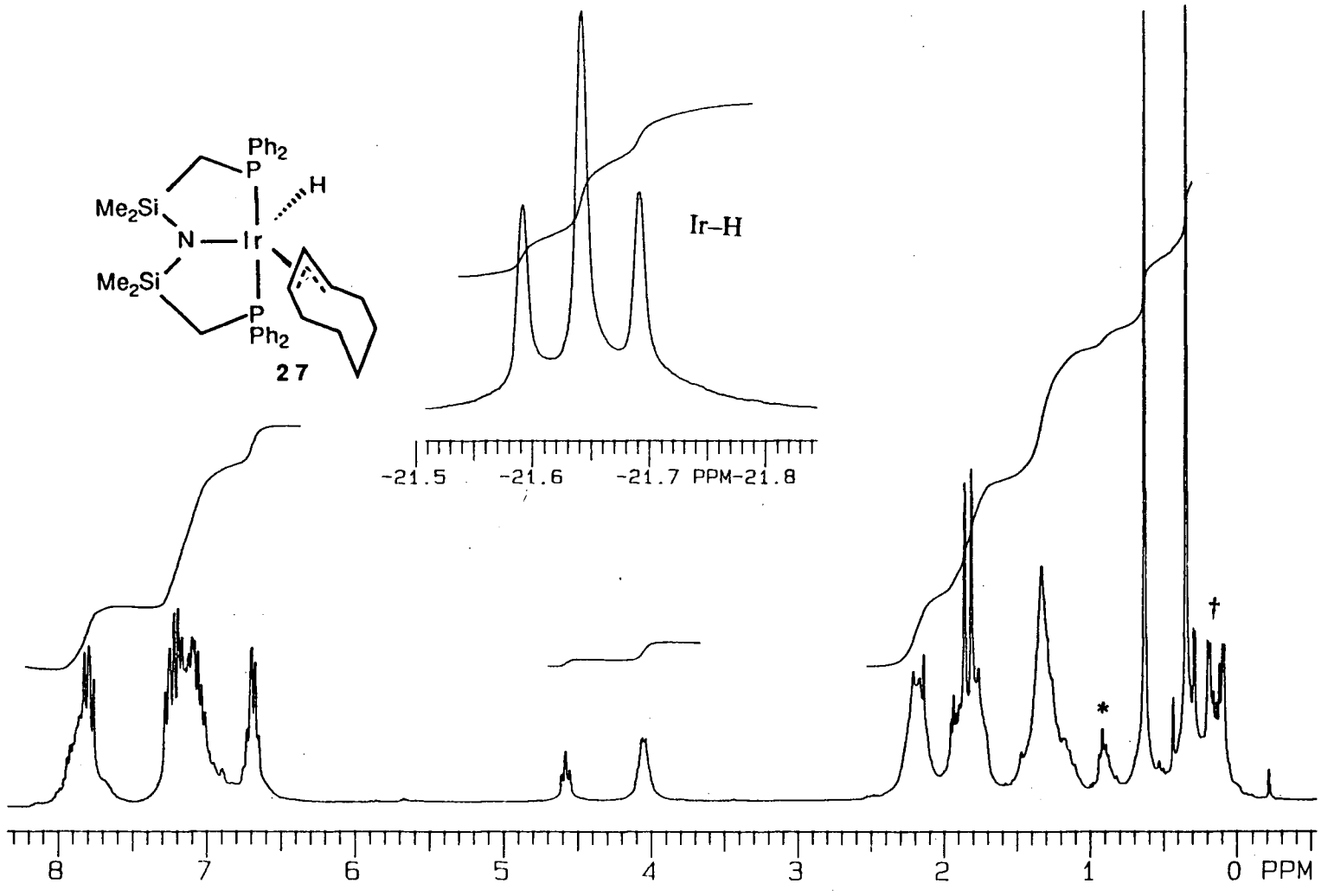

Figure 5.1 ^{1}H NMR spectrum (300 MHz, C_6D_6) of Ir(η^3-C_8H_{13})H[N($SiMe_2CH_2PPh_2$)$_2$], **27**
(* indicates hexanes protons, † indicates $SiMe_2$ resonances of the remaining Ir(η^2-C_8H_{14})[N($SiMe_2CH_2PPh_2$)$_2$], **25**)

From these results, it can be seen that $Ir(H)_2[N(SiMe_2CH_2PPh_2)_2]$ is involved in the isomerisation process of 1,3-COD to 1,5-COD presumably through a 1,4-COD intermediate. Such isomerisation of 1,3-COD to 1,5-COD by some rhodium and iridium systems has been reported in the literature.[6] It is reasonable to assume that the higher ratio of 1,3-COD observed in Scheme 5.3 might be due to the presence of conjugated double bonds in this isomer.

The importance of η^3-allyl hydride complexes in catalytic processes such as conversion of cyclopropanes to olefins (Scheme 5.4)[7] and alkene isomerisation (Scheme 5.5)[8] has long been recognised. However, only a handful examples of stable η^3-allyl hydride complexes are known.[9] One of the early allyl hydride complexes reported in the literature is $Ni(H)(\eta^3\text{-}C_3H_5)PPh_3$.[10] This species could only be prepared *in situ* at low temperatures and decomposed above -40°C. In 1979, a series of stable iridium(III) allyl hydride complexes of formula, $IrClH[\eta^3\text{-}(1\text{-}Ph)\text{-}C_3H_4)]\text{-}(PR_3)_2$, was reported.[11] These species were prepared by the reactions of *trans*-$IrCl(N_2)(PR_3)_2$ with phenylcyclopropane. Recently, Sutton and co-workers described the synthesis and crystallographic characterisation of $Cp^*Re(CO)H(\eta^3\text{-}C_3H_5)$ (both the exo and the endo isomers) produced upon the photolysis of the propene complex, $Cp^*Re(CO)_2(\eta^2\text{-}C_3H_6)$.[12]

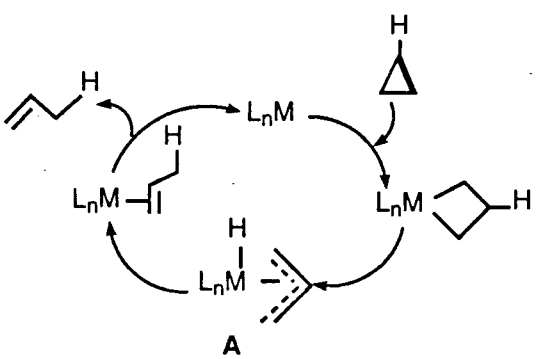

Scheme 5.4

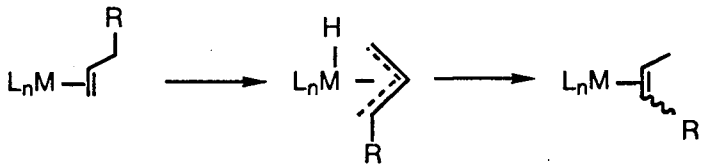

A

Scheme 5.5

5.3 Reactions with Unsaturated Hydrocarbons

As shown in Scheme 5.2, the cyclooctene moiety can be replaced by a ligand such as ethylene. Thus it would appear that other olefin analogues of **25** should be readily accessible by conducting its reactions with other alkenes and dienes. But to our surprise, complex **25** showed no reactivity toward propene, 4-methyl-1-pentene, 1,4-cyclohexadiene or 2,5-norbornadiene over a period of 24 hours. The only dienes which did substitute the cyclooctene ligand were 1,3-butadiene and allene.

5.3.1 Reaction with 1,3-Butadiene

1,3-Butadiene may coordinate to a transition metal in several ways depending upon the ligands on the metal and the substituents on the diene. Early transition metal butadiene complexes generally assume a σ^2-π geometry with the C–C bond lengths in the diene unit alternating as long-short-long (Figure 5.2 **A**).[13] However, the vast majority of the middle and the late transition metal dienes assume the η^4-π structure with the carbons of the diene ligand being nearly equally distant from the metal centre (Figure 5.2 **B**).[14] Only the more common η^4-*cis* mode of diene coordination is shown below, but recently the η^4-*trans* form has been observed as the kinetic product in group 4 metallocenes[15] and the most stable isomer in $(\eta^5\text{-}C_5H_5)$-$Mo(NO)(\eta^4\text{-}C_4H_6)$.[16]

A B

Figure 5.2 Bonding modes of 1,3-butadiene

The iridium(I) η^4-butadiene complex, $Ir(\eta^4\text{-}C_4H_6)[N(SiMe_2CH_2PPh_2)_2]$, **28**, was synthesised from the reaction of the iridium(I) η^2-cyclooctene complex, **25**, $Ir(\eta^2\text{-}C_8H_{14})[N(SiMe_2CH_2PPh_2)_2]$, with excess (~5 equivalents) 1,3-butadiene (Equation 5.2).[17] The reaction proceeded at room temperature without any significant colour change of the initial orange solution. Light yellow crystals of the butadiene complex were isolated in >90% yield from toluene/hexanes solution at room temperature.

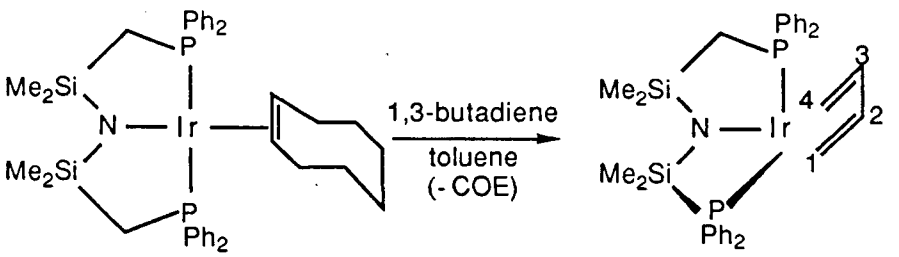

25 28

Equation 5.2

Although five-coordinate d^8 complexes have been studied as prototypes for stereochemical non-rigidity,[18] the complex **28** has a rigid structure from -80° to +85°C (as observed by ^1H and $^{31}P\{^1H\}$ NMR spectroscopy). This lack of fluxionality is quite puzzling in contrast to the hafnium analogue, $Hf(\eta^4\text{-}C_4H_6)Ph[N(SiMe_2CH_2\text{-}PPh_2)_2]$, which is known to display fluxional behaviour.[19]

The spectral features of this complex are indicative of an asymmetric structure. In the ^1H NMR spectrum (Figure 5.3), four singlets of equal intensity for the $Si(CH_3)_2$

protons are observed. The PCH_2Si protons are multiplets centred at 1.85 and 2.12 ppm. Hardly any separation of the *ortho* protons resonance from that of the *meta/para* protons resonance of the phenyl rings is observed, thus suggesting a facial arrangement of the tridentate ligand. The butadiene moiety shows six resonances at -0.60, -0.20, 2.07, 2.61, 4.00 and 5.37 ppm. The corresponding four ^{13}C resonances for the coordinated diene ligand were identified by the use of ^{13}C-^{1}H heteronuclear correlation maps (Figure 5.3). The gated decoupled ^{13}C NMR spectrum shows $^{1}J_{C\text{-}H}$ for C2 and C3 of the diene unit to be 165.5 Hz which is typical of an sp^2 bonded carbon centre;[20] however, $^{1}J_{C\text{-}H}$ for C4 and C1 are lower (155.0 and 150.0 Hz, respectively), but are still suggestive of the sp^2 character around these carbon centres.

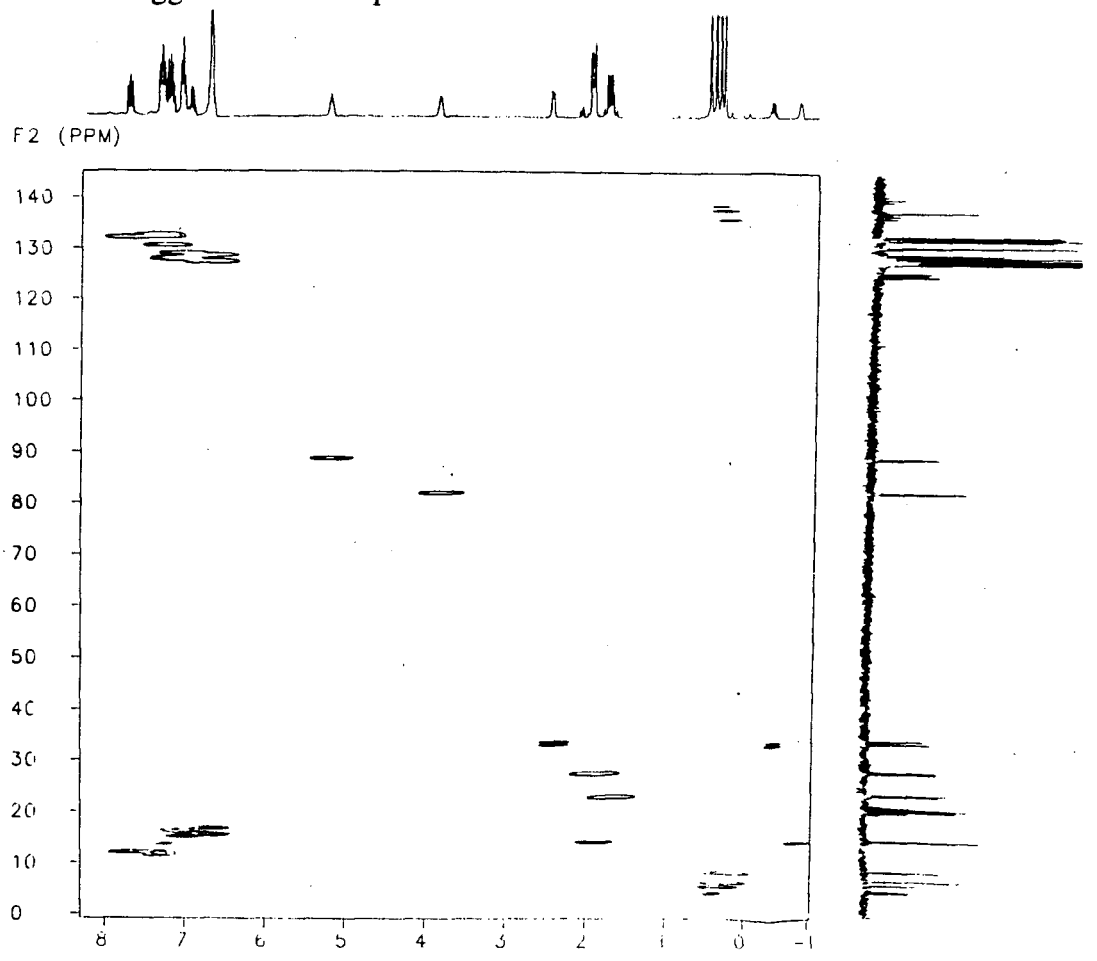

Figure 5.3 ^{13}C-^{1}H HETCOR spectrum (300 MHz, C_6D_6) of $Ir(\eta^4\text{-}C_4H_6)$-$[N(SiMe_2CH_2PPh_2)_2]$, **28**

The solid-state structure of $Ir(\eta^4\text{-}C_4H_6)[N(SiMe_2CH_2PPh_2)_2]$, **28**, complex (Figure 5.4; Tables 5.1 and 5.2) complements the solution data. It reveals that the amido-diphosphine tridentate ligand adopts a facial coordination mode as indicated by the P1–Ir–P2 angle of 107.01(4)°. The metal centre is bonded to each carbon of the butadiene unit with the following bond lengths: Ir–C31, 2.139(4); Ir–C32, 2.167(4); Ir–C33, 2.183(4); and Ir–C34, 2.182(4) Å. These metal-carbon bond lengths parallel the *trans*-influence order,[21] i.e. P>N, since C31 being *trans* to the amide posses a stronger bond with iridium than C34 does which is *trans* to the phosphorus centre. The C-C bond lengths are slightly different and are as follows: C31–C32, 1.430(7); C32–C33,1.409(7); C33–C34,1.421(7) Å.

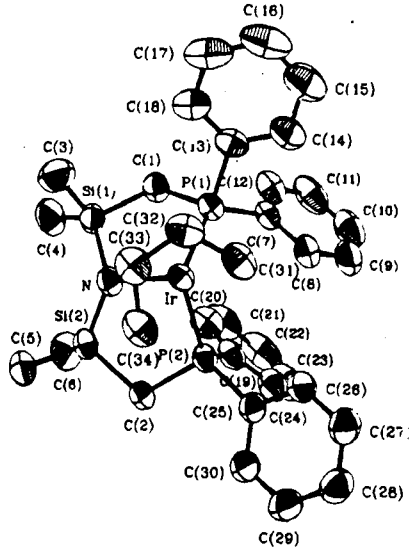

Figure 5.4 X-ray crystal structure of $Ir(\eta^4\text{-}C_4H_6)[N(SiMe_2CH_2PPh_2)_2]$, **28**

Table 5.1 Selected Bond Lengths (Å) for $Ir(\eta^4\text{-}C_4H_6)[N(SiMe_2CH_2PPh_2)_2]$, **28**[a]

Ir—P(1)	2.292(1)	C(31)—C(32)	1.430(7)
Ir—P(2)	2.2879(9)	C(32)—C(33)	1.409(7)
Ir—C(31)	2.139(4)	C(33)—C(34)	1.421(7)
Ir—C(32)	2.167(4)		
Ir—C(33)	2.183(4)		
Ir—C(34)	2.182(4)		

Table 5.2 Selected Bond Angles (deg) for $Ir(\eta^4\text{-}C_4H_6)[N(SiMe_2CH_2PPh_2)_2]$, **28**[a]

P(1)—Ir—P(2)	107.01(4)

a. A complete list of the bond distances and the bond angles is compiled in Appendix A1.

Two different methods have been reported in the literature to compare metal-diene interactions, in particular, to gauge the component of η^4-π versus σ^2-π character of the bonding, from the crystallographic data.[22] The first method deals with the dihedral angle,θ, (subtended by the C1–M–C4 and the C1–C2–C3–C4 planes) and the difference in the bond distances of the metal from the inner and outer carbons of the diene ligand, Δd, {Δd=[d(M-C1)+d(M-C4)]-[d(M-C2)+d(M-C3)]/2}. For the vast majority of the middle and the late transition metal diene complexes, which generally assume the η^4-*cis*-1,3-diene structure, the dihedral angle θ is 75-90° and Δd is between -0.1 and 0.1 Å. For the complex **4**, the value of θ is 92.9° and Δd is -0.01 Å, thus confirming the η^4-π bonding mode of the diene ligand at the iridium centre.

The second mode of comparison shows an approximate linear increase in the dihedral angle, θ, with increasing bond lengths, Δl, {Δl=[l(C1-C2)+l(C3-C4)]/2-l(C2-C3)]}. For the late transition metals, Δl is between -0.1 and 0.0 Å; whereas in the case of early transition metals, Δl falls in the range of 0.0-0.2 Å. The calculated

value of Δl in **28** is 0.02 Å, indicating that the 1,3-butadiene bonding which, is mainly of η^4-π character, might have a small contribution from the σ^2-π mode.

5.3.2 Reaction with Allene

In analogy with transition metal olefin complexes, an allene ligand can bind to a metal centre in one of two possible ways, namely η^2-π (Figure 5.5 **A**) or η^2-σ (Figure 5.5 **B**).[23] Allene complexes of both types have been prepared and in many cases characterised by X-ray crystallography.[23]

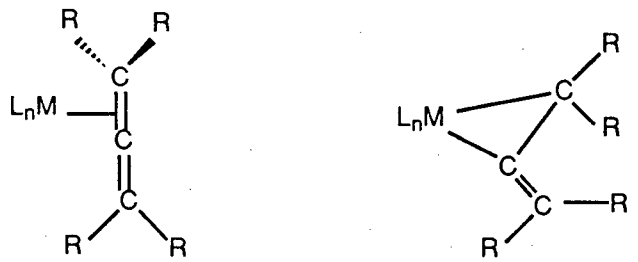

A **B**

Figure 5.5 Modes of allene coordination at a metal centre

The reaction of the iridium(I) η^2-cyclooctene complex, $Ir(\eta^2\text{-}C_8H_{14})$-$[N(SiMe_2CH_2PPh_2)_2]$, **25**, with excess allene (~5 equivalents) proceeded at room temperature to afford the allene derivative, $Ir(\eta^2\text{-}C_3H_4)[N(SiMe_2CH_2PPh_2)_2]$, **29** (Equation 5.3). The orange colour of the starting material changed to yellow over 15 minutes period. The complex **29** was isolated as yellow crystals from hexanes at -30°C.

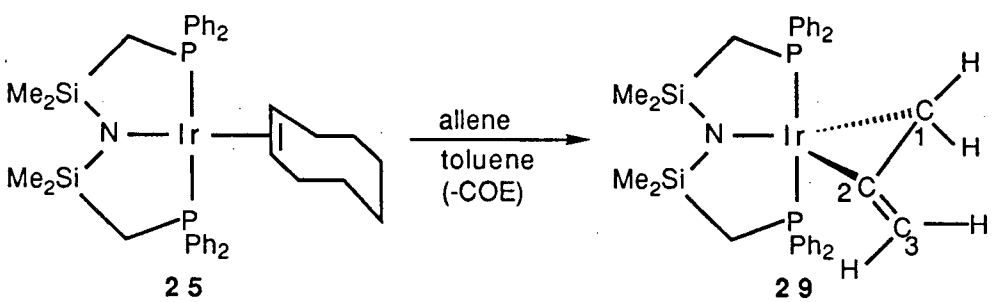

25 **29**

Equation 5.3

From $^{13}C\{^1H\}$ NMR data, it is evident that the allene ligand in **29** is bound to the iridium centre in the η^2-σ fashion. In the $^{13}C\{^1H\}$ NMR spectrum, the resonances for the allene ligand are observed at -3.82 (C1, s), 101.00 (C2, s) and 92.30 ppm (C3, s). Such a high shielding of the C1 carbon is consistent with the data reported for methylene carbons bound to an iridium centre via a σ–bond.[24] In contrast, the olefinic carbons in the iridium(I) η^2-ethylene complex $Ir(\eta^2\text{-}C_2H_4)[N(SiMe_2CH_2PPh_2)_2]$, and also in many other iridium olefin complexes are observed between 40-60 ppm.[25]

The ^1H NMR spectrum (Figure 5.6) of this complex is straightforward. The resonances of the allene ligand appear at 1.12, 5.20 and 5.44 ppm integrating for the protons in the ratio of 2:1:1. They have been assigned to two protons at C1 and two inequivalent protons at C3.

5.4 Reaction with Trimethylaluminum

Alkylaluminum reagents are extensively used in industrial processes like Ziegler-Natta polymerisation.[26] Their use as alkylating agents is important in the formation of "Tebbe's reagent" (Equation 5.4).[27] Other reactions where a transition metal centre brings about aluminum-alkyl bond cleavage involve alkyl/halide or alkyl/alkoxide exchange, as in Equation 5.5.

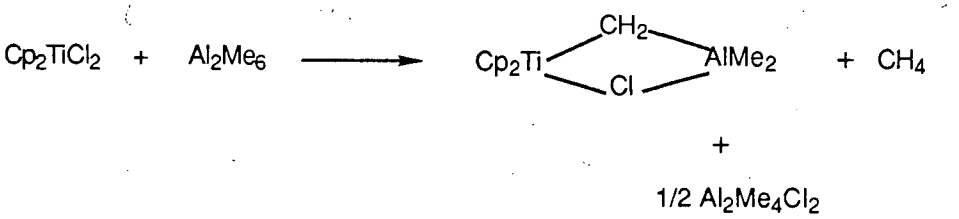

Equation 5.4

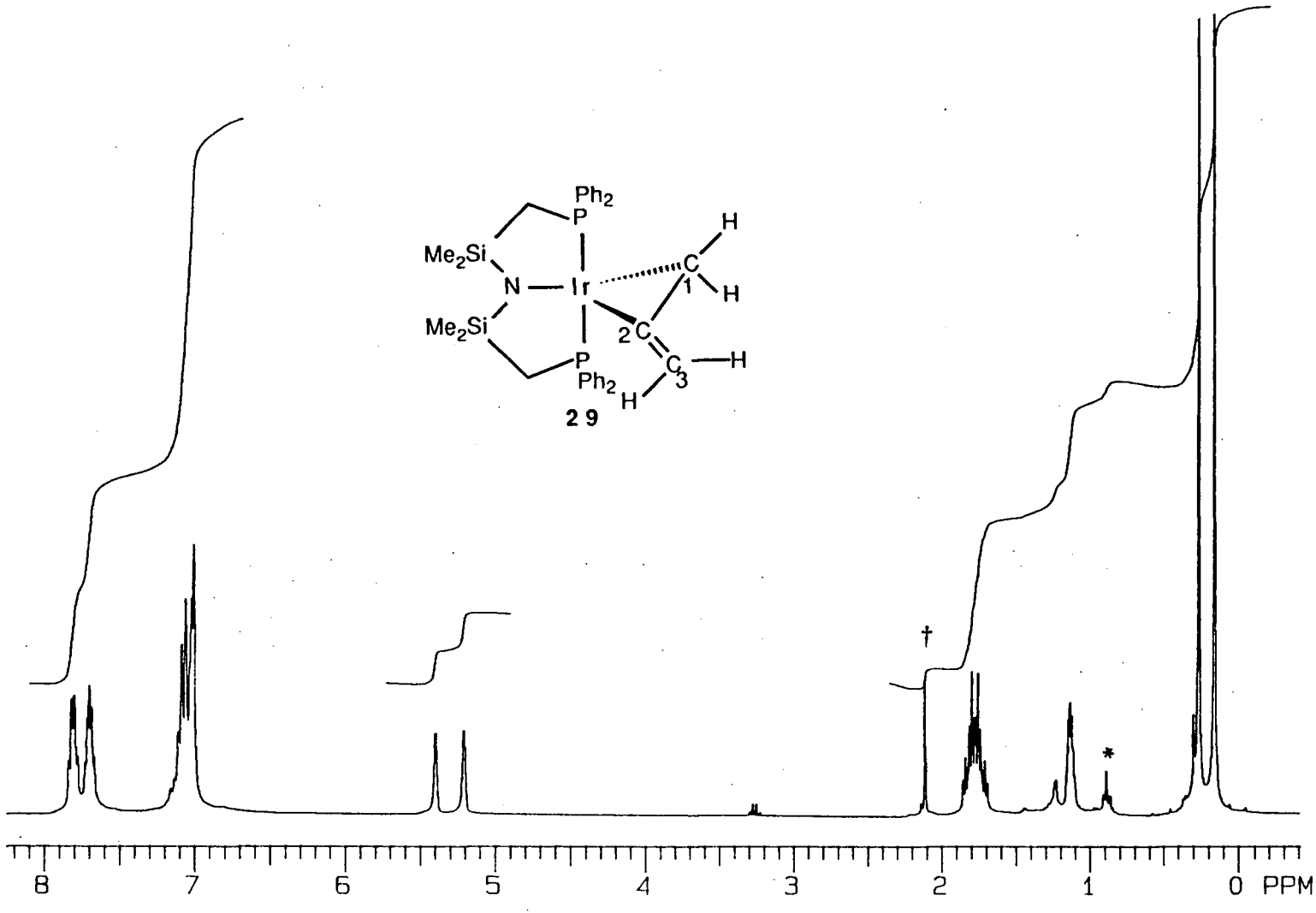

Figure 5.6 ^{1}H NMR spectrum (300 MHz, C_6D_6) of $Ir(\eta^2\text{-}C_3H_4)[N(SiMe_2CH_2PPh_2)_2]$, **29**
(* indicates hexanes protons, † indicates toluene protons)

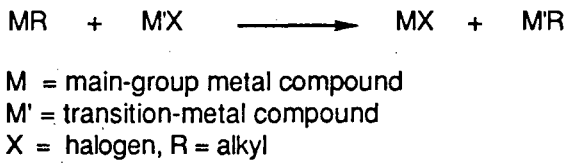

Equation 5.5

Cleavage of group 13 metal–alkyl bonds via oxidative addition at a transition metal centre is a relatively new process. Recently, Thorn and Harlow described the synthesis of *cis*-$Ir(Me)_2InMe_2(PMe_3)_3$ from the oxidative addition reaction of $InMe_3$ with $IrMe(PMe_3)_4$.[28]

Studies on the reactivity of $AlMe_3$ with $Ir{=}CH_2[N(SiMe_2CH_2PPh_2)_2]$ and $Ir{=}C{=}CH_2[N(SiMe_2CH_2PPh_2)_2]$ (Chapter 4, Section 4.3) were extended to $Ir(\eta^2\text{-}C_8H_{14})[N(SiMe_2CH_2PPh_2)_2]$, **25**. In toluene at room temperature, the reaction between trimethylaluminum and the iridium(I) η^2-cyclooctene complex, **25**, proceeded smoothly yielding only one product characterised as $Ir(Me)(\mu\text{-}AlMe_2)[N(SiMe_2CH_2\text{-}PPh_2)_2]$, **30** (Equation 5.6). The orange colour of the cyclooctene complex changed to red within an hour. The reaction was essentially quantitative *in situ* yield (by ^1H NMR spectroscopy).

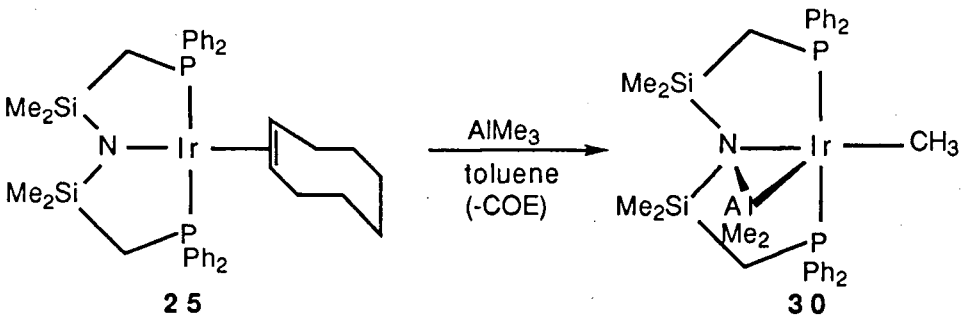

25 **30**

Equation 5.6

The spectral features (Figure 5.7) of this complex are very similar to those of its hydride analogue $Ir(H)(\mu\text{-}AlMe_2)[N(SiMe_2CH_2PPh_2)_2]$ (see Chapter 4, Figure 4.2). The exclusive *trans* disposition of the chelating phosphines was once again

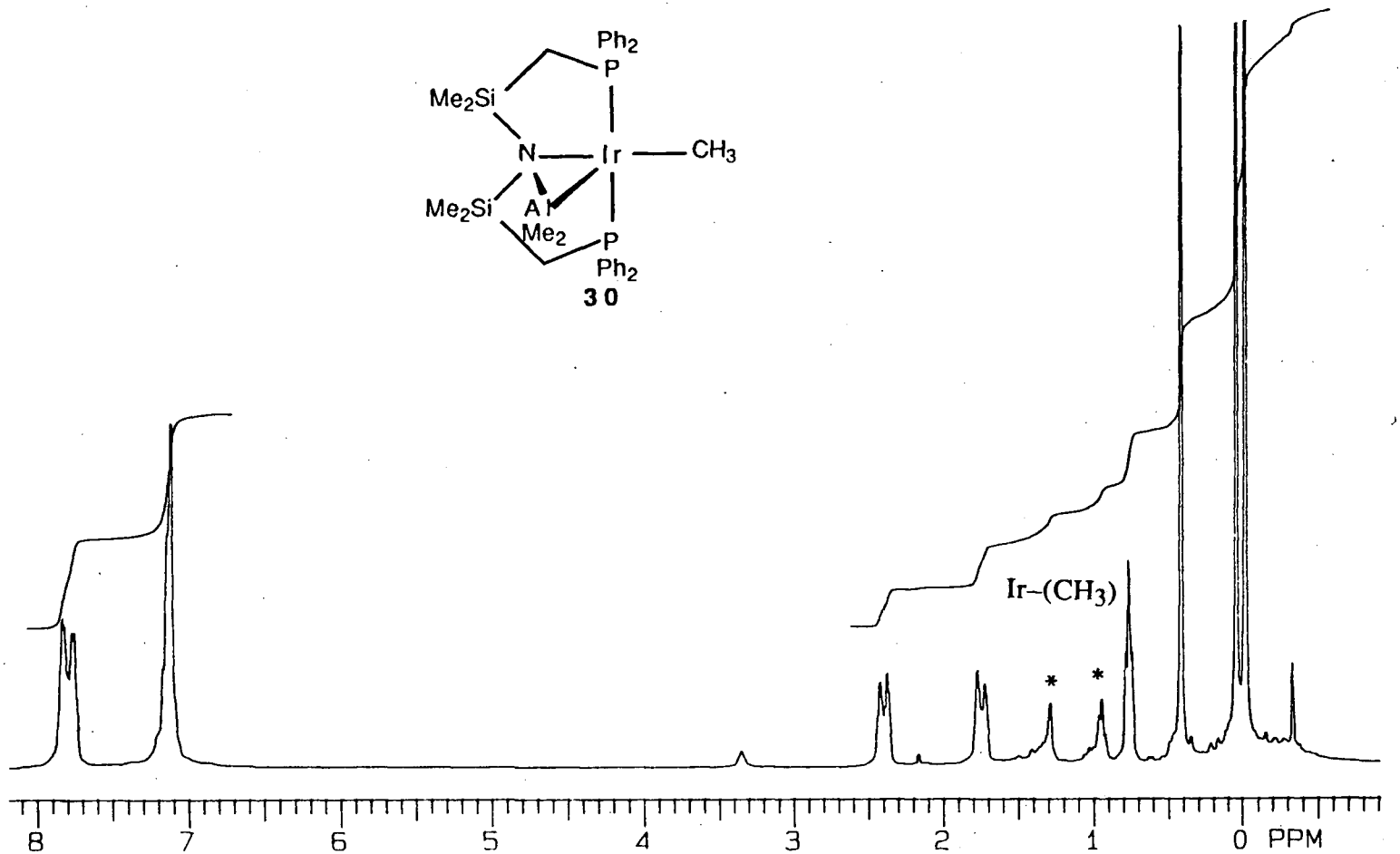

Figure 5.7 ^{1}H NMR spectrum (300 MHz, C_6D_6) of Ir(μ-AlMe$_2$)CH$_3$[N(SiMe$_2$CH$_2$PPh$_2$)$_2$], **30**
(* indicates hexanes protons)

established primarily from ^1H NMR data, in particular the CH_2P and the phenyl resonances. Again, the bridging $AlMe_2$ ligand protons show a singlet at 0.51 ppm. Because of coupling to the two phosphorus nuclei, the Ir-CH_3 resonance is a triplet (0.76 ppm, $^3J_{P,H}$ = 3.1 Hz).

As an extension to the iridium(I) η^2-cyclooctene reactivity with $AlMe_3$, reaction between the analogous rhodium complex was briefly investigated. The rhodium(I) η^2-cyclooctene complex, $Rh(\eta^2\text{-}C_8H_{14})[N(SiMe_2CH_2PPh_2)_2]$, reacted rapidly with $AlMe_3$ to afford a product similar to that observed above namely $Rh(Me)(\mu\text{-}AlMe_2)[N(SiMe_2CH_2PPh_2)_2$, **31**.

5.5 Summary

The results discussed above provide further insight into the reactive nature of the iridium(I) η^2-cyclooctene complex, $Ir(\eta^2\text{-}C_8H_{14})[N(SiMe_2CH_2PPh_2)_2]$. The photolytic conversion of the complex to $Ir(H)_2[N(SiMe_2CH_2PPh_2)_2]$ and free COD through an η^3-allylic hydride intermediate emphasises the importance of such intermediates in dehydrogenation processes. The formation of the iridium(I) olefin complexes via replacement of the cyclooctene ligand by an olefin seems restricted to 1,3-butadiene and allene. The reaction with $AlMe_3$ indicates that an aluminum-alkyl bond cleavage can be achieved under very mild conditions using transition metal complexes.

5.6 References

1 (a) Collman, J. P.; Hegedus, L. S.; Norton, J. R.; Finke, R. G. *Principles and Applications of Organotransition Metal Chemistry*; University Science Books: Mill Valley, CA, **1987**, p.280.
(b) Vaska, L. *Acc. Chem. Res.* **1968**, *1*, 335.

2 (a) Fryzuk, M. D.; MacNeil, P. A.; Rettig, S. J. *Organometallics* **1986**, *5*, 2469.
(b) Fryzuk, M. D.; MacNeil, P. A.; Rettig, S. J. *J. Am. Chem. Soc.* **1987**, *109*, 2803.

3 (a) Crabtree, R. H. *Chem. Rev.* **1985**, *85*, 245.
(b) Shilov, A. E. *Activation of Saturated Hydrocarbons by Transition Metal Complexes*; D. Riedel Publishing Co.: Dordrecht, **1984**.

4 (a) Sakakura, T.; Tanaka, M. *J. Chem. Soc., Chem. Commun.* **1987**, 758.
(b) Sakakura, T.; Sodeyama, T.; Tanaka, M. *Chem. Lett.* **1988**, *4*, 683.
(c) Periana, R. G.; Bergman, R. G. *J. Am. Chem. Soc.* **1986**, *108*, 7332.
(d) Fisher, B. J.; Eisenberg, R. *J. Am. Chem. Soc.* **1986**, *108*, 535.
(e) Kunin, A. J.; Eisenberg, R. *Organometallics* **1983**, *2*, 764.
(f) Maguire, J. A.; Boese, W. T.; Goldman, A. S. *J. Am. Chem. Soc.* **1989**, *111*, 7088.

5 (a) Crabtree, R. H.; Mihelcic, J. M.; Quirk, J. M. *J. Am. Chem. Soc.* **1979**, *101*, 7738.
(b) Crabtree, R. H.; Holt, E. M.; Lavin, M.; Morehouse, S. M. *Inorg. Chem.* **1985**, *24*, 1986.

6 (a) Rinehart, R. E.; Lasky, J. S. *J. Am. Chem. Soc.* **1964**, *86*, 2516.
(b) Gargano, M.; Giannoccaro, M.; Rossi, M. *J. Organomet. Chem.* **1975**, *84*, 389.

7 Bishop, K. C. III *Chem. Rev.* **1976**, *76*, 461.

8 (a) Crabtree, R. H. *The Organometallic Chemistry of the Transition Metals*; Wiley- Interscience: New York, **1988**, p. 188.

(b) Davies, S. G. *Organotransition Metal Chemistry: Applications to Organic Synthesis;* Pergamon Press: Oxford, **1982**, Chapter 7.

9 (a) McGhee, W. S.; Bergman, R. G. *J. Am. Chem. Soc.* **1988**, *110*, 4246.
(b) Siedel, A. R.; Newmark, R. A.; Brown-Wensley, K. A.; Skarjune, R. P.; Haddad, L. C. *Organometallics*, **1988**, *7*, 2078.
(c) McGhee, W. S.; Bergman, R. G. *J. Am. Chem. Soc.* **1985**, *107*, 3388.
(d) Baudry, C.; Boydell, P.; Ephritikhine, M.; Felkin, H.; Guilhem, J.; Pascard, C.; Dau, E. T. H. *J. Chem. Soc., Chem. Commun.* **1985**, 670.
(e) Baudry, C.; Cormier, J. M.; Ephritikhine, M.; Felkin, H. *J. Organomet. Chem.* **1984**, *227*, 99.
(f) Thorn, D. L. *Organometallics* **1982**, *1*, 879.
(g) Claudert, B. N.; Cole-Hamilton, D. J.; Wilkinson, G. *J. Chem. Soc., Dalton Trans.* **1978**, 1739.
(h) Byrne, J. W.; Blaser, H. U.; Osborn, J. A. *J. Am. Chem. Soc.* **1975**, *97*, 3871.

10 Bonnemann, H. *Angew. Chem., Int. Ed. Engl.* **1970**, *9*, 736.

11 Tulip, T. H.; Ibers, J. A. *J. Am. Chem. Soc.* **1979**, *101*, 4201.

12 Batchelor, R. T.; Einstein, F. W. B.; Jones, R. H.; Zhuang, J. M.; Sutton, D. *J. Am. Chem. Soc.* **1989**, *111*, 3468.

13 (a) Blenkers, J.; Hessen, F.; VanBolhuis, A.; Wagner, J.; Teuben, J. H. *Organometallics* **1987**, *6*, 459.
(b) Yasuda, H.; Tatsumi, K.; Nakamura, A. *Acc. Chem. Res.* **1985**, *18*, 120.
(c) Yasuda, H.; Tatsumi, K.; Okamoto, T.; Mashima, K.; Lee, K.; Nakamura, A.; Kai, Y.; Kanehisa, N.; Kasai, N. *J. Am. Chem. Soc.* **1985**, *107*, 2410.
(d) Erker, G.; Kruger, C.; Muller, G. *Adv. Organomet. Chem.* **1985**, *24*, 1.
(e) Datta, S.; Wreford, S. S.; Beatty, R. P.; McNeese, T. J. *J. Am. Chem. Soc.* **1979**, *101*, 1053.

14 See for example: (a) Smith, G. M.; Suzuki, H.; Sonnenberger, D. C.; Day, V. W.; Marks, T. J. *Organometallics*, **1986**, *5*, 549.
(b) Erker, G.; Muhlenberd, T.; Benn, R.; Ruflinska, A. *Organometallics*, **1986**, *5*, 402.

15 (a) Erker, G.; Wicher, J.; Engl, K.; Rosenfeldt, F.; Dietrich, W.; Kruger, C. *J. Am. Chen. Soc.* **1980**, *102*, 6346.
(b) Dorf, U.; Erker, G. *Organometallics* **1983**, *2*, 462.
(c) Czisch, P.; Erker, G.; Korth, H. Sustmann, R. *Organometallics* **1984**, *3*, 945.

16 (a) Hunter, A. D.; Legzdins, P.: Nurse, C. R.; Einstein, F. W. B.; Wills, A. C. *J. Am. Chem. Soc.* **1985**, *107*, 1791.
(b) Christensen, N. J.; Hunter, A. D.; Legzdins, P. *Organometallics* **1989**, *8*, 930.

17 Fryzuk, M. D.; Joshi, K.; Rettig, S. J. *Polyhedron* **1989**, *8*, 2291.

18 Shapley, J. R.; Osborn, J. A. *Acc. Chem. Res.* **1973**, *6*, 305.

19 Fryzuk, M. D.; Haddad, T. S.; Rettig, S. J. *Organometallics* **1989**, *8*, 1723.

20 Okamoto, T.; Yasuda, H.; Nakamura, A.; Kai, Y.; Kanehisa, N.; Kasai, N. *Organometallics* **1988**, *7*, 2266.

21 Appleton, T. G.; Clark, H. C.; Mazner, L. E. *Coord. Chem. Rev.* **1973**, *10*, 335.

22 Yasuda, H.; Nakamura, A. *Angew. Chem. Int. Ed. Engl.* **1987**, *26*, 723.

23 Otsuka, S.; Nakamura, A. *Adv. Organomet. Chem.* **1976**, *14*, 265.

24 (a) Fryzuk, M. D.; MacNeil, P. A.; Massey, R. L.; Ball, R. G. *J. Organomet. Chem.* **1989**, *368*, 231.
(b) Mann, B. E.; Taylor, B. E. *13C NMR Data for Organometallic Compounds*; Academic Press: New York, **1981**, p. 45.

25 Mann, B. E.; Taylor, B. E. *13C NMR Data for Organometallic Compounds*; Academic Press: New York, **1981**, p. 190.

26 (a) Parshall, G. W. *Homogeneous Catalysis*; Wiley: New York, 1980.
(b) Boor, J., Jr. *Ziegler-Natta Catalysis and Polymerisation*; Academic Press: New York, 1979.

27 Tebbe, F. N.; Parshall, G. W.; Reddy, G. S. *J. Am. Chem.Soc.* **1978**, *100*, 3611.

28 Thorn, D. L.; Harlow, R. E. *J. Am. Chem. Soc.* **1989**, *111*, 2575.

CHAPTER 6

General Conclusions and Recommendations for Future Studies

In this thesis work, the synthesis of the six-coordinate iridium(III) cyclometallated hydride complexes of formula, $Ir(\eta^2\text{-}CH_2PR_2)H[N(SiMe_2CH_2\text{-}PPh_2)_2]$, has been achieved by two different unprecedented transformations, namely via thermolysis of the iridium(III) phosphide complexes, and by the reaction of the iridium methylidene complex with primary and secondary phosphines. Kinetic studies show that in the thermolysis process, the rate-determining step is the intramolecular α-hydride abstraction of a methyl C–H, presumably by the phosphide group.

The cyclometallated hydride species convert to the corresponding square-planar iridium(I) phosphine complexes, $Ir(PCH_3R_2)[N(SiMe_2CH_2PPh_2)_2]$, upon thermolysis. The same iridium(I) phosphine complexes are also produced when the phosphide complexes $Ir(CH_3)PR_2[N(SiMe_2CH_2PPh_2)_2]$ are photolysed. It is possible that the photolytic transformation proceeds either through the cyclo-metallated hydride intermediate, or via the migration of the phosphide ligand into the iridium–methyl bond.

The phenylphosphide complex, $Ir(CH_3)PHPh[N(SiMe_2CH_2PPh_2)_2]$, shows dramatically different thermolytic behaviour as compared to its diphenylphosphide

analogue. The only species observed upon the thermolysis is $Ir(PCH_3HPh)$-$[N(SiMe_2CH_2PPh_2)_2]$. Mechanistic studies exclude the involvement of the cyclometallated hydride species in this transformation. A 3-centre transition state is proposed where direct C–P bond formation occurs. This is in contrast to the 4-centre transition state assumed for the thermolysis of the diphenylphosphide complex which might be necessary because of steric strain.

The reactions of $Ir(CH_3)PPh_2[N(SiMe_2CH_2PPh_2)_2]$ with various alkynes have been conducted. Although the initial goal of obtaining the metallacyclophosphinobutene-type complexes could not be achieved (except in the case of the dimethylphosphide complex), some interesting reactivity has emerged from this work. The tridentate ligand undergoes unusual rearrangement when the phosphide complex is exposed to the electron-deficient alkyne DMAD. However, the reactivity with PhC≡CPh and terminal alkynes RC≡CH is readily explained and is consistent with the previous results involving the reactions of the diphenylphosphide complex with CO.

The synthesis of the alkylidene species, $Ir{=}CH_2[N(SiMe_2CH_2PPh_2)_2]$, in relatively good yield has been achieved by the reaction of $Ir(CH_3)I[N(SiMe_2CH_2$-$PPh_2)_2]$ with KO^tBu. The reactions of the alkylidene complex with 1,3-butadiene and allene proceed with complete stereoselectivity which might be a consequence of the hybrid tridentate ligand.

The photochemical dehydrogenation of the η^2-cyclooctene ligand in $Ir(\eta^2$-$C_8H_{14})[N(SiMe_2CH_2PPh_2)_2]$ to yield $Ir(H)_2[N(SiMe_2CH_2PPh_2)_2]$ and free cyclooctadiene through an isolable $Ir(\eta^3$-$C_8H_{13})H[N(SiMe_2CH_2PPh_2)_2]$ intermediate is interesting. Another notable aspect of the iridium(I) cyclooctene chemistry involves Al–Me bond cleavage of the $AlMe_3$ reagent at the iridium centre to yield $Ir(\mu$-$AlMe_2)Me[N(SiMe_2CH_2PPh_2)_2]$

The isolation of and studies on $Ir(\mu\text{-}AlMe_2)Me[N(SiMe_2CH_2PPh_2)_2]$ need to be carried out. In addition, the extension of this work to rhodium analogues and reactivity with other group 13 reagents such as GaR_3 and InR_3 would be of value.

The synthesis of $Ir{=}CH_2[N(SiMe_2CH_2PPh_2)_2]$ from the reaction of $Ir(CH_3)I$-$[N(SiMe_2CH_2PPh_2)_2]$ with $CH_2{=}PR_3$ or potassium enolate (of acetone, for example) would be worth pursuing. Other alkylidene complexes might be accessible via these routes. A preliminary reactivity study of the $^tBuNH_2$ with $Ir{=}CH_2[N(SiMe_2CH_2$-$PPh_2)_2]$ has been conducted (Chapter 4) and the product obtained from this reaction is *fac*-$Ir(\eta^2\text{-}CH_2NH^tBu)H[N(SiMe_2CH_2PPh_2)_2]$. This work can be extended to other amines.

The syntheses of the phosphide complexes containing PR_2 and PHR ligands have been achieved in this thesis work. Phosphide complexes with a PH_2 ligand, namely $Ir(R)PH_2[N(SiMe_2CH_2PPh_2)_2]$, might be prepared from the reaction of $Ir(R)I[N(SiMe_2CH_2PPh_2)_2]$ with PH_3 followed by deprotonation with KO^tBu. Their reactivity studies, in particular thermolysis and photolysis behaviour, would be of interest.

CHAPTER 7

Experimental Procedures

7.1 Materials

7.1.1 Solvents

Spectral or reagent grade solvents were obtained from MCB, BDH, Mallinckrodt, Fisher, Eastman or Aldrich Chemical Co. Hexanes and THF were dried by refluxing over CaH_2 and then distilled from sodium benzophenone ketyl under argon. Toluene was dried by refluxing over CaH_2 and distilled from Na under argon. Benzene was dried over activated 4 Å molecular sieves for 24 hours, vacuum transferred and freeze-pump-thawed several times before being used. The deuterated solvents (C_6D_6 and $CD_3C_6D_5$), used in NMR spectroscopy, were purchased from MSD Isotopes, and were dried over activated 4 Å molecular sieves overnight, vacuum transferred and freeze-pump-thawed several times before being used.

7.1.2 Gases

The gases nitrogen, argon, and carbon monoxide were supplied by Union Carbide of Canada Ltd. The labelled ^{13}CO (90% ^{13}C) gas was obtained from MSD

Isotopes. Acetylene and allene were purchased from Matheson Gas Products and used without further purification. 1,3-Butadiene (obtained from Matheson Gas Products) was condensed into a small gas reactor bomb, and vacuum transferred into a reaction vessel at -10°C.

7.1.3 Reagents

The reagent KO^tBu was purchased from Aldrich Chemical Co. and used as received. CH_3I and CH_2CO_2MeBr were obtained from Aldrich Chemical Co. CH_3I was degassed several times and transferred to a reaction vessel at -10°C. CH_2CO_2MeBr was distilled before being used. BuLi (1.6 M solution in hexanes), $AlMe_3$ (2 M solution in toluene) and DBU were obtained from Aldrich Chemical Co.

The alkynes, DMAD, PhC≡CPh, PhC≡CH, ^{t}BuC≡CH, were purchased from Aldrich Chemical Co. While PhC≡CPh was used without any further purification, the other three alkynes were distilled and stored in dark under a N_2 atmosphere.

The phosphines, $PHPh_2$, $PHMe_2$, PH^tBu_2, HP(*ortho*-tol)$_2$, HP(*meta*-tol)$_2$ and HP^iPr_2, were synthesised by the published procedures.[1] PPh_3 and PH_2Ph were purchased from Aldrich Chemical Co., and used without further purification. The literature procedures were followed to synthesise LiPHPh,[2] $Mg(PHPh)_2$•TMEDA.[3] $KPMe_2$ and KP^tBu_2, were prepared from benzylpotassium and the corresponding phosphines. $LiPPh_2$, LiP(*ortho*-tol)$_2$, LiP(*meta*-tol)$_2$, LiP^iPr_2 were prepared by a dropwise addition of BuLi (1.6 M solution in hexanes) to a hexanes solution of the respective phosphines.

7.1.4 Instrumentation

The ^{1}H NMR spectra were recorded in C_6D_6 or $CD_3C_6D_5$ on the Varian XL-300 or the Bruker WH-400 spectrometer. With C_6D_6 as the solvent, the spectra were

referenced to the residual solvent protons at 7.15 ppm; when $CD_3C_6D_5$ was used, the spectra were referenced to the CD_2H residual proton at 2.09 ppm. The $^{31}P\{^1H\}$ NMR spectra were recorded at 121.421 MHz on the Varian XL-300 and were referenced to external $P(OMe)_3$ set at +141.00 ppm relative to 85% H_3PO_4. The $^{13}C\{^1H\}$ and $^2H\{^1H\}$ were run in C_6D_6 at 75 MHz and 40 MHz, respectively, on the Varian XL-300. The $^{13}C\{^1H\}$ spectra were referenced at 128.00 ppm (triplet for the solvent), and the $^2H\{^1H\}$ spectra were referenced at 7.15 ppm, the residual solvent protons.

Variable temperature NMR spectral studies and various 1D– and 2D–NMR experiments (e.g. selective decoupling studies, APT and HETCOR experiments) were conducted on the Varian XL-300 spectrometer.

Infrared spectra were recorded on a Pye-Unicam SP-1100 or a Nicolet 5DX Fourier Transform spectrophotometer with the samples as KBr pellets or in solution between 0.1 mm NaCl plates.

UV-Vis spectra were recorded on a Perkin Elmer 5523 UV/Vis spectrophotometer stabilised at 20°C.

The X-ray crystal structure of $Ir(\eta^2\text{-}CH_2PPh_2)H[N(SiMe_2CH_2PPh_2)_2]$, **3a**, was carried out by Dr. R. K. Chaddha at the University of Manitoba, and the rest of the structures were determined by Dr. S. J. Rettig of this department.

Carbon, hydrogen and nitrogen analyses were performed by Mr. P. Borda of this department.

7.2 Synthesis and Characterisation of New Complexes

All synthetic reactions were performed under pre-purified nitrogen in a Vacuum Atmosphere HE-533-2 glove box, equipped with a -30°C freezer, or in standard Schlenk-type glassware,[4] as all of the iridium and rhodium complexes prepared in the course of this work were susceptible to oxidation by air. The yields reported for synthetic reactions are generally the average of several repeat preparations.

Iridium and rhodium trichloride hydrates were obtained on loan from Johnson-Matthey and used directly in the preparation of $[M(\eta^2\text{-}C_8H_{14})Cl]_2$ (M = Ir, Rh).[5] The starting materials $Ir(\eta^2\text{-}C_8H_{14})[N(SiMe_2CH_2PPh_2)_2]$ and $Ir(R)X\text{-}[N(SiMe_2CH_2PPh_2)_2]$ (**1**: R = Me, X = I; R = Ph, X = I; **11**: R= CH_2Ph, X = Br; **2a**: R = CH_3, X = PPh_2; **2b**: R = CH_3, X = P(*meta*-tol)$_2$) were prepared by the published procedures.[6] $Rh(\eta^2\text{-}C_8H_{14})[N(SiMe_2CH_2PPh_2)_2]$ and $Rh(CH_3)I[N(SiMe_2CH_2\text{-}PPh_2)_2]$ were also synthesised by the literature procedures.[6]

^1H, $^{31}P\{^1H\}$, $^{13}C\{^1H\}$ NMR data, and IR and UV-Vis data for the new compounds are listed below following their synthesis.

7.2.1 $Ir(CH_3)PMe_2[N(SiMe_2CH_2PPh_2)_2]$, 2c

The complex **2c** was prepared by adding a 2 mL toluene suspension of $KPMe_2$ (46 mg, 0.47 mmol) at -30°C to the toluene solution (10 mL) of $Ir(CH_3)I\text{-}[N(SiMe_2CH_2PPh_2)_2]$, **1**, (400 mg, 0.46 mmol) also at -30°C. The reaction took about an hour to go to completion as the green colour of **1** changed to purple. Because the complex **2c** is thermally unstable, it was prepared only *in situ*. ^1H NMR (300 MHz, C_7D_8, -30°C): $SiMe_2$, -0.03 (s), 0.26 (s); PCH_2Si, 1.99, 2.12 (dt, $^2J_{gem}$ = 12.0 Hz, J_{app} = 4.9 Hz); Ir–CH_3, 1.26 (four line pattern, $^3J_{P,H}$ = 4.0 Hz); PMe_2, 0.55 (d, $^3J_{P,H}$ =

6.7 Hz); PPh_2, 7.17 (m, *para/meta*), 7.75 (m, *ortho*). $^{31}P\{^1H\}$ NMR (C_7D_8, -30°C): PMe_2, 94.30 (t, $^2J_{P,P}$ = 25.1 Hz); PPh_2, 25.11 (d, $^2J_{P,P}$ = 25.0 Hz).

7.2.2 $Ir(CH_3)I(PH_2Ph)[N(SiMe_2CH_2PPh_2)_2]$, 9

Preparation of **9** involved dropwise addition of a toluene solution (5 mL) of PH_2Ph (12 mg, 0.11 mmol) to the toluene solution (10 mL) of $Ir(CH_3)I$-$[N(SiMe_2CH_2PPh_2)_2]$, **1**, (100 mg, 0.11 mmol) at room temperature. The reaction was instantaneous as the green colour of **1** changed to light yellow. The solution was stirred for an hour, and concentrated to ~ 1 mL by pumping off the solvent under vacuum. Addition of ~ 1 mL of hexanes to the reaction mixture afforded light yellow crystals of **9** within few hours. The product was washed with small amounts of hexanes (1/2 mL) and dried *in vacuo*. Yield: 90%. Anal. Calcd. for $C_{37}H_{40}NP_3Si_2Ir$: C, 45.68; H, 4.13; N, 1.44. Found: C, 45.91; H, 4.30; N, 1.20. ^1H NMR (300 MHz, C_6D_6): $SiMe_2$, 0.39 (s), 0.42 (s); PCH_2Si, 1.60, 1.95 (dt, J_{gem} = 12.2 Hz, J_{app} = 4.5 Hz); Ir–CH_3, 1.51 (four line pattern, $^3J_{P,H}$ = 4.7 Hz); P*H*Ph, 5.00 (dt, $^2J_{P,H}$ = 155.1 Hz, $^3J_{P,H}$ = 6.9 Hz); PPh_2, 7.00 (m, *para/meta*), 8.00, 8.17 (m, *ortho*). $^{31}P\{^1H\}$ NMR (C_6D_6): PPh_2, -20.78 (d, $^2J_{P,P}$ = 16.6 Hz); PH_2Ph, -84.57 (t, $^2J_{P,P}$ = 15.8 Hz). $^{13}C\{^1H\}$ NMR (C_6D_6): $SiMe_2$, 5.83 (s), 7.13 (s); PCH_2Si, 21.11 (br t); Ir–CH_3, -6.69 (dt, $^2J_{P,C\ (trans)}$ = 90.1 Hz, $^2J_{P,C\ (cis)}$ = 5.8 Hz; PPh_2, 128-136 (m).

7.2.3 $Ir(CH_3)PHPh[N(SiMe_2CH_2PPh_2)_2]$, 2d

The synthesis of **2d** was achieved by adding KO^tBu (12 mg, 0.10 mmol) to a toluene solution (10 mL) of $Ir(CH_3)I(PH_2Ph)[N(SiMe_2CH_2PPh_2)_2]$, **9**, (100 mg, 0.10 mmol) at room temperature. The reaction proceeded within minutes as the light yellow solution of **9** changed to brick-red due to the formation of **2d**. The excess solvent was pumped off under vacuum. The residual powder was dissolved in hexanes (5 mL) and filtered through Celite in order to remove KI. The solution was

concentrated to ~ 1 mL and stored at -30°C for recrystallisation. The product was isolated as brick-red crystalline material which was washed with hexanes (1/2 mL) and dried *in vacuo*. Yield: 80%. Anal. Calcd. for $C_{37}H_{45}NP_3Si_2Ir$: C, 52.59; H, 5.37; N, 1.66. Found: C, 52.97; H, 5.67; N, 1.49. ^1H NMR (300 MHz, C_7D_8): $SiMe_2$, -0.10 (s), 0.37 (s); PCH_2Si, 1.86 (br); Ir–CH_3, 1.19 (four line pattern, $^3J_{P,H}$ = 4.0 Hz); P*H*Ph, 2.83 (dt, $^1J_{P,H}$ = 195.0 Hz, $^3J_{P,H}$ = 5.4 Hz); PPh_2, 6.81, 6.99, 7.10, 7.29 (m, *para/meta*), 7.35-7.90 (br, *ortho*). $^{31}P\{^1H\}$ NMR (C_6D_6): PHPh, 26.95 (t, $^2J_{P,P}$ = 16.8 Hz); PPh_2, 10.85 (d, $^2J_{P,P}$ = 16.9 Hz). UV-Vis: $\lambda_{(max)}$ (hexanes) = 462 nm, ε = 1820 mol^{-1} L cm^{-1}.

7.2.4 *fac*-Ir(η^2-CH_2PR_2)H[$N(SiMe_2CH_2PPh_2)_2$], (3a: R = Ph, 3b: R = *meta*-tol): General Procedure

The complexes **3a** and **3b** were synthesised by heating a benzene, toluene or hexanes solution (5 mL) of $Ir(CH_3)PR_2[N(SiMe_2CH_2PPh_2)_2]$, **2a** and **2b**, respectively, for ~ 5 hours in an oil bath set at 50°C. The thermolysis was carried out in a reaction vessel sealed under N_2 and wrapped with aluminum foil in order to avoid the photolysis reaction (see Chapter 2). During this time, the purple colour of the phosphide complex discharged to light yellow. The solvent was removed *in vacuo* and the resultant oil was crystallised from hexanes/toluene mixture (1 mL) at room temperature. Light yellow crystals of the product were obtained within few hours which were washed with hexanes (1 mL) and dried *in vacuo*.

7.2.4.1 *fac*-Ir(η^2-CH_2PPh_2)H[$N(SiMe_2CH_2PPh_2)_2$], 3a

$Ir(CH_3)PPh_2[N(SiMe_2CH_2PPh_2)_2]$, **2a** (150 mg, 0.16 mmol). Yield: 82%. Anal. Calcd. for $C_{43}H_{49}NP_3Si_2Ir$: C, 56.07; H, 5.36; N, 1.52. Found: C, 56.28; H, 5.42; N, 1.40. ^1H NMR (300 MHz, C_6D_6): $SiMe_2$, -0.78 (s), 0.65 (s), 0.68 (s), 0.81 (s); PCH_2Si, 1.40 (t, J_{app} = 13.7 Hz), 1.75 (t, J_{app} = 13.7 Hz), 2.10 (m), 2.49 (m); η^2–

CH_2PPh_2, 1.32 (br, m), 2.00 (br, t); PPh_2, 6.60-7.25 (m, *para/meta*), 7.45-8.05 (m, *ortho*); Ir–H, -19.90 (td, $^2J_{P,H}$ = 16.7 Hz, $^2J_{P,H}$ = 9.9 Hz). $^{31}P\{^1H\}$ NMR (C_6D_6): CH_2PPh_2, 12.39 ($^2J_{PA,PX}$ = 32.0 Hz, $^2J_{PM,PX}$ = 5.5 Hz); CH_2PPh_2, 15.60 ($^2J_{PA,PM}$ = 298.2 Hz, $^2J_{PM,PX}$ = 6.4 Hz); η^2-CH_2PPh_2, -46.80 ($^2J_{PA,PM}$ = 297.9 Hz, $^2J_{PA,PX}$ = 30.4 Hz). $^{13}C\{^1H\}$ NMR (C_7D_8): $SiMe_2$, 4.91 (s), 5.62 (s), 5.81 (s), 7.00 (s); PCH_2Si, 23.25 (d, $^1J_{C,P}$ = 12.3 Hz), 28.90 (d, $^1J_{C,P}$ = 21.5 Hz); Ir–CH_2P, -21.62 (m); PPh_2, 127-136 (m). UV-Vis: $\lambda_{(max)}$ (toluene) = 360 nm, ε = 5425 mol^{-1} L cm^{-1}.

7.2.4.2 *fac*-Ir[η^2-CH_2P(*meta*-tol)$_2$]H[$N(SiMe_2CH_2PPh_2)_2$], 3b

Ir(CH_3)[P(*meta*-tol)$_2$][$N(SiMe_2CH_2PPh_2)_2$], **2b** (200 mg, 0.21 mmol). Yield: 80%. Anal. Calcd. for $C_{45}H_{53}NP_3Si_2Ir$: C, 56.94; H, 5.63; N, 1.48. Found: C, 57.30; H, 5.80; N, 1.60. ^1H NMR (400 MHz, C_6D_6): $SiMe_2$, -0.90 (s), 0.71 (s), 0.76 (s), 0.90 (s); PCH_2Si, 1.45 (t, J_{app} = 11.2 Hz), 1.74 (t, J_{app} = 11.2 Hz), 2.19 (m), 2.51 (m); η^2–CH_2P(*meta*-tol)$_2$, 1.30 (br, m), 2.07 (br, overlapped by the tolyl methyl peak); P[$CH_3(C_6H_4)$], 2.10 (s), 2.39 (s); PPh_2, 6.70-8.15 (m); Ir–H, -20.03 (td, $^2J_{P,H}$ = 17.0 Hz, $^2J_{P,H}$ = 8.7 Hz). $^{31}P\{^1H\}$ NMR (C_6D_6): CH_2PPh_2, -1.65 ($^2J_{PA,PX}$ = 33.4 Hz, $^2J_{PM,PX}$ = 4.7 Hz); CH_2PPh_2, 1.82 ($^2J_{PA,PM}$ = 297.1 Hz, $^2J_{PM,PX}$ = 5.0 Hz); η^2-CH_2P(*meta*-tol)$_2$, -61.46 ($^2J_{PA,PM}$ = 297.7 Hz, $^2J_{PA,PX}$ = 33.0 Hz). $^{13}C\{^1H\}$ NMR (C_6D_6): $SiMe_2$, 4.97 (s), 5.77 (s), 5.91 (s), 7.21 (s); PCH_2Si, 23.02 (d, $^1J_{C,P}$ = 12.0 Hz), 29.72 (d, $^1J_{C,P}$ = 21.7 Hz); Ir–CH_2P, -20.65 (m); P[$(CH_3)C_6H_4$] = 21.23 (s), 21.37 (s); PPh_2, 128-139 (m).

7.2.5 *fac*-Ir(η^2-CH_2PMe_2)H[$N(SiMe_2CH_2PPh_2)_2$], 3c

Warming the freshly prepared toluene solution (10 mL) of Ir(CH_3)PMe_2[$N(SiMe_2CH_2PPh_2)_2$], **2c**, from -30°C to room temperature resulted in the formation of **3c** within five minutes. The solution was stirred for an hour. After this time, the solvent was pumped off under vacuum. The residual light yellow powder

was dissolved in toluene (1 mL) and filtered through Celite in order to remove KI generated during the preparation of **2c**. The solution was concentrated to 1/2 mL and left for recrystallisation at room temperature. Light yellow crystals of **3c** were obtained overnight. Yield: 78% (calculated from the amount of **1** used and its 100% conversion to **2c**). Anal. Calcd. for $C_{33}H_{45}NP_3Si_2Ir$: C, 49.75; H, 5.65; N, 1.77. Found: C, 49.67; H, 5.86; N, 1.66. ^1H NMR (300 MHz, C_6D_6): $SiMe_2$, 0.10 (s), 0.51 (s), 0.76 (s), 0.85 (s); PCH_2Si, 1.40 (t, J_{app} = 11.2 Hz), 1.71 (t, J_{app} = 11.2 Hz), 2.18 (m), 2.51 (m); η^2–CH_2PMe_2, 1.30 (br, m), 2.07 (br); PMe_2, 1.40, 1.75 (m), 2.39 (s); PPh_2, 6.70-8.15 (m); Ir–H, -20.10 (td, $^2J_{P,H}$ = 16.8 Hz, $^2J_{P,H}$ = 8.5 Hz). $^{31}P\{^1H\}$ NMR (C_6D_6): CH_2PPh_2, 12.19 ($^2J_{PA,PX}$ = 39.2 Hz, $^2J_{PM,PX}$ = 12.2 Hz); CH_2PPh_2, 14.14 ($^2J_{PA,PM}$ = 300.9 Hz, $^2J_{PM,PX}$ = 12.0 Hz); η^2-CH_2PMe_2, -68.15 ($^2J_{PA,PM}$ = 301.1 Hz, $^2J_{PA,PX}$ = 39.7 Hz).

7.2.6 Ir(PCH_3R_2)[$N(SiMe_2CH_2PPh_2)_2$], (4a: R = Ph, 4b: R = *meta*-tol, 4c: R = Me)

7.2.6.1 Method I: Thermolysis, General Procedure

The complexes **4a-4c** were synthesised by heating a benzene or toluene solution (5 mL) of **3a-3c**, respectively, in a reaction vessel sealed under nitrogen, for 24 h at 100°C. During this time, the light yellow coloured solutions of the species **3a-3c** changed to orange. The excess solvent was pumped off under vacuum and the resultant orange oils were crystallised from hexanes at room temperature.

7.2.6.1a Ir(PCH_3Ph_2)[$N(SiMe_2CH_2PPh_2)_2$], 4a

fac-Ir(η^2-CH_2PPh_2)H[$N(SiMe_2CH_2PPh_2)_2$], **3a** (100 mg, 0.11 mmol). Yield: 85%. Anal. Calcd. for $C_{43}H_{49}NP_3Si_2Ir$: C, 56.07; H, 5.36; N, 1.52. Found: C, 55.80; H, 5.35; N, 1.40. ^1H NMR (400 MHz, C_6D_6): $SiMe_2$, 0.20 (s); PCH_2Si, 1.91 (t, J_{app} = 5.2 Hz); PCH_3Ph_2, 1.38 (d, $^3J_{P,H}$ = 7.5 Hz); PPh_2, 6.90-7.10 (m, *para/meta*), 7.53, 7.62 (m, *ortho*). $^{31}P\{^1H\}$ NMR (C_6D_6): PPh_2, 25.30 (d, $^2J_{P,P}$ = 22.8 Hz); PCH_3Ph_2, -1.79 (t, $^2J_{P,P}$ = 22.3 Hz). UV-Vis: $\lambda_{(max)}$ (toluene) = 388 nm, ε = 2130 mol^{-1} L cm^{-1}.

7.2.6.1b Ir[PCH_3(*meta*-tol)$_2$][$N(SiMe_2CH_2PPh_2)_2$], 4b

fac-Ir[η^2-CH_2P(*meta*-tol)$_2$]H[$N(SiMe_2CH_2PPh_2)_2$], **3b** (100 mg, 0.10 mmol). Yield: 83%. Anal. Calcd. for $C_{45}H_{53}NP_3Si_2Ir$: C, 56.94; H, 5.63; N, 1.48. Found: C, 56.70; H, 5.62; N, 1.42. ^1H NMR (300 MHz, C_6D_6): $SiMe_2$, 0.22 (s); PCH_2Si, 1.85 (t, J_{app} = 5.1 Hz); PCH_3, 0.97 (d, $^3J_{P,H}$ = 6.9 Hz); $CH_3C_6H_4$, 2.45 (s); PPh_2, 7.13 (m, *para/meta*), 8.09 (m, *ortho*). $^{31}P\{^1H\}$ NMR (C_6D_6): PPh_2, 25.56 (d, $^2J_{P,P}$ = 22.3 Hz); PCH_3(*meta*-tol)$_2$, -2.38 (t, $^2J_{P,P}$ = 21.9 Hz).

7.2.6.1c Ir(PMe_3)[$N(SiMe_2CH_2PPh_2)_2$], 4c

fac-Ir(η^2-CH_2PMe_2)H[$N(SiMe_2CH_2PPh_2)_2$], **3c** (100 mg, 0.13 mmol). Yield: 80%. Anal. Calcd. for $C_{33}H_{45}NP_3Si_2Ir$: C, 49.75; H, 5.65; N, 1.77. Found: C, 49.74; H, 5.70; N, 1.71. ^1H NMR (300 MHz, C_6D_6): $SiMe_2$, 0.20 (s); PCH_2Si, 1.88 (t, J_{app} = 5.0 Hz); PMe_3, 0.85 (d, $^3J_{P,H}$ = 7.5 Hz); PPh_2, 7.15 (m, *para/meta*), 8.11 (m, *ortho*). $^{31}P\{^1H\}$ NMR (C_6D_6): PPh_2, 21.51 (d, $^2J_{P,P}$ = 25.2 Hz); PMe_3, -59.54 (t, $^2J_{P,P}$ = 25.2 Hz).

7.2.6.2 Method II: Photolysis, General Procedure

The preparation of the phosphine complexes **4a** and **4b** involved the photolysis, using a 140 W Hg lamp, of the diarylphosphide complexes **2a** and **2b** in a benzene solution (5 mL) at room temperature for 24 h. Because the dimethylphosphide complex **2c** was unstable above -30°C, its photolysis was carried out at -30°C using a N_2 laser in order to produce **4c**. This transformation took approximately 3 hours. The work up of the final orange solutions of **4a-4c** was the same as described above in method I (7.2.6.1).

7.2.6.2a $Ir(PCH_3Ph_2)[N(SiMe_2CH_2PPh_2)_2]$, 4a

$Ir(CH_3)PPh_2[N(SiMe_2CH_2PPh_2)_2]$, **2a** (50 mg, 0.05 mmol). Yield: 78%.

7.2.6.2b $Ir[PCH_3(meta\text{-}tol)_2][N(SiMe_2CH_2PPh_2)_2]$, 4b

$Ir(CH_3)[P(meta\text{-}tol)_2][N(SiMe_2CH_2PPh_2)_2]$, **2b** (100 mg, 0.10 mmol). Yield: 82%.

7.2.6.2c $Ir(PMe_3)[N(SiMe_2CH_2PPh_2)_2]$, 4c

$Ir(CH_3)PMe_2[N(SiMe_2CH_2PPh_2)_2]$, **2c** (50 mg, 0.06 mmol). Yield: 85%.

7.2.7 $Ir(PHCH_3Ph)[N(SiMe_2CH_2PPh_2)_2]$, 4d

The complex **4d** was prepared by heating a benzene, toluene or hexanes solution (5 mL) of the phosphide complex **2d** (100 mg, 0.10 mmol) at 60°C for an hour or by photolysing (140 W Hg lamp) its benzene solution (5 mL) for 18 hours at room temperature. The original brick-red solution turned orange as the transformation proceeded. The reaction mixtures were worked up in usual manner which involved the removal of the solvent *in vacuo* and crystallisation of the orange oil at room

temperature. The isolated yields of **4d** are similar from both the routes (~ 85 %). Anal. Calcd. for $C_{37}H_{45}NP_3Si_2Ir$: C, 52.59; H, 5.37; N, 1.66. Found: C, 52.39; H, 5.30; N, 1.65. ^1H NMR (300 MHz, C_6D_6): $SiMe_2$, 0.26 (s), 0.28 (s); PCH_2Si, 1.93 (m); PCH_3HPh, 1.07 (dd, $^3J_{P,H}$ = 7.9 Hz, $^3J_{H,H}$ = 3.8 Hz); PCH_3HPh, 5.00 (dm, $^1J_{P,H}$ = 140 Hz); PPh_2, 6.90-7.40 (m, *para/meta*), 7.90 (m, *ortho*). $^{31}P\{^1H\}$ NMR (C_6D_6): PPh_2, 22.60 (d, $^2J_{P,P}$ = 18.3 Hz); PHPh, -39.61 (t, $^2J_{P,P}$ = 18.1 Hz). UV-Vis: $\lambda_{(max)}$ (hexanes) = 390 nm, ε = 3000 mol^{-1} L cm^{-1}.

7.2.8 $Ir{=}CH_2[N(SiMe_2CH_2PPh_2)_2]$ + PHR_2 (R = Ph, ^{t}Bu) Reactions: General Procedure

A toluene solution (10 mL) of $Ir{=}CH_2[N(SiMe_2CH_2PPh_2)_2]$, **10**, was cooled to -78°C in a dry ice/ethanol bath for 15 min. To it was added a 1 mL toluene solution containing PHR_2. The original purple colour of **10** turned wine red immediately. As mentioned in chapter 2, this wine red-coloured compound was characterised as $Ir{=}CH_2(PHR_2)[N(SiMe_2CH_2PPh_2)_2]$, **5**. Warming its solution to -30°C resulted in the formation of *fac*-$Ir(\eta^2\text{-}CH_2PR_2)H[N(SiMe_2CH_2PPh_2)_2]$, **6**. The solution was stirred for 10 min at room temperature and then the solvent was removed *in vacuo*. The yellow oil was dissolved in toluene (1 mL) from which pale yellow crystals of **6** were isolated within an hour. The toluene solution of **6** was stirred under an inert atmosphere for 48 hours at room temperature which resulted in its conversion to **3**. The solution was pumped to dryness under vacuum The yellow-coloured oil was crystallised from hexanes/toluene mixture (1 mL) at room temperature.

7.2.8.1 $Ir{=}CH_2(PHPh_2)[N(SiMe_2CH_2PPh_2)_2]$, 5a

$Ir{=}CH_2[N(SiMe_2CH_2PPh_2)_2]$, **10**, (100 mg, 0.14 mmol); $PHPh_2$ (21 mg, 0.15 mmol). ^1H NMR (300 MHz, C_7D_8, -78°C): $SiMe_2$, 0.09 (s), 0.81 (s); PCH_2Si, 1.75 (br); $Ir{=}CH_2$, 12.08 (four line pattern, $^3J_{P,H}$ = 14.4 Hz); $PHPh_2$, 5.90 (other half

obscured by the phenyl resonances); PPh_2, 6.70-7.40 (m, *para/meta*), 8.45 (m, *ortho*). $^{31}P\{^1H\}$ NMR (C_7D_8): CH_2PPh_2, 13.45 (s); $PHPh_2$, 3.90 (s).

7.2.8.2 *fac*-Ir(η^2-CH_2PPh_2)H[$N(SiMe_2CH_2PPh_2)_2$], 6a

Ir=CH_2[$N(SiMe_2CH_2PPh_2)_2$], **10**, (100 mg, 0.14 mmol); $PHPh_2$ (21 mg, 0.15 mmol). Yield: 85%. Anal. Calcd. for $C_{43}H_{49}NP_3Si_2Ir$: C, 56.07; H, 5.36; N, 1.52. Found: C, 56.53; H, 5.52; N, 1.50. ^1H NMR (400 MHz, C_6D_6): $SiMe_2$, 0.52 (s), 0.71 (s), 0.76 (s), 0.82 (s); PCH_2Si, 1.36 (m), 1.40 (m), 1.60 (t, J_{app} = 9.0 Hz), 2.25 (m); η^2–CH_2PPh_2, 1.25 (br, m), 1.58 (m); PPh_2, 6.50-7.49 (m, *para/meta*), 7.90-8.45 (m, *ortho*); Ir–H, -11.88 (dddd, $^2J_{P,H\ (trans)}$ = 133.3 Hz, $^2J_{P,H\ (cis)}$ = 19.8 Hz, $^2J_{P,H\ (cis)}$ = 11.8 Hz). $^{31}P\{^1H\}$ NMR (C_7D_8): CH_2PPh_2, -16.17 (br t, $^2J_{P,\ P}$= 12.6 Hz); CH_2PPh_2, 13.44 ($^2J_{PA,PM}$ = 310.1 Hz, $^2J_{PM,PX}$ = 10.3 Hz); η^2-CH_2PPh_2, -58.20 ($^2J_{PA,PM}$ = 310.8 Hz, $^2J_{PA,PX}$ = 10.3 Hz). $^{13}C\{^1H\}$ NMR (C_7D_8): $SiMe_2$, 3.18 (s), 3.59 (s), 3.73 (s), 7.13 (s); PCH_2Si, 14.38 (br s), 23.08 (br s); Ir–CH_2P, -38.20 (br); PPh_2, 127-136 (m). UV-Vis: $\lambda_{(max)}$ (toluene) = 360 nm, ε = 2205 mol^{-1} L cm^{-1}.

7.2.8.3 *fac*-Ir(η^2-CH_2PPh_2)H[$N(SiMe_2CH_2PPh_2)_2$], 3a

fac-Ir(η^2-CH_2PPh_2)H[$N(SiMe_2CH_2PPh_2)_2$], **6a**, (75 mg, 0.08 mmol). Yield: 80%. The spectroscopic data and elemental analysis of this complex are reported in section 7.2.4.1.

7.2.8.4 Ir=CH_2(PH^tBu_2)[$N(SiMe_2CH_2PPh_2)_2$], 5e

Ir=CH_2[$N(SiMe_2CH_2PPh_2)_2$], **10**, (100 mg, 0.14 mmol); PH^tBu_2 (17 mg, 0.15 mmol). ^1H NMR (300 MHz, C_7D_8, -78°C): $SiMe_2$, 0.70 (s), 0.74 (s); PCH_2Si, 2.30 (br); P^tBu_2, 1.10 (s), 1.15 (s); Ir=CH_2, 16.26 (four line pattern, $^3J_{P,H}$ = 18.0 Hz); PH^tBu_2, 3.36 (br, d, $^1J_{P,H}$ = 216.0 Hz); PPh_2, 6.40-8.15 (m). $^{31}P\{^1H\}$ NMR (C_7D_8): CH_2PPh_2, 17.85 (s); PH^tBu_2, 18.71 (s).

7.2.8.5 *fac*-Ir(η^2-$CH_2P^tBu_2$)H[$N(SiMe_2CH_2PPh_2)_2$], 6e

Ir=CH_2[$N(SiMe_2CH_2PPh_2)_2$], **10**, (100 mg, 0.14 mmol); PH^tBu_2 (17 mg, 0.15 mmol). Yield: 78%. Anal. Calcd. for $C_{39}H_{57}NP_3Si_2Ir$: C, 53.16; H, 6.52; N, 1.59. Found: C, 53.71; H, 6.61; N, 1.70. ^1H NMR (300 MHz, C_7D_8): $SiMe_2$, 0.58 (s), 0.70 (s), 0.85 (s), 0.90 (s); PCH_2Si, 1.49 (m), 1.54 (m), 1.78 (m), 2.46 (m); η^2–$CH_2P^tBu_2$, 1.28 (br, m), 1.67 (m); P^tBu_2, 1.07 (s), 1.09 (s), 1.12 (s), 1.14 (s); PPh_2, 6.70-7.85 (m); Ir–H, -14.34 (dt, $^2J_{P,H\ (trans)}$ = 100.1 Hz, $^2J_{P,H\ (cis)}$ = 15.5 Hz). $^{31}P\{^1H\}$ NMR (C_6D_6): CH_2PPh_2, -17.73 ($^2J_{PA,PX}$ = 15.9 Hz, $^2J_{PM,PX}$ = 14.2 Hz); CH_2PPh_2, 4.55 ($^2J_{PA,PM}$ = 217.9 Hz, $^2J_{PM,PX}$ = 14.7Hz); η^2-$CH_2P^tBu_2$, -23.74 ($^2J_{PA,PM}$ = 323.6 Hz, $^2J_{PA,PX}$ = 15.8 Hz). $^{13}C\{^1H\}$ NMR (C_7D_8): $SiMe_2$, 3.28 (s), 3.84 (s), 3.98 (s), 7.29 (s); PCH_2Si, 18.10 (d, $^2J_{P,C}$ = 13.7 Hz), 25.58 (s); Ir–CH_2P, -38.05 (br); P^tBu_2, 29.54 (s), 31.67 (s); PPh_2, 128-134 (m).

7.2.8.6 *fac*-Ir(η^2-$CH_2P^tBu_2$)H[$N(SiMe_2CH_2PPh_2)_2$], 3e

fac-Ir(η^2-$CH_2P^tBu_2$)H[$N(SiMe_2CH_2PPh_2)_2$], **6e**, (50 mg, 0.06 mmol). Yield: 86%. Anal. Calcd. for $C_{39}H_{57}NP_3Si_2Ir$: C, 53.16; H, 6.52; N, 1.59. Found: C, 53.32; H, 6.43; N, 1.50. ^1H NMR (300 MHz, C_7D_8): $SiMe_2$, 0.65 (s), 0.82 (s), 0.96 (s), 1.14 (s); PCH_2Si, 2.15 (m), 2.35 (m), 2.71 (m); η^2–$CH_2P^tBu_2$, 1.28 (br, m), 1.67 (m); P^tBu_2, 1.50 (s), 1.62 (s), 1.68 (s), 1.74 (s); PPh_2, 6.90-8.42 (m); Ir–H, -21.62 (dt, $^2J_{P,H\ (trans)}$ = 84.0 Hz, $^2J_{P,H\ (cis)}$ = 36.0 Hz). $^{31}P\{^1H\}$ NMR (C_7D_8): CH_2PPh_2, 16.53 ($^2J_{PA,PX}$ = 32.8 Hz, $^2J_{PM,PX}$ = 4.9 Hz); CH_2PPh_2, 18.74 ($^2J_{PA,PM}$ = 289.8 Hz, $^2J_{PM,PX}$ = 5.5 Hz); η^2-$CH_2P^tBu_2$, 3.50 ($^2J_{PA,PM}$ = 289.2 Hz, $^2J_{PA,PX}$ = 32.9 Hz). $^{13}C\{^1H\}$ NMR (C_7D_8): $SiMe_2$, 6.43 (s), 6.58 (s), 7.58 (s), 11.07 (s); PCH_2Si, 22.64 (d, $^2J_{P,C}$ = 11.9 Hz), 27.56 (d, $^2J_{P,C}$ = 21.9 Hz); Ir–CH_2P, -23.00 (br); P^tBu_2, 32.10 (s), 32.28 (s); PPh_2, 125-136 (m).

7.2.9 *fac*-Ir(η^2-CH_2PHPh)H[$N(SiMe_2CH_2PPh_2)_2$], 6d

A solution of Ir=CH_2[$N(SiMe_2CH_2PPh_2)_2$], **10**, (150 mg, 0.27 mmol) in toluene (10 mL) was cooled to -78°C in a dry ice/ethanol bath for 15 min. To it was added 1 mL toluene solution of PH_2Ph (23 mg, 0.21 mmol). The original purple colour of **10** turned light yellow immediately. The solution was warmed to room temperature and stirred for an hour. The solvent was removed under vacuum, and the residue was recrystallised from hexanes/toluene mixture (1/2 mL) at room temperature. Yield: 75%. Anal. Calcd. for $C_{37}H_{45}NP_3Si_2Ir$: C, 52.59; H, 5.37; N, 1.66. Found: C, 52.07; H, 5.54; N, 1.70. ^1H NMR (300 MHz, C_6D_6): $SiMe_2$, -0.05 (s), -0.20 (s), -0.35 (s), -0.69 (s); PCH_2Si, 1.95 (m), 2.10 (m); η^2-C*H*$_2$PHPh, 1.51 (m), 2.75 (br, m); P*H*Ph, 3.86 (br, m); PPh_2, 6.70-7.40 (m, *para*/*meta*), 7.50-7.90 (m, *ortho*); Ir–H, -12.87 (dt, $^2J_{P,H\ (trans)}$ = 149.3 Hz, $^2J_{P,H\ (cis)}$ = 19.1 Hz). $^{31}P\{^1H\}$ NMR (C_6D_6): CH_2PPh_2, 5.50 (m); CH_2PPh_2, -64.21 (m); η^2-CH_2PHPh, -93.25 (t, $^2J_{P,P}$ = 9.1Hz).

7.2.10 *fac*-Ir(η^2-$CHPhPMe_2$)H[$N(SiMe_2CH_2PPh_2)_2$], 6f

The complex **6f** was prepared by adding a 2 mL toluene suspension of $KPMe_2$ (10 mg, 0.09 mmol) to the toluene solution (10 mL) of Ir(CH_2Ph)Br-[$N(SiMe_2CH_2PPh_2)_2$], **11**, (75 mg, 0.08 mmol) at room temperature. The reaction took about half an hour to go to completion as the green colour of **11** changed to yellow. After this time, the solvent was removed *in vacuo*. The residue was dissolved in toluene (1 mL) and filtered through Celite in order to remove KBr. Recrystallisation from toluene/hexanes (1 mL) afforded yellow crystals. Yield: 85%. Anal. Calcd. for $C_{39}H_{49}NP_3Si_2Ir$: C, 53.65; H, 5.66; N, 1.60. Found: C, 53.43; H, 5.80; N, 1.68. ^1H NMR (300 MHz, C_6D_6): $SiMe_2$, 0.17 (s), 0.51 (s), 0.86 (s), 0.95 (s); PCH_2Si, 1.30 (m), 1.59 (m), 1.97 (m); η^2–C*H*$PhPMe_2$, 2.09 (m); PMe_2, 0.35 (d), 1.20 (d, $^3J_{P,H}$ = 15.0 Hz); PPh_2, 6.70-7.75 (m, *para*/*meta*), 8.80 (m, *ortho*); Ir–H,

-10.82 (ddd, $^2J_{P,H\ (trans)}$ = 153.0 Hz, $^2J_{P,H\ (cis)}$ = 20.1 Hz, $^2J_{P,H\ (cis)}$ = 9.0 Hz). $^{31}P\{^1H\}$ NMR (C_6D_6): CH_2PPh_2, -7.39 (4 line pattern, $^2J_{P,P}$ = 9.5 Hz); CH_2PPh_2, -2.60 (4 line pattern, $^2J_{P,P}$ = 9.5 Hz, $^2J_{P,P}$ = 9.3 Hz); η^2-$CHPhPMe_2$, -11.19 (t, $^2J_{P,P}$ = 9.0 Hz).

7.2.11 Ir(PMe_2CH_2Ph)[$N(SiMe_2CH_2PPh_2)_2$], 4f

The complex **4f** was synthesised by stirring a toluene solution (5 mL) of **6f** (50 mg, 0.06 mmol) for two weeks at room temperature (or 48 hours at 80°C) under a N_2 atmosphere. During this time, the light yellow coloured solutions of **6f** darkened to orange. The excess solvent was pumped off under vacuum and the resultant orange oil was recrystallised from hexanes at room temperature. Yield: 80%. Anal. Calcd. for $C_{39}H_{49}NP_3Si_2Ir$: C, 53.65; H, 5.66; N, 1.60. Found: C, 53.53; H, 5.72; N, 1.50. ^1H NMR (300 MHz, C_6D_6): $SiMe_2$, 0.28 (s); PCH_2Si, 1.99 (t, J_{app} = 6.0 Hz); PCH_2PhMe_2, 2.55 (d, $^2J_{P,H}$ = 14.5 Hz); PCH_2PhMe_2, 0.83 (d, $^2J_{P,H}$ = 11.5 Hz); PPh_2, 7.21 (m, *para/meta*), 8.15 (m, *ortho*). $^{31}P\{^1H\}$ NMR (C_6D_6): CH_2PPh_2, 20.23 ($^2J_{P,P}$ = 23.8 Hz); CH_2PhPMe_2, -39.73 ($^2J_{P,P}$ = 23.8 Hz).

7.2.12 Ir(η^1-CH_2PPh_2)H(CO)[$N(SiMe_2CH_2PPh_2)_2$], 7a

A toluene solution (10 mL) of Ir(η^2-CH_2PPh_2)H[$N(SiMe_2CH_2PPh_2)_2$], **2a** or **6a** (100 mg, 0.11 mmol) was loaded in a thick-walled reactor bomb equipped with a 5 mm Kontes needle valve. The vessel was attached to a vacuum line and degassed. The solution was exposed to excess CO gas (1 atm) and stirred for 48 hours at room temperature. Toluene was removed *in vacuo* and the faint yellow residual powder was recrystallised from toluene/hexanes mixture (1 mL). Yield: 90%. Anal. Calcd. for $C_{44}H_{49}NOP_3Si_2Ir$: C, 55.68; H, 5.20; N, 1.48. Found: C, 55.42; H, 5.36; N, 1.60. ^1H NMR (400 MHz, C_6D_6): $SiMe_2$, 0.20 (s), 0.31 (s); PCH_2Si, 2.10 (dt, J_{gem} = 13.3 Hz, J_{app} = 6.6 Hz); η^1–CH_2PPh_2, 1.48 (br); PPh_2, 7.15 (m, *para/meta*), 7.79 , 8.00 (m,

ortho); Ir–H, -6.50 (td, $^2J_{P,H}$ = 18.0 Hz, $^3J_{P,H}$ = 9.0 Hz). $^{31}P\{^1H\}$ NMR (C_6D_6): $SiCH_2PPh_2$, 5.84 (d, $^3J_{P,P}$ = 11.9 Hz); $IrCH_2PPh_2$, 10.51 (t, $^3J_{P,P}$ = 11.6 Hz). $^{13}C\{^1H\}$ NMR (C_6D_6): $SiMe_2$, 2.81 (s), 3.22 (s); PCH_2Si, 32.15 (m); Ir–CO, 179.88 (dt, $^2J_{P,C}$ = 11.0 Hz, $^3J_{P,C}$ = 5.9 Hz); PPh_2, 124-138 (m). IR (toluene): $\nu_{(CO)}$ = 1961 cm^{-1} (vs), $\nu_{(Ir-H)}$ = 2095 cm^{-1} (m).

7.2.13 *fac*-Ir(CH_3)(η^2-CH_2PPh_2)[$N(SiMe_2CH_2PPh_2)_2$]

This complex was prepared by adding a toluene solution of $LiCH_2PPh_2$•TMEDA (40 mg, 0.13 mmol) to the toluene solution (10 mL) of Ir(CH_3)I[$N(SiMe_2CH_2PPh_2)_2$], **1**, (100 mg, 0.11 mmol) at room temperature. The reaction took about an hour to go to completion as the green colour of **1** changed to yellow. The excess solvent was removed *in vacuo*. The residue was dissolved in toluene (1 mL) and filtered through Celite in order to remove LiI. Several attempts were made to isolate the product, but decompositon resulted over 24 hours as the solution was left for recrystallisation at room temperature under a N_2 atmosphere. ^1H NMR (300 MHz, C_6D_6): $SiMe_2$, -0.50 (s), 0.11 (s), 0.39 (s), 0.51 (s); PCH_2Si, 2.62 (m), 2.41 (m), 2.10 (m), 1.65 (m); Ir–CH_3, 1.89 (br); PPh_2, 6.54-7.24 (m, *para*/*meta*), 8.12 (m, *ortho*). $^{31}P\{^1H\}$ NMR (C_6D_6): CH_2PPh_2, 2.11 ($^2J_{PA,PX}$ = 35.2 Hz, $^2J_{PM,PX}$ = 5.1 Hz); CH_2PPh_2, 8.59 ($^2J_{PA,PM}$ = 326.3 Hz, $^2J_{PM,PX}$ = 6.0 Hz); η^2-CH_2PPh_2, -51.23 ($^2J_{PA,PM}$ = 337.8 Hz, $^2J_{PA,PX}$ = 36.4 Hz).

7.2.14 Ir(CH_3)PPh_2{$C_2(CO_2Me)_2$}[$N(SiMe_2CH_2PPh_2)_2$], 12

A toluene solution (10 mL) of Ir(CH_3)PPh_2[$N(SiMe_2CH_2PPh_2)_2$], **2a**, (250 mg, 0.27 mmol) was added to a reactor bomb equipped with a 5 mm Kontes needle valve. The assembly was attached to a vacuum line and cooled to -78°C (dry ice/ethanol). To it was added a toluene solution (1 mL) of DMAD (40 mg, 0.29 mmol) The reaction was instantaneous as the original dark purple colour of the phosphide

complex turned burgundy. The reaction mixture was warmed to room teperature and stirred for an hour. The solvent was removed *in vacuo* and the resultant powder was recrystallised from hexanes/toluene solution (1 mL) at room temperature. Yield: 82%. Anal. Calcd. for $C_{49}H_{55}NO_4P_3Si_2Ir$: C, 55.35; H, 5.21; N, 1.32. Found: C, 55.22; H, 5.37; N, 1.11. ^1H NMR (400 MHz, C_6D_6): $SiMe_2$, 0.54 (s), 0.71 (s), 0.78 (s), 0.90 (s); PCH_2Si, 1.78 (t, J_{gem} = 13.3 Hz), 1.87 (t, J_{gem} = 11.7 Hz), 2.14 (m), 2.72 (m); Ir–CH_3, 0.22 (four line pattren, $^3J_{P,H}$ = 4.0 Hz); OCH_3, 2.92 (s), 3.05 (s); PPh_2, 7.20 (m, *para/meta*), 8.20, 8.45 (m, *ortho*). $^{31}P\{^1H\}$ NMR (C_6D_6): CH_2PPh_2, 41.25 ($^2J_{PA,PM}$ = 398.3 Hz, $^2J_{PA,PX}$ = 6.1 Hz); CH_2PPh_2, -17.65 ($^2J_{PA,PM}$ = 389.3 Hz, $^2J_{PM,PX}$ = 14.6 Hz); PPh, 26.85 ($^2J_{PA,PX}$ = 4.8 Hz, $^2J_{PM,PX}$ = 7.3 Hz). $^{13}C\{^1H\}$ NMR (C_6D_6): $SiMe_2$, 5.38 (s), 5.62 (s), 5.82 (s), 8.89 (s); PCH_2Si, 22.57 (d, $^1J_{P,C}$ = 19.2 Hz), 21.30 (d, $^1J_{P,C}$ = 12.4 Hz); Ir–CH_3, -17.89 (4 line pattern, $^2J_{P,C}$ = 7.3 Hz); OCH_3, 51.13 (s), 51.82 (s); PPh_2, 126-134 (m). IR (KBr): $\nu_{(CO)}$ = 1711.7 (s) and 1746.9 cm^{-1} (s).

7.2.15 $Ir(CH_3)PMe_2\{C_2(CO_2Me)_2\}[N(SiMe_2CH_2PPh_2)_2]$, 13

A toluene solution (10 mL) of $Ir(CH_3)PMe_2[N(SiMe_2CH_2PPh_2)_2]$, **2c**, (100 mg, 0.12 mmol) was prepared at -30°C. To it was added a toluene solution (1 mL, -30°C) of DMAD (20 mg, 0.14 mmol). The reaction was instantaneous as the dark purple-coloured solution turned burgundy. The reaction mixture was warmed to room temperature and stirred for an hour. The solvent was removed *in vacuo* and the resultant powder was recrystallised from hexanes/toluene (1 mL). Yield: 75%. Anal. Calcd. for $C_{39}H_{51}NO_4P_3Si_2Ir$: C, 49.88; H, 5.47; N, 1.49. Found: C, 50.10; H, 5.67; N, 1.21. ^1H NMR (300 MHz, C_6D_6): $SiMe_2$, 0.30 (s), 0.61 (s); PCH_2Si, 2.10 (dt, J_{gem} = 15.6 Hz, J_{app} = 7.1 Hz), 2.38; Ir–CH_3, 0.08 (t, $^3J_{P,H}$ = 4.7 Hz); OCH_3, 3.27 (s), 3.88 (s); PMe_2, 1.19 (d, $^2J_{P,H}$ = 9.5 Hz); PPh_2, 7.15 (m, *para/meta*), 7.66, 7.85 (m, *ortho*). $^{31}P\{^1H\}$ NMR (C_6D_6): CH_2PPh_2, 2.99 ($^2J_{P,P}$ = 23.8 Hz); PMe_2, -106.70

($^2J_{P,P}$ = 23.5 Hz). $^{13}C\{^1H\}$ NMR (C_6D_6): $SiMe_2$, 5.96 (s), 7.96 (s); PCH_2Si, 20.38 (d, $^1J_{P,C}$ = 26.1 Hz), 20.64 (d, $^1J_{P,C}$ = 19.0 Hz); Ir–CH_3, -15.37 (4 line pattern, $^2J_{P,C}$ = 7.0 Hz); OCH_3, 50.25 (s), 50.84 (s); PPh_2, 125-132 (m).

7.2.16 Ir(CH_3)I{$C_2(CO_2Me)_2$}[N($SiMe_2CH_2PPh_2)_2$], 14

To a rapidly stirred solution of Ir(CH_3)I[N($SiMe_2CH_2PPh_2)_2$], **1**, (200 mg, 0.25 mmol) in toluene (10 mL) was added a toluene solution (1 mL) of DMAD (35 mg, 0.25 mmol) at -30°C. An instantaneous reaction occured as the green colour of the starting material changed to burgundy due to the formation of **14**. The solution was stirred for an hour at room temperature, and then the solvent was removed *in vacuo*. The resultant oil was crystallised from toluene. Yield: 90%. Anal. Calcd. for $C_{37}H_{45}NO_4P_3Si_2IIr$: C, 44.22; H, 4.51; N, 1.39. Found: C, 44.17; H, 4.53; N, 1.26. ^1H NMR (400 MHz, C_6D_6): $SiMe_2$, 0.39 (s), 0.46 (s), 0.62 (s), 0.85 (s); PCH_2Si, 1.60 (t, obscured by the Ir-CH_3 peak), 1.76 (t, J_{gem} = 8.8 Hz), 1.93 (m); Ir–CH_3, 1.65 (t, $^3J_{P,H}$ = 3.8 Hz); OCH_3, 3.39 (s), 3.65 (s); PPh_2, 6.90 (m, *para/meta*), 7.95, 8.05, 8.17 (m, *ortho*). $^{31}P\{^1H\}$ NMR (C_6D_6): CH_2PPh_2, 42.34 (d, $^2J_{P,P}$ = 11.0 Hz), -20.56 (d, $^2J_{P,P}$ = 7.4 Hz). $^{13}C\{^1H\}$ NMR (C_6D_6): $SiMe_2$, 0.18 (s), 0.36 (s), 0.99 (s), 1.25 (s); PCH_2Si, 14.99 (s), 15.26 (s); Ir–CH_3, -15.15 (t,$^2J_{P,C}$ = 7.5 Hz); OCH_3, 50.45 (s), 52.04 (s); PPh_2, 126-132 (m). IR(KBr): $\nu_{(CO)}$ = 1676.8 (m) and 1732.8 cm^{-1} (m).

7.2.17 Ir(PhC≡CPh)[N($SiMe_2CH_2PPh_2)_2$], 15

A toluene solution (2 mL) of PhC≡CPh (50 mg, 0.28 mmol) was added dropwise to the toluene solution (10 mL) of Ir(CH_3)PPh_2[N($SiMe_2CH_2PPh_2)_2$], **2a**, (250 mg, 0.27 mmol). The purple colour of **2a** changed to orange over 10 min. After the solution was stirred for an hour, the excess solvent was removed *in vacuo*. Orange crystals of Ir(PhC≡CPh)[N($SiMe_2CH_2PPh_2)_2$], **15**, were isolated from

hexanes (1 mL). Yield: 75%. Anal. Calcd. for $C_{44}H_{46}NP_2Si_2Ir$: C, 58.77; H, 5.16; N, 1.56. Found: C, 59.00; H, 5.16; N, 1.70. The NMR characterisation of **15** is described elsewhere.[7]

7.2.18 $Ir(CH_3)PHPh_2(C{\equiv}CR)[N(SiMe_2CH_2PPh_2)_2]$, 16-18 (R = H, Ph, ^tBu): General Procedure

A toluene solution (10 mL) of the phosphide complex $Ir(CH_3)PPh_2$-$[N(SiMe_2CH_2PPh_2)_2]$, **2a**, was loaded in a reaction bomb equipped with a 5 mm Kontes needle valve. The assembly was connected to a vacuum line and the solution degassed. In the case of HC≡CH, excess alkyne was condensed in the vessel at -78°C (dry ice/ethanol). However, when PhC≡CH or ^tBuC≡CH were reacted with **2a**, the exact amounts of the alkynes dissolved in toluene (1 mL) were syringed into the reaction vessel. Many attempts were made to isolate these complexes, but decomposition resulted as the solutions were left for crystallisation under an inert atmosphere.

7.2.18.1 $Ir(CH_3)PHPh_2(C{\equiv}CH)[N(SiMe_2CH_2PPh_2)_2]$, 16

$Ir(CH_3)PPh_2[N(SiMe_2CH_2PPh_2)_2]$, **2a**, (100 mg, 0.11 mmol). ^1H NMR (300 MHz, C_6D_6): $SiMe_2$, 0.70 (s), 0.85 (s); PCH_2Si, 2.21 (dt), 2.45 (dt, J_{gem} = 12.3 Hz, J_{app} = 7.1 Hz); Ir–CH_3, -0.10 (four line pattern, $^3J_{P,H}$ = 3.8 Hz); C≡CH, 2.10 (s); $PHPh_2$, 5.01 (dt, $^1J_{P,H}$ = 300.1 Hz, $^3J_{P,H}$ = 9.5 Hz); PPh_2, 6.90 (m, *para/meta*), 7.95, 8.17 (m, *ortho*). $^{31}P\{^1H\}$ NMR (C_6D_6): PPh_2, -2.32 (d, $^2J_{P,P}$ = 15.9 Hz); $PHPh_2$, -21.45 (t, $^2J_{P,P}$ = 17.8 Hz).

7.2.18.2 $Ir(CH_3)PHPh_2(C{\equiv}CPh)[N(SiMe_2CH_2PPh_2)_2]$, 17

$Ir(CH_3)PPh_2[N(SiMe_2CH_2PPh_2)_2]$, **2a**, (75 mg, 0.08 mmol). $PhC{\equiv}CH$ (10 mg, 0.08 mmol). ^1H NMR (300 MHz, C_6D_6): $SiMe_2$, 0.56 (s), 0.81 (s); PCH_2Si, 2.00 (dt), 2.21 (dt, J_{gem} = 12.1 Hz, J_{app} = 6.5 Hz); Ir–CH_3, 0.05 (four line pattern, $^3J_{P,H}$ = 3.0 Hz); $PHPh_2$, 5.08 (dt, $^1J_{P,H}$ = 310.6 Hz, $^3J_{P,H}$ = 8.7 Hz); PPh_2, 6.98 (m, *para/meta*), 7.65, 8.10 (m, *ortho*). $^{31}P\{^1H\}$ NMR (C_6D_6): PPh_2, -2.58 (d, $^2J_{P,P}$ = 16.3 Hz); $PHPh_2$, -23.35 (t, $^2J_{P,P}$ = 18.1 Hz).

7.2.18.3 $Ir(CH_3)PHPh_2(C{\equiv}C^tBu)[N(SiMe_2CH_2PPh_2)_2]$, 18

$Ir(CH_3)PPh_2[N(SiMe_2CH_2PPh_2)_2]$, **2a**, (75 mg, mmol). $^tBuC{\equiv}CH$ (10 mg, 0.13 mmol). ^1H NMR (300 MHz, C_6D_6): $SiMe_2$, 0.75 (s), 0.90 (s); PCH_2Si, 2.20 (dt), 2.35 (dt, J_{gem} = 12.3 Hz, J_{app} = 7.1 Hz); Ir–CH_3, -0.09 (four line pattern, $^3J_{P,H}$ = 3.8 Hz); $C{\equiv}C^tBu$, 1.72 (s); $PHPh_2$, 5.30 (dt, $^1J_{P,H}$ = 360.0 Hz, $^3J_{P,H}$ = 7.2 Hz); PPh_2, 6.96 (m, *para/meta*), 7.91, 8.89 (m, *ortho*). $^{31}P\{^1H\}$ NMR (C_6D_6): PPh_2, -3.01 (d, $^2J_{P,P}$ = 16.5 Hz); $PHPh_2$, -22.08 (t, $^2J_{P,P}$ = 17.9 Hz).

7.2.19 $Ir{=}CH_2[N(SiMe_2CH_2PPh_2)_2]$, 10

To a stirred toluene solution (10 mL) of $Ir(CH_3)I[N(SiMe_2CH_2PPh_2)_2]$, **1** (250 mg, 0.29 mmol) was added KO^tBu (160 mg, 1.4 mmol). The reaction proceeded over two hours as the green-coloured solution of **1** turned purple due to the formation of **10**. The reaction mixture was filtered through Celite and pumped to dryness under vacuum. The residue was dissolved in hexanes (2 mL) and recrystallised at -30°C. Yield: 60%. Spectroscopic characterisation of this complex is described elsewhere.[8]

7.2.20 *fac*-Ir(η^2-CH_2NH^tBu)H[$N(SiMe_2CH_2PPh_2)_2$], 19

A solution of Ir=CH_2[$N(SiMe_2CH_2PPh_2)_2$], **10**, (25 mg, 0.03 mmol) in toluene (10 mL) was cooled to -78°C in a dry ice/ethanol bath for 15 min. To it was added a toluene solution (1 mL) of $^tBuNH_2$ (10 mg, 0.09 mmol). The reaction mixture was warmed to room temperature and stirred for two hours. During this time, the initial purple colour of **10** turned light yellow. The solvent was pumped off under vacuum, and the resultant yellow oil was crystallised from hexanes/toluene mixture (1/2 mL) at room temperature. Yield: 75%. Because this study is in its preliminary stages, the product has been characterised only by ^1H and $^{31}P\{^1H\}$ NMR spectroscopy. ^1H NMR (300 MHz, C_6D_6): $SiMe_2$, -0.20 (s), 0.00 (s), 0.33 (s), 0.47 (s); PCH_2Si, 1.40 (m), 2.05 (m); η^2-*CH_2*NH^tBu, 1.62 (t, $^3J_{P,H}$ = 3.8 Hz), 2.60 (br); CH_2N*H*^tBu, 2.79 (br); CH_2NH^t*Bu*, 0.60 (s), PPh_2, 6.30-7.10 (m, *para/meta*), 7.75 (m, *ortho*); Ir–H, -20.85 (dd, $^2J_{P,H\ (cis)}$ = 19.5 Hz, $^2J_{P,H\ (cis)}$ = 9.6 Hz). $^{31}P\{^1H\}$ NMR (C_6D_6): PPh_2, 10.83 (d, $^2J_{P,P}$ = 27.9 Hz), 5.03 (d, $^2J_{P,P}$ = 19.2 Hz)

7.2.21 Ir(μ-$AlMe_2$)H[$N(SiMe_2CH_2PPh_2)_2$], 20

A toluene solution (1 mL) of $AlMe_3$ (100 µl, 0.20 mmol) was added dropwise to the cooled toluene solution (10 mL, -78°C) of Ir=CH_2[$N(SiMe_2CH_2PPh_2)_2$], **10**, (100 mg, 0.14 mmol). The reaction was instantaneous as the purple colour of **10** changed to orange. The reaction mixture was warmed to room temperature and stirred for an hour. The removal of excess solvent from the reaction mixture afforded a yellow oil which was crystallised from minimum hexanes (1/2 mL) at -30°C. Yield: 70%. Anal. Calcd. for $C_{32}H_{42}NAlP_2Si_2Ir$: C, 49.34; H, 5.56; N, 1.80. Found: C, 49.20; H, 5.72; N, 1.69. ^1H NMR (300 MHz, C_6D_6): $SiMe_2$, 0.00 (s), 0.31 (s); PCH_2Si, 2.47 (br, m), 2.65 (br, m); $AlMe_2$, 0.78 (s); PPh_2, 7.40 (m, *para/meta*), 8.15 (br), 8.50 (m, *ortho*); Ir–H, -13.47 (t, $^2J_{P,H}$ = 16.3 Hz). $^{31}P\{^1H\}$ NMR (C_6D_6): PPh_2, 31.20 (s).

$^{13}C\{^1H\}$ NMR (C_6D_6): $SiMe_2$, 4.07 (s), 5.55 (s); PCH_2Si, 24.46 (t, $^1J_{C,P}$ = 6.8 Hz); Al–$(CH_3)_2$, -3.66 (s); PPh_2, 128-140 (m).

7.2.22 $Ir(\eta^2\text{-}C_2H_4)H(I)[N(SiMe_2CH_2PPh_2)_2]$, 21

This species was prepared by vacuum transfering excess MeI (~ 5 equivalents, -10°C) to the toluene solution (10 mL) of $Ir{=}CH_2[N(SiMe_2CH_2PPh_2)_2]$, **10**, (50 mg, 0.07 mmol). The reaction mixture was warmed up slowly from -78°C to room temperature. Within 10 min, the purple solution turned green and then faded to light yellow. Excess MeI and the solvent were pumped off immediately under vacuum to avoid the production of the side product $Ir(CH_3)(I)_2[HN(SiMe_2CH_2PPh_2)_2]$ (see Chapter 4, Section 4.3.1.2). The yellow residue was recrystallised from hexanes/toluene (1/2 mL) at room temperature. Yield: 70%. Anal. Calcd. for $C_{32}H_{45}NP_2SiIIr$: C, 43.83; H, 5.17; N, 1.60. Found: C, 43.80; H, 5.11; N, 1.40. ^1H NMR (300 MHz, C_6D_6): $SiMe_2$, -0.65 (s), 0.51 (s); PCH_2Si, 1.55 (dt, J_{gem} = 14.6 Hz, J_{app} = 6.6 Hz), 2.88 (dt); C_2H_4, 2.56 (t, $^3J_{P,H}$ = 3.6 Hz); PPh_2, 7.00 (m, *para/meta*), 7.25, 7.85 (m, *ortho*); Ir–H, -13.14 (t, $^2J_{P,H}$ = 8.7 Hz). $^{31}P\{^1H\}$ NMR (C_6D_6): PPh_2, 6.01 (s).

7.2.23 $Ir(\eta^3\text{-}C_3H_5)(C{\equiv}CH)[N(SiMe_2CH_2PPh_2)_2]$, 22

Excess HC≡CH (~ 5 equivalents) was condensed (at -196°C, liq. N_2) into a reaction vessel containing 10 mL toluene solution of $Ir{=}CH_2[N(SiMe_2CH_2PPh_2)_2]$, **10**, (50 mg, 0.07 mmol). The reaction proceeded over two hours at room temperature with a gradual colour change from purple to pale yellow. The excess solvent was pumped off under vacuum and the resultant yellow residue was recrystallised from toluene at room temperature. Yield: 85%. Anal. Calcd. for $C_{35}H_{42}NP_2Si_2Ir$: C, 53.41; H, 5.38; N, 1.78. Found: C, 53.30; H, 5.51; N, 1.65. ^1H NMR (300 MHz, C_6D_6): $SiMe_2$, 0.07 (s), 0.25 (s); PCH_2Si, 1.60 (m); C≡CH, 2.30 (s); η^3-C_3H_5: H_{syn} = 3.20

($^3J_{P,H}$ = 8.3 Hz, $J_{Hsyn,Hcentral}$ = 5.2 Hz), H_{anti} = 3.95 (d, $J_{Hanti,Hcental}$ = 9.3 Hz), $H_{central}$ = 4.28 (m); PPh_2, 7.00 (m, *para/meta*), 7.74, 8.38 (m, *ortho*). $^{31}P\{^1H\}$ NMR (C_6D_6): PPh_2, -15.2 (s). $SiMe_2$, 6.10 (s), 7.02 (s); PCH_2Si, 25.25 (d, $^1J_{P,C}$ = 21.0 Hz); η^3-C_3H_5 : $C_{(apical)}$ = 53.61 (s), 54.2 (s), $C_{(central)}$ = 110.34 (s); C≡CH: α-carbon = 90.15 (s), β-carbon = 140.02 (s); PPh_2, 128-140 (m).

7.2.24 Ir(σ-η^3-C_5H_8)[N($SiMe_2CH_2PPh_2$)$_2$], 23

Ir=CH_2[N($SiMe_2CH_2PPh_2$)$_2$], **10**, (100 mg, 0.14 mmol) was dissolved in toluene (10 mL) and loaded into a reactor bomb. An excess of 1,3-butadiene was condensed at -196°C into the reaction vessel and the reaction mixture warmed gradually to room temperature. Over a one hour period, the purple colour of the reaction mixture changed to light yellow. The excess solvent and 1,3-butadiene were removed *in vacuo*. The yellow residue was recrystallised from hexanes/toluene solution (1 mL) at room temperature. Yield: 82%. Anal. Calcd. for $C_{35}H_{44}NP_2Si_2Ir$: C, 53.28; H,5.62; N, 1.77. Found: C, 53.70; H, 5.73; N, 1.84. ^1H NMR (300 MHz, C_6D_6): $SiMe_2$, 0.32 (s), 0.35 (s), 0.38 (s), 0.53 (s); PCH_2Si, 1.98, 2.17 (m); PPh_2, 6.70-7.82 (m). $^{31}P\{^1H\}$ NMR (C_6D_6): PPh_2, -4.87 (d, $^2J_{P,P}$ = 7.3 Hz), -7.81 (d, $^2J_{P,P}$ = 6.8 Hz). $^{13}C\{^1H\}$ NMR (C_6D_6): $SiMe_2$, 5.23 (s), 5.36 (s), 5.92 (s), 9.04 (s); PCH_2Si, 24.26 (d, $^1J_{P,C}$ = 16.4 Hz), 30.10 (d, $^1J_{P,C}$ = 22.3 Hz); σ-η^3-C_5H_8 ligand (starting from the σ side): C1 = 44.16 (d, $^2J_{C,P}$ = 35.1 Hz), C2 = 108.35 (s), C3 = 54.90 (d,$^2J_{C,P}$ = 23.5 Hz), C4 = 28.01 (s), C5 = -37.29 (s); PPh_2, 127-133 (m).

7.2.25 *fac*-Ir{η^4-$C(CH_2)_3$}[N($SiMe_2CH_2PPh_2$)$_2$], 24

An excess of allene was condensed into a toluene solution (5 mL) of Ir=CH_2[N($SiMe_2CH_2PPh_2$)$_2$], **10**, (100 mg, 0.14 mmol). At -78°C, the purple colour of the methylidene complex faded to light yellow over an hour. At which time, the solution was warmed to room temperatutre. The toluene and excess allene were

removed *in vacuo*. The off-white residue was recrystallised from hexanes/toluene at room temperature. Yield: 75%. Anal. Calcd. for $C_{34}H_{42}NP_2Si_2Ir$: C, 52.69; H, 5.46; N, 1.81. Found: C, 52.90; H, 5.67; N, 1.71. ^1H NMR (300 MHz, C_6D_6): $SiMe_2$, 0.36 (s), 0.63 (s); PCH_2Si, 1.80, 2.10 (m); $C(CH_2)_3$, 1.54 (m), 1.45 (m), 2.38 (m); PPh_2, 6.70-7.82 (m). $^{31}P\{^1H\}$ NMR (C_6D_6): PPh_2, 0.45 (s). $^{13}C\{^1H\}$ NMR (C_6D_6): $SiMe_2$, 5.35 (s), 6.18 (s); PCH_2Si, 24.13 (m); η^4-$C(CH_2)_3$: CH_2 = 31.89 (d, $^2J_{C,P}$ = 4.2 Hz), 47.64 (d, $^2J_{C,P}$ = 44.3 Hz), C = 101.00 (s); PPh_2, 126-134 (m).

7.2.26 Ir(η^3-C_8H_{13})H[$N(SiMe_2CH_2PPh_2)_2$], 27

A benzene solution (5 mL) of Ir(η^2-C_8H_{14})[$N(SiMe_2CH_2PPh_2)_2$], **25**, (100 mg, 0.12 mmol) was sealed under N_2 in a reactor bomb. The sample was photolysed using 140 W Hg lamp for six hours. During this time, the orange-coloured solution of **25** darkened to red. The solvent was removed under vacuum and the resultant red powder was recrystallised from hexanes (1 mL) at -30°C. Yield: 75%. Anal. Calcd. for $C_{38}H_{50}NP_2Si_2Ir$: C, 54.94; H, 6.02; N, 1.69. Found: C, 55.47; H, 6.28; N, 1.60. ^1H NMR (300 MHz, C_6D_6): $SiMe_2$, 0.47 (s), 0.65 (s); PCH_2Si, 1.80 (m); η^3-C_8H_{13} (non allylic protons), 1.25 (br m), 2.15 (br m), η^3-C_8H_{13} (allylic protons), 4.08 (H_{syn}, m), 4.56 ($H_{central}$, $^2J_{H,H}$ = 7.6 Hz); PPh_2, 6.60-8.00 (m); Ir–H, -21.65 (t, $^2J_{P,H}$ = 16.7 Hz). $^{31}P\{^1H\}$ NMR (C_6D_6): PPh_2, 4.77 (s). $^{13}C\{^1H\}$ NMR (C_6D_6): $SiMe_2$, 6.95 (s), 8.49 (s); PCH_2Si, 23.58 (d, $^1J_{P,C}$ = 17.9 Hz); η^3-C_8H_{13}: $C_{(\text{inner C of the allyl unit})}$ = 102.80 (s), $C_{(\text{outer carbons of the allyl unit})}$ = 37.42 (s), 57.20 (s), $C_{(\text{five octenyl ring carbons})}$ = 37.42 (s), 29.18 (s), 28.34 (s), 26.62 (s), 24.92 (s); PPh_2, 126-140 (m).

7.2.27 Ir(η^4-C_4H_6)[$N(SiMe_2CH_2PPh_2)_2$], 28

A solution of Ir(η^2-C_8H_{14})[$N(SiMe_2CH_2PPh_2)_2$], **25**, (100 mg, 0.12 mmol) in toluene (10 mL) was loaded in a reactor bomb. The vessel was attached to a vacuum line, degassed and cooled to liquid N_2 temperature. Excess 1,3-butadiene was

condensed in the bomb. The reaction mixture was stirred for one hour at room temperature. Toluene was removed *in vacuo* and the residue recrystallised from hexanes/toluene at room temperature. Yield: 95%. Anal. Calcd. for $C_{34}H_{42}NP_2Si_2Ir$: C, 52.70; H, 5.51; N, 1.81. Found: C, 53.27; H, 5.50; N, 1.60. ^1H NMR (300 MHz, C_6D_6): $SiMe_2$, 0.40 (s), 0.45 (s), 0.50 (s), 0.55 (s); PCH_2Si, 1.85, 2.12 (m); η^4-C_4H_6, -0.60 (m, H_{anti}), -0.20 (m, H_{anti}) 2.07 (m, H_{syn}), 2.61 (m, H_{syn}), 4.00 (m, $H_{central}$), 5.37 (m, $H_{central}$); PPh_2, 7.30 (m, *para/meta*), 7.90 (m, *ortho*). $^{31}P\{^1H\}$ NMR (C_6D_6): PPh_2, 17.82 (s), -5.90 (s). $^{13}C\{^1H\}$ NMR (C_6D_6): $SiMe_2$, 4.40 (d, $^3J_{P,C}$ = 9.7 Hz), 6.60 (s), 8.40 (s); PCH_2Si, 23.39 (d, $^1J_{P,C}$ = 15.2 Hz), 27.85 (d, $^1J_{P,C}$ = 18.8 Hz); C_1, 14.44 (s), C_2, 88.93 (d, $^2J_{P,C}$ = 2.3 Hz), C_3, 82.27 (d, $^2J_{P,C}$ = 6.3 Hz), C_4, 33.75 (dd, $^2J_{P,C}$ = 41.6 Hz, $^2J_{P,C}$ = 3.3 Hz); PPh_2, 126-135 (m).

7.2.28 Ir(η^2-C_3H_4)[$N(SiMe_2CH_2PPh_2)_2$], 29

An excess of allene was condensed at -78°C into a reactor vessel containing a toluene solution (10 mL) of Ir(η^2-C_8H_{14})[$N(SiMe_2CH_2PPh_2)_2$], **25**, (50 mg, 0.06 mmol). The reaction mixture was warmed to room temperature and stirred for 15 minutes. During this time, the orange colour of **25** changed to yellow due to the formation of **29**. The solvent and allene were pumped off under vacuum. The yellow residue was recrystallised from hexanes at -30°C. Yield: 80%. Anal. Calcd. for $C_{33}H_{40}NP_2Si_2Ir$: C, 52.08; H, 5.30; N, 1.84. Found: C, 52.07; H, 5.54; N, 1.70. ^1H NMR (300 MHz, C_6D_6): $SiMe_2$, 0.12 (s), 0.25 (s); PCH_2Si, 1.79 (m); η^4-C_3H_4, 1.12 (m), 5.21 (m), 5.44 (m); PPh_2, 7.10 (m, *para/meta*), 7.78, 7.82 (m, *ortho*). $^{31}P\{^1H\}$ NMR (C_6D_6): PPh_2, 20.56 (s). $^{13}C\{^1H\}$ NMR (C_6D_6): $SiMe_2$, 4.79 (s), 5.08 (s); PCH_2Si, 23.41 (t, $^1J_{P,C}$ = 15.5 Hz); η^2-C_3H_4: $CH_{2\ (\sigma\text{-bound})}$ = -3.82 (s), CH_2 = 92.30 (s), C = 101.00 (s); PPh_2, 125-137 (m).

7.2.29 $Ir(\mu\text{-}AlMe_2)Me[N(SiMe_2CH_2PPh_2)_2]$, 30

A toluene solution (1 mL) of $AlMe_3$ (75 µl, 0.15 mmol) was added dropwise to the toluene solution (10 mL) of $Ir(\eta^2\text{-}C_8H_{14})[N(SiMe_2CH_2PPh_2)_2]$, **25**, (100 mg, 0.12 mmol). The reaction proceeded over an hour as the orange colour of **25** changed to red. The removal of excess solvent from the reaction mixture afforded red oil. Because this study is in its preliminary stages, the crude product has been characterised only by ^1H and $^{31}P\{^1H\}$ NMR spectroscopy. ^1H NMR (300 MHz, C_6D_6): $SiMe_2$, -0.07 (s), 0.05 (s); PCH_2Si, 1.75 (br, m), 2.40 (br, m); $AlMe_2$, 0.48 (s); Ir–CH_3, 0.76 (t, $^3J_{P,H}$ = 3.1 Hz); PPh_2, 7.10 (m, *para/meta*), 7.90 (m, *ortho*). $^{31}P\{^1H\}$ NMR (C_6D_6): PPh_2, 23.39 (s).

7.2.30 $Rh(\mu\text{-}AlMe_2)Me[N(SiMe_2CH_2PPh_2)_2]$, 31

The same procedure was followed as reported above for the synthesis of the iridium analogue, **30**. The reaction was instantaneous. Addition of a toluene solution (1 mL) of $AlMe_3$ (50 µl, 0.10 mmol) to the toluene solution (10 mL) of the rhodium(I) cyclooctene derivative $Rh(\eta^2\text{-}C_8H_{14})[N(SiMe_2CH_2PPh_2)_2]$ (50 mg, 0.07 mmol) afforded complex **31**. The complex **31** has been characterised only by ^1H and $^{31}P\{^1H\}$ NMR spectroscopy, because this investigation is in early stages. ^1H NMR (300 MHz, C_6D_6): $SiMe_2$, -0.05 (s), 0.06 (s); PCH_2Si, 1.72 (br, m), 2.45 (br, m); $AlMe_2$, 0.50 (s); Rh–CH_3, 0.78 (t, $^3J_{P,H}$ = 3.2 Hz); PPh_2, 7.10 (m, *para/meta*), 7.90 (m, *ortho*). $^{31}P\{^1H\}$ NMR (C_6D_6): PPh_2, 26.06 (d, $^1J_{Rh,P}$ = 145.9 Hz).

7.3 Kinetic Experiments

7.3.1 Thermolysis Experiments

The details for the kinetic procedures are given in chapter 2. In a typical experiment, a stock solution of known concentration was prepared in an appropriate solvent and stored at -30°C in the glove box. 5 mL aliquots of the solution were placed in a solvent reservoir fused to an anaerobic 1 cm optical cell. During the thermolysis of the light-sensitive phosphide complexes, aluminum foil was wrapped around the vessel. The sample was thermolysed in a temperature-controlled oil bath. As mentioned in chapter 2, the disappearence (or appearence in some cases) of the appropriate absorption band was followed with time using a Perkin Elmer 5523 UV/Vis spectrophotometer stabilised at 20°C. Treatment of the data is also described in chapter 2.

7.3.2 Carbonylation Experiment

A toluene solution of **6a** of exact concentration (see Appendix A2) was prepared in the glove box and loaded into a solvent reservoir fused to an anaerobic 1 cm optical cell. The vessel was attached to a vacuum line and degassed once. Then the solution was exposed to CO gas (1 atm). The absorbance of the solution at 360 nm was recorded using a Perkin Elmer 5523 UV/Vis spectrophotometer stabilised at 20°C. The sample was thermolysed at 46°C in a temperature-controlled oil bath, and the disappearence of the absorption band at 360 nm was followed with time. The data for this run are compiled in Appendix A2.

7.4 References

1 (a) Parshall, G. W. *Inorg. Synth.* **1968**, *11*, 157.
(b) Sollot, G. P.; Snead, J. L. Strecker, R. A. *J. Am. Chem. Soc.* **1973**, *95*, 210.

2 Issleib, K.; Kummel, R. *J. Organomet. Chem.* **1965**, *3*, 84.

3 King, R. B.; Eisch, J. J. (Eds.) *Organometallic Syntheses vol. 3*; Elsevier: Amsterdam, **1986**.

4 Most of the techniques used in this work are described in: Wayda, A. L.; Darensbourg, M. Y. (Eds.) *ACS Symp. Ser. vol. 357; Experimental Organometallic Chemistry*; American Chemical Society, Washington, D. C; **1987**.

5 Van der Ent, A.; Onderlinden, A. L. *Inorg. Synth.* **1973**, *14*, 93.

6 (a) Fryzuk, M. D.; MacNeil, P. A.; Rettig, S. J. *Organometallics* **1986**, *5*, 2469.
(b) Fryzuk, M. D.; Joshi, K. *Organometallics* **1989**, *8*, 1722.

7 Block, G. *B. Sc. Thesis*, University of British Columbia, Vancouver, Canada, **1986**.

8 Fryzuk, M. D.; MacNeil, P. A.; Rettig, S. J. *J. Am. Chem. Soc.* **1985**, *107*, 6709.

APPENDIX

A1 X-ray Crystallographic Analyses

A1.1 X-ray Crystallographic Analysis of $Ir(CH_3)PPh_2[N(SiMe_2CH_2PPh_2)_2]$, 2a

Experimental Details

Empirical Formula	C(43)H(49)Ir(1)N(1)P(3)Si(2)
Formula Weight	921.18
Crystal System	Monoclinic
Lattice Parameters:	a = 13.506 (3) angstroms b = 13.665 (3) angstroms c = 22.816 (7) angstroms beta = 92.35 (2) degrees V = 4207 (2) angstroms**3
Space Group	P21/c (#14)
Z value	4
Dcalc	1.45 g/cm**3
F000	1856
mu(Mo K-alpha)	33.59 cm**-1
Diffractometer	Rigaku AFC6
Radiation	Mo K-alpha (lambda= 0.71069) Graphite-monochromated
Temperature	21 degrees Cent.
2-theta(max)	55.0 degrees
No. Observations (I>3.00(sig(I)))	3993
No. Variables	451
Residuals: R; Rw	0.034; 0.037
Goodness of Fit Indicator	1.13
Maximum Shift in Final Cycle	0.05
Largest Peak in Final Diff. Map	1.25 e/angstrom**3

Table A1.1.1 Bond Lengths (Å) with estimated standard deviations in parentheses

atom	atom	distance	atom	atom	distance
Ir	C(43)	2.126(9)	P(3)	C(31)	1.80(1)
Ir	N	2.126(6)	P(3)	C(37)	1.834(9)
Ir	P(3)	2.297(2)	Si(1)	N	1.714(7)
Ir	P(1)	2.309(2)	Si(1)	C(3)	1.86(1)
Ir	P(2)	2.312(2)	Si(1)	C(4)	1.89(1)
P(1)	C(1)	1.808(9)	Si(1)	C(1)	1.91(1)
P(1)	C(7)	1.831(8)	Si(2)	N	1.729(8)
P(1)	C(13)	1.84(1)	Si(2)	C(6)	1.85(1)
P(2)	C(2)	1.807(9)	Si(2)	C(5)	1.85(1)
P(2)	C(25)	1.818(8)	Si(2)	C(2)	1.87(1)
P(2)	C(19)	1.824(9)			

Table A1.1.2 Bond Angles (deg) with estimated standard deviations in parentheses

atom	atom	atom	angle	atom	atom	atom	angle
C(43)	Ir	N	159.0(3)	C(19)	P(2)	Ir	112.1(3)
C(43)	Ir	P(3)	87.4(2)	C(31)	P(3)	C(37)	100.3(4)
C(43)	Ir	P(1)	91.2(2)	C(31)	P(3)	Ir	108.4(3)
C(43)	Ir	P(2)	90.3(2)	C(37)	P(3)	Ir	117.7(3)
N	Ir	P(3)	113.2(2)	N	Si(1)	C(3)	113.6(5)
N	Ir	P(1)	87.4(2)	N	Si(1)	C(4)	115.6(4)
N	Ir	P(2)	86.5(2)	N	Si(1)	C(1)	105.9(4)
P(3)	Ir	P(1)	105.35(9)	C(3)	Si(1)	C(4)	107.8(5)
P(3)	Ir	P(2)	87.95(8)	C(3)	Si(1)	C(1)	109.1(5)
P(1)	Ir	P(2)	166.68(8)	C(4)	Si(1)	C(1)	104.3(5)
C(1)	P(1)	C(7)	100.9(5)	N	Si(2)	C(6)	114.7(5)
C(1)	P(1)	C(13)	106.4(5)	N	Si(2)	C(5)	113.4(5)
C(1)	P(1)	Ir	108.8(3)	N	Si(2)	C(2)	106.0(4)
C(7)	P(1)	C(13)	101.3(5)	C(6)	Si(2)	C(5)	107.0(6)
C(7)	P(1)	Ir	111.7(3)	C(6)	Si(2)	C(2)	105.2(5)
C(13)	P(1)	Ir	125.0(3)	C(5)	Si(2)	C(2)	110.2(5)
C(2)	P(2)	C(25)	108.8(4)	Si(1)	N	Si(2)	121.8(4)
C(2)	P(2)	C(19)	104.2(4)	Si(1)	N	Ir	119.2(4)
C(2)	P(2)	Ir	105.3(3)	Si(2)	N	Ir	118.9(4)
C(25)	P(2)	C(19)	101.9(4)	P(1)	C(1)	Si(1)	106.3(5)
C(25)	P(2)	Ir	123.1(3)	P(2)	C(2)	Si(2)	107.1(5)

Table A1.1.3 Final Atomic Coordinates (Fractional) and B(eq)

atom	x	y	z	B(eq)
Ir	0.28896(2)	0.24657(3)	0.17779(1)	2.83(1)
P(1)	0.3295(1)	0.2494(2)	0.08048(8)	3.38(8)
P(2)	0.2825(2)	0.2239(1)	0.2780(1)	3.3(1)
P(3)	0.1359(2)	0.3194(2)	0.1802(1)	3.5(1)
Si(1)	0.3123(2)	0.0369(2)	0.1063(1)	4.0(1)
Si(2)	0.2512(2)	0.0239(2)	0.2313(1)	4.9(1)
N	0.2815(6)	0.0916(4)	0.1706(3)	4.4(4)
C(1)	0.2934(8)	0.1342(7)	0.0470(4)	4.1(5)
C(2)	0.2099(7)	0.1142(7)	0.2868(4)	4.6(5)
C(3)	0.4427(8)	-0.0072(8)	0.1066(5)	6.1(6)
C(4)	0.2292(7)	-0.0677(7)	0.0806(5)	5.9(6)
C(5)	0.356(1)	-0.0502(8)	0.2624(5)	8.3(8)
C(6)	0.145(1)	-0.0602(9)	0.2190(6)	9.2(9)
C(7)	0.4638(6)	0.2464(8)	0.0725(3)	3.8(3)
C(8)	0.5025(8)	0.2259(8)	0.0181(4)	5.5(6)
C(9)	0.604(1)	0.2181(8)	0.0130(5)	6.4(6)
C(10)	0.6671(8)	0.2293(8)	0.0593(6)	6.1(6)
C(11)	0.6306(6)	0.252(1)	0.1128(4)	5.5(4)
C(12)	0.5295(7)	0.261(1)	0.1186(4)	5.2(5)
C(13)	0.2922(8)	0.3455(7)	0.0276(4)	4.0(5)
C(14)	0.2059(8)	0.3388(7)	-0.0070(4)	4.9(5)
C(15)	0.1780(8)	0.4136(8)	-0.0440(4)	5.1(5)
C(16)	0.237(1)	0.4949(8)	-0.0471(5)	5.8(6)
C(17)	0.3210(8)	0.5042(7)	-0.0132(4)	4.8(5)
C(18)	0.3496(8)	0.4307(7)	0.0247(4)	4.8(5)
C(19)	0.4035(6)	0.1934(6)	0.3116(4)	3.5(4)

Table (continued).

atom	x	y	z	B(eq)
C(20)	0.4128(7)	0.1625(7)	0.3685(4)	4.9(5)
C(21)	0.5021(8)	0.1335(9)	0.3933(5)	6.1(6)
C(22)	0.5844(8)	0.1367(8)	0.3612(6)	5.9(6)
C(23)	0.5771(8)	0.167(1)	0.3038(6)	7.1(7)
C(24)	0.4886(8)	0.195(1)	0.2801(5)	6.8(6)
C(25)	0.2389(6)	0.3172(6)	0.3275(4)	3.6(4)
C(26)	0.1445(8)	0.3156(7)	0.3484(4)	4.9(5)
C(27)	0.1126(8)	0.389(1)	0.3849(5)	6.2(6)
C(28)	0.173(1)	0.463(1)	0.3997(5)	7.4(8)
C(29)	0.269(1)	0.4663(8)	0.3799(6)	6.8(7)
C(30)	0.3001(7)	0.3936(7)	0.3431(5)	5.0(5)
C(31)	0.0653(8)	0.2859(7)	0.1145(5)	4.0(5)
C(32)	0.0643(8)	0.1878(7)	0.0965(5)	4.2(5)
C(33)	0.0081(9)	0.1533(8)	0.0489(6)	5.9(7)
C(34)	-0.0494(9)	0.2178(9)	0.0157(5)	5.6(6)
C(35)	-0.0533(9)	0.3153(9)	0.0319(5)	6.0(7)
C(36)	0.0026(8)	0.3472(7)	0.0803(5)	5.0(6)
C(37)	0.1303(6)	0.4532(6)	0.1748(4)	3.8(4)
C(38)	0.1514(7)	0.5102(7)	0.1276(5)	4.8(5)
C(39)	0.144(1)	0.6119(8)	0.1284(6)	6.8(7)
C(40)	0.114(1)	0.6572(8)	0.1770(8)	8.2(9)
C(41)	0.096(1)	0.605(1)	0.2255(7)	8.3(9)
C(42)	0.1038(8)	0.5016(8)	0.2258(5)	5.7(6)
C(43)	0.3513(6)	0.3879(6)	0.1917(4)	3.4(4)

Calculated hydrogen atom parameters

Atom	x	y	z	B(iso)
H(1)	0.2237	0.1364	0.0333	4.9
H(2)	0.3349	0.1200	0.0138	4.9
H(3)	0.2211	0.0878	0.3264	5.5
H(4)	0.1393	0.1288	0.2800	5.5
H(5)	0.4537	-0.0550	0.1382	7.3
H(6)	0.4552	-0.0382	0.0689	7.3
H(7)	0.4879	0.0483	0.1128	7.3
H(8)	0.1613	-0.0438	0.0742	7.1
H(9)	0.2530	-0.0943	0.0438	7.1
H(10)	0.2305	-0.1192	0.1105	7.1
H(11)	0.3347	-0.0843	0.2976	10.0
H(12)	0.3756	-0.0982	0.2333	10.0
H(13)	0.4117	-0.0072	0.2728	10.0
H(14)	0.0872	-0.0231	0.2041	11.0
H(15)	0.1621	-0.1102	0.1902	11.0
H(16)	0.1297	-0.0919	0.2560	11.0
H(17)	0.4579	0.2170	-0.0165	6.6
H(18)	0.6307	0.2042	-0.0255	7.7
H(19)	0.7386	0.2214	0.0551	7.3
H(20)	0.6761	0.2612	0.1469	6.6
H(21)	0.5044	0.2784	0.1569	6.2
H(22)	0.1646	0.2801	-0.0051	5.9
H(23)	0.1165	0.4089	-0.0681	6.1
H(24)	0.2171	0.5476	-0.0744	7.0
H(25)	0.3615	0.5634	-0.0157	5.7

Calculated hydrogen atom parameters

Atom	x	y	z	B(iso)
H(26)	0.4100	0.4376	0.0496	5.7
H(27)	0.3539	0.1611	0.3923	5.8
H(28)	0.5066	0.1106	0.4340	7.3
H(29)	0.6488	0.1177	0.3789	7.1
H(30)	0.6360	0.1674	0.2801	8.5
H(31)	0.4846	0.2173	0.2393	8.1
H(32)	0.0996	0.2618	0.3373	5.9
H(33)	0.0456	0.3869	0.3998	7.5
H(34)	0.1500	0.5160	0.4248	8.8
H(35)	0.3141	0.5195	0.3920	8.2
H(36)	0.3667	0.3966	0.3278	6.0
H(37)	0.1059	0.1411	0.1189	5.0
H(38)	0.0091	0.0836	0.0387	7.1
H(39)	-0.0874	0.1947	-0.0191	6.7
H(40)	-0.0952	0.3613	0.0092	7.2
H(41)	-0.0017	0.4163	0.0914	6.0
H(42)	0.1729	0.4783	0.0918	5.8
H(43)	0.1597	0.6502	0.0938	8.2
H(44)	0.1047	0.7283	0.1769	9.8
H(45)	0.0783	0.6394	0.2613	10.0
H(46)	0.0905	0.4644	0.2614	6.8
H(47)	0.4238	0.3831	0.1933	4.1
H(48)	0.3298	0.4313	0.1594	4.1
H(49)	0.3291	0.4145	0.2288	4.1

A1.2 X-ray Crystallographic Analysis of *fac*-Ir(η^2-CH_2PPh_2)H[N($SiMe_2CH_2PPh_2$)$_2$], 3a

Experimental Details

formula	$C_{43}H_{49}IrNP_3Si_2$
mol. wt. (g/mol)	920.4
crystal size , mm	0.14 x 0.19 x 0.60
crystal system	monoclinic
space group	$P2_1/c$
a, Å	9.253(2)
b, Å	21.950(5)
c, Å	20.081(4)
β, deg	90.74(2)
U, Å^3	4448
Z	4
D_C, g/cm^3	1.50
F(000)	1856
radiation	Mo
wavelength (Å)	0.71069
μ, cm^{-1}	33.27
transmission factors	0.883-0.959
scan type	ω-2θ
scan speed, deg/min	3.91-14.65 (variable)
data collected	$+h, +k, \pm l$
$2\theta_{max}$, deg	48
total no. of reflections	7299
no. of reflcns with $I \geq 3\sigma(I)$	4448
R	0.036
R_w	0.037
g.o.f.	1.1

Table A1.2.1 Bond Lengths (Å) with estimated standard deviations in parentheses

Ir—P(1)	2.241(2)	P(3)—C(61)	1.816(7)
Ir—P(2)	2.272(2)	Si(1)—N	1.695(6)
Ir—P(3)	2.291(2)	Si(1)—C(2)	1.897(7)
Ir—C(1)	2.203(7)	Si(1)—C(4)	1.871(8)
Ir—N	2.277(6)	Si(1)—C(5)	1.885(9)
Ir—H	1.51(6)	Si(2)—N	1.684(6)
P(1)—C(1)	1.760(8)	Si(2)—C(3)	1.927(7)
P(1)—C(11)	1.828(7)	Si(2)—C(6)	1.882(9)
P(1)—C(21)	1.817(8)	Si(2)—C(7)	1.87(1)
P(2)—C(31)	1.833(7)		
P(2)—C(41)	1.831(7)		
P(3)—C(3)	1.824(8)		
P(3)—C(51)	1.847(7)		

Table A1.2.2 Bond Angles (deg) with estimated standard deviations in parentheses

C(1)—Ir—N	97.6(3)	P(1)—Ir—H	70(3)
C(1)—Ir—H	87(3)	P(2)—Ir—H	157.5(2)
C(1)—Ir—P(1)	46.7(2)	P(3)—Ir—H	112(3)
C(1)—Ir—P(2)	157.5(2)	N—Ir—H	167(3)
C(1)—Ir—P(3)	97.9(2)	Ir—P(1)—C(11)	123.9(2)
N—Ir—P(1)	103.8(2)	C(1)—P(1)—C(11)	114.6(3)
N—Ir—P(2)	88.4(2)	Ir—P(1)—C(21)	127.4(3)
N—Ir—P(3)	79.7(1)	Ir—P(2)—C(2)	109.5(2)
P(1)—Ir—P(2)	110.9(1)	Ir—P(3)—C(3)	106.8(2)
P(1)—Ir—P(3)	144.5(1)	Ir—P(3)—C(51)	117.3(2)
P(2)—Ir—P(3)	104.5(1)	Ir—P(3)—C(61)	120.4(2)
N—Si(1)—C(2)	106.5(3)	N—Si(2)—C(3)	105.2(3)
N—Si(1)—C(5)	117.6(4)	N—Si(2)—C(6)	118.0(4)
C(2)—Si(1)—C(5)	103.3(4)	N—Si(2)—C(7)	116.5(4)
C(4)—Si(1)—C(5)	103.8(4)	Ir—N—Si(1)	113.4(3)
Ir—N—Si(2)	114.1(1)	Si(1)—N—Si(2)	131.0(4)
Ir—C(1)—P(1)	67.8(2)		

Table A1.2.3 Final Atomic Coordinates (Fractional) and B(eq)

Ir	0.14352(3)	0.35691(1)	0.22349(1)	28.9(1)
P(1)	0.3110(2)	0.3170(1)	0.1567(1)	35(1)
P(2)	-0.0732(2)	0.3099(1)	0.2080(1)	30(1)
P(3)	0.1048(2)	0.4247(1)	0.3081(1)	33(1)
Si(1)	-0.0952(2)	0.4210(1)	0.1192(1)	41(1)
Si(2)	0.1291(2)	0.5051(1)	0.1861(1)	42(1)
N	0.0554(6)	0.4377(3)	0.1645(3)	38(3)
C(1)	0.3751(8)	0.3754(4)	0.2094(4)	45(4)
C(2)	-0.1987(8)	0.3621(3)	0.1686(4)	40(4)
C(3)	0.1720(8)	0.4983(3)	0.2800(4)	43(4)
C(4)	-0.0553(11)	0.3941(4)	0.0329(4)	62(6)
C(5)	-0.2317(10)	0.4837(4)	0.1059(5)	69(6)
C(6)	0.0169(11)	0.5758(3)	0.1735(4)	60(6)
C(7)	0.2993(11)	0.5268(4)	0.1432(5)	70(6)
C(11)	0.3961(7)	0.2429(3)	0.1704(4)	37(4)
C(12)	0.5100(8)	0.2238(4)	0.1299(4)	48(5)
C(13)	0.5794(9)	0.1691(4)	0.1427(5)	59(6)
C(14)	0.5363(10)	0.1329(4)	0.1936(5)	65(6)
C(15)	0.4219(11)	0.1504(4)	0.2322(5)	67(6)
C(16)	0.3551(9)	0.2049(4)	0.2211(4)	53(5)
C(21)	0.3356(8)	0.3322(4)	0.0686(4)	45(4)
C(22)	0.4171(12)	0.3794(5)	0.0462(5)	74(7)
C(23)	0.4307(16)	0.3911(6)	-0.0201(6)	107(10)
C(24)	0.3584(17)	0.3555(7)	-0.0652(6)	107(10)
C(25)	0.2767(13)	0.3069(7)	-0.0449(5)	95(9)

C(26)	0.2642(10)	0.2944(5)	0.0241(4)	65(6)
C(31)	-0.1613(7)	0.2766(3)	0.2806(3)	36(4)
C(32)	-0.0786(9)	0.2515(4)	0.3313(4)	48(5)
C(33)	-0.1415(10)	0.2245(4)	0.3860(4)	57(5)
C(34)	-0.2880(11)	0.2237(4)	0.3908(4)	67(6)
C(35)	-0.3727(10)	0.2492(5)	0.3406(5)	67(6)
C(36)	-0.3094(9)	0.2745(4)	0.2858(4)	54(5)
C(41)	-0.0659(7)	0.2445(3)	0.1515(3)	34(4)
C(42)	-0.0002(9)	0.1907(3)	0.1732(4)	50(4)
C(43)	0.0174(10)	0.1414(4)	0.1305(5)	60(5)
C(44)	-0.0294(11)	0.1448(4)	0.0657(4)	62(6)
C(45)	-0.0971(11)	0.1967(4)	0.0443(4)	66(6)
C(46)	-0.1155(9)	0.2458(4)	0.0858(4)	52(5)
C(51)	-0.0841(8)	0.4372(3)	0.3334(3)	34(4)
C(52)	-0.1419(8)	0.3993(4)	0.3818(4)	44(4)
C(53)	-0.2867(9)	0.4039(4)	0.3972(4)	56(5)
C(54)	-0.3734(9)	0.4444(5)	0.3645(5)	67(6)
C(55)	-0.3167(9)	0.4812(4)	0.3173(5)	64(6)
C(56)	-0.1722(9)	0.4778(4)	0.3023(4)	54(5)
C(61)	0.1953(8)	0.4150(3)	0.3882(3)	40(5)
C(62)	0.2777(8)	0.3647(4)	0.4036(4)	46(4)
C(63)	0.3495(10)	0.3599(4)	0.4654(4)	63(6)
C(64)	0.3385(11)	0.4055(5)	0.5107(4)	74(7)
C(65)	0.2568(12)	0.4554(5)	0.4971(4)	79(7)
C(66)	0.1867(10)	0.4600(4)	0.4358(4)	58(5)

H	0.1884	0.2949	0.2489	100
H(1A)	0.4412	0.3652	0.2442	60
H(1B)	0.4026	0.4131	0.1901	60
H(2A)	-0.2616	0.3401	0.1395	60
H(2B)	-0.2538	0.3819	0.2018	60
H(3A)	0.1252	0.5302	0.3034	60
H(3B)	0.2734	0.5009	0.2875	60
H(4A)	0.0135	0.3620	0.0349	70
H(4B)	-0.0175	0.4269	0.0076	70
H(4C)	-0.1419	0.3797	0.0123	70
H(5A)	-0.2584	0.5002	0.1477	80
H(5B)	-0.3149	0.4676	0.0839	80
H(5C)	-0.1906	0.5148	0.0792	80
H(6A)	-0.0746	0.5703	0.1936	70
H(6B)	0.0037	0.5830	0.1272	70
H(6C)	0.0647	0.6096	0.1934	70
H(7A)	0.3664	0.4941	0.1462	80
H(7B)	0.3396	0.5619	0.1639	80
H(7C)	0.2786	0.5354	0.0977	80
H(12)	0.5397	0.2486	0.0938	60
H(13)	0.6575	0.1568	0.1156	70
H(14)	0.5847	0.0955	0.2022	70
H(15)	0.3900	0.1247	0.2671	80
H(16)	0.2779	0.2168	0.2490	60
H(22)	0.4657	0.4048	0.0776	80

H(23)	0.4900	0.4235	-0.0349	110
H(24)	0.3642	0.3645	-0.1114	110
H(25)	0.2289	0.2818	-0.0768	100
H(26)	0.2083	0.2610	0.0393	70
H(32)	0.0238	0.2522	0.3281	60
H(33)	-0.0829	0.2074	0.4204	70
H(34)	-0.3319	0.2054	0.4283	70
H(35)	-0.4749	0.2489	0.3445	70
H(36)	-0.3686	0.2907	0.2510	70
H(42)	0.0340	0.1877	0.2179	60
H(43)	0.0608	0.1049	0.1466	70
H(44)	-0.0152	0.1117	0.0360	70
H(45)	-0.1314	0.1992	-0.0004	70
H(46)	-0.1631	0.2812	0.0692	60
H(52)	-0.0818	0.3706	0.4042	60
H(53)	-0.3259	0.3791	0.4313	70
H(54)	-0.4738	0.4461	0.3736	70
H(55)	-0.3762	0.5106	0.2956	70
H(56)	-0.1338	0.5040	0.2693	60
H(62)	0.2864	0.3328	0.3719	60
H(63)	0.4057	0.3247	0.4753	80
H(64)	0.3886	0.4023	0.5522	80
H(65)	0.2471	0.4869	0.5292	90
H(66)	0.1313	0.4955	0.4262	70

A1.3 X-ray Crystallographic Analysis of $Ir(CH_3)PPh_2\{C_2(CO_2Me)_2\}[N(SiMe_2CH_2PPh_2)_2]$, 12

Experimental Details

Empirical Formula	$C_{49}H_{55}IrNO_4P_3Si_2$
Formula Weight	1063.29
Crystal Color, Habit	green, prism
Crystal Dimensions (mm)	0.200 X 0.200 X 0.250
Crystal System	monoclinic
No. Reflections Used for Unit Cell Determination (2θ range)	25 (30.1 - 34.9°)
Omega Scan Peak Width at Half-height	0.34
Lattice Parameters:	
	a = 20.04 (2)Å
	b = 23.764 (4)Å
	c = 20.496 (4)Å
	β = 100.40 (4)°
	V = 9599 (9)Å^3
Space Group	$P2_1/n$ (#14)
Z value	8
D_{calc}	1.471 g/cm^3
F_{000}	4304
$\mu_{(MoK\alpha)}$	29.60 cm^{-1}

B. Intensity Measurements

Diffractometer	Rigaku AFC6S
Radiation	MoKα (λ = 0.71069 Å)
Temperature	21°C
Take-off Angle	6.0°
Detector Aperture	6.0 mm horizontal 6.0 mm vertical

Crystal to Detector Distance	285 mm
Scan Type	ω
Scan Rate	16.0°/min (in omega) (6 rescans)
Scan Width	(0.79 + 0.35 tanθ)°
$2\theta_{max}$	55.0°
No. of Reflections Measured	Total: 22625 Unique: 21995 (R_{int} = .057)
Corrections	Lorentz-polarization Absorption (trans. factors: 0.75 - 1.00) Secondary Extinction (coefficient: 0.10956E-07)

C. Structure Solution and Refinement

Structure Solution	Patterson Method
Refinement	Full-matrix least-squares
Function Minimized	Σ w (|Fo| - |Fc|)^2
Least-squares Weights	$4Fo^2/\sigma^2(Fo^2)$
p-factor	0.03
Anomalous Dispersion	All non-hydrogen atoms
No. Observations (I>3.00σ(I))	11022
No. Variables	1082
Reflection/Parameter Ratio	10.19
Residuals: R; R_w	0.036; 0.036
Goodness of Fit Indicator	1.16
Max Shift/Error in Final Cycle	0.05
Maximum Peak in Final Diff. Map	0.67 $e^-/Å^3$
Minimum Peak in Final Diff. Map	-0.57 $e^-/Å^3$

Table A1.3.1 Bond Lengths (Å) with estimated standard deviations in parentheses

atom	atom	distance	atom	atom	distance
Ir(1)	P(1)	2.352(2)	P(5)	C(87)	1.843(6)
Ir(1)	P(2)	2.288(2)	P(6)	C(74)	1.852(7)
Ir(1)	P(3)	2.335(2)	P(6)	C(80)	1.841(6)
Ir(1)	N(1)	2.281(5)	P(6)	C(88)	1.851(7)
Ir(1)	C(43)	2.145(7)	Si(1)	N(1)	1.694(6)
Ir(1)	C(49)	2.119(7)	Si(1)	C(1)	1.878(7)
Ir(2)	P(4)	2.343(2)	Si(1)	C(3)	1.891(8)
Ir(2)	P(5)	2.284(2)	Si(1)	C(4)	1.885(8)
Ir(2)	P(6)	2.335(2)	Si(2)	N(1)	1.707(6)
Ir(2)	N(2)	2.281(5)	Si(2)	C(2)	1.898(8)
Ir(2)	C(92)	2.123(7)	Si(2)	C(5)	1.868(8)
Ir(2)	C(98)	2.140(7)	Si(2)	C(6)	1.882(8)
P(1)	C(1)	1.833(7)	Si(3)	N(2)	1.689(6)
P(1)	C(7)	1.832(7)	Si(3)	C(50)	1.896(7)
P(1)	C(13)	1.841(7)	Si(3)	C(52)	1.882(8)
P(2)	C(2)	1.789(7)	Si(3)	C(53)	1.882(8)
P(2)	C(19)	1.827(7)	Si(4)	N(2)	1.709(6)
P(2)	C(38)	1.851(7)	Si(4)	C(51)	1.909(8)
P(3)	C(25)	1.831(7)	Si(4)	C(54)	1.876(8)
P(3)	C(31)	1.837(7)	Si(4)	C(55)	1.868(8)
P(3)	C(39)	1.825(7)	O(1)	C(37)	1.332(9)
P(4)	C(50)	1.806(7)	O(1)	C(41)	1.44(1)
P(4)	C(56)	1.822(7)	O(2)	C(37)	1.202(9)
P(4)	C(62)	1.833(7)	O(3)	C(40)	1.335(8)
P(5)	C(51)	1.795(7)	O(3)	C(42)	1.44(1)
P(5)	C(68)	1.822(7)	O(4)	C(40)	1.192(8)

Table . (continued)

atom	atom	distance
O(5)	C(86)	1.311(9)
O(5)	C(90)	1.447(9)
O(6)	C(86)	1.196(9)
O(7)	C(89)	1.323(8)
O(7)	C(91)	1.45(1)
O(8)	C(89)	1.191(8)
C(37)	C(38)	1.50(1)
C(38)	C(39)	1.34(1)
C(39)	C(40)	1.52(1)
C(86)	C(87)	1.51(1)
C(87)	C(88)	1.316(9)
C(88)	C(89)	1.517(9)

Table A1.3.2 Bond Angles (deg) with estimated standard deviations in parentheses

atom	atom	atom	angle	atom	atom	atom	angle
P(1)	Ir(1)	P(2)	169.98(6)	P(6)	Ir(2)	C(98)	90.2(2)
P(1)	Ir(1)	P(3)	96.16(7)	N(2)	Ir(2)	C(92)	90.0(2)
P(1)	Ir(1)	N(1)	84.9(1)	N(2)	Ir(2)	C(98)	174.0(2)
P(1)	Ir(1)	C(43)	98.8(2)	C(92)	Ir(2)	C(98)	86.2(3)
P(1)	Ir(1)	C(49)	90.9(2)	Ir(1)	P(1)	C(1)	106.7(2)
P(2)	Ir(1)	P(3)	84.88(7)	Ir(1)	P(1)	C(7)	120.4(3)
P(2)	Ir(1)	N(1)	85.1(1)	Ir(1)	P(1)	C(13)	119.5(2)
P(2)	Ir(1)	C(43)	81.1(2)	C(1)	P(1)	C(7)	105.9(3)
P(2)	Ir(1)	C(49)	99.1(2)	C(1)	P(1)	C(13)	104.1(3)
P(3)	Ir(1)	N(1)	96.1(1)	C(7)	P(1)	C(13)	98.5(3)
P(3)	Ir(1)	C(43)	164.5(2)	Ir(1)	P(2)	C(2)	109.0(3)
P(3)	Ir(1)	C(49)	89.2(2)	Ir(1)	P(2)	C(19)	125.8(2)
N(1)	Ir(1)	C(43)	89.2(2)	Ir(1)	P(2)	C(38)	108.6(2)
N(1)	Ir(1)	C(49)	173.6(2)	C(2)	P(2)	C(19)	107.3(3)
C(43)	Ir(1)	C(49)	86.7(3)	C(2)	P(2)	C(38)	104.4(3)
P(4)	Ir(2)	P(5)	170.57(6)	C(19)	P(2)	C(38)	99.6(3)
P(4)	Ir(2)	P(6)	95.97(6)	Ir(1)	P(3)	C(25)	126.3(2)
P(4)	Ir(2)	N(2)	85.3(1)	Ir(1)	P(3)	C(31)	116.3(2)
P(4)	Ir(2)	C(92)	98.5(2)	Ir(1)	P(3)	C(39)	106.7(2)
P(4)	Ir(2)	C(98)	90.7(2)	C(25)	P(3)	C(31)	104.3(3)
P(5)	Ir(2)	P(6)	85.25(7)	C(25)	P(3)	C(39)	97.9(3)
P(5)	Ir(2)	N(2)	85.3(1)	C(31)	P(3)	C(39)	101.0(3)
P(5)	Ir(2)	C(92)	81.1(2)	Ir(2)	P(4)	C(50)	106.7(2)
P(5)	Ir(2)	C(98)	98.7(2)	Ir(2)	P(4)	C(56)	118.8(2)
P(6)	Ir(2)	N(2)	94.7(1)	Ir(2)	P(4)	C(62)	121.3(2)
P(6)	Ir(2)	C(92)	165.1(2)	C(50)	P(4)	C(56)	104.8(3)

Table . (continued)

atom	atom	atom	angle	atom	atom	atom	angle
C(50)	P(4)	C(62)	105.4(3)	N(2)	Si(3)	C(50)	105.2(3)
C(56)	P(4)	C(62)	98.2(3)	N(2)	Si(3)	C(52)	118.8(3)
Ir(2)	P(5)	C(51)	108.9(2)	N(2)	Si(3)	C(53)	114.0(3)
Ir(2)	P(5)	C(68)	124.2(2)	C(50)	Si(3)	C(52)	105.3(3)
Ir(2)	P(5)	C(87)	108.2(2)	C(50)	Si(3)	C(53)	109.2(3)
C(51)	P(5)	C(68)	107.4(3)	C(52)	Si(3)	C(53)	103.9(4)
C(51)	P(5)	C(87)	105.0(3)	N(2)	Si(4)	C(51)	106.3(3)
C(68)	P(5)	C(87)	101.5(3)	N(2)	Si(4)	C(54)	113.9(3)
Ir(2)	P(6)	C(74)	127.3(2)	N(2)	Si(4)	C(55)	114.8(3)
Ir(2)	P(6)	C(80)	115.9(2)	C(51)	Si(4)	C(54)	107.0(4)
Ir(2)	P(6)	C(88)	106.0(2)	C(51)	Si(4)	C(55)	108.1(3)
C(74)	P(6)	C(80)	104.4(3)	C(54)	Si(4)	C(55)	106.4(4)
C(74)	P(6)	C(88)	97.1(3)	C(37)	O(1)	C(41)	116.5(7)
C(80)	P(6)	C(88)	101.5(3)	C(40)	O(3)	C(42)	116.9(6)
N(1)	Si(1)	C(1)	105.0(3)	C(86)	O(5)	C(90)	116.9(7)
N(1)	Si(1)	C(3)	119.0(3)	C(89)	O(7)	C(91)	114.9(6)
N(1)	Si(1)	C(4)	114.2(3)	Ir(1)	N(1)	Si(1)	118.6(3)
C(1)	Si(1)	C(3)	107.2(3)	Ir(1)	N(1)	Si(2)	117.5(3)
C(1)	Si(1)	C(4)	107.7(3)	Si(1)	N(1)	Si(2)	123.2(3)
C(3)	Si(1)	C(4)	103.2(4)	Ir(2)	N(2)	Si(3)	117.8(3)
N(1)	Si(2)	C(2)	106.6(3)	Ir(2)	N(2)	Si(4)	117.8(3)
N(1)	Si(2)	C(5)	113.9(3)	Si(3)	N(2)	Si(4)	123.4(3)
N(1)	Si(2)	C(6)	113.9(3)	P(1)	C(1)	Si(1)	108.2(4)
C(2)	Si(2)	C(5)	106.7(3)	P(2)	C(2)	Si(2)	108.1(4)
C(2)	Si(2)	C(6)	108.7(3)	O(1)	C(37)	O(2)	125.6(8)
C(5)	Si(2)	C(6)	106.7(3)	O(1)	C(37)	C(38)	112.0(7)

Table . (continued)

atom	atom	atom	angle
O(2)	C(37)	C(38)	122.4(7)
P(2)	C(38)	C(37)	120.7(5)
P(2)	C(38)	C(39)	117.4(5)
C(37)	C(38)	C(39)	121.7(6)
P(3)	C(39)	C(38)	120.3(5)
P(3)	C(39)	C(40)	120.8(5)
C(38)	C(39)	C(40)	118.9(6)
O(3)	C(40)	O(4)	124.7(7)
O(3)	C(40)	C(39)	110.2(6)
O(4)	C(40)	C(39)	125.0(7)
P(4)	C(50)	Si(3)	108.1(4)
P(5)	C(51)	Si(4)	108.4(3)
O(5)	C(86)	O(6)	124.5(8)
O(5)	C(86)	C(87)	112.3(7)
O(6)	C(86)	C(87)	123.2(7)
P(5)	C(87)	C(86)	120.9(5)
P(5)	C(87)	C(88)	119.0(5)
C(86)	C(87)	C(88)	120.0(6)
P(6)	C(88)	C(87)	119.5(5)
P(6)	C(88)	C(89)	118.1(5)
C(87)	C(88)	C(89)	122.3(6)
O(7)	C(89)	O(8)	125.4(7)
O(7)	C(89)	C(88)	108.9(6)
O(8)	C(89)	C(88)	125.6(6)

Table A1.3.3 Final Atomic Coordinates (Fractional) and B(eq)

atom	x	y	z	B(eq)
Ir(1)	0.19315(1)	0.17228(1)	0.20660(1)	2.03(1)
Ir(2)	0.71633(1)	0.04935(1)	0.21258(1)	1.85(1)
P(1)	0.16796(9)	0.26887(8)	0.20891(9)	2.40(8)
P(2)	0.23256(9)	0.08315(8)	0.19501(9)	2.43(8)
P(3)	0.25994(8)	0.16856(8)	0.31240(8)	2.30(7)
P(4)	0.68629(9)	0.14476(8)	0.20761(9)	2.20(7)
P(5)	0.75940(9)	-0.03930(8)	0.20824(9)	2.34(8)
P(6)	0.78084(8)	0.05251(8)	0.31943(8)	2.07(7)
Si(1)	0.2862(1)	0.2692(1)	0.1371(1)	2.88(9)
Si(2)	0.3217(1)	0.1484(1)	0.1205(1)	2.90(9)
Si(3)	0.8090(1)	0.1453(1)	0.1427(1)	2.83(9)
Si(4)	0.8493(1)	0.0249(1)	0.1319(1)	3.02(9)
O(1)	0.3770(3)	0.0091(2)	0.2211(3)	4.8(3)
O(2)	0.3380(3)	-0.0201(3)	0.3119(3)	5.8(3)
O(3)	0.4287(2)	0.0817(2)	0.3487(2)	4.2(3)
O(4)	0.3701(3)	0.1043(2)	0.4282(2)	4.3(3)
O(5)	0.8932(3)	-0.1175(2)	0.2400(3)	4.7(3)
O(6)	0.8718(4)	-0.1310(3)	0.3414(3)	7.2(4)
O(7)	0.9539(3)	-0.0198(3)	0.3622(3)	6.2(3)
O(8)	0.8922(2)	-0.0056(2)	0.4413(2)	4.0(3)
N(1)	0.2781(3)	0.1998(2)	0.1530(3)	2.4(2)
N(2)	0.8033(2)	0.0764(2)	0.1615(2)	2.3(2)
C(1)	0.2457(3)	0.3067(3)	0.2006(3)	2.7(3)
C(2)	0.2717(3)	0.0808(3)	0.1233(3)	3.0(3)

Table . (continued)

atom	x	y	z	B(eq)
C(3)	0.2461(4)	0.2977(4)	0.0530(4)	4.4(4)
C(4)	0.3768(4)	0.2941(4)	0.1471(4)	4.6(4)
C(5)	0.3286(4)	0.1601(3)	0.0319(4)	4.0(4)
C(6)	0.4105(4)	0.1372(3)	0.1674(4)	4.0(4)
C(7)	0.1005(3)	0.2994(3)	0.1468(3)	2.8(3)
C(8)	0.1002(4)	0.3556(4)	0.1311(4)	4.3(4)
C(9)	0.0470(5)	0.3804(4)	0.0897(5)	5.4(5)
C(10)	-0.0087(5)	0.3478(5)	0.0620(5)	5.5(5)
C(11)	-0.0096(4)	0.2914(4)	0.0762(5)	5.4(5)
C(12)	0.0449(4)	0.2675(3)	0.1179(4)	3.9(4)
C(13)	0.1434(3)	0.2994(3)	0.2837(3)	2.9(3)
C(14)	0.1891(4)	0.3299(3)	0.3288(4)	3.6(3)
C(15)	0.1701(5)	0.3511(4)	0.3861(4)	4.5(4)
C(16)	0.1060(5)	0.3425(4)	0.3977(4)	4.7(4)
C(17)	0.0591(4)	0.3134(4)	0.3528(4)	4.7(4)
C(18)	0.0779(4)	0.2913(3)	0.2961(4)	3.4(4)
C(19)	0.1838(4)	0.0183(3)	0.1960(4)	3.1(3)
C(20)	0.1597(4)	0.0035(4)	0.2524(4)	4.8(4)
C(21)	0.1247(5)	-0.0463(4)	0.2550(5)	6.3(5)
C(22)	0.1135(5)	-0.0817(4)	0.2010(6)	6.6(6)
C(23)	0.1347(6)	-0.0664(4)	0.1437(5)	6.8(6)
C(24)	0.1708(5)	-0.0173(4)	0.1422(4)	5.2(5)
C(25)	0.3251(3)	0.2194(3)	0.3479(3)	2.6(3)
C(26)	0.3733(3)	0.2314(3)	0.3082(4)	3.2(3)
C(27)	0.4268(4)	0.2662(4)	0.3321(5)	4.6(4)

Table . (continued)

atom	x	y	z	B(eq)
C(28)	0.4329(4)	0.2902(4)	0.3936(5)	5.2(5)
C(29)	0.3856(5)	0.2803(4)	0.4317(4)	4.7(4)
C(30)	0.3322(4)	0.2444(4)	0.4099(4)	3.9(4)
C(31)	0.2156(3)	0.1519(3)	0.3810(3)	2.9(3)
C(32)	0.1831(4)	0.1952(3)	0.4079(4)	3.7(4)
C(33)	0.1465(4)	0.1836(4)	0.4578(4)	5.3(5)
C(34)	0.1405(4)	0.1296(5)	0.4796(5)	5.6(5)
C(35)	0.1717(4)	0.0872(4)	0.4512(4)	4.4(4)
C(36)	0.2093(4)	0.0980(3)	0.4025(4)	3.4(4)
C(37)	0.3406(4)	0.0140(3)	0.2691(4)	3.5(4)
C(38)	0.3026(3)	0.0687(3)	0.2651(3)	2.7(3)
C(39)	0.3149(3)	0.1072(3)	0.3137(3)	2.3(3)
C(40)	0.3729(4)	0.0973(3)	0.3712(4)	3.0(3)
C(41)	0.4219(5)	-0.0388(4)	0.2251(5)	6.6(6)
C(42)	0.4861(4)	0.0641(4)	0.3974(5)	5.8(5)
C(43)	0.1323(3)	0.1515(3)	0.1125(3)	2.6(3)
C(44)	0.1462(3)	0.1709(3)	0.0522(3)	3.4(3)
C(45)	0.1128(4)	0.1506(4)	-0.0082(4)	4.2(4)
C(46)	0.0633(4)	0.1100(4)	-0.0118(4)	4.5(4)
C(47)	0.0469(4)	0.0898(4)	0.0463(4)	3.9(4)
C(48)	0.0810(4)	0.1101(3)	0.1072(4)	3.6(4)
C(49)	0.1070(3)	0.1524(3)	0.2488(3)	3.0(3)
C(50)	0.7623(3)	0.1839(3)	0.2019(3)	2.9(3)
C(51)	0.8017(3)	-0.0439(3)	0.1383(3)	2.9(3)
C(52)	0.7689(4)	0.1702(4)	0.0575(4)	4.2(4)

Table . (continued)

atom	x	y	z	B(eq)
C(53)	0.8986(4)	0.1723(4)	0.1536(4)	4.6(4)
C(54)	0.8564(4)	0.0339(4)	0.0425(4)	4.6(4)
C(55)	0.9377(4)	0.0162(4)	0.1788(4)	4.3(4)
C(56)	0.6550(3)	0.1759(3)	0.2775(3)	2.4(3)
C(57)	0.6946(3)	0.2125(3)	0.3222(3)	3.2(3)
C(58)	0.6698(4)	0.2334(3)	0.3765(4)	4.0(4)
C(59)	0.6068(5)	0.2188(4)	0.3872(4)	4.4(4)
C(60)	0.5664(4)	0.1839(4)	0.3425(5)	4.5(4)
C(61)	0.5897(3)	0.1629(3)	0.2886(4)	3.1(3)
C(62)	0.6210(3)	0.1721(3)	0.1408(3)	2.4(3)
C(63)	0.6153(4)	0.2299(3)	0.1283(4)	3.1(3)
C(64)	0.5641(4)	0.2513(3)	0.0822(4)	3.5(4)
C(65)	0.5177(4)	0.2168(4)	0.0458(4)	3.5(4)
C(66)	0.5215(3)	0.1596(3)	0.0563(4)	3.1(3)
C(67)	0.5722(3)	0.1374(3)	0.1038(3)	2.8(3)
C(68)	0.7101(3)	-0.1036(3)	0.2099(4)	3.0(3)
C(69)	0.6850(4)	-0.1179(4)	0.2667(4)	4.6(4)
C(70)	0.6460(5)	-0.1659(4)	0.2686(5)	5.7(5)
C(71)	0.6313(5)	-0.2003(4)	0.2143(6)	5.6(5)
C(72)	0.6548(5)	-0.1871(4)	0.1579(5)	5.4(5)
C(73)	0.6939(4)	-0.1391(4)	0.1560(4)	4.4(4)
C(74)	0.8457(3)	0.1055(3)	0.3533(3)	2.4(3)
C(75)	0.8964(4)	0.1155(3)	0.3171(4)	3.7(4)
C(76)	0.9510(4)	0.1487(4)	0.3408(4)	4.4(4)
C(77)	0.9537(4)	0.1753(4)	0.4009(4)	4.6(4)

Table . (continued)

atom	x	y	z	B(eq)
C(78)	0.9034(4)	0.1672(4)	0.4363(4)	4.7(4)
C(79)	0.8497(4)	0.1319(4)	0.4136(4)	3.8(4)
C(80)	0.7345(3)	0.0391(3)	0.3877(3)	2.4(3)
C(81)	0.6995(3)	0.0818(3)	0.4121(3)	3.0(3)
C(82)	0.6623(4)	0.0721(4)	0.4617(4)	3.5(4)
C(83)	0.6572(4)	0.0188(4)	0.4847(4)	4.5(4)
C(84)	0.6887(4)	-0.0251(4)	0.4595(4)	4.2(4)
C(85)	0.7290(3)	-0.0151(3)	0.4122(4)	3.0(3)
C(86)	0.8666(4)	-0.1036(3)	0.2917(4)	3.3(4)
C(87)	0.8269(3)	-0.0491(3)	0.2813(3)	2.4(3)
C(88)	0.8384(3)	-0.0090(3)	0.3261(3)	2.2(3)
C(89)	0.8968(3)	-0.0115(3)	0.3846(4)	2.7(3)
C(90)	0.9338(4)	-0.1682(4)	0.2455(5)	6.0(5)
C(91)	1.0144(5)	-0.0212(7)	0.4127(5)	11.9(9)
C(92)	0.6596(3)	0.0236(3)	0.1197(3)	2.4(3)
C(93)	0.6069(4)	-0.0160(3)	0.1133(4)	3.0(3)
C(94)	0.5734(4)	-0.0358(3)	0.0532(4)	4.1(4)
C(95)	0.5901(4)	-0.0166(4)	-0.0053(4)	4.5(4)
C(96)	0.6410(4)	0.0216(4)	-0.0020(4)	4.0(4)
C(97)	0.6753(4)	0.0417(3)	0.0583(3)	3.2(3)
C(98)	0.6279(3)	0.0290(3)	0.2528(3)	2.9(3)

Calculated hydrogen atom coordinates and B(iso)

atom	x	y	z	B(iso)
H(1)	0.2347	0.3454	0.1862	3.3
H(2)	0.2769	0.3071	0.2433	3.3
H(3)	0.3024	0.0484	0.1261	3.6
H(4)	0.2369	0.0777	0.0832	3.6
H(5)	0.2494	0.3389	0.0534	5.2
H(6)	0.2699	0.2826	0.0191	5.2
H(7)	0.1983	0.2866	0.0429	5.2
H(8)	0.3998	0.2878	0.1929	5.5
H(9)	0.4002	0.2732	0.1167	5.5
H(10)	0.3774	0.3344	0.1368	5.5
H(11)	0.3538	0.1949	0.0281	4.9
H(12)	0.3526	0.1284	0.0161	4.9
H(13)	0.2831	0.1631	0.0050	4.9
H(14)	0.4089	0.1273	0.2135	4.8
H(15)	0.4321	0.1067	0.1467	4.8
H(16)	0.4367	0.1720	0.1665	4.8
H(17)	0.1394	0.3788	0.1501	5.2
H(18)	0.0481	0.4206	0.0796	6.5
H(19)	-0.0471	0.3651	0.0324	6.6
H(20)	-0.0487	0.2682	0.0569	6.5
H(21)	0.0443	0.2271	0.1272	4.7
H(22)	0.2350	0.3367	0.3205	4.3
H(23)	0.2029	0.3722	0.4182	5.4
H(24)	0.0932	0.3571	0.4385	5.7

Calculated hydrogen atom coordinates and B(iso) (cont.)

atom	x	y	z	B(iso)
H(25)	0.0127	0.3084	0.3608	5.6
H(26)	0.0449	0.2699	0.2646	4.1
H(27)	0.1674	0.0286	0.2910	5.8
H(28)	0.1078	-0.0564	0.2954	7.6
H(29)	0.0904	-0.1178	0.2036	7.9
H(30)	0.1242	-0.0902	0.1041	8.1
H(31)	0.1877	-0.0074	0.1017	6.2
H(32)	0.3689	0.2151	0.2637	3.9
H(33)	0.4612	0.2740	0.3047	5.5
H(34)	0.4717	0.3146	0.4102	6.2
H(35)	0.3894	0.2987	0.4750	5.7
H(36)	0.2989	0.2365	0.4384	4.7
H(37)	0.1859	0.2338	0.3918	4.4
H(38)	0.1246	0.2145	0.4777	6.4
H(39)	0.1145	0.1215	0.5146	6.8
H(40)	0.1671	0.0484	0.4658	5.3
H(41)	0.2316	0.0670	0.3833	4.1
H(42)	0.3952	-0.0736	0.2218	7.9
H(43)	0.4474	-0.0373	0.1886	7.9
H(44)	0.4536	-0.0381	0.2675	7.9
H(45)	0.4730	0.0323	0.4227	7.0
H(46)	0.5232	0.0528	0.3751	7.0
H(47)	0.5011	0.0954	0.4277	7.0
H(48)	0.1809	0.2000	0.0526	4.1

Calculated hydrogen atom coordinates and B(iso) (cont.)

atom	x	y	z	B(iso)
H(49)	0.1246	0.1655	-0.0493	5.1
H(50)	0.0401	0.0957	-0.0549	5.4
H(51)	0.0114	0.0612	0.0449	4.7
H(52)	0.0688	0.0950	0.1480	4.3
H(53)	0.1178	0.1577	0.2969	3.6
H(54)	0.0692	0.1771	0.2300	3.6
H(55)	0.0940	0.1131	0.2389	3.6
H(56)	0.7502	0.2218	0.1850	3.5
H(57)	0.7912	0.1865	0.2458	3.5
H(58)	0.8338	-0.0754	0.1444	3.4
H(59)	0.7682	-0.0498	0.0977	3.4
H(60)	0.7711	0.2114	0.0558	5.0
H(61)	0.7933	0.1542	0.0246	5.0
H(62)	0.7214	0.1581	0.0478	5.0
H(63)	0.9209	0.1676	0.2000	5.6
H(64)	0.9236	0.1511	0.1248	5.6
H(65)	0.8981	0.2123	0.1418	5.6
H(66)	0.8811	0.0019	0.0283	5.5
H(67)	0.8109	0.0357	0.0154	5.5
H(68)	0.8809	0.0688	0.0372	5.5
H(69)	0.9364	0.0069	0.2251	5.2
H(70)	0.9603	-0.0142	0.1588	5.2
H(71)	0.9628	0.0514	0.1770	5.2
H(72)	0.7399	0.2234	0.3152	3.9

Calculated hydrogen atom coordinates and B(iso) (cont.)

atom	x	y	z	B(iso)
H(73)	0.6979	0.2590	0.4075	4.8
H(74)	0.5902	0.2329	0.4263	5.2
H(75)	0.5207	0.1742	0.3494	5.4
H(76)	0.5604	0.1384	0.2574	3.7
H(77)	0.6488	0.2556	0.1532	3.7
H(78)	0.5606	0.2921	0.0752	4.2
H(79)	0.4816	0.2326	0.0121	4.2
H(80)	0.4882	0.1346	0.0300	3.7
H(81)	0.5740	0.0967	0.1117	3.3
H(82)	0.6951	-0.0937	0.3059	5.5
H(83)	0.6289	-0.1753	0.3092	6.9
H(84)	0.6039	-0.2343	0.2160	6.7
H(85)	0.6441	-0.2114	0.1187	6.5
H(86)	0.7105	-0.1300	0.1151	5.3
H(87)	0.8930	0.0983	0.2732	4.4
H(88)	0.9876	0.1535	0.3154	5.3
H(89)	0.9920	0.2000	0.4182	5.5
H(90)	0.9053	0.1867	0.4786	5.7
H(91)	0.8144	0.1257	0.4402	4.6
H(92)	0.7010	0.1199	0.3940	3.6
H(93)	0.6398	0.1034	0.4802	4.2
H(94)	0.6308	0.0118	0.5197	5.4
H(95)	0.6829	-0.0636	0.4747	5.0
H(96)	0.7536	-0.0462	0.3960	3.6

Calculated hydrogen atom coordinates and B(iso) (cont.)

atom	x	y	z	B(iso)
H(97)	0.9059	-0.2004	0.2533	7.2
H(98)	0.9512	-0.1740	0.2042	7.2
H(99)	0.9720	-0.1644	0.2826	7.2
H(100)	1.0112	-0.0521	0.4435	14.3
H(101)	1.0542	-0.0267	0.3917	14.3
H(102)	1.0189	0.0146	0.4370	14.3
H(103)	0.5933	-0.0303	0.1538	3.6
H(104)	0.5374	-0.0639	0.0519	4.9
H(105)	0.5658	-0.0302	-0.0482	5.4
H(106)	0.6537	0.0354	-0.0431	4.8
H(107)	0.7117	0.0692	0.0585	3.9
H(108)	0.6366	0.0366	0.3006	3.5
H(109)	0.5896	0.0520	0.2311	3.5
H(110)	0.6170	-0.0109	0.2451	3.5

A1.4 X-ray Crystallographic Analysis of $Ir(CH_3)I\{C_2(CO_2Me)_2\}[N(SiMe_2CH_2PPh_2)_2]$, 14

Experimental Details

Empirical Formula	C(37)H(45)I(1)Ir(1)N(1)O(4)P(2)Si(2)
Formula Weight	923.94
Crystal System	Monoclinic
Lattice Parameters:	a = 11.911 (2) angstroms b = 19.998 (2) angstroms c = 16.502 (2) angstroms beta = 94.05 (1) degrees V = 3920.9 (8) angstroms**3
Space Group	P21/n (#14)
Z value	4
Dcalc	1.57 g/cm**3
F000	1812
mu(Cu K-alpha)	146.69 cm**-1
Diffractometer	Rigaku AFC6
Radiation	Cu K-alpha (lambda= 1.54178) Graphite-monochromated
Temperature	21 degrees Cent.
2-theta(max)	155.3 degrees
No. Observations (I>3.00(sig(I)))	4945
No. Variables	434
Residuals: R; Rw	0.047; 0.057
Goodness of Fit Indicator	1.66
Maximum Shift in Final Cycle	0.02
Largest Peak in Final Diff. Map	1.75 e/angstrom**3

Table A1.4.1 Bond Lengths (Å) with estimated standard deviations in parentheses

atom	atom	distance	atom	atom	distance
Ir	N	2.044(9)	Si(1)	C(1)	1.87(1)
Ir	C(37)	2.146(9)	Si(2)	C(8)	1.86(1)
Ir	P(1)	2.278(3)	Si(2)	C(7)	1.86(1)
Ir	C(3)	2.32(1)	Si(2)	C(4)	1.87(1)
Ir	P(2)	2.433(2)	Si(2)	C(3)	1.87(1)
Ir	I	2.6929(9)	O(1)	C(9)	1.33(1)
P(1)	C(1)	1.81(1)	O(1)	C(35)	1.44(2)
P(1)	C(11)	1.82(1)	O(2)	C(9)	1.18(1)
P(1)	C(17)	1.82(1)	O(3)	C(10)	1.35(1)
P(2)	C(4)	1.83(1)	O(3)	C(36)	1.44(1)
P(2)	C(23)	1.83(1)	O(4)	C(10)	1.21(1)
P(2)	C(29)	1.84(1)	N	C(2)	1.28(1)
Si(1)	N	1.796(9)	C(2)	C(3)	1.51(1)
Si(1)	C(5)	1.85(1)	C(2)	C(9)	1.52(1)
Si(1)	C(6)	1.85(1)	C(3)	C(10)	1.46(1)

Table A1.4.2 Bond Angles (deg) with estimated standard deviations in parentheses

atom	atom	atom	angle	atom	atom	atom	angle
N	Ir	C(37)	85.1(4)	C(29)	P(2)	Ir	122.8(3)
N	Ir	P(1)	91.1(2)	N	Si(1)	C(5)	111.0(5)
N	Ir	C(3)	64.3(3)	N	Si(1)	C(6)	112.9(5)
N	Ir	P(2)	93.7(2)	N	Si(1)	C(1)	98.8(4)
N	Ir	I	165.6(2)	C(5)	Si(1)	C(6)	112.0(7)
C(37)	Ir	P(1)	91.5(3)	C(5)	Si(1)	C(1)	110.7(6)
C(37)	Ir	C(3)	83.6(4)	C(6)	Si(1)	C(1)	110.8(5)
C(37)	Ir	P(2)	172.1(3)	C(8)	Si(2)	C(7)	108.7(6)
C(37)	Ir	I	84.7(3)	C(8)	Si(2)	C(4)	110.9(5)
P(1)	Ir	C(3)	155.2(3)	C(8)	Si(2)	C(3)	112.0(5)
P(1)	Ir	P(2)	96.37(9)	C(7)	Si(2)	C(4)	108.9(6)
P(1)	Ir	I	99.24(7)	C(7)	Si(2)	C(3)	112.9(5)
C(3)	Ir	P(2)	88.8(2)	C(4)	Si(2)	C(3)	103.4(5)
C(3)	Ir	I	104.5(2)	C(9)	O(1)	C(35)	116(1)
P(2)	Ir	I	95.13(7)	C(10)	O(3)	C(36)	115.9(9)
C(1)	P(1)	C(11)	105.3(5)	C(2)	N	Si(1)	137.8(8)
C(1)	P(1)	C(17)	106.6(5)	C(2)	N	Ir	99.7(7)
C(1)	P(1)	Ir	102.8(3)	Si(1)	N	Ir	120.2(4)
C(11)	P(1)	C(17)	99.6(5)	P(1)	C(1)	Si(1)	114.0(6)
C(11)	P(1)	Ir	121.8(3)	N	C(2)	C(3)	113(1)
C(17)	P(1)	Ir	119.3(4)	N	C(2)	C(9)	124(1)
C(4)	P(2)	C(23)	105.3(5)	C(3)	C(2)	C(9)	122.2(9)
C(4)	P(2)	C(29)	100.1(5)	C(10)	C(3)	C(2)	114.2(9)
C(4)	P(2)	Ir	104.9(4)	C(10)	C(3)	Si(2)	110.2(7)
C(23)	P(2)	C(29)	100.8(5)	C(10)	C(3)	Ir	121.0(7)
C(23)	P(2)	Ir	120.1(4)	C(2)	C(3)	Si(2)	120.0(7)

Table . (continued)

atom	atom	atom	angle
C(2)	C(3)	Ir	82.2(6)
Si(2)	C(3)	Ir	107.3(4)
P(2)	C(4)	Si(2)	108.4(5)
O(2)	C(9)	O(1)	125(1)
O(2)	C(9)	C(2)	125(1)
O(1)	C(9)	C(2)	110(1)
O(4)	C(10)	O(3)	121(1)
O(4)	C(10)	C(3)	126(1)
O(3)	C(10)	C(3)	113.1(9)

Table A1.4.3 Final Atomic Coordinates (Fractional) and B(eq)

atom	x	y	z	B(eq)
Ir	0.54293(4)	0.28052(2)	0.27601(3)	2.21(1)
I	0.65116(7)	0.37548(4)	0.36706(5)	3.92(4)
P(1)	0.4653(2)	0.3460(1)	0.1739(2)	2.5(1)
P(2)	0.3783(2)	0.2776(1)	0.3552(2)	2.5(1)
Si(1)	0.4378(3)	0.2016(2)	0.1099(2)	3.1(1)
Si(2)	0.5284(3)	0.1719(1)	0.4322(2)	3.0(1)
O(1)	0.5583(9)	0.0708(4)	0.1570(6)	5.1(5)
O(2)	0.5636(8)	0.0344(4)	0.2854(6)	4.8(4)
O(3)	0.7634(6)	0.1291(4)	0.2915(5)	3.6(4)
O(4)	0.7808(7)	0.1813(5)	0.4113(5)	5.2(5)
N	0.4981(7)	0.1958(4)	0.2125(5)	2.6(3)
C(1)	0.3778(8)	0.2880(5)	0.1142(6)	2.8(4)
C(2)	0.5494(9)	0.1520(5)	0.2582(6)	2.6(4)
C(3)	0.6018(8)	0.1805(5)	0.3364(6)	2.4(4)
C(4)	0.3797(9)	0.1943(5)	0.4005(6)	2.8(4)
C(5)	0.548(1)	0.1978(8)	0.0368(8)	5.3(7)
C(6)	0.325(1)	0.1394(6)	0.0866(7)	4.0(5)
C(7)	0.532(1)	0.0851(7)	0.4727(8)	4.8(7)
C(8)	0.587(1)	0.2292(7)	0.5130(7)	4.1(6)
C(9)	0.5577(9)	0.0783(5)	0.2373(7)	3.0(5)
C(10)	0.7214(9)	0.1653(5)	0.3517(6)	2.8(4)
C(11)	0.374(1)	0.4161(5)	0.1936(6)	2.9(4)
C(12)	0.259(1)	0.4159(6)	0.1713(8)	4.4(6)
C(13)	0.191(1)	0.4699(7)	0.1878(8)	4.7(6)
C(14)	0.236(1)	0.5249(6)	0.2277(7)	4.3(6)

atom	x	y	z	B(eq)
C(15)	0.351(1)	0.5258(6)	0.2498(9)	4.9(7)
C(16)	0.418(1)	0.4723(6)	0.2339(8)	3.9(5)
C(17)	0.557(1)	0.3859(6)	0.1044(7)	3.3(5)
C(18)	0.536(1)	0.3839(8)	0.0205(8)	5.3(7)
C(19)	0.608(1)	0.416(1)	-0.0272(8)	6.8(9)
C(20)	0.699(1)	0.4529(8)	0.004(1)	5.7(8)
C(21)	0.722(1)	0.4544(7)	0.0868(9)	4.9(7)
C(22)	0.650(1)	0.4218(6)	0.1363(7)	3.7(5)
C(23)	0.367(1)	0.3355(5)	0.4399(7)	3.0(5)
C(24)	0.377(1)	0.4032(6)	0.4237(8)	4.8(7)
C(25)	0.365(1)	0.4503(6)	0.486(1)	5.8(8)
C(26)	0.350(1)	0.4295(7)	0.562(1)	5.6(8)
C(27)	0.339(1)	0.3630(7)	0.5786(7)	4.7(7)
C(28)	0.347(1)	0.3161(6)	0.5168(7)	3.5(5)
C(29)	0.2333(8)	0.2798(6)	0.3085(6)	3.0(4)
C(30)	0.200(1)	0.2285(6)	0.2553(8)	4.0(5)
C(31)	0.091(1)	0.2252(7)	0.2202(8)	4.7(6)
C(32)	0.012(1)	0.273(1)	0.2354(8)	5.8(7)
C(33)	0.044(1)	0.322(1)	0.288(1)	6.6(9)
C(34)	0.155(1)	0.3267(8)	0.3246(8)	5.1(7)
C(35)	0.563(2)	0.0029(8)	0.129(1)	9(1)
C(36)	0.879(1)	0.1073(7)	0.3060(8)	5.0(7)
C(37)	0.6979(8)	0.2730(6)	0.2177(7)	3.3(5)

Hydrogen atom coordinates and B(iso).

atom	x	y	z	B(iso)
H(1)	0.3048	0.2852	0.1379	3.4
H(2)	0.3672	0.3053	0.0587	3.4
H(3)	0.3347	0.1943	0.4480	3.4
H(4)	0.3484	0.1618	0.3606	3.4
H(5)	0.5882	0.1552	0.0430	6.3
H(6)	0.5131	0.2015	-0.0186	6.3
H(7)	0.6010	0.2348	0.0472	6.3
H(8)	0.2643	0.1464	0.1227	4.8
H(9)	0.2955	0.1447	0.0300	4.8
H(10)	0.3558	0.0943	0.0946	4.8
H(11)	0.4866	0.0825	0.5197	5.8
H(12)	0.5020	0.0543	0.4304	5.8
H(13)	0.6101	0.0728	0.4892	5.8
H(14)	0.6654	0.2166	0.5285	4.9
H(15)	0.5850	0.2752	0.4926	4.9
H(16)	0.5425	0.2259	0.5604	4.9
H(17)	0.2259	0.3768	0.1433	5.3
H(18)	0.1104	0.4687	0.1710	5.7
H(19)	0.1888	0.5629	0.2404	5.1
H(20)	0.3844	0.5652	0.2772	5.9
H(21)	0.4986	0.4738	0.2512	4.7
H(22)	0.4707	0.3597	-0.0043	6.4
H(23)	0.5945	0.4134	-0.0863	8.2
H(24)	0.7461	0.4774	-0.0325	6.8
H(25)	0.7878	0.4783	0.1106	5.9

Hydrogen atom coordinates and B(iso) (continued).

atom	x	y	z	B(iso)
H(26)	0.6661	0.4239	0.1954	4.4
H(27)	0.3932	0.4181	0.3692	5.8
H(28)	0.3664	0.4982	0.4732	7.0
H(29)	0.3468	0.4624	0.6055	6.7
H(30)	0.3260	0.3484	0.6339	5.6
H(31)	0.3377	0.2684	0.5287	4.2
H(32)	0.2547	0.1942	0.2424	4.8
H(33)	0.0693	0.1880	0.1837	5.6
H(34)	-0.0640	0.2714	0.2091	6.9
H(35)	-0.0113	0.3552	0.3013	7.9
H(36)	0.1746	0.3638	0.3616	6.1
H(37)	0.4965	-0.0215	0.1443	10.3
H(38)	0.5643	0.0027	0.0693	10.3
H(39)	0.6311	-0.0187	0.1528	10.3
H(40)	0.8856	0.0789	0.3544	6.0
H(41)	0.9010	0.0818	0.2590	6.0
H(42)	0.9278	0.1464	0.3143	6.0
H(43)	0.7344	0.2303	0.2321	4.0
H(44)	0.6822	0.2754	0.1586	4.0
H(45)	0.7478	0.3099	0.2357	4.0

A1.5 X-ray Crystallographic Analysis of *fac*-Ir{η^4-C$(CH_2)_3$}[N$(SiMe_2CH_2PPh_2)_2$], 24

Experimental Details

Empirical Formula	$C_{34}H_{42}IrNP_2Si_2$
Formula Weight	775.05
Crystal Color, Habit	colorless, prism
Crystal Dimensions (mm)	0.120 X 0.250 X 0.350
Crystal System	triclinic
No. Reflections Used for Unit Cell Determination (2θ range)	25 (25.3 - 30.0°)
Omega Scan Peak Width at Half-height	0.36
Lattice Parameters:	a = 11.202 (2)Å b = 13.829 (2)Å c = 10.972 (2)Å α = 90.43 (2)° β = 90.80 (2)° γ = 96.67 (2)° V = 1687.9 (6)Å^3
Space Group	$P\bar{1}$ (#2)
Z value	2
D_{calc}	1.525 g/cm^3
F_{000}	776
$\mu_{(MoK\alpha)}$	41.27 cm^{-1}

B. Intensity Measurements

Diffractometer	Rigaku AFC6S
Radiation	MoKα (λ = 0.71069 Å)
Temperature	21°C
Take-off Angle	6.0°

Detector Aperture	6.0 mm horizontal 6.0 mm vertical
Crystal to Detector Distance	285 mm
Scan Type	ω-2θ
Scan Rate	32.0°/min (in omega) (8 rescans)
Scan Width	(1.10 + 0.35 tanθ)°
$2\theta_{max}$	59.9°
No. of Reflections Measured	Total: 10289 Unique: 9822 (R_{int} = .030)
Corrections	Lorentz-polarization Absorption (trans. factors: 0.54 - 1.00)

C. Structure Solution and Refinement

Structure Solution	Patterson Method
Refinement	Full-matrix least-squares
Function Minimized	Σ w (|Fo| - |Fc|)^2
Least-squares Weights	$4Fo^2/\sigma^2(Fo^2)$
p-factor	0.03
Anomalous Dispersion	All non-hydrogen atoms
No. Observations (I>3.00σ(I))	6397
No. Variables	385
Reflection/Parameter Ratio	16.62
Residuals: R; R_w	0.034; 0.036
Goodness of Fit Indicator	1.27
Max Shift/Error in Final Cycle	0.08
Maximum Peak in Final Diff. Map	1.29 $e^-/Å^3$
Minimum Peak in Final Diff. Map	-1.35 $e^-/Å^3$

Table A1.5.1 Bond Lengths (Å) with estimated standard deviations in parentheses

atom	atom	distance	atom	atom	distance
Ir(1)	P(1)	2.296(1)	C(9)	C(10)	1.35(1)
Ir(1)	P(2)	2.295(1)	C(10)	C(11)	1.39(1)
Ir(1)	N(1)	2.198(4)	C(11)	C(12)	1.376(8)
Ir(1)	C(31)	2.055(5)	C(13)	C(14)	1.390(7)
Ir(1)	C(32)	2.189(5)	C(13)	C(18)	1.386(8)
Ir(1)	C(33)	2.222(5)	C(14)	C(15)	1.393(8)
Ir(1)	C(34)	2.202(5)	C(15)	C(16)	1.36(1)
P(1)	C(1)	1.827(5)	C(16)	C(17)	1.38(1)
P(1)	C(7)	1.840(5)	C(17)	C(18)	1.395(9)
P(1)	C(13)	1.826(5)	C(19)	C(20)	1.399(8)
P(2)	C(2)	1.821(5)	C(19)	C(24)	1.396(7)
P(2)	C(19)	1.834(5)	C(20)	C(21)	1.366(8)
P(2)	C(25)	1.823(5)	C(21)	C(22)	1.39(1)
Si(1)	N(1)	1.688(4)	C(22)	C(23)	1.36(1)
Si(1)	C(1)	1.898(5)	C(23)	C(24)	1.400(9)
Si(1)	C(3)	1.861(7)	C(25)	C(26)	1.400(6)
Si(1)	C(4)	1.868(6)	C(25)	C(30)	1.390(7)
Si(2)	N(1)	1.694(4)	C(26)	C(27)	1.386(7)
Si(2)	C(2)	1.897(5)	C(27)	C(28)	1.362(8)
Si(2)	C(5)	1.873(6)	C(28)	C(29)	1.388(8)
Si(2)	C(6)	1.887(6)	C(29)	C(30)	1.395(8)
C(7)	C(8)	1.387(7)	C(31)	C(32)	1.426(7)
C(7)	C(12)	1.374(7)	C(31)	C(33)	1.437(7)
C(8)	C(9)	1.379(8)	C(31)	C(34)	1.441(7)

Table A1.5.2 Bond Angles (deg) with estimated standard deviations in parentheses

atom	atom	atom	angle	atom	atom	atom	angle
P(1)	Ir(1)	P(2)	106.49(5)	C(7)	P(1)	C(13)	100.5(2)
P(1)	Ir(1)	N(1)	87.0(1)	Ir(1)	P(2)	C(2)	104.7(2)
P(1)	Ir(1)	C(31)	123.1(1)	Ir(1)	P(2)	C(19)	121.8(2)
P(1)	Ir(1)	C(32)	101.9(2)	Ir(1)	P(2)	C(25)	118.1(2)
P(1)	Ir(1)	C(33)	97.1(2)	C(2)	P(2)	C(19)	103.0(2)
P(1)	Ir(1)	C(34)	161.9(1)	C(2)	P(2)	C(25)	105.8(2)
P(2)	Ir(1)	N(1)	83.0(1)	C(19)	P(2)	C(25)	101.5(2)
P(2)	Ir(1)	C(31)	120.7(1)	N(1)	Si(1)	C(1)	104.7(2)
P(2)	Ir(1)	C(32)	105.3(2)	N(1)	Si(1)	C(3)	115.5(3)
P(2)	Ir(1)	C(33)	156.3(2)	N(1)	Si(1)	C(4)	114.9(3)
P(2)	Ir(1)	C(34)	90.4(2)	C(1)	Si(1)	C(3)	111.0(3)
N(1)	Ir(1)	C(31)	126.2(2)	C(1)	Si(1)	C(4)	105.2(3)
N(1)	Ir(1)	C(32)	165.3(2)	C(3)	Si(1)	C(4)	105.1(3)
N(1)	Ir(1)	C(33)	101.1(2)	N(1)	Si(2)	C(2)	106.3(2)
N(1)	Ir(1)	C(34)	101.6(2)	N(1)	Si(2)	C(5)	115.1(2)
C(31)	Ir(1)	C(32)	39.1(2)	N(1)	Si(2)	C(6)	114.7(3)
C(31)	Ir(1)	C(33)	39.0(2)	C(2)	Si(2)	C(5)	107.5(2)
C(31)	Ir(1)	C(34)	39.4(2)	C(2)	Si(2)	C(6)	107.4(3)
C(32)	Ir(1)	C(33)	66.4(2)	C(5)	Si(2)	C(6)	105.4(3)
C(32)	Ir(1)	C(34)	66.7(2)	Ir(1)	N(1)	Si(1)	112.4(2)
C(33)	Ir(1)	C(34)	65.8(2)	Ir(1)	N(1)	Si(2)	114.6(2)
Ir(1)	P(1)	C(1)	109.0(2)	Si(1)	N(1)	Si(2)	132.9(2)
Ir(1)	P(1)	C(7)	122.5(2)	P(1)	C(1)	Si(1)	109.2(2)
Ir(1)	P(1)	C(13)	113.5(2)	P(2)	C(2)	Si(2)	109.1(2)
C(1)	P(1)	C(7)	104.5(2)	P(1)	C(7)	C(8)	120.0(4)
C(1)	P(1)	C(13)	105.2(2)	P(1)	C(7)	C(12)	121.9(4)

Intramolecular Bond Angles Involving the Nonhydrogen Atoms (cont)

atom	atom	atom	angle	atom	atom	atom	angle
C(8)	C(7)	C(12)	118.1(5)	C(26)	C(27)	C(28)	120.6(5)
C(7)	C(8)	C(9)	120.0(6)	C(27)	C(28)	C(29)	120.1(5)
C(8)	C(9)	C(10)	121.2(6)	C(28)	C(29)	C(30)	119.6(5)
C(9)	C(10)	C(11)	119.8(6)	C(25)	C(30)	C(29)	121.0(5)
C(10)	C(11)	C(12)	119.0(6)	Ir(1)	C(31)	C(32)	75.5(3)
C(7)	C(12)	C(11)	121.7(6)	Ir(1)	C(31)	C(33)	76.8(3)
P(1)	C(13)	C(14)	120.7(4)	Ir(1)	C(31)	C(34)	75.8(3)
P(1)	C(13)	C(18)	121.7(4)	C(32)	C(31)	C(33)	115.2(5)
C(14)	C(13)	C(18)	117.6(5)	C(32)	C(31)	C(34)	114.7(5)
C(13)	C(14)	C(15)	121.1(6)	C(33)	C(31)	C(34)	113.3(5)
C(14)	C(15)	C(16)	120.5(6)	Ir(1)	C(32)	C(31)	65.4(3)
C(15)	C(16)	C(17)	119.7(6)	Ir(1)	C(33)	C(31)	64.2(3)
C(16)	C(17)	C(18)	120.1(7)	Ir(1)	C(34)	C(31)	64.8(3)
C(13)	C(18)	C(17)	121.1(6)				
P(2)	C(19)	C(20)	117.7(4)				
P(2)	C(19)	C(24)	123.0(5)				
C(20)	C(19)	C(24)	119.3(5)				
C(19)	C(20)	C(21)	121.0(6)				
C(20)	C(21)	C(22)	119.6(8)				
C(21)	C(22)	C(23)	120.2(6)				
C(22)	C(23)	C(24)	121.4(7)				
C(19)	C(24)	C(23)	118.5(7)				
P(2)	C(25)	C(26)	120.1(4)				
P(2)	C(25)	C(30)	121.9(4)				
C(26)	C(25)	C(30)	117.8(5)				
C(25)	C(26)	C(27)	120.9(5)				

Table A1.5.3 Final Atomic Coordinates (Fractional) and B(eq)

atom	x	y	z	B(eq)
Ir(1)	0.12381(2)	0.21981(1)	0.18561(2)	3.049(7)
P(1)	0.2688(1)	0.13678(9)	0.2724(1)	3.61(5)
P(2)	0.0644(1)	0.32045(8)	0.3347(1)	3.33(5)
Si(1)	0.4000(1)	0.3022(1)	0.1287(1)	4.50(6)
Si(2)	0.2192(1)	0.4530(1)	0.1665(1)	3.87(6)
N(1)	0.2661(3)	0.3410(3)	0.1595(4)	3.8(2)
C(1)	0.4165(4)	0.2028(4)	0.2438(5)	4.3(2)
C(2)	0.0826(5)	0.4413(3)	0.2679(4)	3.9(2)
C(3)	0.4167(6)	0.2570(6)	-0.0296(6)	6.9(3)
C(4)	0.5332(5)	0.3946(5)	0.1559(7)	7.1(3)
C(5)	0.1729(5)	0.5023(4)	0.0168(5)	5.3(3)
C(6)	0.3323(6)	0.5509(4)	0.2350(6)	6.3(3)
C(7)	0.2720(5)	0.1086(3)	0.4360(5)	3.9(2)
C(8)	0.1665(5)	0.1009(4)	0.5018(5)	5.1(3)
C(9)	0.1689(7)	0.0801(5)	0.6245(6)	6.5(3)
C(10)	0.2727(8)	0.0691(4)	0.6834(5)	6.5(3)
C(11)	0.3795(7)	0.0765(5)	0.6195(6)	6.2(3)
C(12)	0.3770(5)	0.0954(4)	0.4966(5)	4.9(2)
C(13)	0.2739(5)	0.0156(4)	0.2067(5)	4.4(2)
C(14)	0.2082(5)	-0.0654(4)	0.2571(5)	5.1(3)
C(15)	0.2076(6)	-0.1575(4)	0.2046(7)	6.7(3)
C(16)	0.2721(7)	-0.1701(5)	0.1024(8)	7.1(4)
C(17)	0.3381(7)	-0.0910(6)	0.0506(7)	7.6(4)
C(18)	0.3384(6)	0.0014(4)	0.1024(6)	6.3(3)

Table . (continued)

atom	x	y	z	B(eq)
C(19)	0.1461(5)	0.3392(3)	0.4806(4)	4.1(2)
C(20)	0.2716(6)	0.3566(4)	0.4775(5)	5.4(3)
C(21)	0.3384(7)	0.3727(5)	0.5824(7)	7.4(4)
C(22)	0.281(1)	0.3724(5)	0.6938(7)	8.5(5)
C(23)	0.159(1)	0.3539(5)	0.6988(5)	7.9(4)
C(24)	0.0887(6)	0.3381(4)	0.5928(5)	5.7(3)
C(25)	-0.0909(4)	0.3004(3)	0.3848(4)	3.7(2)
C(26)	-0.1414(5)	0.2070(4)	0.4176(5)	4.4(2)
C(27)	-0.2564(5)	0.1916(4)	0.4641(5)	5.0(3)
C(28)	-0.3227(5)	0.2673(5)	0.4790(6)	5.4(3)
C(29)	-0.2753(5)	0.3609(4)	0.4475(6)	5.6(3)
C(30)	-0.1604(5)	0.3766(4)	0.3988(5)	4.8(2)
C(31)	0.0037(4)	0.1598(4)	0.0550(5)	4.1(2)
C(32)	-0.0262(5)	0.1046(4)	0.1618(5)	4.5(2)
C(33)	0.1183(5)	0.1473(4)	0.0039(5)	4.8(2)
C(34)	-0.0187(5)	0.2602(4)	0.0624(5)	4.4(2)

A1.6 X-ray Crystallographic Analysis of $Ir(\eta^4\text{-}C_4H_6)[N(SiMe_2CH_2PPh_2)_2]$, 28

Experimental Details

compound	$[(Ph_2PCH_2SiMe_2)_2N]Ir(\eta^4\text{-}C_4H_6)$
formula	$C_{34}H_{42}IrNP_2Si_2$
fw	775.05
crystal system	triclinic
space group	$P\bar{1}^b$
a (Å)	10.9061(5)
b (Å)	11.1193(9)
c (Å)	14.0083(5)
α (deg)	95.040(6)
β (deg)	91.127(4)
γ (deg)	90.520(6)
V (Å^3)	1691.8(2)
Z	2
D_c (g/cm^3)	1.521
$F(000)$	776
μ(Mo-K_α) (cm^{-1})	41.2
crystal dimensions (mm)	0.27x0.35x0.45
scan type	$\omega - 2\theta$
scan range (deg in ω)	0.80 + 0.35 tan θ
scan speed (deg/min)	1.7-20.0
data collected	$\pm h, \pm k, +l$
$2\theta_{max}$ (deg)	60
crystal decay	negligible
unique reflections	9810
reflections with $I \geq 3\sigma(I)$	7666
number of variables	362
R	0.025
R_w	0.033
S	1.143
mean Δ/σ (final cycle)	0.002
max Δ/σ (final cycle)	0.017
residual density (e/Å^3)	-0.76 to +1.55 (near Ir)

Table A1.6.1 Bond Lengths (Å) with estimated standard deviations in parentheses

Bond	Length(Å)	Bond	Length(Å)
Ir -P(1)	2.292(1)	C(9)-C(10)	1.35(1)
Ir -P(2)	2.2879(9)	C(10)-C(11)	1.38(1)
Ir -N	2.214(3)	C(11)-C(12)	1.384(8)
Ir -C(31)	2.139(4)	C(13)-C(14)	1.386(7)
Ir -C(32)	2.167(4)	C(13)-C(18)	1.386(7)
Ir -C(33)	2.183(4)	C(14)-C(15)	1.390(7)
Ir -C(34)	2.182(4)	C(15)-C(16)	1.36(1)
Ir -Bu	1.770(2)	C(16)-C(17)	1.37(1)
P(1)-C(1)	1.829(4)	C(17)-C(18)	1.399(8)
P(1)-C(7)	1.837(4)	C(19)-C(20)	1.388(7)
P(1)-C(13)	1.837(4)	C(19)-C(24)	1.389(6)
P(2)-C(2)	1.826(4)	C(20)-C(21)	1.384(7)
P(2)-C(19)	1.832(4)	C(21)-C(22)	1.41(1)
P(2)-C(25)	1.828(4)	C(22)-C(23)	1.36(1)
Si(1)-N	1.683(4)	C(23)-C(24)	1.389(8)
Si(1)-C(1)	1.891(4)	C(25)-C(26)	1.389(6)
Si(1)-C(3)	1.863(7)	C(25)-C(30)	1.396(6)
Si(1)-C(4)	1.864(6)	C(26)-C(27)	1.390(7)
Si(2)-N	1.696(4)	C(27)-C(28)	1.369(7)
Si(2)-C(2)	1.905(4)	C(28)-C(29)	1.392(7)
Si(2)-C(5)	1.888(5)	C(29)-C(30)	1.362(7)
Si(2)-C(6)	1.883(5)	C(31)-C(32)	1.430(7)
C(7)-C(8)	1.376(7)	C(32)-C(33)	1.409(7)
C(7)-C(12)	1.397(6)	C(33)-C(34)	1.421(7)
C(8)-C(9)	1.404(7)		

Bu refers to the centroid of the butadiene ligand.

Table A1.6.2 Bond Angles (deg) with estimated standard deviations in parentheses

Bonds	Angle(deg)	Bonds	Angle(deg)
P(1)-Ir -P(2)	107.01(4)	P(1)-C(7)-C(8)	119.6(3)
P(1)-Ir -N	87.49(9)	P(1)-C(7)-C(12)	121.2(4)
P(1)-Ir -Bu	122.23(8)	C(8)-C(7)-C(12)	119.2(4)
P(2)-Ir -N	83.43(9)	C(7)-C(8)-C(9)	120.4(5)
P(2)-Ir -Bu	123.22(8)	C(8)-C(9)-C(10)	120.2(6)
N -Ir -Bu	122.3(1)	C(9)-C(10)-C(11)	119.8(5)
Ir -P(1)-C(1)	108.5(1)	C(10)-C(11)-C(12)	121.2(6)
Ir -P(1)-C(7)	121.8(1)	C(7)-C(12)-C(11)	119.2(5)
Ir -P(1)-C(13)	114.3(1)	P(1)-C(13)-C(14)	121.1(4)
C(1)-P(1)-C(7)	106.1(2)	P(1)-C(13)-C(18)	120.2(4)
C(1)-P(1)-C(13)	105.1(2)	C(14)-C(13)-C(18)	118.5(4)
C(7)-P(1)-C(13)	99.6(2)	C(13)-C(14)-C(15)	120.7(6)
Ir -P(2)-C(2)	106.1(1)	C(14)-C(15)-C(16)	120.8(6)
Ir -P(2)-C(19)	122.4(1)	C(15)-C(16)-C(17)	119.1(5)
Ir -P(2)-C(25)	116.5(1)	C(16)-C(17)-C(18)	121.4(6)
C(2)-P(2)-C(19)	101.8(2)	C(13)-C(18)-C(17)	119.5(6)
C(2)-P(2)-C(25)	106.4(2)	P(2)-C(19)-C(20)	118.3(3)
C(19)-P(2)-C(25)	101.8(2)	P(2)-C(19)-C(24)	123.3(4)
N -Si(1)-C(1)	105.5(2)	C(20)-C(19)-C(24)	118.3(4)
N -Si(1)-C(3)	113.4(2)	C(19)-C(20)-C(21)	121.5(5)
N -Si(1)-C(4)	115.7(2)	C(20)-C(21)-C(22)	118.8(6)
C(1)-Si(1)-C(3)	110.2(3)	C(21)-C(22)-C(23)	120.0(5)
C(1)-Si(1)-C(4)	105.9(2)	C(22)-C(23)-C(24)	120.6(6)
C(3)-Si(1)-C(4)	105.9(4)	C(19)-C(24)-C(23)	120.7(6)
N -Si(2)-C(2)	106.3(2)	P(2)-C(25)-C(26)	119.5(3)
N -Si(2)-C(5)	115.2(2)	P(2)-C(25)-C(30)	122.0(3)
N -Si(2)-C(6)	115.2(2)	C(26)-C(25)-C(30)	118.4(4)
C(2)-Si(2)-C(5)	107.2(2)	C(25)-C(26)-C(27)	120.7(4)
C(2)-Si(2)-C(6)	108.7(2)	C(26)-C(27)-C(28)	120.3(5)
C(5)-Si(2)-C(6)	104.0(2)	C(27)-C(28)-C(29)	119.0(5)
Ir -N -Si(1)	109.8(2)	C(28)-C(29)-C(30)	121.3(5)
Ir -N -Si(2)	116.5(2)	C(25)-C(30)-C(29)	120.3(4)
Si(1)-N -Si(2)	133.7(2)	C(31)-C(32)-C(33)	116.6(4)
P(1)-C(1)-Si(1)	108.5(2)	C(32)-C(33)-C(34)	117.4(4)
P(2)-C(2)-Si(2)	109.2(2)		

Table A1.6.3 Final Atomic Coordinates (Fractional) and B(eq)

Atom	x	y	z	U_{eq}
Ir	313715(12)	375874(13)	282414(9)	40
P(1)	22792(9)	22874(9)	36538(7)	45
P(2)	16511(9)	43637(9)	18003(6)	43
Si(1)	38224(11)	10392(11)	21053(9)	57
Si(2)	32880(10)	27538(11)	5152(8)	49
N	3451(3)	2340(3)	1647(2)	49
C(1)	2636(4)	815(4)	3042(3)	53
C(2)	2283(4)	4149(4)	600(3)	50
C(3)	5392(5)	1060(7)	2655(6)	96
C(4)	3735(7)	-342(5)	1249(5)	93
C(5)	4760(5)	3176(5)	-66(4)	68
C(6)	2562(5)	1579(5)	-375(4)	77
C(7)	630(4)	2248(4)	3895(3)	50
C(8)	-25(4)	3302(5)	3940(3)	64
C(9)	-1284(5)	3291(7)	4130(4)	84
C(10)	-1862(5)	2243(8)	4277(4)	93
C(11)	-1212(6)	1181(7)	4227(4)	88
C(12)	30(4)	1168(5)	4045(3)	65
C(13)	2895(4)	2240(4)	4880(3)	56
C(14)	2317(5)	2833(5)	5655(3)	73
C(15)	2830(7)	2856(7)	6573(4)	95
C(16)	3911(7)	2304(7)	6730(4)	95
C(17)	4507(6)	1740(7)	5967(5)	94
C(18)	4010(5)	1695(6)	5037(4)	80
C(19)	163(4)	3588(4)	1628(3)	53
C(20)	147(5)	2337(5)	1484(3)	67
C(21)	-935(6)	1695(6)	1283(4)	89
C(22)	-2044(6)	2331(9)	1256(5)	101
C(23)	-2038(5)	3555(8)	1406(4)	92
C(24)	-945(4)	4191(5)	1593(3)	69
C(25)	1194(4)	5944(4)	1976(3)	50
C(26)	977(5)	6460(4)	2895(3)	59
C(27)	539(5)	7630(5)	3042(4)	68
C(28)	333(5)	8297(4)	2280(4)	67
C(29)	579(5)	7791(5)	1361(4)	73
C(30)	1008(5)	6645(4)	1207(3)	62
C(31)	3360(5)	5065(4)	4031(3)	62
C(32)	4474(4)	4404(4)	3919(3)	61
C(33)	5033(4)	4393(4)	3020(3)	62
C(34)	4446(4)	5038(5)	2311(4)	63

A2 Raw Data for the Kinetic Studies of the Thermolysis and Carbonylation Processes

A2.1a Thermolysis of $Ir(CH_3)PPh_2[N(SiMe_2CH_2PPh_2)_2]$, 2a, in toluene

Temperature = 73°C
[**2a**] = 3.26 x 10^{-3} mol L^{-1}

Time (s)	A_t (538 nm)
0	0.893
500	0.788
1000	0.686
1500	0.609
2000	0.534
2550	0.479
3300	0.385
4800	0.253
6800	0.155
A_∞	0.060

k_{obs} = 0.54 x 10^{-3} s^{-1}

Temperature = 83°C
[**2a**] = 3.26 x 10^{-3} mol L^{-1}

Time (s)	A_t (538 nm)
0	0.881
200	0.824
400	0.765
700	0.658
1000	0.573
1300	0.509
1800	0.388
2300	0.298
4000	0.127
A_∞	0.060

k_{obs} = 0.84 x 10^{-3} s^{-1}

Temperature = 97°C
[**2a**] = 3.26 x 10^{-3} mol L^{-1}

Time (s)	A_t (538 nm)
0	0.879
200	0.700
350	0.610
500	0.535
650	0.480
800	0.422
1000	0.344
1500	0.222
2000	0.165
A_∞	0.060

k_{obs} = 1.04 x 10^{-3} s^{-1}

Temperature = 97°C
[**2a**] = 3.26 x 10^{-3} mol L^{-1}

Time (s)	A_t (538 nm)
0	0.879
200	0.688
350	0.598
500	0.522
650	0.472
800	0.414
1000	0.337
1200	0.277
1500	0.215
2000	0.097
A_∞	0.060

k_{obs} = 1.07 x 10^{-3} s^{-1}

Temperature = 108°C
[**2a**] = 3.26 x 10^{-3} mol L^{-1}

Time (s)	A_t (538 nm)
0	0.914
100	0.849
250	0.653
400	0.520
550	0.410
700	0.327
900	0.223
1100	0.151
A_∞	0.058

k_{obs} = 1.07 x 10^{-3} s^{-1}

A2.1b Thermolysis of $Ir(CH_3)PPh_2[N(SiMe_2CH_2PPh_2)_2]$, 2a, in hexanes

Temperature = 60°C
[**2a**] = 4.34 x 10^{-4} mol L^{-1}

Time (s)	A_t (538 nm)
0	1.010
1500	0.859
3000	0.738
4500	0.654
6000	0.592
8000	0.536
12000	0.440
15000	0.379
19000	0.320
24000	0.260
30000	0.136
35000	0.091
A_∞	0.060

k_{obs} = 6.06 x 10^{-5} s^{-1}

Temperature = 67°C
[**2a**] = 4.34 x 10^{-4} mol L^{-1}

Time (s)	A_t (538 nm)
0	0.912
1000	0.803
2000	0.701
3000	0.613
4000	0.547
5000	0.483
7500	0.361
8500	0.322
9500	0.289
15000	0.106
A_∞	0.045

k_{obs} = 1.37 x 10^{-4} s^{-1}

Temperature = 78°C
[**2a**] = 4.88 x 10^{-4} mol L^{-1}

Time (s)	A_t (538 nm)
0	1.490
200	1.400
600	1.215
1000	1.050
1400	0.920
1800	0.800
2200	0.693
2700	0.580
3500	0.420
4500	0.275
5500	0.190
A_∞	0.050

k_{obs} = 4.20 x 10^{-4} s^{-1}

Temperature = 87°C
[**2a**] = 4.88 x 10^{-4} mol L^{-1}

Time (s)	A_t (538 nm)
0	1.503
200	1.178
400	0.926
550	0.803
700	0.705
900	0.577
1100	0.465
1300	0.383
1500	0.320
1700	0.270
2350	0.138
A_∞	0.040

k_{obs} = 1.10 x10^{-3} s^{-1}

Temperature = 67°C
[**2a-CD_3**] = 6.44 x 10^{-4} mol L^{-1}

Time (s)	A_t (538 nm)
0	1.353
500	1.307
1250	1.216
3405	1.081
4405	0.986
5405	0.895
7405	0.745
9405	0.609
11405	0.505
20000	0.241
25000	0.146
A_∞	0.053

k_{obs} = 8.77 x10^{-5} s^{-1}

A2.2 Thermolysis of *fac*-Ir(η^2-CH_2PPh_2)H[$N(SiMe_2CH_2PPh_2)_2$], 3a, in toluene

Temperature = 91°C
[**3a**] = 2.04 x 10^{-4} mol L^{-1}

Time (s)	A_t (360 nm)
0	1.054
6000	1.000
12000	0.940
18650	0.908
27650	0.852
86870	0.660
96370	0.622
106370	0.610
183870	0.520
216770	0.503
A_∞	0.400

k_{obs} = 0.87 x 10^{-5} s^{-1}

Temperature = 91°C
[**3a**] = 2.04 x 10^{-4} mol L^{-1}

Time (s)	A_t (360 nm)
0	1.014
4100	0.973
8100	0.930
12500	0.916
23450	0.835
32450	0.800
81800	0.663
99800	0.610
161800	0.532
A_∞	0.400

k_{obs} = 0.94 x 10^{-5} s^{-1}

Temperature = 94°C
[**3a**] = 2.04 x 10^{-4} mol L^{-1}

Time (s)	A_t (360 nm)
0	0.945
5000	0.906
9200	0.868
16500	0.828
61300	0.680
65300	0.673
72850	0.640
89050	0.603
94450	0.607
100000	0.582
200000	0.466
A_∞	0.400

k_{obs} = 1.03 x 10^{-5} s^{-1}

Temperature = 102°C
[**3a**] = 2.04 x 10^{-4} mol L^{-1}

Time (s)	A_t (360 nm)
0	1.108
4000	1.053
8100	0.994
12000	0.940
17700	0.876
25350	0.798
63950	0.563
A_∞	0.400

k_{obs} = 2.31 x 10^{-5} s^{-1}

Temperature = 112°C
[**3a**] = 2.04 x 10^{-4} mol L^{-1}

Time (s)	A_t (360 nm)
0	1.066
4000	0.928
8000	0.810
12550	0.697
16550	0.621
20550	0.584
38270	0.454
A_∞	0.400

k_{obs} = 6.59 x 10^{-5} s^{-1}

Temperature = 112°C
[**3a-CD_2**]=2.32x10^{-4} mol L^{-1}

Time (s)	A_t (360 nm)
0	1.258
4000	1.081
8000	0.950
12000	0.844
16000	0.783
20570	0.746
33070	0.588
A_∞	0.366

k_{obs} = 4.19 x 10^{-5} s^{-1}

A2.3 Thermolysis of *fac*-Ir(η^2-CH_2PPh_2)H[N($SiMe_2CH_2PPh_2$)$_2$], 6a, in toluene

Temperature = 36°C
[**6a**] = 2.08 x 10^{-4} mol L^{-1}

Time (s)	A_t (360 nm)
0	0.458
1000	0.479
2000	0.500
6150	0.596
8150	0.641
10150	0.720
26550	0.904
32000	0.965
45000	1.032
A_∞	1.100

k_{obs} = 0.50 x 10^{-4} s^{-1}

Temperature = 46°C
[**6a**] = 2.08 x 10^{-4} mol L^{-1}

Time (s)	A_t (360 nm)
0	0.458
600	0.528
1200	0.581
1800	0.633
2400	0.678
3200	0.732
4200	0.792
5200	0.840
6200	0.883
8200	0.963
9700	0.992
A_∞	1.100

k_{obs} = 1.84 x 10^{-4} s^{-1}

Temperature = 56°C
[**6a**] = 2.08 x 10^{-4} mol L^{-1}

Time (s)	A_t (360 nm)
0	0.455
200	0.511
400	0.545
600	0.571
900	0.629
1900	0.784
2300	0.860
2700	0.903
3300	0.964
3800	0.995
4400	1.024
A_∞	1.100

k_{obs} = 4.87 x 10^{-4} s^{-1}

Temperature = 59°C
[**6a**] = 2.08 x 10^{-4} mol L^{-1}

Time (s)	A_t (360 nm)
0	0.460
150	0.516
300	0.557
450	0.585
650	0.659
850	0.719
1050	0.779
1300	0.827
2000	0.926
3000	1.026
A_∞	1.100

k_{obs} = 7.15 x 10^{-4} s^{-1}

A2.4a Thermolysis of $Ir(CH_3)PHPh[N(SiMe_2CH_2PPh_2)_2]$, 2d, in toluene

Temperature = 69°C
[**2d**] = 2.84 x 10^{-4} mol L^{-1}

Time (s)	A_t (460 nm)
0	0.688
320	0.650
650	0.595
1020	0.550
1620	0.496
2620	0.434
A_∞	0.310

k_{obs} = 0.430 x 10^{-3} s^{-1}

Temperature = 82°C
[**2d**] = 2.84 x 10^{-4} mol L^{-1}

Time (s)	A_t (460 nm)
0	0.628
110	0.581
260	0.535
500	0.460
800	0.378
1200	0.304
1700	0.249
A_∞	0.310

k_{obs} = 1.600 x 10^{-3} s^{-1}

Temperature = 86°C
[**2d**] = 2.84 x 10^{-4} mol L^{-1}

Time (s)	A_t (460 nm)
0	0.690
100	0.660
300	0.577
550	0.472
800	0.405
1100	0.356
1400	0.331
A_∞	0.310

k_{obs} =2.102 x 10^{-3} s^{-1}

Temperature = 93°C
[**2d**] = 2.84 x 10^{-4} mol L^{-1}

Time (s)	A_t (460 nm)
0	0.690
150	0.647
305	0.539
510	0.449
700	0.386
1000	0.336
A_∞	0.310

k_{obs} = 2.800 x 10^{-3} s^{-1}

A2.4b Thermolysis of $Ir(CH_3)PHPh[N(SiMe_2CH_2PPh_2)_2]$, 2d, in hexanes

Temperature = 54°C
[**2d**] = 1.15 x 10^{-3} mol L^{-1}

Time (s)	A_t (515 nm)
0	1.630
500	1.617
1000	1.510
2020	1.305
2800	1.178
4000	0.999
6000	0.763
8000	0.587
12000	0.410
A_∞	0.236

k_{obs} = 0.176 x 10^{-3} s^{-1}

Temperature = 54°C
[**2d**] = 1.15 x 10^{-3} mol L^{-1}

Time (s)	A_t (515 nm)
0	1.628
1000	1.490
2000	1.299
2800	1.169
4000	0.989
6000	0.759
8000	0.585
A_∞	0.230

k_{obs} = 0.178 x 10^{-3} s^{-1}

Temperature = 65°C
[**2d**] = 1.15 x 10^{-3} mol L^{-1}

Time (s)	A_t (515 nm)
0	1.632
400	1.520
800	1.238
1000	1.160
1300	1.040
1600	0.936
1900	0.845
2300	0.738
2900	0.585
4000	0.463
5000	0.373
A_∞	0.238

k_{obs} = 0.476 x 10^{-3} s^{-1}

Temperature = 74°C
[**2d**] =1.15 x 10^{-3} mol L^{-1}

Time (s)	A_t (515 nm)
0	1.650
400	1.185
600	1.020
800	0.902
1000	0.787
1200	0.686
1400	0.607
1600	0.542
1850	0.460
A_∞	0.253

k_{obs} = 1.008 x 10^{-3} s^{-1}

Temperature = 79°C
[**2d**]=1.15 x 10^{-3} mol L^{-1}

Time (s)	A_t (515 nm)
0	1.634
150	1.540
350	1.156
450	1.079
600	0.940
750	0.806
900	0.703
1050	0.620
1250	0.508
1525	0.380
A_∞	0.240

k_{obs} = 1.008 x 10^{-3} s^{-1}

Temperature = 74°C
[**2d-CD_3**]=1.12x10^{-3}mol L^{-1}

Time (s)	A_t (515 nm)
0	1.611
150	1.225
400	1.185
600	1.020
800	0.879
1000	0.771
1200	0.678
1400	0.604
1700	0.485
2000	0.397
2500	0.283
A_∞	0.214

k_{obs} = 0.994 x 10^{-3} s^{-1}

A2.5 Carbonylation of *fac*-Ir(η^2-CH_2PPh_2)H[N($SiMe_2CH_2PPh_2$)$_2$], 6a, in toluene

Temperature = 46°C

[**6a**] = 4.22 x 10^{-4} mol L^{-1}

Time (s)	A_t (360 nm)
0	0.929
600	0.842
1000	0.795
1400	0.752
1900	0.706
2400	0.657
3200	0.581
4000	0.510
5010	0.425
6010	0.365
7010	0.305
8110	0.247
9210	0.201
10210	0.158
11010	0.140
A_∞	0.020

k_{obs} = 1.82 x 10^{-4} s^{-1}